

ISSN: 2687 - 4539

# CHAOS

## THEORY AND APPLICATIONS

IN APPLIED SCIENCES AND ENGINEERING



VOLUME 6, ISSUE 1, MARCH 2024

AN INTERDISCIPLINARY JOURNAL OF NONLINEAR SCIENCE

**Chaos Theory and Applications (CHTA)**  
 Volume: 6 – Issue No: 1 (March 2024)  
<https://dergipark.org.tr/en/pub/chaos/issue/83761>  
**Editorial Board Members**

Honorary Editorial Board

Otto E. ROSSLER, University of Tuebingen, GERMANY, oeross00@yahoo.com  
 Julien C. SPROTT, University of Wisconsin–Madison, USA, csprott@wisc.edu  
 Guanrong CHEN, City University of Hong Kong, HONG KONG, eegchen@cityu.edu.hk  
 José A. Tenreiro MACHADO<sup>†</sup>, Polytechnic Institute of Porto, PORTUGAL, jtm@isep.ipp.pt  
 Ravi P. AGARWAL, Texas A&M University, USA, Ravi.Agarwal@tamuk.edu

Editor-in-Chief

Akif AKGUL, Hitit University, TURKEY, akifakgul@hitit.edu.tr

Associate Editors

Miguel A. F. SANJUAN, Universidad Rey Juan Carlos, SPAIN, miguel.sanjuan@urjc.es  
 Chunbiao LI, Nanjing University of Information Science & Technology, CHINA, goontry@126.com  
 Dumitru BALEANU, Lebanese American University, LEBANON, dumitru.baleanu@gmail.com  
 Yeliz KARACA, University of Massachusetts Chan Medical School, USA, yeliz.karaca@ieee.org  
 J. M. MUÑOZ PACHECO, Benemérita Universidad Autónoma de Puebla, MEXICO, jesusm.pacheco@correo.buap.mx  
 Martin BOHNER, Missouri University of Science and Technology, USA, bohner@mst.edu  
 Nikolay V. KUZNETSOV, Saint Petersburg State University, RUSSIA, n.v.kuznetsov@spbu.ru  
 Sifeu T. KINGNI, University of Maroua, CAMEROON, stkingni@gmail.com  
 Fahrettin HORASAN, Kırkkale University, TURKEY, fhorasan@kku.edu.tr  
 Vinod PATIDAR, School of Computer Science UPES, INDIA, vinod.patidar@ddn.upes.ac.in  
 Hijaz AHMAD, International Telematic University, ITALY, hijaz555@gmail.com  
 Eyyüp Ensari ŞAHİN, Nigde Omer Halisdemir University, TURKEY, ensarisahin@ohu.edu.tr

Editorial Board Members

Jun MA, Lanzhou University of Technology, CHINA, hyperchaos@lut.edu.cn  
 René LOZI, University Côte D'azur, FRANCE, Rene.LOZI@univ-cotedazur.fr  
 Herbert Ho-Ching LU, The University of Western Australia, AUSTRALIA, herbert.lu@uwa.edu.au  
 Praveen AGARWAL, Anand International College of Engineering, INDIA, goyal.praveen2011@gmail.com  
 Shaher MOMANI, Ajman University, UAE, shaherm@yaho.com  
 Edmon PERKINS, North Carolina State University, USA, edmonperkins@gmail.com  
 Alexander PCHELINTSEV, Tambov State Technical University, RUSSIA, pchelintsev.an@yandex.ru  
 Yudong ZHANG, University of Leicester, UK, yudongzhang@ieee.org  
 Wesley Joo-Chen THIO, The Ohio State University, USA, wesley.thio@gmail.com  
 Yong WANG, Chongqing University of Posts and Telecommunications, CHINA, wangyong\_cqupt@163.com  
 Mustafa Zahid YILDIZ, Sakarya University of Applied Sciences, TURKEY, mustafayildiz@sakarya.edu.tr  
 Anastasios (Tassos) BOUNTIS, University of Patras, GREECE, anastasios.bountis@nu.edu.kz  
 Marcelo MESSIAS, São Paulo State University, BRAZIL, marcelo.messias1@unesp.br  
 Sajad JAFARI, Ton Duc Thang University, VIETNAM, sajadjafari83@gmail.com  
 Jesús M. SEOANE, Universidad Rey Juan Carlos, SPAIN, jesus.seoane@urjc.es  
 G. Cigdem YALCIN, Istanbul University, TURKEY, gcyalcin@istanbul.edu.tr  
 Marcelo A. SAVI, Universidade Federal do Rio de Janeiro, BRAZIL, savi@mecanica.coppe.ufrj.br  
 Christos K. VOLOS, Aristotle University of Thessaloniki, GREECE, volos@physics.auth.gr  
 Charalampos (Haris) SKOKOS, University of Cape Town, SOUTH AFRICA, haris.skokos@uct.ac.za  
 Ihsan PEHLIVAN, Sakarya University of Applied Sciences, TURKEY, ipehlivan@sakarya.edu.tr  
 Olfa BOUBAKER, University of Carthage, TUNUSIA, olfa\_insat@yahoo.com  
 Karthikeyan RAJAGOPAL, Defence University, ETHIOPIA, rkarthikeyan@gmail.com  
 Binoy Krishna ROY, National Institute of Technology Silchar, INDIA, bkr\_nits@yahoo.co.in  
 Jacques KENGNE, Université de Dschang, CAMEROON, kengnemozart@yahoo.fr  
 Fatih KURUGOLLU, University of Sharjah, UAE, fkurugollu@sharjah.ac.ae  
 Denis BUTUSOV, Petersburg State Electrotechnical University, RUSSIA, butusovdn@mail.ru  
 Iqtadar HUSSAIN, Qatar University, QATAR, iqtadarqau@qu.edu.qa  
 Sundarapandian VAIDYANATHAN, Vel Tech - Technical University, INDIA, sundarvту@gmail.com  
 Irene M. MOROZ, University of Oxford, UK, Irene.Moroz@maths.ox.ac.uk  
 Serdar CICEK, Tarsus University, TURKEY, serdarcicek@gmail.com  
 Zhouchao WEI, China University of Geosciences, CHINA, weizhouchao@163.com  
 Qiang LAI, East China Jiaotong University, CHINA, laiqiang87@126.com  
 Viet-thanh PHAM, Phenikaa University, VIETNAM, pvt3010@gmail.com  
 Günyaz ABLAY, Abdullah Gul University, TURKEY, gunyaz.ablay@agu.edu.tr  
 Jay Prakash SINGH, Rewa Engineering College, INDIA, jp4ssm@gmail.com

Yılmaz UYAROĞLU, Sakarya University, TURKEY, uyaroglu@sakarya.edu.tr  
Shaobo HE, Central South University, CHINA, heshabo\_123@163.com  
Esteban Tlelo CUAUTLE, Instituto Nacional de Astrofísica, MEXICO, etlelo@inaoep.mx  
Dan-gheorghe DIMITRIU, Alexandru Ioan Cuza University of Iasi, ROMANIA, dimitriu@uaic.ro  
Jawad AHMAD, Edinburgh Napier University, UK, jawad.saj@gmail.com  
Metin VARAN, Sakarya University of Applied Sciences, TURKEY, mvaran@sakarya.edu.tr  
Ashish ASHISH, Government College Satnali, INDIA, drashishkumar108@gmail.com  
Murat TUNA, Kırklareli University, TURKEY, murat.tuna@klu.edu.tr  
Orhan Ozgur AYBAR, Piri Reis University, TURKEY, oaybar@pirireis.edu.tr  
Mehmet YAVUZ, Necmettin Erbakan University, TURKEY, mehmetyavuz@erbakan.edu.tr

#### Editorial Advisory Board Members

Ayhan ISTANBULLU, Balıkesir University, TURKEY, ayhanistan@yahoo.com  
Ismail KOYUNCU, Afyon Kocatepe University, TURKEY, ismailkoyuncu@aku.edu.tr  
Fatih OZKAYNAK, Fırat University, TURKEY, ozkaynak@firat.edu.tr  
Sezgin KACAR, Sakarya University of Applied Sciences, TURKEY, skacar@subu.edu.tr  
Ugur Erkin KOCAMAZ, Bursa Uludağ University, TURKEY, ugurkocamaz@gmail.com  
Erdinc AVAROĞLU, Mersin University, TURKEY, eavaroglu@mersin.edu.tr  
Ali DURDU, Social Sciences University of Ankara, TURKEY, ali.durdu@asbu.edu.tr  
Hakan KOR, Hitit University, TURKEY, hakankor@hitit.edu.tr

#### Language Editors

Muhammed Maruf OZTURK, Suleyman Demirel University, TURKEY, muhammedozturk@sdu.edu.tr  
Mustafa KUTLU, Sakarya University of Applied Sciences, TURKEY, mkutlu@subu.edu.tr  
Hamid ASADI DERESHGİ, Istanbul Arel University, TURKEY, hamidasadi@arel.edu.tr  
Emir AVCIOĞLU, Hitit University, TURKEY, emiravciogluhitit.edu.tr

#### Managing Editor

Akif AKGUL, Hitit University, TURKEY, akifakgul@hitit.edu.tr

#### Technical Coordinator


Muhammed Ali PALA, Sakarya University of Applied Sciences, TURKEY, pala@subu.edu.tr  
Murat Erhan CIMEN, Sakarya University of Applied Sciences, TURKEY, muratcimen@sakarya.edu.tr  
Harun Emre KIRAN, Hitit University, TURKEY, harunemre@hitit.edu.tr  
Berkay EMİN, Hitit University, TURKEY, berkayeminn@gmail.com

Chaos Theory and Applications (CHTA)  
Volume: 6 – Issue No: 1 (March 2024)  
<https://dergipark.org.tr/en/pub/chaos/issue/83761>

## Contents:

- Chaos in Physiological Control Systems: Health or Disease?** 1-12  
(Review Article)  
Olfa BOUBAKER
- In Search of Chaos in Genetic Systems** (Research Article) 13-18  
Olga KOZLOVSKA, Felix SADYRBAEV
- A Novel Hypothesis for Migraine Disease Mechanism: The Creation of a New Attractor Responsible for Migraine Disease Symptoms** (Research Article) 19-25  
Farnaz GAREHDAGHI, Yashar SARBAZ, Elham BARADARI
- A Novel Hyperchaotic Financial System with Sinusoidal Hyperbolic Nonlinearity: From Theoretical Analysis to Adaptive Neural Fuzzy Controller Method** (Research Article) 26-40  
Muhamad Deni JOHANSYAH, Seyed Mohamad HAMIDZADEH, Khaled BENKOUIDER, Sundarapandian VAIDYANATHAN, Aceng SAMBAS, Mohamad Afendee MOHAMED, Azwa Abdul AZIZ
- Chaotic and Quasi-periodic Regimes in the Covid-19 Mortality Data** (Research Article) 41-50  
Erkan YILMAZ, Ekrem AYDINER
- Improved Set-point Tracking Control of an Unmanned Aerodynamic MIMO System Using Hybrid Neural Networks** (Research Article) 51-62  
David Mohammed EZEKIEL, Ravi SaAMIKANNU, Oduetse MATSEBE
- Future Prediction for Tax Complaints to Turkish Ombudsman by Models from Polynomial Regression and Parametric Distribution** (Research Article) 63-72  
Mehmet Niyazi CANKAYA, Murat AYDIN

## Chaos in Physiological Control Systems: Health or Disease?

Olfa Boubaker <sup>\*</sup>,<sup>1</sup>

<sup>\*</sup>University of Carthage, National Institute of Applied Sciences and Technology, Tunis, Tunisia.

**ABSTRACT** During the nineties, the Rössler's have reported in their famous book "Chaos in Physiology," that "physiology is the mother of Chaos." Moreover, several researchers have proved that Chaos is a generic characteristic of systems in physiology. In the context of disease, like for example growth of cancer cell populations, Chaos often refers to irregular and unpredictable patterns. In such cases, Chaos signatures can be used to prove the existence of some pathologies. However, for other physiological behaviors, Chaos is a form of order disguised as disorder and can be a signature of healthy physiological functions. This is for example the case of human brain behavior. As the boundary between health and disease is not always clear-cut in chaotic systems in physiology, some conditions may involve transitions between ordered and chaotic states. Understanding these transitions and identifying critical points can be crucial for predicting Healthy vs. pathological Chaos. Using recent advances in physiological Chaos and disease dynamics, this survey paper tries to answer the crucial question: when Chaos be a sign of health or disease?

### KEYWORDS

Modelling in physiology  
Homeostasis  
Physiological chaos  
Chaos in disease  
Pathological chaos  
Healthy chaotic patterns

### INTRODUCTION

In Chaos theory, Chaos dynamics refer to a complex, unpredictable, and random behavior within a system. The concept of Chaos is often associated with nonlinear and complex dynamics showing inherent sensitivity to initial conditions where small effects lead to large and unexpected consequences (Sprott 2003; Lassoued and Boubaker 2016; Devaney 2018; Lozi 2023). While in the vast literature, Chaos theory and its applications to various fields, including mathematics, physics, engineering and so on have been extensively discussed (Boubaker and Jafari 2018), its application in medicine remains both intriguing and challenging. Figure 1 shows the production per year as well as the production by country or territory for a literature review done in January 2024 via the Scopus database using the keyword "Chaos".

The investigation shows the considerable number of journal papers published in the field. It is found 40.169 journal papers written in English with a peak of production in 2023. The search also reveals that China, United States and India are the three countries with the highest production in the field. Figure 2 presents

the classification of production by subject area. It is noticed that mathematics, physics, and engineering are the fields with the highest production. To my surprise, among this considerable number of papers dedicated to Chaos theory, I found only 883 articles devoted for medicine and 638 documents for neurosciences. This little production stands for simply 3.8% of the total. The production per year related to these two categories is shown in Figure 3 and Figure 4, respectively. In the opposite way, it is important to note here that the most cited paper in all categories presented in Figure 2 is the paper titled "Approximate entropy as a measure of system complexity," published in 1991 by Pincus presenting an application of Chaos theory to the analysis of heart rate data, and its effectively discriminated between healthy and sick groups of neonates (Pincus 1991).

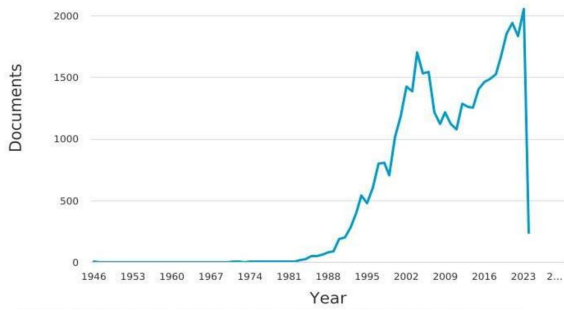
This observation is consistent with the statements of Rössler in his famous book "Chaos in Physiology" published in 1994 in which he has reported that "the physiology is the mother of Chaos" and that "It appears that physiology has a particularly high affinity to Chaos" (Rossler and Rossler 1994). It was during the nineties that researchers have proved that Chaos is a regular characteristic for systems in physiology (Mackey and An Der Heiden 1984; Mpitos *et al.* 1988; Glass *et al.* 1988; da Silva 1991; Goldberger *et al.* 1990; Elbert *et al.* 1994)

Manuscript received: 3 January 2024,

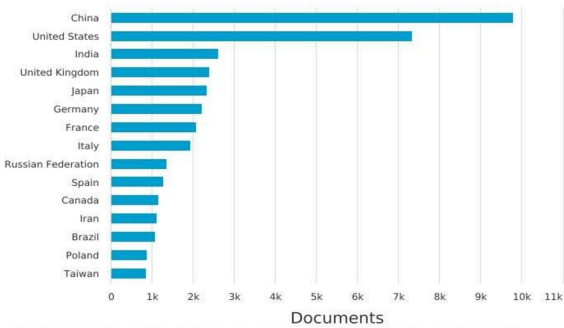
Revised: 19 February 2024,

Accepted: 21 February 2024.

<sup>1</sup>olfa.boubaker@insat.ucar.tn (Corresponding author).

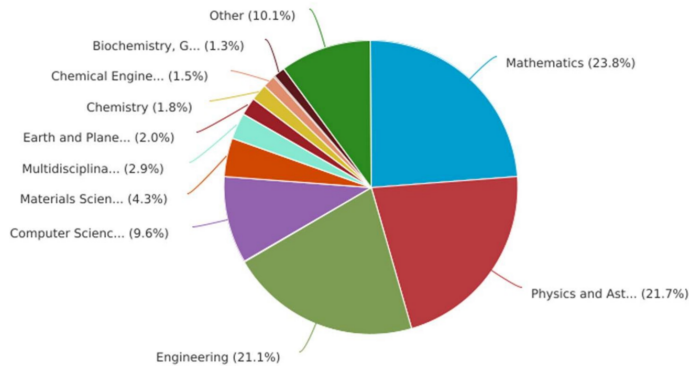


(a)



(b)

**Figure 1** Data from Scopus database. Query: KEY (Chaos) AND (LIMIT-TO (SRCTYPE, «j»)) AND (LIMIT-TO (LANGUAGE, «English»)). (a) Production per year, (b) Production by country or territory.



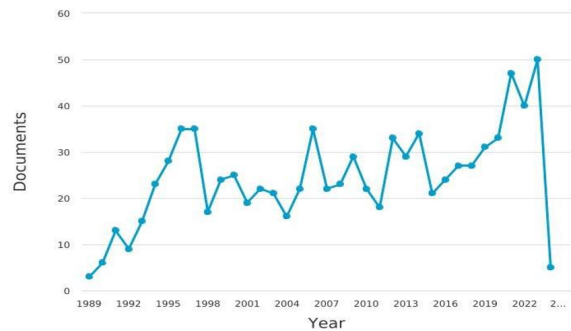
**Figure 2** Data from Scopus database: Documents by subject area. Query: KEY (Chaos) AND (LIMIT-TO (SRCTYPE, «j»)) AND (LIMIT-TO (LANGUAGE, «English»)). The category “Other (10.1%)” includes medicine and neurosciences with 3.7%.

In this framework, I should note that cardiovascular system, with a specific focus on heart rate variability (HRV), was the pioneering area of application of Chaos theory in physiology recognizing that the heart rate does not exhibit a constant rhythm over time (Leaning *et al.* 1983; Pincus and Goldberger 1994; Mansier *et al.* 1996). Early investigations within Chaos in physiological control systems had also considered respiratory control model (Flower *et al.* 1993), blood pressure regulation (Persson 1996; Wagner *et al.* 1996), autonomic nervous system dynamics (Korn and Faure 2003) and neuroendocrine system (Lipsitz and Goldberger 1992). Let us

recognize here that the study of Chaos in physiology is a complex and evolving field, and the understanding of its implications in medicine is continually expanding. Researchers use mathematical models, computational simulations, and empirical observations to explore the dynamic nature of physiological systems and their relationship to human health (Lassoued and Boubaker 2020).

Chaotic behavior in physiology was often associated within certain pathological conditions and may be linked to disease (Cross and Cotton 1994). For example, for the glucose-insulin regulatory system numerous anomalies are perceived in form of chaotic dynamics such as hypoglycemia, hyperinsulinemia, and type 2 diabetes (Rajagopal *et al.* 2020). The chaotic pathological signatures of migraine headache (Bayani *et al.* 2018), the epileptic seizures (Panahi *et al.* 2017, 2019) and the attention deficit hyperactivity disorder (Ansarinassab *et al.* 2023) are recently considered. Complex dynamics for type 1 diabetes (Ginoux *et al.* 2018) and cancer model (Xuan *et al.* 2022) are also studied.

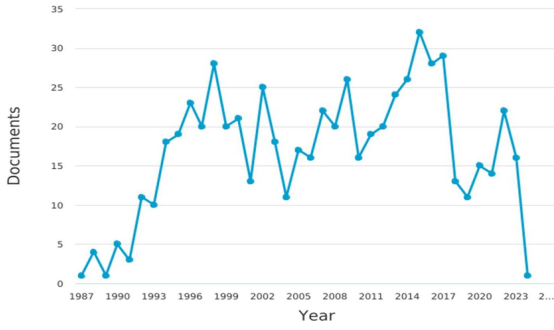
On another side, Chaos can be a normal and healthy aspect of certain physiological processes like for example the heartbeat, the respiratory patterns, and the neural activity which often show complex irregular patterns falling under the umbrella of Chaos dynamics. These dynamics can contribute to the adaptability and resilience of the organism (Golbin and Umantsev 2006; Goldberger and West 1987). As physiological systems are highly interconnected and dynamic, Chaos theory can help us appreciate the complexity of these interactions, perturbations, or changes. Some complex dynamics of the system can lead to unpredictable consequences, which may have implications for health or disease.



**Figure 3** Data from Scopus database: Production per year in the field of medicine. Query: KEY (Chaos) AND (LIMIT-TO (SRCTYPE, «j»)) AND (LIMIT-TO (LANGUAGE, «English»)) AND (LIMIT-TO (SUBJAREA, «MEDI»))

In this paper, after reviewing the fundamental basics in modeling and control in physiology, I will try to answer the three following key questions:

1. How does manifest pathological Chaos in physiological control systems and what are the motivation behind studying these dynamics?
2. What are the control systems in physiology showing healthy chaotic patterns?
3. How can we distinguish between healthy and pathological Chaos?



**Figure 4** Data from Scopus database: Production per year in the field of neurosciences. Query: KEY (Chaos) AND (LIMIT-TO (SRCTYPE, «j»)) AND (LIMIT-TO (LANGUAGE, «English»)) AND (LIMIT-TO (SUBJAREA, «NEUR»))

This paper is organized as follows: the following section introduces fundamentals in modeling and control in physiology. In section 3, main pathological and healthy chaotic systems are reviewed and discussed. Finally, general principles and approaches to help differentiate between healthy and pathological chaotic dynamics are exposed.

## FUNDAMENTALS IN MODELING AND CONTROL IN PHYSIOLOGY

This section will expose motivations and used approaches for modelling dynamic systems in physiology. It also introduces the importance of the principle of Homeostasis in controlling physiological systems.

### Motivations

Modeling and controlling complex physiological systems is a new research area compared to other applications in control systems like robotics, aeronautics, and industrial systems. The results of this new research field are of huge importance as they can be used to understand the complexity of physiological systems, to establish a diagnosis and to forecast the dynamics of some diseases (Lassoued and Boubaker 2020). Furthermore, in many cases, certain failures in the body process require external control laws to normalize the performances of the body (Boubaker 2020) or use of artificial organs and robotic assistive technologies (Boubaker 2023).

### Modelling in physiology

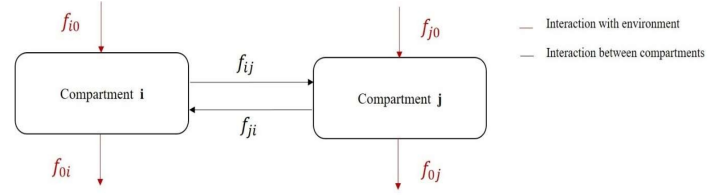
Modelling in physiology can be organized via three main approaches: the compartmental modelling approach, the equivalent modeling approach and the data driven modelling approach (see (Lassoued and Boubaker 2020) and related references).

**Compartmental modeling approach** It is one of the oldest approaches used for modelling physiological systems (Enderle and Bronzino 2012). The related basic equations are expressed as follows (Lassoued and Boubaker 2020):

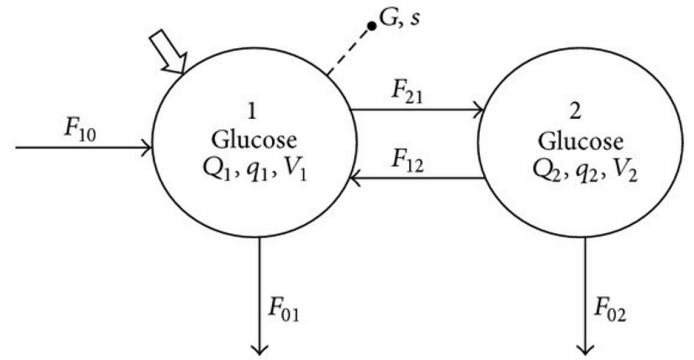
$$\frac{dx_i}{dt} = f_{i0} + \sum_{\substack{j=1 \\ j \neq i}}^n (f_{ij} - f_{ji}) - f_{oi} \quad ; \quad x_i(0) = x_{oi} \quad ; \quad i = 1, 2, \dots, n \quad (1)$$

where  $x_i$  denotes the amount of material in compartment  $i$  and  $x_{oi}$  represents the related initial value.  $f_{ji}$  is the mass flow rate of

compartment  $j$  from compartment  $i$ . Figure 5 shows its arrangement. The index zero represents the environment of the physiological system (Lassoued and Boubaker 2020). Applications of this approach can be found in (Alvarez-Arenas *et al.* 2019; Yousefnezhad *et al.* 2021; Rajeswari and Vijayakumar 2023; Giakoumi *et al.* 2023; Boudin *et al.* 2023; McKnight *et al.* 2013). Figure 6 describes the example of the insulin-independent two-compartment model.



**Figure 5** Basics in compartmental modelling approach (Lassoued and Boubaker 2020).




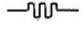
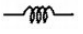
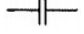
**Figure 6** Insulin-independent two-compartment model for describing glucose kinetics. First compartment holds the vascular space. Arrowed solid lines are flows, hollow arrow is glucose application (infusion or dose), and broken line sampling (McKnight *et al.* 2013).

**Equivalent modeling approach** By such an approach, physiological variables are modelled via physical mechanisms such as electrical or mechanical components (see Table.1). Figure 7. shows an example of an equivalent electronic circuit of blood-vessels system (Lassoued and Boubaker 2020). Figure 8. shows an example of the equivalent electronic circuit for a short segment of squid giant axon proposed by Hodgkin and Huxley (Hodgkin and Huxley 1952). Furthermore, an example of a physiological system modelled by an equivalent electronic circuit for the cardiovascular system is found in (Ismail *et al.* 2018; Zhang *et al.* 2020).

**Data driven modeling approach** It is here an empirical approach that does not imply mathematical modelling derived from physical systems but machine learning and deep learning modeling approaches using time series data. Applications of such an approach can be found in many recent papers (see for example (Dutta *et al.* 2018; Paoletti *et al.* 2019) for diabetes management, (Fong *et al.* 2018; Yoo *et al.* 2022) for immune system modelling, (Dritsas and Trigka 2023) for cardiovascular disease modelling and (Khan *et al.* 2022) for brain disease modelling).

**Classification of mathematical models** Dynamical systems in physiology can be described using lumped models described by

■ Table 1 Physical, mechanical, and electrical analogues (Lassoued and Boubaker 2020).

Physiological measurements	Mechanical analogues			Electrical analogues		
	Name	Notation	Symbol	Name	Notation	Symbol
Pressure	Force	$F$	-	Voltage	$V$	-
Volume	Displacement	$x$	-	Charge	$q$	-
Flow	Velocity	$v = \frac{dx}{dt}$	-	Current	$I = \frac{dq}{dt}$	-
Viscous drag	Viscous resistance	$B = \frac{F}{v}$		Resistance	$R = \frac{V}{I}$	
Compliance	Compliance	$C' = \frac{x}{F}$		Capacitance	$C = \frac{q}{V}$	

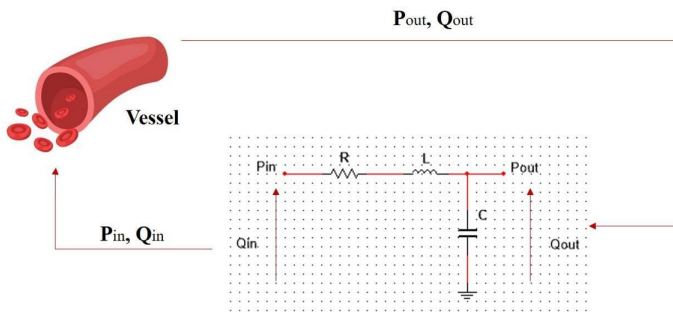


Figure 7 Equivalent electronic circuit of blood-vessels system (Lassoued and Boubaker 2020).

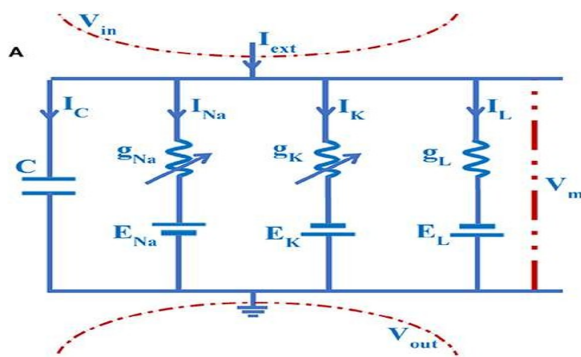


Figure 8 Electrical equivalent circuit for a short segment of squid giant axon proposed by Hodgkin and Huxley. The capacitor represents the capacitance of the cell membrane; the two variable resistors represent voltage-dependent Na<sup>+</sup> and K<sup>+</sup> conductance, the fixed resistor represents a voltage-independent leakage conductance, and the three batteries represent reversal potentials for the corresponding conductance (Fang and Wang 2021).

ordinary differential equations or distributed parameter models described by partial differential equations (Shi *et al.* 2011). They can be also described by deterministic or stochastic models, continuous-time, or discrete-time models or by, parametric or non-parametric models.

Many recent papers have described physiological systems using fractional-order derivatives. Some other papers have included time-delays in mathematical models. In fact, “fractional calculus is recognized as one suitable option to increase the accuracy of the mathematical models and to provides a memory effect into the time evolution of the system since its future solutions will depend on all past times and not only from recent event” (Fernández-Carreón *et al.* 2022).

### Homeostasis principle

“In physiology, control refers to the process of stabilizing a physiological variable to a specified set point, either by reversing perturbations via negative feedback closed loops or via anticipatory open loops. In the human body, the control process is designed by Homeostasis” (Lassoued and Boubaker 2020). Homeostasis principle was discovered by Walter Bradford Cannon in 1929 (Cannon 1929). A literature survey of this principle can be found in (Chapelot and Charlot 2019). “The Homeostasis principle is the property of a physiological system to regulate its internal environment to a given set point in presence of a specific stimulus producing changes in that variable” (Lassoued and Boubaker 2020).

As shown by Figure 9, the control activity in the body is guaranteed by the arrangement of the control center (composed by nervous and endocrine systems), sensors and effectors. Figure 10 gives several examples of Homeostasis. The example of temperature regulation in the human body is described by Figure 11. As reported in (Houk 1988), three basic control strategies guarantying Homeostasis exist: negative feedback, feedforward, and adaptive control. These approaches are summarized in Figure 12. Figure 13 and Figure 14 present the two examples of postural balance homeostasis and glucose homeostasis, respectively, using feedback control laws. For further examples of physiological systems using feedforward and adaptive control, the reader can refer to (Lassoued and Boubaker 2020).

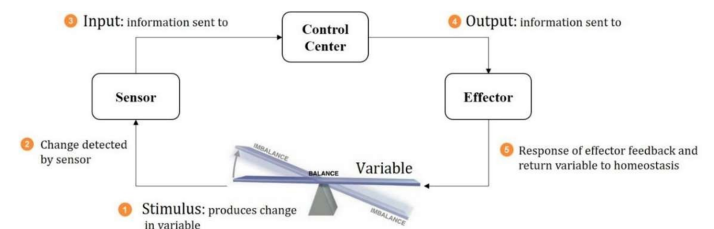
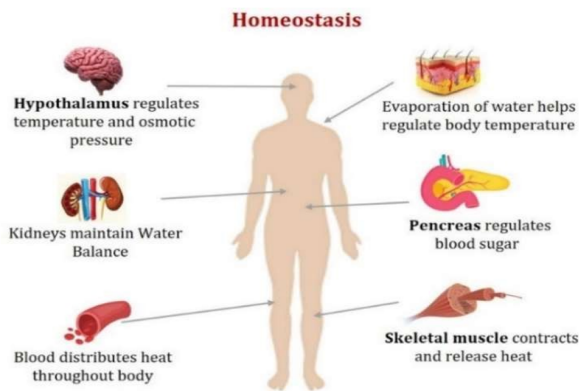
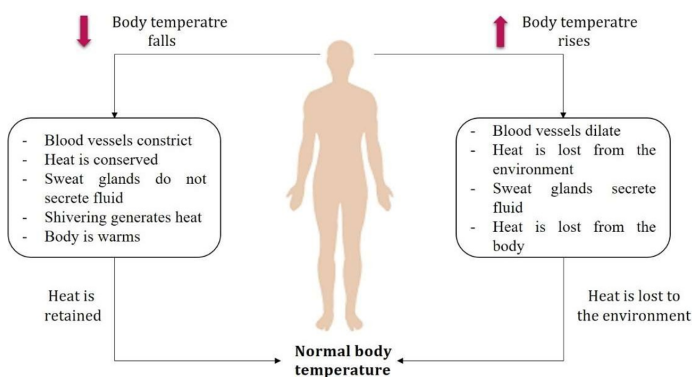


Figure 9 Homeostasis principle (Lassoued and Boubaker 2020).

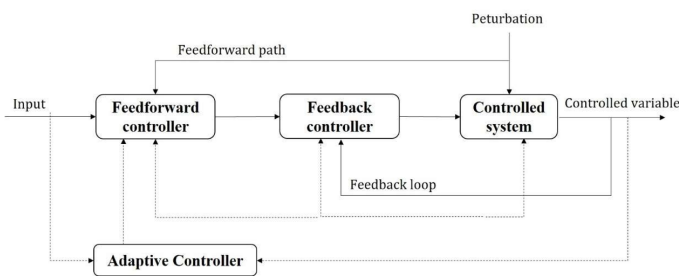




**Figure 10** Homeostasis examples including energy and fluid balances (Lassoued and Boubaker 2020).



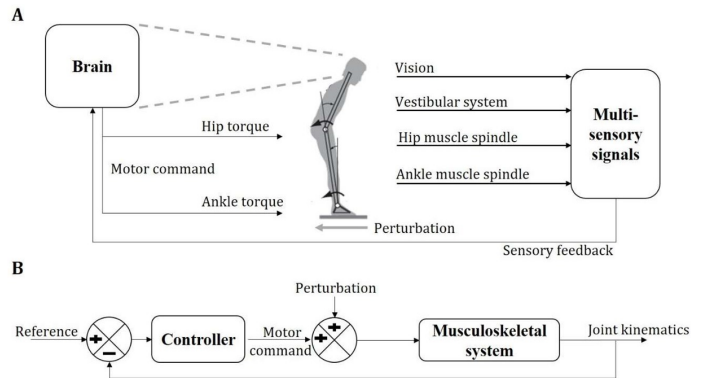
**Figure 11** Human temperature Homeostasis (Lassoued and Boubaker 2020).



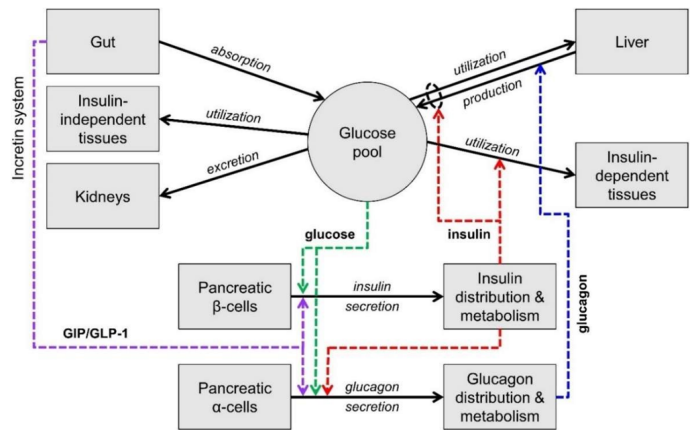
**Figure 12** Basic control strategies in Homeostasis principle (Lassoued and Boubaker 2020).

## CHAOS IN PHYSIOLOGY

According to classical concepts of physiological control, healthy systems are self-regulated to reduce variability and keep physiological constancy. However, contrary to the predictions of homeostasis, the output of a wide range of systems fluctuates in a complex manner that is underpinned by non-linear mechanisms and the low dimensional dynamics of Chaos. Chaos supplies new concepts and methods of analysis that help to understand the dynamics of neural networks in both health and disease that complement existing approaches and may lead to new investigative opportunities (Kernick 2005).



**Figure 13** Postural balance via feedback control laws; (A) schematic model (B) Block diagram (Lassoued and Boubaker 2020).



**Figure 14** Scheme of the main mechanisms of glucose homeostasis. Colored dashed arrows are control signals (glucose or hormone concentrations) that regulate glucose fluxes or insulin and glucagon secretion. The scheme does not show adaptive control mechanisms (e.g., insulin secretion upregulation with insulin resistance) (Mari et al. 2020).

Really, Peng et al. were between the first researchers claiming that the classical theory of homeostasis, according to which stable physiological processes seek to maintain constancy and its more recently proposed modifications under the rubric of hemodynamics, need to be revised and extended to account explicitly for this far from equilibrium behavior (Peng et al. 1994).

## Nonlinear dynamics in physiology

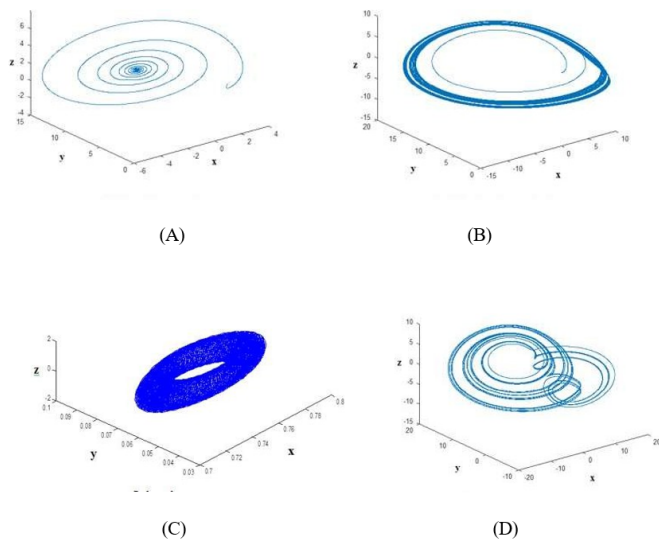
In (Goldberger et al. 2002), Goldberger et al., have given an exhaustive list of nonlinear dynamics that a physiological system can generate. These complex behaviors include abrupt changes (like bifurcations, bistability and multistability), hysteresis, nonlinear oscillations (including limit cycles, phase-resetting, entrainment...), scale invariant (including fractal and multi-fractal scaling, long range correlation, self-organized criticality), nonlinear waves (like spirals, scrolls, solitons) and deterministic Chaos.

Even controlled via Homeostasis principle, it is proved in many other research papers that physiological controlled systems are, at least, capable of the four kinds of behaviors described by Figure 15 (Lassoued and Boubaker 2020; Uthamacumaran 2021). These dynamics can include fixed point, limit cycle, limit torus and strange attractor behavior. It is important to note that the term Chaos in

physiology does not imply randomness in the traditional sense but rather a complex and often nonlinear behavior that deviates from typical physiological patterns (Kernick 2005; Coffey 1998). Studying these chaotic dynamics is crucial for understanding diseases mechanisms and developing targeted interventions.

### Healthy chaotic patterns

Chaotic physiological systems in healthy organisms refer to systems that show complex, unpredictable behavior despite being in a state of normal health. It is important to note that Chaos in physiological systems does not always imply dysfunction; rather, it reflects the inherent complexity and dynamic nature of these systems. It is important to emphasize that Chaos in these systems is often related to their adaptability and responsiveness to changing internal and external conditions as healthy and stable living systems are set up as chaotic and fractal in nature (Golbin and Umantsev 2006; Goldberger and West 1987; Korolj et al. 2019). While Chaos might be present in healthy physiological systems, it is typically controlled and contributes to the overall stability and resilience of the organism. It is proved in many research papers that a healthy dose of Chaos is always necessary (Korolj et al. 2019). I give below some examples.



**Figure 15** Various behaviors shown by complex systems in physiology (Lassoued and Boubaker 2020). (A) Fixed point; (B) Limit Cycle; (C) Limit Torus; (D) Strange attractor.

**Chaos in healthy cardiovascular and respiratory systems** The cardiovascular system is composed of the heart and vessels. Its main function is to pump the blood in the body in order to supply all tissues and organs with oxygen and other nutrients (Formaggia et al. 2010). The earliest model of this system was proposed in (Grodins 1959). The modeling of this system was then determined via different point of view (Golbin and Umantsev 2006; Gois and Savi 2009; Noble et al. 2012; Cheffer et al. 2021; Yadav and Jadhav 2021). For example, in (Golbin and Umantsev 2006), the authors prove via the cardiac Hodgkin–Huxley equation that hearts are poised near the edge of Chaos. They find that the potassium ion-channel and the sodium ion-channel are memristors.

In (Zhang et al. 2020; Coffey 1998), the authors prove that cardiac Chaos is prevalent in healthy heart, and a decrease in such Chaos may be indicative of congestive heart failure. Let us note

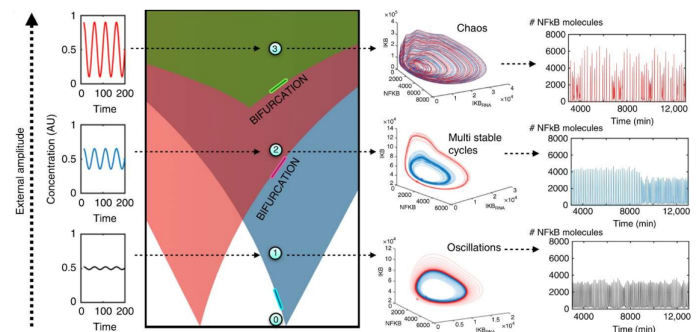
that during intense physical exercise, the interaction between the cardiovascular and respiratory systems can also show chaotic behavior. This complexity is often seen as a normal adaptive response to the increased demands on the body (Golbin and Umantsev 2006; Goldberger and West 1987). The HRV may show a more irregular pattern during exercise, and this variability is often considered a sign of a healthy cardiovascular system (Pincus and Goldberger 1994; Mansier et al. 1996).

**Chaos in healthy neural activity in the brain** Neural networks in the brain often display complex patterns of activity (Poon and Merrill 1997). Some level of Chaos in neural activity is considered healthy and necessary for cognitive function. Indeed, neuronal firing patterns and the interactions between different brain regions contribute to the complexity of brain function. This complexity is not only normal but is also thought to be essential for cognitive processes such as learning, memory, information processing and adaptability (Xuan et al. 2022; Pritchard and Duke 1995; Breakspear 2017; Kavakci 2021). The concept of Chaos in neural dynamics is often explored through the study of brain waves. For example, it is proved that the EEG frequencies of aging subjects show a loss of low-voltage fast waves and an increase in slow waves with diffusion of slow periodicity. Measures of complexity using fractals and Chaos theory always help to assess age-related anatomic and physiologic changes and predict pathologies (Goldberger et al. 2002).

**Healthy Chaos in gait and locomotion system** Human movement and locomotion involve a complex interplay of muscles, joints, and neural signals. Walking, for example, is not a perfectly regular and predictable activity. Gait patterns show variability and chaotic dynamics, allowing individuals to adapt to changes in terrain and keep balance. This variability is considered a sign of a healthy and adaptable motor control system (Müller et al. 2017).

**Healthy chaos in immune system** According to (Heltberg et al. 2019), Chaos in bodily regulation can optimize our immune system and can have of great significance for avoiding serious diseases such as cancer and diabetes.

Heltberg et al. (2019) show how chaotic dynamics create a heterogeneous population of cell states and describe how this can be beneficial in multi-toxic environments. The dynamics of the transcription factor of the immune system when driven by an external periodic signal and exhibiting chaotic signals are described by Figure 16.



**Figure 16** Dynamics emerging from a transcription factor of the immune system when driven by a periodic tumor necrosis factor (TNF) signal exhibiting chaotic output signals when amplitude of external signals increase (Heltberg et al. 2019).

## Chaos in disease

Chaos in the context of disease often refers to irregular and unpredictable patterns or behaviors within physiological systems (Cross and Cotton 1994). There are diverse ways in which chaotic dynamics contribute to the complexity and unpredictability of various diseases across different physiological systems. Understanding these chaotic patterns is essential for developing effective diagnostic and therapeutic strategies. Here are examples where chaotic dynamics may be seen in the context of various diseases.

**Cardiovascular and respiratory disorders** Cardiac fibrillation, with its complex and disordered patterns, can be seen as a manifestation of Chaos in space and time within the heart muscle (Garfinkel et al. 1997; Cheffer et al. 2021). The chaotic electrical activity can disrupt the normal pumping function of the heart, leading to compromised blood circulation (Gupta et al. 2020, 2021; Gupta 2023). On the other hand, other studies focusing on chronic obstructive pulmonary disease, and asthma have shown the chaotic behavior within these diseases. In this framework, (Mansour et al. 2023) have proposed a new chaotic system that investigates the connection between weather patterns and respiratory illness.

**Cancer progression** Cancers are complex systems, consisting of groups of adaptive malignant cells that self-organize in time and space, far from thermodynamic equilibrium (Uthamacumaran 2021). They are considered as of the most curious physiologic problems in these last years. The growth and spread of cancer cells can show chaotic patterns (Fong et al. 2018; Yoo et al. 2022; Sedivy and Mader 1997; Debbouche et al. 2022; Uthamacumaran 2020; Naik et al. 2020). Tumor growth is influenced by complex interactions between cancer cells, the immune system, and the surrounding microenvironment, resulting in unpredictable disease progression (Russo et al. 2021). Several mathematical models were proposed to predict the evolution of this disease. They are based on the Volterra–Lotka type prey–predator models. One of the most interesting models was proposed by Itik and Banks in (Itik and Banks 2010). The non-dimensional model considering a three-cell population is described by:

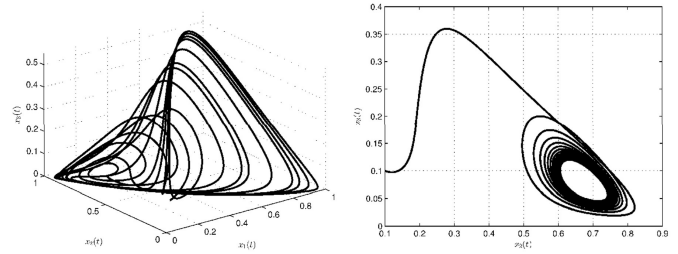
$$\begin{aligned} \frac{dx_1}{dt} &= x_1(1 - x_1) - a_1x_1x_2 - a_2x_1x_3 \\ \frac{dx_2}{dt} &= a_3x_2(1 - x_2) - a_4x_1x_2 \\ \frac{dx_3}{dt} &= \frac{a_5x_1x_3}{x_1 + a_6} - a_7x_1x_3 - a_8x_3 \end{aligned} \quad (2)$$

where  $x_1$  represents the number of tumor cells,  $x_2$  indicates the number of host cells,  $x_3$  refers to the number of effectors cells in the single tumor compartment and  $a_i$  ( $i = 1, \dots, 8$ ) are system's parameters. Let us note that a patient is healthy when the effector cells are equal to zero, more precisely when the chaotic-cancer system converges to an equilibrium point. Several papers have proved that entropy in individual cells change with cancer induction and increasing anaplasticity (See (Uthamacumaran 2021) and related papers).

Recent works in this field have considered fractional-order differential systems to describe cancer models. The most recent model is described by (Karaca 2023):

$$\begin{aligned} D_t^\gamma x_1 &= x_1(1 - x_1) - a_1x_1x_2 - a_2x_1x_3 \\ D_t^\gamma x_2 &= a_3x_2(1 - x_2) - a_4x_1x_2 \\ D_t^\gamma x_3 &= \frac{a_5x_1x_3}{x_1 + a_6} - a_7x_1x_3 - a_8x_3 \end{aligned} \quad (3)$$

where  $D_t^\gamma$  is the Caputo-Fabrizio-Caputo fractional derivative and  $0 < \gamma \leq 1$  is the fractional order. Figure 17 describes the numerical simulation for the model (3).



**Figure 17** Numerical simulation for cancer model via Atangana-Baleanu-Caputo fractional operator. (A): Simulation in the three dimensional-space; (B): projected onto  $x_2(t)$ - $x_3(t)$  planes, respectively (Karaca 2023).

**Metabolic disorders** It was proved through several research works that metabolic disorders including obesity, hyperglycemia, hypertension, dyslipidemia, hypercholesterolemia, hypertriglyceridemia, non-alcoholic fatty liver disease and type I and type II diabetes have complex dynamic patterns. Diabetes involves dysregulation of blood glucose levels, and the metabolic Chaos associated with insulin resistance and impaired insulin secretion can lead to erratic fluctuations in blood sugar levels (Ginoux et al. 2018; Rajeswari and Vijayakumar 2023; Dutta et al. 2018; Paoletti et al. 2019; Shabestari et al. 2019; Borah et al. 2021).

One of the most interesting integer-order models for human glucose-insulin regulatory system is described by (Shabestari et al. 2019):

$$\begin{aligned} \frac{dx_1}{dt} &= a_1x_2(t - \tau_1)x_3(t - \tau) - a_2x_1 + a_3x_3(t - \tau_1) \\ \frac{dx_2}{dt} &= \frac{a_4}{x_3} - a_5x_1(t - \tau_2) + a_6 \\ \frac{dx_3}{dt} &= a_7(x_2 - \hat{x}_2)(T - x_3) + a_8x_3(T - x_3) - a_9x_3 \end{aligned} \quad (4)$$

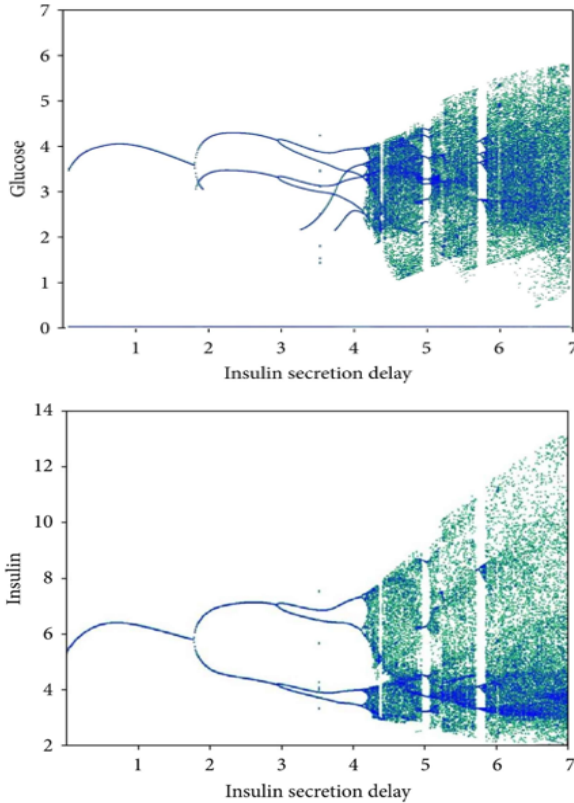
where  $x_1$ ,  $x_2$ ,  $x_3$  and  $\hat{x}_2$  are the insulin level, glucose level, beta-cells number and the glucose metabolism considering its basal state, respectively.  $\tau_1$  is the delay for the insulin production, because of blood glucose level rising. The delay between augmented insulin level and glucose reduction is  $\tau_2$ . Figure 18. Shows the bifurcation diagrams for the glucose-insulin system (4) depending on the bifurcation delays  $\tau_1$  and  $\tau_2$  and showing routes to Chaos.

Fractional-order modelling of glucose-insulin biological systems was also considered by some researchers (see for example (Rajagopal et al. 2020; Munoz-Pacheco et al. 2020; Fernández-Carreón et al. 2022)). In (Fernández-Carreón et al. 2022), the authors derived the fractional-order model corresponding to the integer-order model (5) as follow:

$$\begin{aligned} D_t^\gamma x_1 &= a_1x_2(t - \tau_1)x_3(t - \tau) - a_2x_1 + a_3x_3(t - \tau_1) \\ D_t^\gamma x_2 &= \frac{a_4}{x_3} - a_5x_1(t - \tau_2) + a_6 \\ D_t^\gamma x_3 &= a_7(x_2 - \hat{x}_2)(T - x_3) + a_8x_3(T - x_3) - a_9x_3 \end{aligned} \quad (5)$$

By using the fractional-order operator and representing the phase portraits and bifurcations diagrams, the authors conclude

that numerical simulations remain in good agreement with the theoretical findings and that a memory profile, can provide improved accuracy of the physiological disorders. Furthermore, in (Munoz-Pacheco *et al.* 2020), the authors who proposed an electronic realization of the fractional glucose-insulin regulatory model confirm that the use of fractional-order modelling for chaotic systems is more interesting for embedded technologies.



**Figure 18** Bifurcation diagram for the glucose-insulin system (5) depending on the bifurcation delays  $\tau_1$  and  $\tau_2$  and showing routes to Chaos (Shabestari *et al.* 2019).

**Neurological disorder** Neurological disorders are conditions that affect the nervous system, which includes the brain, spinal cord, and peripheral nerves. These disorders can result from abnormalities in the structure, function, or chemistry of the nervous system and often lead to a variety of symptoms affecting movement, sensation, cognition, or other functions. Examples of specific neurological disorders showing chaotic patterns, contributing to the characteristic motor symptoms are Alzheimer’s disease (Khan *et al.* 2022), neurodegenerative diseases like Parkinson’s disease and Huntington’s disease (Yulmetyev *et al.* 2006; Borah *et al.* 2021; Shabestari *et al.* 2019) and Epilepsy (Panahi *et al.* 2017, 2019; Sarbadhikari and Chakrabarty 2001).

However, the application of chaos theory to these diseases is still an area of ongoing research, and the nature of the dynamics may vary between individuals. Between neurological diseases I can also cite migraines attacks involving severe headaches often accompanied by nausea, sensitivity to light, and sound. The triggers and the unpredictable nature of migraine attacks are also examples of chaotic behavior in the nervous system (Bayani *et al.* 2018; Kernick 2005; Khan *et al.* 2022). Other examples of neuronal diseases can also be cited such as the chaotic model of memristive

nature of autapsis when an axon is injured. This involves poisoning in ion channels or heterogeneity in a local area of the axon for which signal transmission may be interrupted or blocked during neuronal communication (Muni *et al.* 2022).

**Viral diseases impacting the immune system** There are many fatal diseases impacting the immune system like HIV / AIDS, Hepatitis C (HCV) and Herpes Simplex Virus (HSV) which are caused by virus. For example, HIV-1 infection is a hazardous disease that can lead to cancer, AIDS, and other serious illnesses. The progression of HIV to AIDS involves chaotic dynamics in the immune system. The virus attacks and depletes CD4 T cells, disrupting the body’s ability to mount an effective immune response (Borah *et al.* 2021; Ye *et al.* 2009; Duarte *et al.* 2018). The related model can be described by (Naik *et al.* 2020):

$$\begin{aligned} \frac{dx_1}{dt} &= x_1 \left[ a_1 \left( 1 - \frac{x_1 + x_2 + x_3}{a_2} \right) - a_3 x_2 \right] \\ \frac{dx_2}{dt} &= x_2 \left[ a_4 \left( 1 - \frac{x_1 + x_2 + x_3}{a_2} \right) - a_5 x_1 - a_6 x_3 \right] \\ \frac{dx_3}{dt} &= a_6 x_2 x_3 - a_7 x_3 \end{aligned} \quad (6)$$

where  $x_1$  is the population number of cancer cells,  $x_2$  represents the number of healthy cells,  $x_3$  refers to the number of HIV-infected cells  $a_i$  ( $i = 1, \dots, 7$ ) are system’s parameters. Once again, stability investigations and results obtained in (Naik *et al.* 2020) indicate that fractional models are better predictors, among others.

## HOW DISTINGUISHING BETWEEN HEALTHY AND DISEASE CHAOS?

Distinguishing between healthy Chaos and chaotic patterns associated with disease is a complex task that often requires a thorough understanding of the specific physiological system under consideration. Interdisciplinary collaboration, combining ability from clinicians, researchers, and data scientists, is essential for a comprehensive assessment of chaotic dynamics in physiological systems. This collaborative approach enables a more nuanced interpretation of Chaos, considering both the specific characteristics of the system under study and the broader clinical context. Here are some general principles and approaches to help differentiate between healthy and pathological chaotic dynamics.

### Temporal Patterns

In physiology, there are several types of physiological signals that can be collected. They include the electroencephalogram (EEG) measuring the electrical activity of the brain, the electrocardiogram (ECG) recording the electrical activity of the heart, Electromyogram (EMG) recording the electrical activity of muscles, the Electrodermal Activity (EDA) measuring the electrical activity of the skin, the Oxygen Saturation (SpO2) measuring the percentage of oxygen in the blood, the body Temperature, the respiratory rate, the blood pressure, the blood glucose, the bioelectrical impedance analysis (BIA), the Capnography measuring the concentration of carbon dioxide in exhaled air and so on (Shirmohammadi *et al.* 2016). Examining the temporal patterns and dynamics of physiological systems over time is especially important (Stam 2005).

We should recognize that time series often hold "hidden information" including chaotic signals for a wide range of physiological systems. Healthy Chaos often shows short-term dynamics within a stable overall pattern. In contrast, chaotic patterns associated with disease may be characterized by sustained instability, irregularities,

or a lack of right regulation (Goldberger *et al.* 2002). Nonlinear analysis of time series of physiological signals such as EEG and HRV signals can be used to support the diagnosis of many diseases like cardiovascular diseases (Poon and Merrill 1997).

### Integration of multiple parameters

Combining information from multiple physiological parameters can supply a more comprehensive understanding. Examining the interactions between different systems and their chaotic patterns can reveal insights into overall health or the presence of disease (Poon and Merrill 1997; Borah *et al.* 2021; Stam 2005; Garland 2013; Cashin and Yorke 2016).

### Using quantitative measures

Employing quantitative measures can supply objective assessments of Chaos. Analyzing specific parameters, such as largest Lyapunov exponent, fractal dimensions, Hausdorff dimension D, correlation dimension D2, wavelet transform modulus maxima, time asymmetry/irreversibility parameters, Renyi's entropy (REN), Shannon spectral, entropy and so on can offer insights into the nature of chaotic behavior and whether it aligns with healthy or pathological patterns (Faust and Bairy 2012; Müller *et al.* 2017; Pereda *et al.* 2005).

### Integration of imaging techniques

Utilizing advanced imaging techniques (Choquet *et al.* 2021), such as functional magnetic resonance imaging (MRI) and electroencephalography (EEG), can supply insights into the spatial and temporal patterns of chaotic behavior within the body. It can enhance the understanding of Chaos dynamics within a physiological system. Recent advancements in deep learning, particularly convolutional networks, have rapidly become the preferred methodology for analyzing medical images, facilitating tasks like disease segmentation, classification, and pattern quantification of a range of diseases including Alzheimer's, breast cancer, brain tumors, glaucoma, heart murmurs, retinal microaneurysms, colorectal liver metastases, and more (Rasool and Bhat 2023).

### Baseline variability, population-based Comparisons, and genetic factors

Healthy physiological systems often show a certain degree of variability or Chaos within a defined range. Understanding the normal range of variability for a given parameter, such as heart rate, neural activity, or hormone levels, is crucial. Deviations that fall outside the normal range may show pathology. Furthermore, comparing individual physiological patterns to population-based norms can be informative (Poon and Merrill 1997).

Deviations that are consistent with a healthy range in the population may suggest adaptive Chaos, while patterns that diverge significantly may show disease-related Chaos. Genetic and epigenetic factors play a role in deciding the baseline characteristics of physiological systems. Understanding how genetic and epigenetic factors influence chaotic patterns can contribute to distinguishing between healthy and pathological dynamics (Sedivy and Mader 1997).

### Adaptability and responsiveness to interventions

Healthy chaotic patterns are often associated with adaptability and responsiveness to internal and external stimuli (Cross and Cotton 1994). Interventions or modifications, such as lifestyle changes, medications, or therapeutic approaches, can supply valuable information. These adaptive responses contribute to the system's

ability to support homeostasis. In contrast, chaotic patterns in disease may be maladaptive, resulting in dysfunction or failure to respond appropriately to challenges (Golbin and Umantsev 2006). Indeed, healthy systems often have a reserve ability that allows them to adapt to stressors and challenges. Assessing the functional reserve ability of a physiological system can help distinguish between adaptive, healthy Chaos and dysfunction. Showing specific associated with healthy or pathological chaotic patterns can be useful. Certain biomarkers may say adaptive responses in a healthy context or dysregulation in the presence of disease.

### Contextual understanding, functional outcome, and clinical symptoms

Understanding the purpose and context of chaos within a system is important. For example, chaotic neural activity during certain cognitive processes is normal (Tsuda 2015), but chaotic patterns in neural activity associated with seizures may say pathology (Tsatsaris *et al.* 2016; Kavakci 2021). Furthermore, symptoms and signs associated with disease should not be overlooked. The presence of abnormal clinical symptoms, in conjunction with chaotic physiological patterns, may say pathology. Assessing the functional outcome of chaotic dynamics is crucial. Healthy chaotic behavior contributes to the proper functioning of physiological systems, supporting best performance. Chaotic patterns associated with disease may lead to impaired function, symptoms, and negative health outcomes.

### Examining network analysis

Utilizing network analysis techniques can help understand the connectivity and interactions within a physiological system. Indeed Healthy and stable living systems are proved as chaotic and fractal in nature. A few of the most accessible examples include neurons and neural networks, heart rate variability, and the branching vasculature (Korolj *et al.* 2019). Healthy chaotic networks often exhibit organized complexity, while aging and disease-related may disrupt normal network dynamics (Alves *et al.* 2017). Lets' note for example that physiologic aging is associated with a generalized loss of such complexity in the network showing loss of complex variability in multiple physiologic processes including cardiovascular control, pulsatile hormone release, and electroencephalographic potentials and leading to an impaired ability to adapt to physiologic stress (Peng *et al.* 1994; Alves *et al.* 2017; Goldberger *et al.* 2002; Uthamacumaran 2021).

## CONCLUSION

In this paper, after reviewing basics in modeling and control in physiology, I have examined through a state of art pathological vs healthy chaotic patterns in physiological systems. I have listed a number of principles and approaches to help differentiate between healthy and pathological chaotic dynamics. In all examples, the presence of chaos does not always show dysfunction or disease. Instead, it can reflect the intrinsic adaptability of physiological systems. Researchers have studied these chaotic dynamics to better understand the baseline behavior of healthy systems, which can provide valuable insights for distinguishing normal variations from patterns associated with pathology. Several prospectives can be suggested for this complex research domain including improving the performance of disease diagnostic models and exploring a new paradigm for intelligent assisted disease diagnosis (Liu *et al.* 2024; Rasool and Bhat 2023), diseases prediction (Mansour *et al.* 2023) and disease's optimal control (Mohammadi and Hejazi 2023).

## Availability of data and material

Not applicable.

## Conflicts of interest

The author declares that there is no conflict of interest regarding the publication of this paper.

## Ethical standard

The author has no relevant financial or non-financial interests to disclose.

## LITERATURE CITED

- Alvarez-Arenas, A., K. E. Starkov, G. F. Calvo, and J. Belmonte-Beitia, 2019 Ultimate dynamics and optimal control of a multi-compartment model of tumor resistance to chemotherapy. *Discrete & Continuous Dynamical Systems-Series B* **24**.
- Alves, L. G., P. B. Winter, L. N. Ferreira, R. M. Brielmann, R. I. Morimoto, *et al.*, 2017 Long-range correlations and fractal dynamics in *c. elegans*: Changes with aging and stress. *Physical Review E* **96**: 022417.
- Ansarinassab, S., F. Parastesh, F. Ghassemi, K. Rajagopal, S. Jafari, *et al.*, 2023 Synchronization in functional brain networks of children suffering from adhd based on hindmarsh-rose neuronal model. *Computers in Biology and Medicine* **152**: 106461.
- Bayani, A., S. Jafari, J. Sprott, and B. Hatef, 2018 A chaotic model of migraine headache considering the dynamical transitions of this cyclic disease. *Europhysics Letters* **123**: 10006.
- Borah, M., D. Das, A. Gayan, F. Fenton, and E. Cherry, 2021 Control and anticontrol of chaos in fractional-order models of diabetes, hiv, dengue, migraine, parkinson's and ebola virus diseases. *Chaos, Solitons & Fractals* **153**: 111419.
- Boubaker, O., 2020 *Control theory in biomedical engineering: applications in physiology and medical robotics*. Academic Press.
- Boubaker, O., 2023 *Medical and Healthcare Robotics: New Paradigms and Recent Advances*. Elsevier.
- Boubaker, O. and S. Jafari, 2018 *Recent advances in chaotic systems and synchronization: from theory to real world applications*. Academic Press.
- Boudin, L., C. Grandmont, B. Grec, and S. Martin, 2023 A coupled model for the dynamics of gas exchanges in the human lung with haldane and bohr's effects. *Journal of Theoretical Biology* **573**: 111590.
- Breakspear, M., 2017 Dynamic models of large-scale brain activity. *Nature neuroscience* **20**: 340–352.
- Cannon, W. B., 1929 Organization for physiological homeostasis. *Physiological reviews* **9**: 399–431.
- Cashin, A. and J. Yorke, 2016 Overly regulated thinking and autism revisited. *Journal of Child and Adolescent Psychiatric Nursing* **29**: 148–153.
- Chapelot, D. and K. Charlot, 2019 Physiology of energy homeostasis: Models, actors, challenges and the glucoadipostatic loop. *Metabolism* **92**: 11–25.
- Cheffer, A., M. A. Savi, T. L. Pereira, and A. S. de Paula, 2021 Heart rhythm analysis using a nonlinear dynamics perspective. *Applied Mathematical Modelling* **96**: 152–176.
- Choquet, D., M. Sainlos, and J.-B. Sibarita, 2021 Advanced imaging and labelling methods to decipher brain cell organization and function. *Nature Reviews Neuroscience* **22**: 237–255.
- Coffey, D. S., 1998 Self-organization, complexity and chaos: the new biology for medicine. *Nature medicine* **4**: 882–885.
- Cross, S. S. and D. W. Cotton, 1994 Chaos and antichaos in pathology. *Human pathology* **25**: 630–637.
- da Silva, F. L., 1991 Neural mechanisms underlying brain waves: from neural membranes to networks. *Electroencephalography and clinical neurophysiology* **79**: 81–93.
- Debbouche, N., A. Ouannas, G. Grassi, A.-B. A. Al-Hussein, F. R. Tahir, *et al.*, 2022 Chaos in cancer tumor growth model with commensurate and incommensurate fractional-order derivatives. *Computational and Mathematical Methods in Medicine* **2022**.
- Devaney, R., 2018 *An introduction to chaotic dynamical systems*. CRC press.
- Dritsas, E. and M. Trigka, 2023 Efficient data-driven machine learning models for cardiovascular diseases risk prediction. *Sensors* **23**: 1161.
- Duarte, J., C. Januário, N. Martins, C. C. Ramos, C. Rodrigues, *et al.*, 2018 Optimal homotopy analysis of a chaotic hiv-1 model incorporating aids-related cancer cells. *Numerical Algorithms* **77**: 261–288.
- Dutta, S., T. Kushner, and S. Sankaranarayanan, 2018 Robust data-driven control of artificial pancreas systems using neural networks. In *Computational Methods in Systems Biology: 16th International Conference, CMSB 2018, Brno, Czech Republic, September 12-14, 2018, Proceedings 16*, pp. 183–202, Springer.
- Elbert, T., W. J. Ray, Z. J. Kowalik, J. E. Skinner, K. E. Graf, *et al.*, 1994 Chaos and physiology: deterministic chaos in excitable cell assemblies. *Physiological reviews* **74**: 1–47.
- Enderle, J. and J. Bronzino, 2012 *Introduction to biomedical engineering*. Academic press.
- Fang, X. and L. Wang, 2021 Memristive hodgkin-huxley spiking neuron model for reproducing neuron behaviors. *Frontiers in Neuroscience* **15**: 730566.
- Faust, O. and M. G. Bairy, 2012 Nonlinear analysis of physiological signals: a review. *Journal of Mechanics in Medicine and Biology* **12**: 1240015.
- Fernández-Carreón, B., J. Muñoz-Pacheco, E. Zambrano-Serrano, and O. Félix-Beltrán, 2022 Analysis of a fractional-order glucose-insulin biological system with time delay. *Chaos Theory and Applications* **4**: 10–18.
- Flower, A., G. Kalamangalam, and G. Kember, 1993 A mathematical analysis of the grodins model of respiratory control. *Mathematical Medicine and Biology: A Journal of the IMA* **10**: 249–280.
- Fong, L. E., A. R. Muñoz-Rojas, and K. Miller-Jensen, 2018 Advancing systems immunology through data-driven statistical analysis. *Current opinion in biotechnology* **52**: 109–115.
- Formaggia, L., A. Quarteroni, and A. Veneziani, 2010 *Cardiovascular Mathematics: Modeling and simulation of the circulatory system*, volume 1. Springer Science & Business Media.
- Garfinkel, A., P.-S. Chen, D. O. Walter, H. S. Karagueuzian, B. Kogan, *et al.*, 1997 Quasiperiodicity and chaos in cardiac fibrillation. *The Journal of clinical investigation* **99**: 305–314.
- Garland, J., 2013 Energy management—a critical role in cancer induction? *Critical reviews in oncology/hematology* **88**: 198–217.
- Giakoumi, M., P. S. Stephanou, K. Kapnisis, and A. Anayiotos, 2023 On the development of physiologically based toxicokinetic (pbtk) models for cardiovascular implants. *Regulatory Toxicology and Pharmacology* **144**: 105489.
- Ginoux, J.-M., H. Ruskeepää, M. Perc, R. Naeck, V. Di Costanzo, *et al.*, 2018 Is type 1 diabetes a chaotic phenomenon? *Chaos, Solitons & Fractals* **111**: 198–205.
- Glass, L., A. Beuter, and D. Larocque, 1988 Time delays, oscillations, and chaos in physiological control systems. *Mathematical Biosciences* **90**: 111–125.

- Gois, S. R. and M. A. Savi, 2009 An analysis of heart rhythm dynamics using a three-coupled oscillator model. *Chaos, Solitons & Fractals* **41**: 2553–2565.
- Golbin, A. and A. Umantsev, 2006 Adaptive chaos: mild disorder may help contain major disease. *Medical hypotheses* **66**: 182–187.
- Goldberger, A. L., L. A. Amaral, J. M. Hausdorff, P. C. Ivanov, C.-K. Peng, *et al.*, 2002 Fractal dynamics in physiology: alterations with disease and aging. *Proceedings of the national academy of sciences* **99**: 2466–2472.
- Goldberger, A. L., D. R. Rigney, and B. J. West, 1990 Chaos and fractals in human physiology. *Scientific American* **262**: 42–49.
- Goldberger, A. L. and B. J. West, 1987 Chaos in physiology: health or disease? In *Chaos in biological systems*, pp. 1–4, Springer.
- Grodins, F. S., 1959 Integrative cardiovascular physiology: a mathematical synthesis of cardiac and blood vessel hemodynamics. *The Quarterly Review of Biology* **34**: 93–116.
- Gupta, V., 2023 Application of chaos theory for arrhythmia detection in pathological databases. *International Journal of Medical Engineering and Informatics* **15**: 191–202.
- Gupta, V., M. Mittal, and V. Mittal, 2020 Chaos theory: an emerging tool for arrhythmia detection. *Sensing and Imaging* **21**: 10.
- Gupta, V., M. Mittal, and V. Mittal, 2021 Chaos theory and artifa: emerging tools for interpreting ecg signals to diagnose cardiac arrhythmias. *Wireless Personal Communications* **118**: 3615–3646.
- Heltberg, M. L., S. Krishna, and M. H. Jensen, 2019 On chaotic dynamics in transcription factors and the associated effects in differential gene regulation. *Nature communications* **10**: 71.
- Hodgkin, A. L. and A. F. Huxley, 1952 A quantitative description of membrane current and its application to conduction and excitation in nerve. *The Journal of physiology* **117**: 500.
- Houk, J. C., 1988 Control strategies in physiological systems. *The FASEB journal* **2**: 97–107.
- Ismail, L. S., S. A. Zulkifl, and N. H. Hamid, 2018 Circuit modeling and analysis of cardiovascular system using analog circuit analogy. In *2018 International Conference on Intelligent and Advanced System (ICIAS)*, pp. 1–6, IEEE.
- Itik, M. and S. P. Banks, 2010 Chaos in a three-dimensional cancer model. *International Journal of Bifurcation and Chaos* **20**: 71–79.
- Karaca, Y., 2023 Computational complexity-based fractional-order neural network models for the diagnostic treatments and predictive transdifferentiability of heterogeneous cancer cell propensity. *Chaos Theory and Applications* **5**: 34–51.
- Kavakci, M., 2021 Neurochaos: Analyzing the brain and its disorders from a physics perspective. In *Chaos, Complexity and Leadership 2020: Application of Nonlinear Dynamics from Interdisciplinary Perspective*, pp. 15–24, Springer.
- Kernick, D., 2005 Migraine—new perspectives from chaos theory. *Cephalalgia* **25**: 561–566.
- Khan, A. F., Q. Adewale, T. R. Baumeister, F. Carbonell, K. Zilles, *et al.*, 2022 Personalized brain models identify neurotransmitter receptor changes in alzheimer’s disease. *Brain* **145**: 1785–1804.
- Korn, H. and P. Faure, 2003 Is there chaos in the brain? ii. experimental evidence and related models. *Comptes rendus biologies* **326**: 787–840.
- Korolj, A., H.-T. Wu, and M. Radisic, 2019 A healthy dose of chaos: Using fractal frameworks for engineering higher-fidelity biomedical systems. *Biomaterials* **219**: 119363.
- Lassoued, A. and O. Boubaker, 2016 On new chaotic and hyperchaotic systems: a literature survey. *Nonlinear Analysis: Modelling and Control* **21**: 770–789.
- Lassoued, A. and O. Boubaker, 2020 Modeling and control in physiology. In *Control Theory in Biomedical Engineering*, pp. 3–42, Elsevier.
- Leaning, M., H. Pullen, E. Carson, and L. Finkelstein, 1983 Modelling a complex biological system: the human cardiovascular system—1. methodology and model description. *Transactions of the Institute of Measurement and Control* **5**: 71–86.
- Lipsitz, L. A. and A. L. Goldberger, 1992 Loss of ‘complexity’ and aging: potential applications of fractals and chaos theory to senescence. *Jama* **267**: 1806–1809.
- Liu, Y., C. Chen, X. Tian, E. Zuo, Z. Cheng, *et al.*, 2024 A prospective study: Advances in chaotic characteristics of serum raman spectroscopy in the field of assisted diagnosis of disease. *Expert Systems with Applications* **238**: 121787.
- Lozi, R., 2023 Are chaotic attractors just a mathematical curiosity or do they contribute to the advancement of science? *Chaos Theory and Applications* **5**: 133–140.
- Mackey, M. C. and U. An Der Heiden, 1984 The dynamics of recurrent inhibition. *Journal of Mathematical Biology* **19**: 211–225.
- Mansior, P., J. Clairambault, N. Charlotte, C. Médigue, C. Vermeiren, *et al.*, 1996 Linear and non-linear analyses of heart rate variability: a minireview. *Cardiovascular research* **31**: 371–379.
- Mansour, M., T. B. Donmez, M. Ç. Kutlu, and C. Freeman, 2023 Respiratory diseases prediction from a novel chaotic system. *Chaos Theory and Applications* **5**: 20–26.
- Mari, A., A. Tura, and E. Grespan, 2020 Mathematical modeling for the physiological and clinical investigation of glucose homeostasis and diabetes. *Frontiers in Physiology* **11**: 575789.
- McKnight, L. L., S. Lopez, A. K. Shoveller, and J. France, 2013 Models for the study of whole-body glucose kinetics: a mathematical synthesis. *International Scholarly Research Notices* **2013**.
- Mohammadi, S. and S. R. Hejazi, 2023 Lie symmetry, chaos optimal control in non-linear fractional-order diabetes mellitus, human immunodeficiency virus, migraine parkinson’s diseases models: using evolutionary algorithms. *Computer Methods in Biomechanics and Biomedical Engineering* pp. 1–29.
- Mpitsos, G. J., R. M. Burton Jr, and H. C. Creech, 1988 Connectionist networks learn to transmit chaos. *Brain Research Bulletin* **21**: 539–546.
- Müller, W., A. Jung, and H. Ahammer, 2017 Advantages and problems of nonlinear methods applied to analyze physiological time signals: human balance control as an example. *Scientific reports* **7**: 2464.
- Muni, S. S., Z. Njitacke, C. Feudjio, T. Fozin, and J. Awrejcewicz, 2022 Route to chaos and chimera states in a network of memristive hindmarsh-rose neurons model with external excitation. *Chaos Theory and Applications* **4**: 119–127.
- Munoz-Pacheco, J. M., C. Posadas-Castillo, and E. Zambrano-Serrano, 2020 The effect of a non-local fractional operator in an asymmetrical glucose-insulin regulatory system: Analysis, synchronization and electronic implementation. *Symmetry* **12**: 1395.
- Naik, P. A., K. M. Owolabi, M. Yavuz, and J. Zu, 2020 Chaotic dynamics of a fractional order hiv-1 model involving aids-related cancer cells. *Chaos, Solitons & Fractals* **140**: 110272.
- Noble, D., A. Garny, and P. J. Noble, 2012 How the hodgkin–huxley equations inspired the cardiac physiome project. *The Journal of physiology* **590**: 2613–2628.
- Panahi, S., Z. Aram, S. Jafari, J. Ma, and J. Sprott, 2017 Modeling of epilepsy based on chaotic artificial neural network. *Chaos, Solitons & Fractals* **105**: 150–156.
- Panahi, S., T. Shirzadian, M. Jalili, and S. Jafari, 2019 A new chaotic

- network model for epilepsy. *Applied Mathematics and Computation* **346**: 395–407.
- Paoletti, N., K. S. Liu, H. Chen, S. A. Smolka, and S. Lin, 2019 Data-driven robust control for a closed-loop artificial pancreas. *IEEE/ACM transactions on computational biology and bioinformatics* **17**: 1981–1993.
- Peng, C.-K., S. V. Buldyrev, J. M. Hausdorff, S. Havlin, J. E. Mietus, *et al.*, 1994 Non-equilibrium dynamics as an indispensable characteristic of a healthy biological system. *Integrative Physiological and Behavioral Science* **29**: 283–293.
- Pereda, E., R. Q. Quiroga, and J. Bhattacharya, 2005 Nonlinear multivariate analysis of neurophysiological signals. *Progress in neurobiology* **77**: 1–37.
- Persson, P. B., 1996 Modulation of cardiovascular control mechanisms and their interaction. *Physiological reviews* **76**: 193–244.
- Pincus, S. M., 1991 Approximate entropy as a measure of system complexity. *Proceedings of the national academy of sciences* **88**: 2297–2301.
- Pincus, S. M. and A. L. Goldberger, 1994 Physiological time-series analysis: what does regularity quantify? *American Journal of Physiology-Heart and Circulatory Physiology* **266**: H1643–H1656.
- Poon, C.-S. and C. K. Merrill, 1997 Decrease of cardiac chaos in congestive heart failure. *Nature* **389**: 492–495.
- Pritchard, W. S. and D. W. Duke, 1995 Measuring chaos in the brain—a tutorial review of eeg dimension estimation. *Brain and cognition* **27**: 353–397.
- Rajagopal, K., A. Bayani, S. Jafari, A. Karthikeyan, and I. Hussain, 2020 Chaotic dynamics of a fractional order glucose-insulin regulatory system. *Frontiers of Information Technology & Electronic Engineering* **21**: 1108–1118.
- Rajeswari, S. and P. Vijayakumar, 2023 Mathematical approaches in the study of diabetes mellitus. In *Computer Vision and Robotics: Proceedings of CVR 2022*, pp. 229–248, Springer.
- Rasool, N. and J. I. Bhat, 2023 Unveiling the complexity of medical imaging through deep learning approaches. *Chaos Theory and Applications* **5**: 267–280.
- Rossler, O. E. and R. Rossler, 1994 Chaos in physiology. *Integrative Physiological and Behavioral Science* **29**: 328–333.
- Russo, G., A. Tramontano, I. Iodice, L. Chiariotti, and A. Pezone, 2021 Epigenome chaos: stochastic and deterministic dna methylation events drive cancer evolution. *Cancers* **13**: 1800.
- Sarbadhikari, S. N. and K. Chakrabarty, 2001 Chaos in the brain: a short review alluding to epilepsy, depression, exercise and lateralization. *Medical engineering & physics* **23**: 447–457.
- Sedivy, R. and R. M. Mader, 1997 Fractals, chaos, and cancer: do they coincide? *Cancer investigation* **15**: 601–607.
- Shabestari, P. S., Z. Rostami, V.-T. Pham, F. E. Alsaadi, and T. Hayat, 2019 Modeling of neurodegenerative diseases using discrete chaotic systems. *Communications in Theoretical Physics* **71**: 1241.
- Shi, Y., P. Lawford, and R. Hose, 2011 Review of zero-d and 1-d models of blood flow in the cardiovascular system. *Biomedical engineering online* **10**: 1–38.
- Shirmohammadi, S., K. Barbe, D. Grimaldi, S. Rapuano, and S. Grassini, 2016 Instrumentation and measurement in medical, biomedical, and healthcare systems. *IEEE Instrumentation & Measurement Magazine* **19**: 6–12.
- Sprott, J. C., 2003 *Chaos and time-series analysis*. Oxford university press.
- Stam, C. J., 2005 Nonlinear dynamical analysis of eeg and meg: review of an emerging field. *Clinical neurophysiology* **116**: 2266–2301.
- Tsatsaris, A., S. Domenikos, C. Psychos, and D. Moutsionas, 2016 Chaos theory and behavioural patterns: a theoretical approach to psychosis, bipolar disorders and depression. *Journal of Advanced Biotechnology and Bioengineering* **4**.
- Tsuda, I., 2015 Chaotic itinerancy and its roles in cognitive neurodynamics. *Current opinion in neurobiology* **31**: 67–71.
- Uthamacumaran, A., 2020 Cancer: A turbulence problem. *Neoplasia* **22**: 759–769.
- Uthamacumaran, A., 2021 A review of dynamical systems approaches for the detection of chaotic attractors in cancer networks. *Patterns* **2**.
- Wagner, C., B. Nafz, and P. Persson, 1996 Chaos in blood pressure control. *Cardiovascular research* **31**: 380–387.
- Xuan, L., S. Ahmad, A. Ullah, S. Saifullah, A. Akgül, *et al.*, 2022 Bifurcations, stability analysis and complex dynamics of caputo fractal-fractional cancer model. *Chaos, Solitons & Fractals* **159**: 112113.
- Yadav, S. S. and S. M. Jadhav, 2021 Detection of common risk factors for diagnosis of cardiac arrhythmia using machine learning algorithm. *Expert systems with applications* **163**: 113807.
- Ye, H., Y. Ding, *et al.*, 2009 Nonlinear dynamics and chaos in a fractional-order hiv model. *Mathematical Problems in Engineering* **2009**.
- Yoo, J., Z. Sun, M. Greenacre, Q. Ma, D. Chung, *et al.*, 2022 A guideline for the statistical analysis of compositional data in immunology. arXiv preprint arXiv:2201.07945 .
- Yousefnezhad, M., C.-Y. Kao, and S. A. Mohammadi, 2021 Optimal chemotherapy for brain tumor growth in a reaction-diffusion model. *SIAM Journal on Applied Mathematics* **81**: 1077–1097.
- Yulmetyev, R. M., S. A. Demin, and P. Hänggi, 2006 Manifestation of chaos in real complex systems: Case of parkinson’s disease. In *The logistic map and the route to chaos: From the beginnings to modern applications*, pp. 175–196, Springer.
- Zhang, X., Z. Wu, and L. Chua, 2020 Hearts are poised near the edge of chaos. *International Journal of Bifurcation and Chaos* **30**: 2030023.

**How to cite this article:** Boubaker, O. Chaos in Physiological Control Systems: Health or Disease? *Chaos Theory and Applications*, 6(1), 1-12, 2024.

**Licensing Policy:** The published articles in *Chaos Theory and Applications* are licensed under a [Creative Commons Attribution-NonCommercial 4.0 International License](https://creativecommons.org/licenses/by-nc/4.0/).





# In Search of Chaos in Genetic Systems

Olga Kozlovskā <sup>1</sup> and Felix Sadyrbaev <sup>2</sup>

\*Institute of Applied Mathematics, Riga Technical University, LV-1048 Riga, Latvia, <sup>α</sup>Institute of Life Sciences and Technology, Daugavpils University, LV-1459, Riga, Latvia.

**ABSTRACT** A three-dimensional multiparametric system of ordinary differential equations, arising in the theory of genetic networks, is considered. Examples of chaotic behavior are constructed using the methodology by Shilnikov. This methodology requires the existence of saddle-focus points satisfying some additional conditions. As the result, rich dynamical behavior of solutions can be observed, including chaotic behavior of solutions.

**KEYWORDS**  
Mathematical model  
Dynamical system  
Attractors  
Genetic regulatory networks

## INTRODUCTION

Genetic regulatory networks are in a focus of investigation of biologists (Peter 2020) and theoreticians (Samuilik and Sadyrbaev 2023; Jong 2002; Schlitt 2013; Vijesh et al. 2013). Mathematical models of GRN can be formulated in terms of ordinary differential equations (Barbuti et al. 2020). This modeling method is preferable if the evolution of a network is to be studied. Each equation in a system corresponds to an element of a network. So realistic networks and the respective systems are large (Kardynska et al. 2023). To understand the principles of functioning of gene networks small networks should be investigated first. The systems of differential equations also consist of several equations only.

The two-dimensional systems can be studied using the phase plane method. The results can be visualized easily and the respective conclusions are at hand. We mention briefly the main properties of two-dimensional systems. They are quasi-linear, and the right sides contain a nonlinear term and a linear one. The non-linearity is represented usually by a sigmoidal function, such as the logistic one,  $f(z) = 1/(1 + e^{-\mu z})$  (Samuilik 2022), Hill's function  $h(z) = z^\mu / (z^\mu + \theta^\mu)$  (Santillan 2008) or Gompertz function  $g(z) = \exp(-\exp(-\mu z))$  (Ogorelova et al. 2020).

Sigmoidal functions are monotone, smooth and bounded. They are convenient for mathematical treatment and reflect the main properties of a modeled object. To predict future states of a network, a researcher should analyze the mathematical model. The following questions should be answered: 1) Does the system have attracting sets in the phase space; 2) What they (attractors) are; 3) How attractors depend on the parameters of a system; 4) Is it possible to regulate the model by changing parameters. The main

issue is, of course, the ability of a model to adequately describe a modeled object. In other words, could a researcher rely on the predictions, formulated when mathematically studied a network. More or less full analysis can be made for two-dimensional (2D) systems. They have attractors, which are stable critical points, limit cycles and their combinations. New information is obtained when studying three-dimensional (3D) systems of the form

$$\begin{cases} \frac{dx}{dt} = \frac{1}{1 + e^{-\mu_1(w_{11}x + w_{12}y + w_{13}z - \theta_1)}} - v_1x, \\ \frac{dy}{dt} = \frac{1}{1 + e^{-\mu_2(w_{21}x + w_{22}y + w_{23}z - \theta_2)}} - v_2y, \\ \frac{dz}{dt} = \frac{1}{1 + e^{-\mu_3(w_{31}x + w_{32}y + w_{33}z - \theta_3)}} - v_3z. \end{cases} \quad (1)$$

Here the three variables  $x, y, z$  are for the elements of a network. The dynamics of the system and future states of a network depend on solutions of this system and its attractors. There are many examples of attractors which are stable critical points, stable periodic solutions (limit cycles) and more (Ogorelova et al. 2020; Brokan and Sadyrbaev 2016, 2018). There are many examples of three-dimensional autonomous systems, which exhibited chaotic behavior. Recall Lorenz system, Rössler system, Duffing type equations written as 3D-systems, and many nice examples collected by J.C. Sprott (Sprott 2010) and N.A. Magnitskii (Magnitskii and Sidorov 2006).

To find a chaotic attractor, which is none of the above mentioned, is a non-trivial task. "Chaos should occur often in gene regulatory networks which have been widely described by nonlinear coupled ordinary differential equations, if their dimensions are no less than 3. It is therefore puzzling that chaos is also extremely rare in models of GRN," write the authors in (Zhang et al. 2012). In (Zhang et al. 2012) two tables are provided, which show the number of chaotic samples reached in three-dimensional GRN by

Manuscript received: 24 October 2023,  
Revised: 21 November 2023,  
Accepted: 23 December 2023.

<sup>1</sup>olga.kozlovskaa@rtu.lv (Corresponding author).  
<sup>2</sup>felix@latnet.lv

$10^6$  tests with random network structures, parameter distributions and initial variable conditions. This number is one. The same measurement within networks possessing the structure of periodic oscillations is 195. We knew only the work (Das *et al.* 2000) where a chaotic attractor was discovered for the system of the form (1).

The attempts to find new chaotic attractors in the system (1) were time and work consuming without any guarantees. Literature review related to the subject led us to early works by L.P. Shilnikov. We plan to study this system under the assumptions formulated in the work (Shilnikov 1965). In this work, a three-dimensional system was considered, which had a saddle-focus type critical point (see also (Gonchenko *et al.* 2019; Deng *et al.* 2017)). Our intent is to construct examples of genetic systems which have a critical point of this type. It is known that the behavior of trajectories in a neighborhood of such point can be complicated. We are looking for chaotic behavior.

## SHILNIKOV SYSTEM

In the work (Shilnikov 1965) the following system

$$\begin{cases} \frac{dx}{dt} = \rho x - \omega y + P, \\ \frac{dy}{dt} = \omega x + \rho y + Q, \\ \frac{dz}{dt} = \lambda z + R \end{cases} \quad (2)$$

was studied under the conditions  $\rho < 0$ ,  $\lambda > 0$ , functions  $P, Q, R$  are zeros together with their derivatives at the point  $(0,0,0)$ .

The linearized system around  $(0,0,0)$  is

$$\begin{cases} \frac{dx}{dt} = \rho x - \omega y, \\ \frac{dy}{dt} = \omega x + \rho y, \\ \frac{dz}{dt} = \lambda z. \end{cases} \quad (3)$$

If we assume that  $\omega$  is positive, then the origin in the system (3) is a saddle-focus with 2D stable focus and repulsion in  $z$ -direction. If this repulsion dominates over an attraction in the 2D focus ( $\lambda > -\rho$ ), the behavior of trajectories near the origin in a nonlinear system (2) can be complicated (Shilnikov 1965). Our intent is to construct GRN system with similar properties and to test it on attractors.

Characteristic values for  $(0,0,0)$  are  $\Lambda_1 = \lambda > 0$ ,  $\Lambda_{2,3} = \rho \pm \omega i$ ,  $\rho < 0$ ,  $\omega > 0$ . The phase space around  $(0,0,0)$  is the spiral going away of the plane where its (spiral) projection approaches the stable focus. According to (Shilnikov 1965), there is a trajectory of the system (2), which emanates from  $(0,0,0)$  and ends in  $(0,0,0)$  in an infinite time. It was denoted  $\Gamma_0$ . The following condition according to (Shilnikov 1965) is important for the complicated behavior of trajectories: If  $\lambda > -\rho$ , then in a vicinity of  $\Gamma_0$  there are infinitely many periodic solutions.

It was mentioned in (Gonchenko *et al.* 2019, page 9) that there are two interesting cases of a saddle-focus behavior. The first case is called saddle-focus I. Then the equilibrium has a stable 2D manifold and unstable 1D manifold. In terms of characteristic numbers  $\lambda_1 > 0$ ,  $\lambda_{2,3} = \alpha \pm \beta i$ ,  $\alpha < 0$ ,  $\beta \neq 0$ . Conversely, the saddle-focus II case has  $\lambda_1 < 0$ ,  $\lambda_{2,3} = \alpha \pm \beta i$ ,  $\alpha > 0$ ,  $\beta \neq 0$ .

## EXAMPLES

We wish to construct examples of systems of the form (1), which have critical points with the characteristic numbers  $\lambda_1 < 0$ ,  $\lambda_{2,3} = \alpha \pm \beta i$ , where  $\alpha > 0$ . Alternatively, we are interested in the case  $\lambda_1 > 0$ ,  $\lambda_{2,3} = \alpha \pm \beta i$ ,  $\alpha < 0$ . The notation in this section is independent of the notation in the previous section. We wish also the following condition to be satisfied

$$|\lambda_1| > \alpha. \quad (4)$$

To construct examples, we will use material in the article (Kozlovska and Sadyrbaev 2022). We set  $v_i = 1$ ,  $\mu_i = 4$  in the system (1). Suppose that the regulatory matrix

$$W = \begin{pmatrix} w_{11} & w_{12} & w_{13} \\ w_{21} & w_{22} & w_{23} \\ w_{31} & w_{32} & w_{33} \end{pmatrix} \quad (5)$$

is already defined. A critical point can be found from the system

$$\begin{cases} x = \frac{1}{1 + e^{-\mu_1(w_{11}x + w_{12}y + w_{13}z - \theta_1)}}, \\ y = \frac{1}{1 + e^{-\mu_2(w_{21}x + w_{22}y + w_{23}z - \theta_2)}}, \\ z = \frac{1}{1 + e^{-\mu_3(w_{31}x + w_{32}y + w_{33}z - \theta_3)}} \end{cases} \quad (6)$$

where

$$\begin{aligned} w_{11} + w_{12} + w_{13} &= 2\theta_1, \\ w_{21} + w_{22} + w_{23} &= 2\theta_2, \\ w_{31} + w_{32} + w_{33} &= 2\theta_3. \end{aligned} \quad (7)$$

This choice of  $\theta_i$  puts a critical point to a central location  $(0.5, 0.5, 0.5)$ . Notice that the right sides of equations in the system (6) then are equal to 0.5.

Choose  $\lambda_1 = -2$ ,  $\lambda_{2,3} = 1 \pm i$ . The numbers  $\Lambda_1 = \lambda_1 + 1 = -1$ ,  $\Lambda_{2,3} = \lambda_{2,3} \pm i = 2 \pm i$  (do not mix with  $\Lambda$  in the previous section) are solutions (Kozlovska and Sadyrbaev 2022) of the characteristic equation

$$\begin{aligned} \Lambda^3 - (w_{11} + w_{22} + w_{33})\Lambda^2 - (w_{21}w_{12} - w_{11}w_{22} + w_{31}w_{13} \\ + w_{32}w_{23} - w_{11}w_{33} - w_{22}w_{33})\Lambda - (-w_{31}w_{22}w_{13} + w_{21}w_{32}w_{13} \\ + w_{31}w_{12}w_{23} - w_{11}w_{32}w_{23} - w_{21}w_{12}w_{33} + w_{11}w_{22}w_{33}) = 0. \end{aligned} \quad (8)$$

For our choice of  $\Lambda_1 = -1$ ,  $\Lambda_{2,3} = 2 \pm i$  we obtain the cubic equation

$$(\Lambda + 1)(\Lambda^2 - 4\Lambda + 5) = \Lambda^3 - 3\Lambda^2 + \Lambda + 5 = 0. \quad (9)$$

Comparing (11) and (9), we are led to the conclusion that

$$\begin{aligned} (w_{11} + w_{22} + w_{33}) &= 3, \\ (w_{21}w_{12} - w_{11}w_{22} + w_{31}w_{13} + w_{32}w_{23} - w_{11}w_{33} - w_{22}w_{33}) &= -1, \\ (-w_{31}w_{22}w_{13} + w_{21}w_{32}w_{13} + w_{31}w_{12}w_{23} - w_{11}w_{32}w_{23} \\ - w_{21}w_{12}w_{33} + w_{11}w_{22}w_{33}) &= -5. \end{aligned} \quad (10)$$

This is an over-determined system of equations to find elements of matrix  $W$ . The central point  $(0.5, 0.5, 0.5)$  will be a critical point with the characteristic values  $\lambda_1 = -2, \lambda_{2,3} = 1 \pm i$ .

In such a way multiple examples can be constructed. The central point  $(0.5, 0.5, 0.5)$  need not be a unique critical point. To find the rest of the critical points (if any), one needs to analyze the location of the nullclines, which are given by the relations (6).

**Example of system (1) with the required critical point**

Suppose we wish to construct the system with the critical point at  $(0.5, 0.5, 0.5)$  and with prescribed characteristic numbers. Since the parameters  $\mu$  and  $v$  are already defined, we need to construct the regulatory matrix  $W$  only. The parameters  $\theta$  will then be defined by the relations (7). Choose the characteristic numbers  $\lambda_1 = -0.8, \lambda_{2,3} = 0.1 \pm 2i$ . The numbers  $\Lambda_1 = \lambda_1 + 1 = 0.2, \Lambda_{2,3} = \lambda_{2,3} \pm 2i = 1.1 \pm 2i$  are solutions (Kozlovska and Sadyrbaev 2022) of the characteristic equation

$$\Lambda^3 - (w_{11} + w_{22} + w_{33})\Lambda^2 - (w_{21}w_{12} - w_{11}w_{22} + w_{31}w_{13} + w_{32}w_{23} - w_{11}w_{33} - w_{22}w_{33})\Lambda - (-w_{31}w_{22}w_{13} + w_{21}w_{32}w_{13} + w_{31}w_{12}w_{23} - w_{11}w_{32}w_{23} - w_{21}w_{12}w_{33} + w_{11}w_{22}w_{33}) = 0. \tag{11}$$

For our choice of  $\Lambda_1 = 0.2, \Lambda_{2,3} = 1.1 \pm 2i$  we obtain the cubic equation

$$(\Lambda - 0.2)(\Lambda^2 - 2.2\Lambda + 5.21) = \Lambda^3 - 2.4\Lambda^2 + 5.65\Lambda - 1.042 = 0. \tag{12}$$

Comparing (11) and (9), we are led to the conclusion that

$$\begin{aligned} (w_{11} + w_{22} + w_{33}) &= 2.4, (w_{21}w_{12} - w_{11}w_{22} + w_{31}w_{13} \\ + w_{32}w_{23} - w_{11}w_{33} - w_{22}w_{33}) &= -5.65, (-w_{31}w_{22}w_{13} + w_{21}w_{32}w_{13} \\ + w_{31}w_{12}w_{23} - w_{11}w_{32}w_{23} - w_{21}w_{12}w_{33} + w_{11}w_{22}w_{33}) &= 1.042. \end{aligned} \tag{13}$$

This is an over-determined system of equations to find elements of matrix  $W$ . The central point  $(0.5, 0.5, 0.5)$  will be a critical point with the characteristic values  $\lambda_1 = -0.8, \lambda_{2,3} = 0.1 \pm 2i$ .

The regulatory matrix

$$W = \begin{pmatrix} 0 & 0 & 1.042 \\ -1 & 0 & 5.65 \\ 0 & -1 & 2.4 \end{pmatrix} \tag{14}$$

is good. It is not unique, of course.

**EXAMPLES WITH ATTRACTORS**

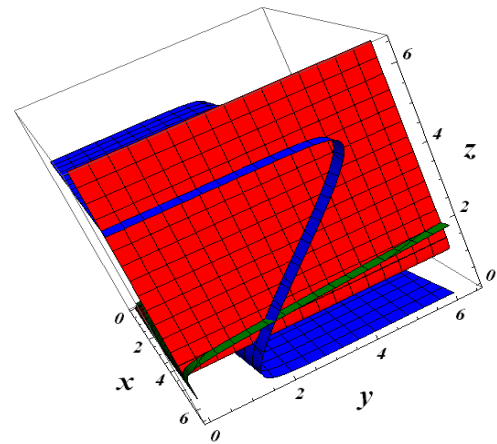
We consider system (1), where parameters are  $\mu_i, \theta_i, v_i$  and  $w_{ij}$ . In any of our examples we will have a critical point with the characteristic values, satisfying the condition (4). Our goal is to obtain attractors which are neither stable equilibria, nor limit cycles, but something else. We provide 3D visualizations of attractors, as well as graphs of  $x(t), y(t)$  and  $z(t)$ . The behavior of solutions is irregular. We also made a test on the sensitive dependence of solutions on the initial data. For this, we compute Lyapunov exponents. Recall, that there are three Lyapunov curves. If one of them is positive, this is an evidence of the chaotic behavior of solutions. For calculations, we use Wolfram Mathematica programming written by M. Sandri (Sandri 1996) and available online.

**Example 1**

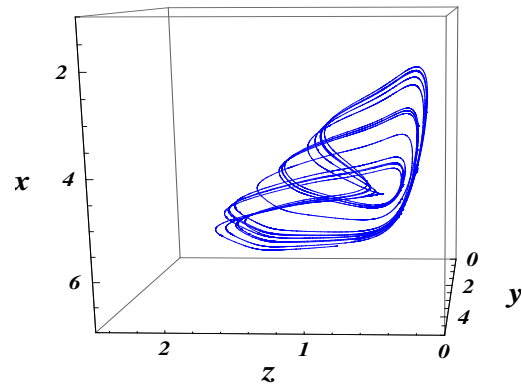
Consider the three-dimensional system (1) with the regulatory matrix

$$W = \begin{pmatrix} 0 & 0 & 2 \\ -0.82 & -0.2 & 4.55 \\ 0.1 & -0.87 & 1.11 \end{pmatrix} \tag{15}$$

and  $v_1 = 0.164, v_2 = 0.1, v_3 = 0.2; \mu_1 = 4.38, \mu_2 = 4, \mu_3 = 3.1; \theta_1 = 0.77, \theta_2 = 1.09, \theta_3 = 0.62$ . Let initial conditions be  $(0.41; 0.1; 0.4)$ . There is the critical point  $P = (6.096; 2.085; 1.356)$ . The nullclines of the system (1) with the regulatory matrix (15) are demonstrated in Fig.1 and the trajectory of the system (1) with the regulatory matrix (15) is shown in Fig.2.

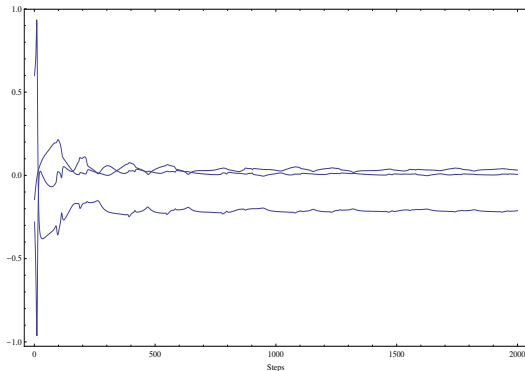


**Figure 1** The nullclines of the system (1) with the regulatory matrix (15).

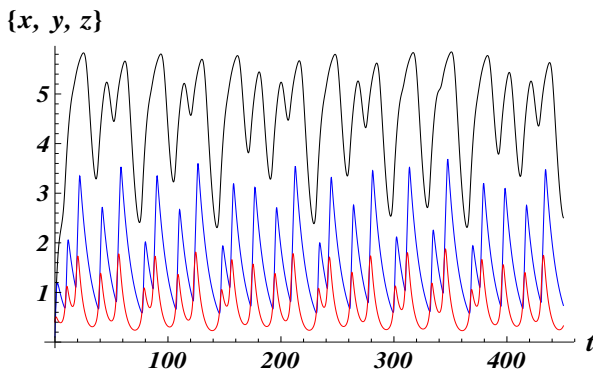


**Figure 2** The trajectory of the system (1) with the regulatory matrix (15).

The characteristic values for the critical point  $P$  are  $\lambda_1 = -0.16, \lambda_{2,3} = 0.12 \pm 1.21i$ . This is a saddle-focus II with the condition (4) fulfilled. The dynamics of Lyapunov exponents for the system (1) with the regulatory matrix (15) are demonstrated in Fig.3 and the graphs of the system (1) with regulatory matrix (15) are shown in Fig.4.



**Figure 3** The dynamics of Lyapunov exponents for the system (1) with the regulatory matrix (15).



**Figure 4** The graphs  $(x(t), y(t), z(t))$  of the system (1) with regulatory matrix (15).

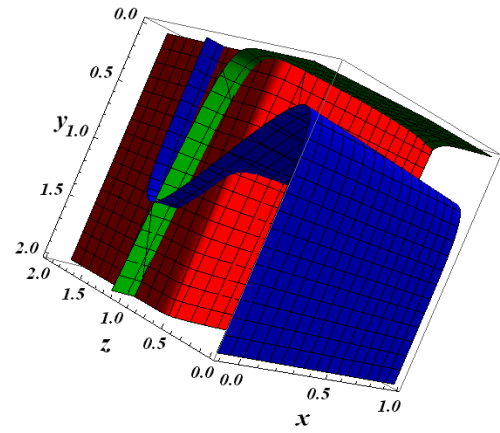
The Lyapunov exponents are  $(0.032, 0.005, -0.212)$  with the initial condition  $(0.41; 0.1; 0.4)$ , where  $LE_1 > 0, LE_2 = 0$  and  $LE_3 < 0$  (Saeed et al. 2023).

**Example 2**

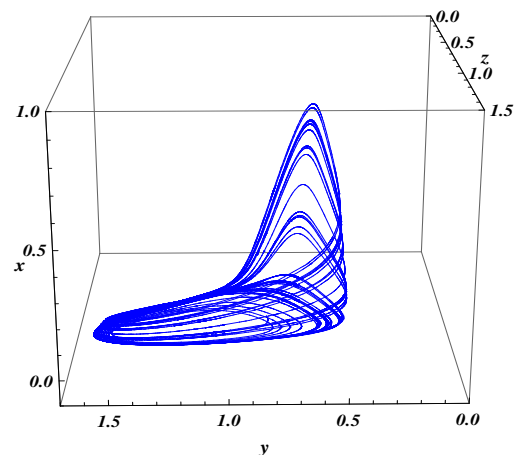
Consider the three-dimensional system (1) with the regulatory matrix

$$W = \begin{pmatrix} 0 & 0.262 & -7.12 \\ 1.46 & 0 & 4 \\ 0.1425 & -1 & 2 \end{pmatrix} \quad (16)$$

and  $v_1 = 0.708, v_2 = 0.307, v_3 = 0.767; \mu_1 = 5.63, \mu_2 = 4.538, \mu_3 = 4; \theta_1 = -4, \theta_2 = 4.44, \theta_3 = 0.5$ . The initial conditions are  $(0.4; 0.9; 0.4)$ . The nullclines of the system (1) with the regulatory matrix (16) are demonstrated in Fig.5 and the trajectory of the system (1) with the regulatory matrix (16) is shown in Fig.6.

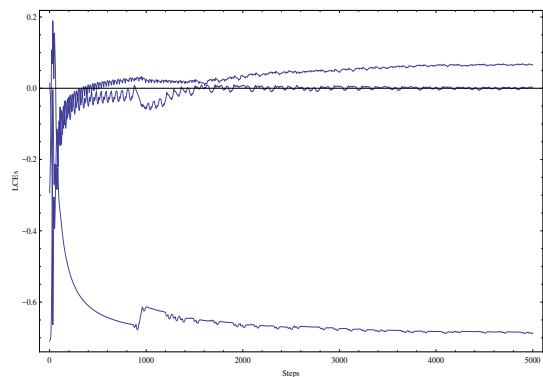


**Figure 5** The nullclines of the system (1) with the regulatory matrix (16).

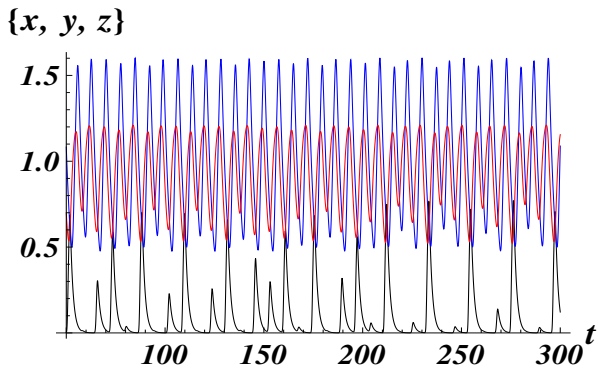


**Figure 6** The trajectory of the system (1) with the regulatory matrix (16).

The critical point has coordinates  $P = (0; 1.269; 1.085)$ . Characteristic values for the critical point  $P$  are  $\lambda_1 = -0.71, \lambda_{2,3} = 0.02 \pm 1.51i$ . This point is a saddle-focus II again. The dynamics of Lyapunov exponents for the system (1) with the regulatory matrix (16) are demonstrated in Fig.7 and the graphs of the system (1) with regulatory matrix (16) are shown in Fig.8.

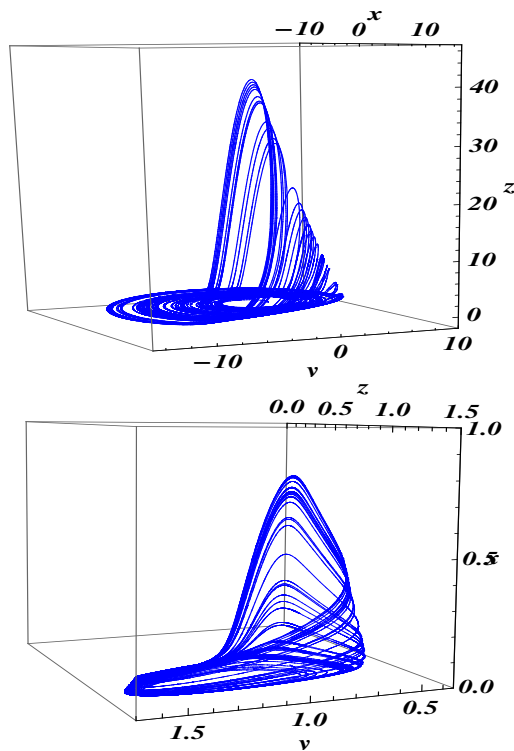


**Figure 7** The dynamics of Lyapunov exponents for the system (1) with the regulatory matrix (16).



**Figure 8** The graphs  $(x(t), y(t), z(t))$  of the system(1) with the regulatory matrix (16).

The Lyapunov exponents are  $(0.065; 0.002; -0.686)$  with the initial condition  $(0.4; 0.9; 0.4)$ , where  $LE_1 > 0, LE_2 = 0$  and  $LE_3 < 0$ . The trajectory of Rössler system and the trajectory of the system (1) with the regulatory matrix (16) are shown in Fig.9.



**Figure 9** The trajectory of the Rössler system ( top picture). The trajectory of the system (1) with the regulatory matrix (16) ( bottom picture).

The second attractor looks similar to the Rössler one (Ibraheem and Raied 2022). They are different, however. The Rössler attractor is based on two critical points, one in the basement and the second one in the upper part of the attractor. The critical point in the basement is a saddle focus II point, while the second critical point has one-dimensional unstable manifold and two-dimensional stable one. The attractor in the system (1) with the regulatory matrix (16) has a single saddle focus II type point.

## CONCLUSION

Chaotic attractors in GRN are extremely rare, according to the evidences of researchers. So any indications on how to get chaotic behavior are of great importance. In our study, the examples with a critical point of saddle-focus type were considered. The condition  $\lambda > -\rho$  was essential. In our examples, we were looking for systems with the critical point of this type. So the number of tests in search of chaos was significantly narrowed. We provide the GRN system having a critical point of saddle-focus type II, where  $\lambda_1 < 0, \lambda_{2,3} = \alpha \pm i\beta, \alpha > 0, \beta \neq 0$  and  $|\lambda_1| > \alpha$ . In two cases the chaotic behavior was confirmed by analysis using the Lyapunov exponents.

## Availability of data and material

Not applicable.

## Conflicts of interest

The authors declare that there is no conflict of interest regarding the publication of this paper.

## Ethical standard

The authors have no relevant financial or non-financial interests to disclose.

## LITERATURE CITED

- Barbuti, R., Gori, Milazzo, and Nasti, 2020 A survey of gene regulatory networks modelling methods: from differential equations, to Boolean and qualitative bioinspired models. *Journal of Membrane Computing* 2: 207–226.
- Brokan, E. and F. Sadyrbaev, 2016 On attractors in gene regulatory systems. *AIP Conf. Proc.* 1809, 020010 .
- Brokan, E. and F. Sadyrbaev, 2018 Attraction in n-dimensional differential systems from network regulation theory. *Mathematical Methods in the Applied Sciences* 41: 7498–7509.
- Das, A., P. Das, and A. Roy, 2000 Chaos In A Three-Dimensional General Model Of Neural Network. *Applied Mathematical Modelling* pp. 511–522.
- Das, A., P. Das, and A. Roy, 2002 Chaos In A Three-Dimensional General Model Of Neural Network. *International Journal of Bifurcation and Chaos* 12: 2271–2281.
- Deng, B., M. Han, and S.-B. Hsu, 2017 Numerical Proof For Chemostat Chaos of Shilnikov Type. *Chaos* 27.
- Gonchenko, S., A.Gonchenko, Kazakov, Kozlov, and Bakhanova, 2019 Spiral chaos of three-dimensional flows. *Izvestija vuzov* 27: 7–52.
- Ibraheem and K. Raied, 2022 Generating a Novel Chaotic System by Coupling (Rossler-Chen) Systems. *Research Square* .
- Jong, D., 2002 Modeling and simulation of genetic regulatory systems. *Journal of Computational Biology* 9: 67–103.
- Kardynska, M., D. Kogut, M. Pacholczyk, and J. Smieja, 2023 Mathematical modeling of regulatory networks of intracellular processes. *Computational and Structural Biotechnology Journal* 21: 1523–1532.
- Kozlovskaya, O. and F. Sadyrbaev, 2022 Models of genetic networks with given properties. *Transactions on Computer Research* 10: 43–49.
- Magnitskii, N. and Sidorov, 2006 New methods for chaotic dynamics. *World Scientific* .
- Ogorelova, D., F. Sadyrbaev, and V. Sengilejev, 2020 Control in Inhibitory Genetic Regulatory Network Models. *Contemporary Mathematics* 1: 393–400.

- Peter, I., 2020 The function of architecture and logic in developmental gene regulatory networks. *Current Topics in Developmental Biology*, Academic Press **139**: 267–295.
- Saeed, N. A., H. A. Saleh, W. A. El-Ganaini, M. Kamel, and M. S. Mohamed, 2023 On a new three-dimensional chaotic system with adaptive control and chaos synchronization. *Shock and Vibration* pp. 1–19.
- Samuilik, I., 2022 Genetic engineering construction of a network of four dimensions with a chaotic attractor. *Vibroengineering Procedia* **44**: 66–70.
- Samuilik, I. and F. Sadyrbaev, 2023 On trajectories of a system modeling evolution of genetic networks. *Mathematical Biosciences and Engineering* **20**: 2232–2242.
- Sandri, M., 1996 Numerical calculation of Lyapunov exponents. *Mathematica Journal* **6**: 78–84.
- Santillan, M., 2008 On the Use of the Hill Functions in Mathematical Models of Gene Regulatory Networks. *Mathematical Modelling of Natural Phenomena* **3**: 85–97.
- Schlitt, T., 2013 Approaches to Modeling Gene Regulatory Networks: A Gentle Introduction. In *Silico Systems Biology* p. 13–35.
- Shilnikov, L., 1965 A case of the existence of a denumerable set of periodic motions. *Doklady Akademii Nauk SSSR*, 1965 **160**: 558–561.
- Sprott, J., 2010 *Elegant Chaos*. World Scientific .
- Vijesh, N., S. K.Chakrabarti, and J. Sreekumar, 2013 Modeling of gene regulatory networks. *Biomedical Science and Engineering* pp. 223–231.
- Zhang, Z., Y.Weiming, and *et al.*, 2012 Chaotic motifs in gene regulatory networks. *PLOS ONE* **7**: 1–11.

**How to cite this article:** Kozlovska, O., and Sadyrbaev, F. In Search of Chaos in Genetic Systems. *Chaos Theory and Applications*, 6(1), 13-18, 2024.

**Licensing Policy:** The published articles in *Chaos Theory and Applications* are licensed under a [Creative Commons Attribution-NonCommercial 4.0 International License](https://creativecommons.org/licenses/by-nc/4.0/).



# A Novel Hypothesis for Migraine Disease Mechanism: The Creation of a New Attractor Responsible for Migraine Disease Symptoms

Farnaz Garehdaghi<sup>1</sup>, Yashar Sarbaz<sup>2</sup> and Elham Baradari<sup>3</sup>

\*Modeling Biological System's Laboratory, Department of Biomedical Engineering, Faculty of Electrical and Computer Engineering, University of Tabriz, Tabriz, Iran.

**ABSTRACT** Migraine Disease (MD) is one of the common primary headaches that can prevent patients from their everyday life. Despite the high prevalence, the pathophysiology of the disease has not been clearly understood yet. Here, the brain is considered as a dynamical system. The Chua's circuit with a chaotic attractor is the proposed model. This attractor has a one-scroll mode representing a healthy brain and a double-scroll mode representing a migraine sufferer brain. We believe that MD and Chua's systems have certain behavioral similarities. The boundaries of the attractor are the sensitive brain areas in which any small trigger can start the ictal phase of the migraine. The transition from the inter-ictal phase to the ictal phase in migraine patients occurs due to a decrease in serotonin levels when the brain is within the boundaries of the first attractor. Here, this is the results of the increase of system parameters. In addition, the transition from the ictal phase to the inter-ictal phase in a migraine sufferer brain is caused by a disruption of coordination in the brain's structures and this lasts for a certain period for every migraine patient. The structures which are the result of the Migraine Generator Network (MGN) and Cortical Spreading Depression (CSD). This explanation may propose newer methods for preventing or curing MD. To better understand MD to control it and shrink the areas involved in this disease, it is better to know the dynamic systems better. It may help prevent the formation of migraine ictal attractor or even make the migraine ictal phase attractor smaller even after it has been formed.

## KEYWORDS

Headache  
Ictal  
Migraine sufferer  
Complex dynamic system  
Chaotic attractor  
Chua's system

## INTRODUCTION

Migraine Disease (MD) is one of the primary headaches affecting one in every seven individuals worldwide (Aslan 2021). This prevalent disease is a neurological disorder characterized by numerous symptoms, including headache, nausea, vomiting, photophobia, phonophobia, osmophobia, etc. The foremost critical and bothering symptom of the MD is the throbbing headache. The frequency of incidence of the migraine ictal can range from infrequent to weekly or even daily. MD is regarded as a chronic disorder with

episodic manifestations (Ashina *et al.* 2021). The mechanism of MD is still not fully understood. However, the activation of some regions in the brainstem called Migraine Generator Network (MGN) and activation of Cortical Spreading Depression (CSD) during a migraine ictal are considered to be theories involved in the pathophysiology of MD. These theories have difficulty explaining the difference between a healthy brain and a migraine sufferer's brain in the inter-ictal phase. In this disease, there are one normal phase and four abnormal phases, including the pre-ictal, aura, ictal, and post-ictal phases. In some patients, only one or two phases of the disease are observed (Lane and davies 2006).

Two common subtypes of MD are migraine with aura (MA) and migraine without aura (MO), depending on whether the migraine sufferer experiences the aura phase. The diagnosis of MD is based on the clinical symptoms described by the patient and the opin-

Manuscript received: 25 August 2023,

Revised: 27 November 2023,

Accepted: 14 December 2023.

<sup>1</sup>f.garehdaghi@tabrizu.ac.ir

<sup>2</sup>yashar.sarbaz@tabrizu.ac.ir (Corresponding author).

<sup>3</sup>elham.baradari94@gmail.com

ion of the physician. Some studies focus on the classification of migraine patients and healthy controls based on the extracted features from the electroencephalography (EEG) signal (Aslan 2021; Bellotti et al. 2007; Jindal et al. 2018). According to some researchers, the brain is a dynamic system that enters the MD state by alternation in its parameters (Dahlem et al. 2013, 2015; Scheffer et al. 2013). In 2003, Charles described migraine as a brain state. He stated that headache happens due to changes in the state of the brain. During the start of the ictal phase, certain brain networks either become active or inactive. As a result, coordination between different parts of the brain is disrupted. Also, during the ictal phase, arousal decreases and symptoms like fatigue and yawning occur. As awareness grows, the brain becomes more responsive to light, smell, and other stimuli.

In migraine, not only does it activate pain-sensing networks, but it also disrupts the physiological communication between different parts of the brain. Several studies have indicated alterations in neuronal connections during the inter-ictal phase, along with a reduction in theta wave activity on Quantitative Electroencephalography (QEEG) during the pre-ictal and ictal phases (Charles 2013). In 2013, Scheffer et al. considered a minimal model for migraine. According to their report, when a group of neurons is stimulated by an input stimulus, it causes an increase in the intracellular level of potassium and glutamate, which enhances the excitability of the neurons. This excitability is further amplified by the local neuronal activity and positive feedback, ultimately leading to the initiation of a contagious process called CSD by a small trigger in the neurons. This study suggests that within each small region of the brain, there exists a dynamic equilibrium. This equilibrium arises from the generation and decay of pulses. When the baseline excitability increases, this equilibrium is disrupted, and the brain reaches a tipping point. In this case, every small trigger initiates the ictal phase (Scheffer et al. 2013).

Dahlem et al. in 2013 considered migraine to be a dynamic disease. It was stated that when the headache starts, the brain transitions from the normal phase and enters a tipping point or bifurcation point and then enters the headache phase. They declared this stage as the prodromal stage and stated that it could be detected with dynamical network biomarkers. It is important to identify the prodromal stage since it is reversible while the headache stage is not, and this may help prevent the headache (Dahlem et al. 2013). Dahlem et al. in 2014 also found that when the brain reaches a tipping point, even a small trigger can start the headache. In contrast, if the brain is not in this area, even things known to be major triggers of migraine headaches do not cause pain.

They considered a path with one or two wells as two states of health and pain. As the height between the two wells decreases, the brain enters the tipping point area, and any small trigger causes the onset of the headache (Dahlem et al. 2015). In 2018, Bayani et al. extended the model proposed by Scheffer et al. and considered a group of neurons for 3 different trigeminovascular, descending modulatory brainstem, and cortex units, then obtained 3 equations for neuronal activity. They also announced that the inter-ictal and the ictal stages are chaotic phases, and the pre-ictal phase is unstable and periodic (Bayani et al. 2018).

According to previous studies, it may be an appropriate method to consider the brain as a dynamic system and then propose a complex system model for that as a migraine patient or a healthy subject. For this reason, it seems possible to gain a good understanding of the performance of MD by studying the behavior of dynamic systems that exhibit similar behavior to MD. This may

also serve a better understanding of the changes in the brain during the ictal phase to enable better diagnosis and possibly better therapy.

## HYPOTHESIS

MD is considered a chronic disease with episodic manifestations. If the frequency of headaches increases, it can lead to chronicity of the disease. A chronic migraine is present if the headaches occur 15 times or more per month and last longer than 3 months. It is assumed that there is a pre-ictal phase prior to the ictal phase of the migraine. This phase can be a warning sign of the headache initiation. Symptoms that accompany this phase include behavioral changes, hunger, fatigue, and etc. Despite some theories about the cause of the MD such as CSD or MGN, the pathophysiological mechanism of MD is still not fully understood.

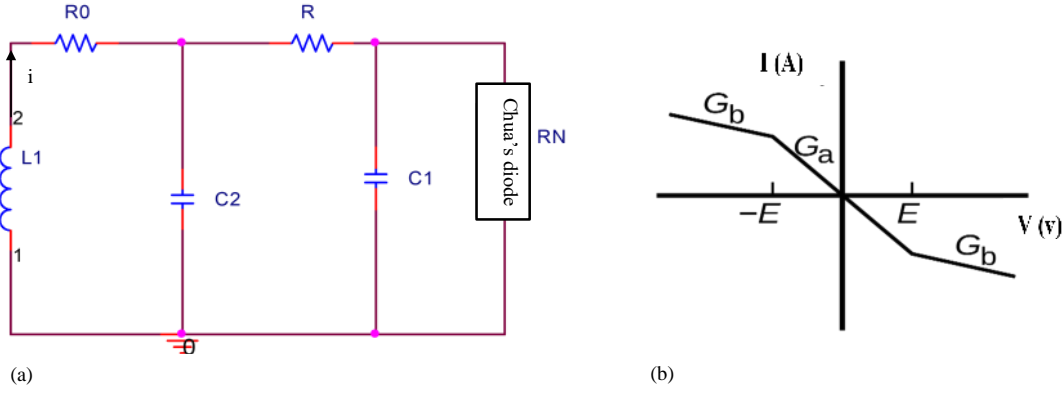
Since 1970s, there have been numerous computational models attempting to explain the spreading depression. Some studies also considered the role of Central Nervous System (CNS) as a function of a complex dynamic system. When the parameters of the dynamic system change, the symptoms of the disease become visible. A theoretical model from the perspective of the complex dynamic system is presented here. This is used to explain the clinical signs and manifestation of MD. The dynamics of individual neurons are not considered here, but the interaction between whole neurons is analyzed. As a model for the healthy brain, a complex system with a chaotic strange attractor is considered. It is assumed that this attractor changes from one scroll to double scroll when the system parameters in the brain of migraine patients change. It is considered that the one scroll attractor can represent a healthy brain, while the double scroll attractor represents the brain of a migraine patient.

The size of the two scrolls can change by varying the model parameters to represent the Chronic Daily Migraine (CDM) or episodic migraine. For a migraine patient, certain triggers such as neck pain, bright light, certain foods, and other factors can sometimes initiate the ictal phase, while having no effect on other days. It is believed that the brain becomes sensitive in certain situations where any trigger can initiate the ictal phase. In the proposed system, the boundaries of the normal attractor are the regions where any small trigger can change the phase and thus initiate the ictal phase. In the proposed model, the inner regions of the normal attractor are the non-sensitive brain situations.

## COMPUTATIONAL MODEL

In order to choose a suitable model for MD, different dynamic systems were considered. Our goal was to find a system that has one attractor representing a healthy brain and able to generate two attractors by changing the parameters. This attractor can simulate the behavior of the brain of a migraine patient. The assumed system should have a "one scroll" mode and a "double scroll" mode representing a healthy brain and the brain of a migraine patient. Switching between the modes is done with a parameter change. One of the best-known systems with these features is Chua's system. Chua is a non-linear and well-known dynamic model (Chua 1993). In 1983 Leon Chua developed a chaotic electronic circuit with 2 linear capacitors ( $C_1$ ,  $C_2$ ), a linear inductor ( $L$ ), a linear resistor ( $R$ ), and a voltage-controlled non-linear resistor ( $R_N$ ) known as Chua's diode. The Chua's diode is capable of generating chaotic behavior. This circuit is shown in Figure 1(a). The Chua's diode has 3 regions; a piecewise linear region with 2 unstable points. The driving points of Chua's diode are shown in Figure 1(b).





**Figure 1** Representation of (a) Chua's circuit and (b) the driving point characteristics of the voltage controlled resistor (Chua's diode)

The equations of the circuit, which are derived by applying Kirchoff's laws to nodes and loops, are as follows:

$$C_1 V_{C1}' = \frac{V_{C2} - V_{C1}}{R - g(V_{C1})} \quad (1)$$

$$C_2 V_{C2}' = \frac{V_{C1} - V_{C2}}{R + i} \quad (2)$$

$$L i' = -V_{C2} - R_0 i \quad (3)$$

$C_1$  and  $C_2$  are the capacitances of the capacitors,  $L$  is the inductance of the inductor,  $R$  is the resistance of the resistor, and  $g(x)$  is the three-segment piecewise linear characteristic of the Chua's diode, which is shown in Figure 1(b) and mentioned here:

$$g(x) = G_b x + 0.5(G_a - G_b)(|x + 1| - |x - 1|) \quad (4)$$

$G_a$  is the slope of the inner region of the non-linear resistor, and  $G_b$  is the slope of the outer part. Then the variables of these equations are replaced with  $x_1 = v_1$ ,  $x_2 = v_2$ ,  $x_3 = Ri$ , and the parameters with

$$\alpha = \frac{C_2}{C_1}, \beta = \frac{R^2 C_2}{L}, \gamma = \frac{R R_0 C_2}{L}, m_0 = R G_a, m_1 = R G_b \quad (5)$$

Chua's system equations are achieved as:

$$x_1' = \alpha(x_2 - x_1 - h(x_1)) \quad (6)$$

$$x_2' = x_1 - x_2 + x_3 \quad (7)$$

$$x_3' = \beta x_2 - \gamma x_3 \quad (8)$$

Where

$$h(x) = m_1 x + 0.5(m_0 - m_1)(|x + 1| - |x - 1|) \quad (9)$$

For different values of the parameters, this attractor changes from a spiral attractor to a double scroll attractor. The spiral attractor can be the representation of a healthy brain, while the double scroll attractor can be the representation of the brain of a migraine patient. Each region can show the ictal or inter-ictal phases, and the lines connecting the two areas show the pre-ictal and post-ictal phases.

### The similarities between MD and Chua's system

A healthy brain that does not experience a migraine ictal has only one normal phase. This mode is the one scroll or spiral mode of Chua's attractor, as shown in Figure 2(a).

The value of the parameters for this mode is as:

$$\alpha = 6.5792, \beta = 10.9, \gamma = -0.446, m_0 = -1.182, m_1 = -0.652 \quad (10)$$

A healthy brain has only the normal phase, which is free of headaches. In the proposed model, changing the alpha parameter can transform the healthy brain into a migraine prone one. Increasing the alpha parameter, gives the attractor, which has two scrolls indicating two phases of a migraine patient's brain. The inter-ictal or headache-free phase and the ictal or headache phase are connected by some lines. Figure 2(b) is a representation of the double scroll attractor. The value of the parameters are as:

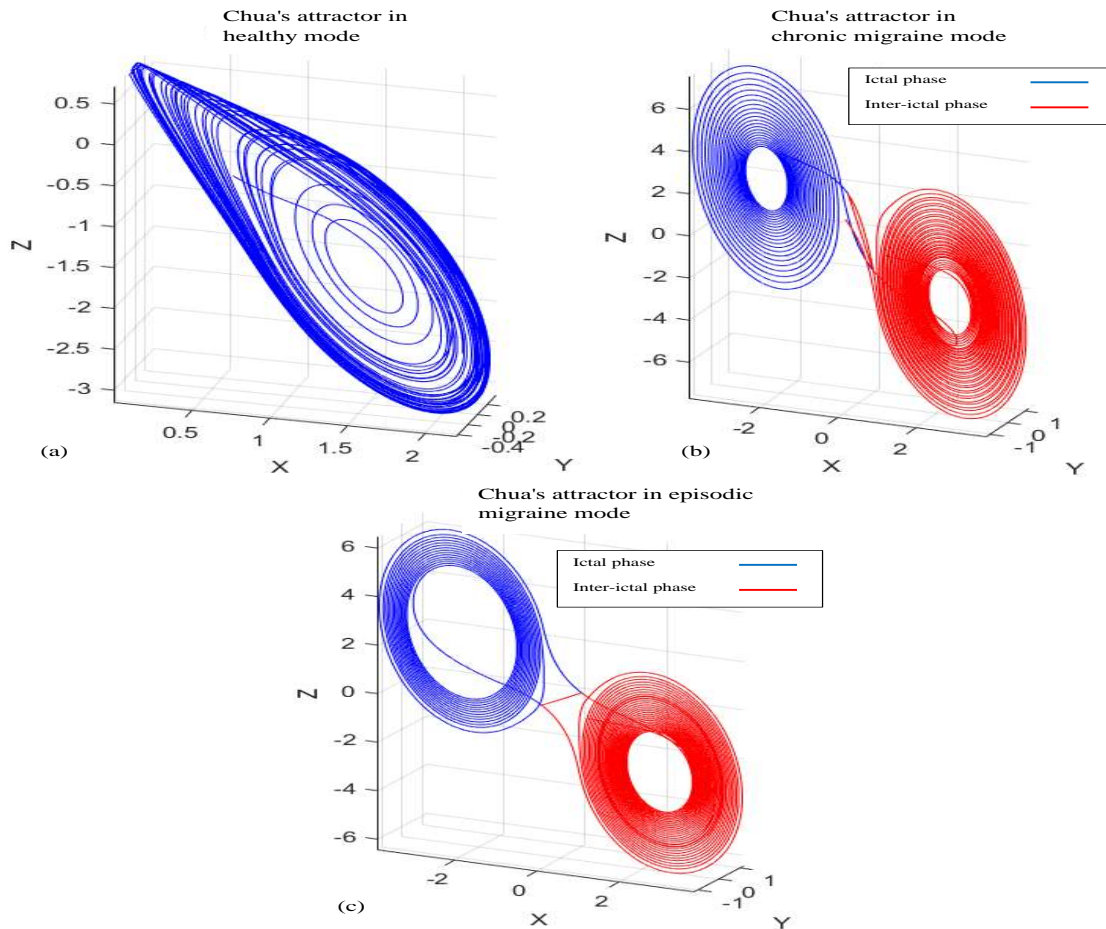
$$\alpha = 10.3515, \beta = 16.79, \gamma = -0, m_0 = -2, m_1 = -0.2601 \quad (11)$$

Each region of the attractor represents the ictal and inter-ictal phases. Suppose the size of one of the regions is smaller than the size of the other one as shown in Figure 2(c). In this case, the small region may represent the ictal phase for the situation of episodic migraine, in which the headache occur with less frequency. However, if the two areas are the same size, this may represent the brain of a chronic migraine sufferer, where the migraine sufferer experiences headaches 15 days of a month or more. For the parameter values as:

$$\alpha = 11.3515, \beta = 10.79, \gamma = -0.14, m_0 = -2, m_1 = -0.2601 \quad (12)$$

The representation of the Chua's attractor for the given parameter values is in Figure 2(c). This is the proposed model for the brain of an episodic migraine sufferer.

The representation of  $x(t)$  in healthy mode, in the ictal phase, and in the inter-ictal phase are shown in Figures 3(a), 3(b), and 3(c). As can be seen in figure 3, the behavior of  $x(t)$  in the 3 states of healthy mode, inter-ictal phase, and ictal phase of migraine does not seem to make any significant difference. When we compare the EEG of these 3 groups, there is no noticeable difference in the appearance of the EEG in the time domain of these 3 groups. But in general, these behaviors indicate whether there is MD or not. As a result, we can say that what happens in epilepsy does not occur in MD. In epilepsy, these differences can be seen in the EEG



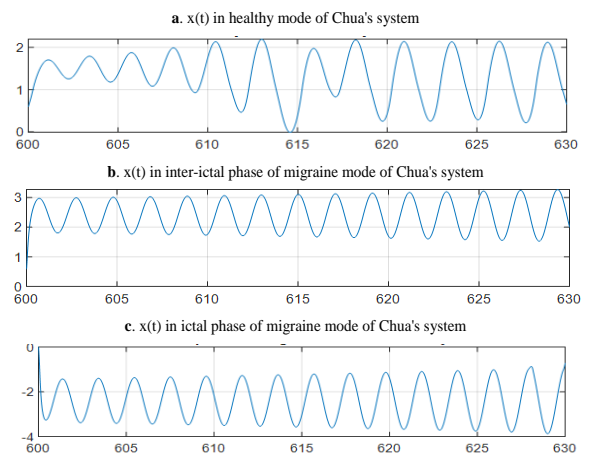
**Figure 2** (a) Chua's system in the spiral mode representing a healthy brain and (b) . Double scroll Chua's attractor representing a chronic migraine sufferer brain (c) Double scroll Chua's attractor representing an episodic migraine sufferer brain

due to synchronization. In MD, however, there is no noticeable difference in the appearance of the EEG. In this figure, there is also no significant difference between the behavior of the three groups. Nevertheless, they originate from different phases and modes of the Chua's attractor and lead to different states.

The energy level of  $x(t)$  in the different modes of the Chua's system was also compared. The energy level was lower in Chua's spiral mode (considered here as the healthy mode), than the double scroll mode (considered as the MD mode). By calculating the energy levels of the EEG recordings of the migraine patients and healthy controls in the inter-ictal phase using the publicly available Carnegie Mellon University dataset (Chamanzar *et al.* 2020), this higher value of average energy was also seen in migraine sufferer brain compared to a healthy brain. These values are listed in Table 1.

The researchers also point out that the glutamate level is higher in migraine sufferer brain than a healthy brain (Hoffmann and Charles 2018). Since glutamate plays an important role in the energy metabolism of the brain and the neuron excitation (Ramadan 2003), the reason for the higher energy level could be the higher glutamate level in a migraine sufferer brain.

Migraine patients believe that sometimes any small trigger can

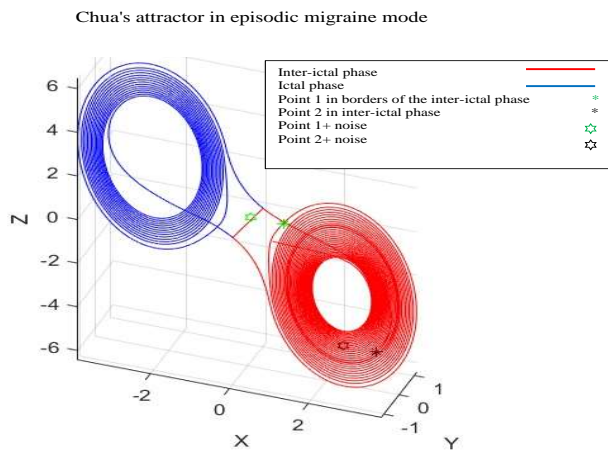


**Figure 3** Shape of the  $x(t)$  in the healthy mode. (b). Shape of the  $x(t)$  in inter-ictal phase of the migraine mode. (c). Shape of the  $x(t)$  in ictal phase of the migraine mode.

**Table 1 Comparison of the average energy of different modes of the Chua's system and EEG recordings of the migraine patients and healthy controls**

Energy level in one scroll mode of chua's system (healthy mode)	Energy level in double scroll mode of chua's system (disease mode)	Average energy level in healthy controls' EEG recordings in rest (mean of all channels)	Average energy level in migraine patients' EEG recordings in rest (mean of all channels)
1.9574e+06	5.8743e+06	15839	22957

initiate a migraine ictal, while in other situations even major triggers may not initiate the ictal phase. To test whether this situation occurs in the proposed model, a point at the edge of the inter-ictal phase is chosen, as shown in Figure 4. Here, a small noise is added to test if the point enters the ictal phase or not. This point enters the lines between two phases, which represent a path to the ictal phase. This noise can simulate the small trigger which initiates a headache. In addition, the lines between the two phases can be considered pre-ictal and post-ictal phases of the migraine. Another point is also selected in the inner region of the inter-ictal phase; then the same noise is added to the system. Since the trajectory is in the inter-ictal phase and far from the boundaries, the same noise cannot trigger the headache and bring the trajectory into the ictal phase.



**Figure 4** A point in the edge of the inter-ictal phase entering ictal phase while adding noise

## DISCUSSION

Headaches are one of the most common disorders that 90% of people experience at least once in their lives. Episodic migraine is a common primary type of headache, affecting 15% of women and 6% of men worldwide (Hauser and Josephson 2010). 20% of the migraine patients suffer from migraine with aura (Lane and Davies 2006). The prevalence of migraine increases from childhood to the age of 40 after which it decreases (Stovner et al. 2007). In some migraine patients, the frequency of the headaches increases. These people experience migraine without aura 15 times a month. If it lasts longer than three months, this disorder is referred to as CDM (Lipton and Bigal 2006). MD has affected many people globally, particularly young individuals, and has prevented the patients

from their daily activities. 53% of migraine patients report a need for bed rest, and one third miss one day a year of school or work (Lipton and Bigal 2006). There is no specific cure to prevent the onset of this disease.

Despite the high prevalence of MD and the disability attributed to the severe pain during the migraine ictal phase, the cause of the disease is not yet clearly understood. Although many studies have addressed the pathophysiology of the disease (Goadsby et al. 2017; Hargreaves and Shephard 1999; Pietrobon and Moskowitz 2013), some questions about MD have remained unanswered. What is the real reason for the onset of MD? Medical texts cite two mechanisms for MD, but it is not yet clear how these mechanisms relate to the headaches and why new manners occur? How are the periods of migraine ictal determined? Why can any minor trigger sometimes initiate a migraine headache and even major triggers may not start the headache in other situations? What is the reason that the headache gets stronger or weaker? What are the pre-ictal and post-ictal phases of migraine headaches?

It seems that the study of individual neurons and changes in MD is not very suitable to assess and recognize the function of the disease. We believe that we will get a better understanding if we have a global view of the neuronal areas. Given what we know about the performance of the dynamical systems and various studies that have compared CNS performance of dynamical systems, it can be concluded that looking at dynamical systems to analyze brain function can lead to a better understanding of MD. Therefore, we hypothesize that different neuronal regions from the normal behavior of the brain can be considered as attractors and the system response remains in this healthy attractor. In the case of MD, a new attractor is added to the responses of different areas of the CNS, which may indicate the disease attractor.

Entering the abnormal area distorts brain function and forms classic migraine pain. Although there are no sensors for pain recognition in large parts of the brain (Hauser and Josephson 2010), severe migraine pain can be caused by a mismatch of information between the different brain regions. The best example of this mechanism is the moment an airplane take off. The vestibular system detects high acceleration during take-off, but the visual and auditory systems do not, resulting in mismatch of information that leads to headaches. According to this theory, some neuronal regions, referred to as MGN in medical texts, form migraine attractor regions. When the number of these neuronal regions greater, the mismatch rate is higher and severe headaches occur.

The model of the creation of a new attractor is closer to reality. In fact, there is no headache when the brain is in the first attractor, and headaches occur when the second attractor is created and the brain enters this attractor. It can be said that the creation of the second attractor occurs through the activation of MGN or CSD as a result of changes in the content of substances such as serotonin, glutamate (Park and Chu 2022) or potassium. Then the brain enters the second attractor. After the creation of the second attractor, when the brain enters this attractor, it has been observed that the

brain energy function increases. This results in an elevation of the cell metabolism, an increased number of action potentials and an enhancement of ATP consumption. The dysfunction of energy metabolism and demonstrable mitochondrial damage has also been reported for migraine patients in recent studies (Haemmerl and Kraya 2023).

The EEG recordings of the brains of the migraine patients also show an increase in energy levels and more spikes than in healthy controls. This ATP consumption cannot continue indefinitely and must be reduced to a certain extent to return to the previous state. The creation of the second attractor occurs through the activation of MGN and CSD, then the increased glutamate level leads to entry into the second attractor. The increase in the glutamate levels have been seen in plasma of the migraine patients which can be the result of its increase in platelets and neurons (Park and Chu 2022). Then there is an increase in energy levels and ATP consumption. After a while, the brain is forced to leave this second attractor and return to the normal state.

It has recently been demonstrated that ATP sensitive potassium channels (KATP) open during migraine attacks (Al-Karagholi *et al.* 2021). This study assumes that the energy level in one part of the brain suddenly rises due to an increase in glutamate levels and that other parts of the brain are unable to adapt to these energy changes, resulting in a mismatch. One of the standard dynamical systems that exhibit complex behavior is Chua's system. Chua's system has been widely studied and applied in various fields of science and engineering, such as mathematics, physics, biology, and control theory. A remarkable similarity can be observed between the behavior of this system and that of MD. The proposed theory is that when a person does not experience migraine, the glutamate and serotonin levels are a little altered, the brain compensates for these changes and most of the neuronal areas of the MGN in the attractor function normally. Then the maladaptation rate in different areas of the brain is low and the headache does not occur. When the alternation of glutamate and serotonin is high, the neuronal states of the MGN are activated, the brain enters the second attractor, energy increases and there is a mismatch of information, resulting in headaches. As only the normal attractor is formed in healthy people, the attractor associated with the headache area gradually develops in migraine patients.

Therefore, the growth of the disease can be explained by an enlargement of the ictal area of the attractor. By comparing the size of the ictal migraine attractor with the inter-ictal attractor, the length and brevity of the headaches and the frequency of migraine headaches can be justified. In some cases, patients become severely sensitive to stimuli, depending on how close the trajectory is to the branch area, which represents the transition to the ictal attractor. The farther the trajectory is from the branch, the greater the stimulus required to enter the ictal area. In contrast, the closer the trajectory is to the branch, the less stimulus is required to enter the migraine ictal area. According to the drawn trajectory and the phase space of Figure 4, the attractor transition areas can be medically considered pre-ictal and post-ictal areas. In the pre-ictal area (the transition pathway from an inter-ictal attractor to the ictal attractor), it gradually deviates from normal function. The headache rate gradually increases. The transition period can be short or long in different people. In the post-ictal area (the transition pathway from the ictal attractor of migraine to the inter-ictal attractor), we move away from the migraine-related areas with severe headaches and approach the inter-ictal attractor, then the amount of pain gradually decreases.

## CONCLUSION

It is assumed that the anatomical differences between the brains of healthy people and migraine patients, which may be caused by genetic factors or other circumstances, are the reason for the creation of the second attractor, which is the attractor of the ictal phase of migraine. CSD and MGN can occur in a migraine sufferer brain leading to the ictal phase of migraine. Then the differences between the structure of a migraine sufferer brain and a healthy brain has created a second attractor.

The transition from the inter-ictal phase (first attractor) to the ictal phase (second attractor) in migraine patients occurs due to a decrease in serotonin levels when the brain is within the boundaries of the first attractor. When the serotonin level drops in a migraine sufferer brain for any reason, which is normal in the daily behavior of the brain, and the brain is also at the boundaries of the attractor, it enters the ictal phase of migraine (second attractor). On the other hand, if the brain is not at the attractor boundaries can compensate the decrease in serotonin level and does not enter the second attractor. For this reason, minor triggers can sometimes cause a headache, while in some cases, even major stimuli have no impact.

The transition from the ictal phase to the inter-ictal phase in a migraine sufferer brain is caused by a disruption of coordination in the brain's structures. The structures which are a result of CSD and MGN activation. When the neurons in this region fail to generate necessary action potentials, these structures become disconnected. When the neurons' ATP intake increases due to high energy levels, a lack of ATP and energy can occur resulting in the neurons being unable to generate action potentials, causing the cessation of the headaches. In other words, a migraine sufferer brain has a higher energy level. Eventually, the body cannot sustain this level of energy, leading to deactivation of neurons in the affected area of the brain and interruption of the second attractor. This results in a reversal to the first attractor, ultimately stopping the headache.

The cause of headaches in migraine sufferers is due to a mismatch of energy levels in the brain. A migraine sufferer brain is initially adapted to a lower energy level. When a certain part of the brain experiences a sudden increase in energy level, the brain is unable to adapt to this heightened level of energy, leading to the onset of a headache. According to the above mentioned items, ATP plays a key role in the migraine cycle. Thus, high fat and high calorie foods keep the second attractor on standby. In this case, a brief stimulus starts the headache phase. When migraine patients consume high-fat and high-calorie foods, they are more likely to experience headaches and enter a the second attractor (Bic *et al.* 1999). In addition, high-calorie and high-fat foods consumption during an ictal phase can prolong headaches. It is recommended that migraine patients reduce their fat and calorie intake, especially when they feel a migraine attack coming on.

In this study, we attempt to explain the disease function and offer a theory that reasonably justifies the behavior of the MD. This explanation may propose newer methods for preventing or curing MD. To better understand MD to control it and shrink the areas involved in this disease, it is better to know the dynamic systems better. It may help prevent the formation of migraine ictal attractor or even make the migraine ictal phase attractor smaller even after it has been formed. A series of electrical stimuli when the headache starts can take us back from the migraine ictal area to the inter-ictal area, which should be further studied.

### Availability of data and material

Not applicable.

## Conflicts of interest

The authors declare that there is no conflict of interest regarding the publication of this paper.

## Ethical standard

The authors have no relevant financial or non-financial interests to disclose.

## LITERATURE CITED

- Al-Karagholi, M. A.-M., H. Ghanizada, C. A. W. Nielsen, C. Skandarioon, J. Snellman, *et al.*, 2021 Opening of bkca channels causes migraine attacks: a new downstream target for the treatment of migraine. *Pain* **162**: 2512–2520.
- Ashina, S., E. Bentivegna, P. Martelletti, and K. Eikermann-Haerter, 2021 Structural and functional brain changes in migraine. *Pain and Therapy* **10**: 211–223.
- Aslan, Z., 2021 Migraine detection from eeg signals using tunable q-factor wavelet transform and ensemble learning techniques. *Physical and Engineering Sciences in Medicine* **44**: 1201–1212.
- Bayani, A., S. Jafari, J. Sprott, and B. Hatef, 2018 A chaotic model of migraine headache considering the dynamical transitions of this cyclic disease. *Europhysics Letters* **123**: 10006.
- Bellotti, R., F. De Carlo, M. de Tommaso, and M. Lucente, 2007 Migraine detection through spontaneous eeg analysis. In *2007 29th Annual International Conference of the IEEE Engineering in Medicine and Biology Society*, pp. 1834–1837, IEEE.
- Bic, Z., G. G. Blix, H. P. Hopp, F. M. Leslie, and M. J. Schell, 1999 The influence of a low-fat diet on incidence and severity of migraine headaches. *Journal of women's health & gender-based medicine* **8**: 623–630.
- Chamanzar, A., M. Behrmann, and P. Grover, 2020 Ultra high-density eeg recording of interictal migraine and controls: Sensory and rest.
- Charles, A., 2013 Migraine: a brain state. *Current opinion in neurology* **26**: 235–239.
- Chua, L. O., 1993 A zoo of strange attractors from the canonical chua's circuits. volume 35, pp. 916–916.
- Dahlem, M. A., J. Kurths, M. D. Ferrari, K. Aihara, M. Scheffer, *et al.*, 2015 Understanding migraine using dynamic network biomarkers. *Cephalalgia* **35**: 627–630.
- Dahlem, M. A., S. Rode, A. May, N. Fujiwara, Y. Hirata, *et al.*, 2013 Towards dynamical network biomarkers in neuromodulation of episodic migraine. *Translational neuroscience* **4**: 282–294.
- Goadsby, P. J., P. R. Holland, M. Martins-Oliveira, J. Hoffmann, C. Schankin, *et al.*, 2017 Pathophysiology of migraine: a disorder of sensory processing. *Physiological reviews*.
- Haemmerl, L. and T. Kraya, 2023 Migraine and mitochondrial diseases: Energy deficit in the brain. *Schmerz (Berlin, Germany)*.
- Hargreaves, R. and S. Shephard, 1999 Pathophysiology of migraine—new insights. *Canadian journal of neurological sciences* **26**: 12–19.
- Hauser, S. and S. A. Josephson, 2010 *Harrison's neurology in clinical medicine*. McGraw Hill Professional.
- Hoffmann, J. and A. Charles, 2018 Glutamate and its receptors as therapeutic targets for migraine. *Neurotherapeutics* **15**: 361–370.
- Jindal, K., R. Upadhyay, H. Singh, M. Vijay, A. Sharma, *et al.*, 2018 Migraine disease diagnosis from eeg signals using non-linear feature extraction technique. In *2018 IEEE International Conference on Computational Intelligence and Computing Research (ICIC)*, pp. 1–4, IEEE.
- Lane, R. and P. davies, 2006 *Migraine*. CRC Press.

- Lipton, R. B. and M. E. Bigal, 2006 *Migraine and other Headache Disorders*. CRC Press.
- Park, C. G. and M. K. Chu, 2022 Interictal plasma glutamate levels are elevated in individuals with episodic and chronic migraine. *Scientific Reports* **12**: 6921.
- Pietrobon, D. and M. A. Moskowitz, 2013 Pathophysiology of migraine. *Annual review of physiology* **75**: 365–391.
- Ramadan, N. M., 2003 The link between glutamate and migraine. *CNS spectrums* **8**: 446–449.
- Scheffer, M., A. van den Berg, and M. D. Ferrari, 2013 Migraine strikes as neuronal excitability reaches a tipping point. *PloS one* **8**: e72514.
- Stovner, L., K. Hagen, R. Jensen, Z. Katsarava, R. Lipton, *et al.*, 2007 The global burden of headache: a documentation of headache prevalence and disability worldwide. *Cephalalgia* **27**: 193–210.

**How to cite this article:** Garehdaghi, F., Sarbaz, Y., and Baradari, E. A Novel Hypothesis for Migraine Disease Mechanism: The Creation of a New Attractor Responsible for Migraine Disease Symptoms *Chaos Theory and Applications*, 6(1), 19-25, 2024.

**Licensing Policy:** The published articles in *Chaos Theory and Applications* are licensed under a [Creative Commons Attribution-NonCommercial 4.0 International License](https://creativecommons.org/licenses/by-nc/4.0/).



# A Novel Hyperchaotic Financial System with Hyperbolic Sinusoidal Nonlinearity: From Theoretical Analysis to Adaptive Neural Fuzzy Controller Design

Muhamad Deni Johansyah<sup>1</sup>, Seyed Mohammad Hamidzadeh<sup>2</sup>, Khaled Benkouider<sup>3</sup>, Sundarapandian Vaidyanathan<sup>4</sup>, Aceng Sambas<sup>5</sup>, Mohamad Afendee Mohamed<sup>6</sup> and Azwa Abdul Aziz<sup>7</sup>

<sup>\*</sup>Department of Mathematics, Universitas Padjadjaran, Jatinangor, Sumedang, 45363, Indonesia, <sup>a</sup>Department of Electrical Engineering, Khorasan Institute of Higher Education, Mashhad, 91898, Iran, <sup>β</sup>Department of Electronics, Faculty of Technology, Badji-Mokhtar University, Annaba 23000, Algeria, <sup>γ</sup>Centre for Control Systems, Vel Tech University, Vel Nagar, Avadi, Chennai 600 062, Tamil Nadu, India, <sup>δ</sup>Faculty of Informatics and Computing, Universiti Sultan Zainal Abidin, Campus Besut, 22200, Malaysia, <sup>†</sup>Department of Mechanical Engineering, Universitas Muhammadiyah Tasikmalaya, Tasikmalaya, Jawa Barat, 46196, Indonesia.

**ABSTRACT** Chaotic systems are known to be extremely sensitive to initial conditions, meaning small changes can have a significant impact on the outcomes. By analyzing the average profit margin in relation to chaotic dynamics, companies can conduct sensitivity analysis to assess the potential impact of various factors on their profitability. This analysis can help identify critical variables or scenarios that may significantly affect profit margins. In this article, we have proposed a hyperchaotic financial system with hyperbolic sinusoidal non-linear variables applied to the average profit margin. Furthermore, we have investigated the stability of the hyperchaotic financial dynamics model to provide information to companies to assess the consistency and reliability of their profitability. In addition, fundamental dynamic behavior like Lyapunov exponents, bifurcation analysis, coexisting attractors have been reported. Finally, a nonlinear feedback control approach is developed to train an adaptive neural fuzzy controller. The application of Lyapunov theory confirms that this nonlinear feedback controller can effectively minimize the synchronization error within a finite duration. The results from simulations establish the effectiveness of the proposed neural fuzzy controller architecture in controlling the synchronization of two hyperchaotic financial models. Additionally, the simulation includes a comparison between the performance of the nonlinear controller and the adaptive neural fuzzy controller.

## KEYWORDS

Chaotic system  
Financial system  
Dynamical analysis  
Complexity analysis  
Adaptive neural fuzzy controller

## INTRODUCTION

Chaotic behavior in financial systems often leads to increased volatility and unpredictability (Guegan 2009; Vogl 2022; Inglada-Perez 2020). By studying the average profit margin in relation to

chaotic dynamics, companies can gain a better understanding of the potential risks they face (Lux 1998; Shi *et al.* 2022; Xin *et al.* 2013). This understanding can help in developing risk management strategies and contingency plans to mitigate the adverse effects of financial instability on profitability. Moreover, chaotic behavior in financial markets can create opportunities for profit. The market fluctuations and price volatility can allow skilled investors and traders to capitalize on short-term price movements and generate profits through strategic buying and selling (Ma and Li 2020; Musaev *et al.* 2022). The ability to identify patterns or trends within chaotic behavior can provide a competitive advantage in capturing these profit opportunities.

Financial chaotic systems arise in business modelling and they have many applications in science and engineering. Many studies

**Manuscript received:** 5 August 2023,

**Revised:** 12 November 2023,

**Accepted:** 6 February 2024.

<sup>1</sup>muhamad.deni@unpad.ac.id (Corresponding author).

<sup>2</sup>s.m.hamidzadeh@khorasan.ac.ir

<sup>3</sup>benkouider.khaled@gmail.com

<sup>4</sup>sundarvtu@gmail.com

<sup>5</sup>acengssambas@unisza.edu.my, acengs@umtas.ac.id

<sup>6</sup>mafendee@unisza.edu.my

<sup>7</sup>azwaaziz@unisza.edu.my

have discussed the financial model using hyperchaotic systems approach, such as [Yu et al. \(2012\)](#) proposed hyperchaos financial system with addition variable average profit margin using quadratic nonlinear term and designed speed feedback controllers and linear feedback controllers for stabilizing hyperchaos to unstable equilibrium points. [Xin \(2009\)](#) constructed a new 4D continuous autonomous financial hyperchaotic system using a nonlinear state feedback controller. In their study, [Vargas et al. \(2015\)](#) introduced an adaptive controller aimed at achieving synchronization in hyperchaotic finance systems. The proposed controller addresses uncertainties that may arise from factors such as unknown system parameters and disturbances that vary over time or are dependent on the system's state. [Szumiński \(2018\)](#) conducted an analysis of integrability for complex dynamical systems within the context of the financial hyperchaotic model, utilizing differential Galois theory.

The primary focus of this study was to demonstrate the non-integrability of the examined system across a broad range of functions. Additionally, the research aimed to identify specific parameter values that may indicate integrability within the system. [Jahanshahi et al. \(2019\)](#) apply the four-dimensional financial hyperchaotic system and propose a unique control method for suppressing chaos and achieving synchronization in this nonlinear system. This study approach combines fuzzy logic with a fast disturbance observer and ITSMC. [Chen et al. \(2021\)](#) developed suitable control strategies for achieving synchronization between two financial systems that have different initial conditions. They also provided mathematical evidence demonstrating the effectiveness of the control law employed in their study. [Kai et al. \(2017\)](#) proposed a 4D hyperchaotic financial system derived from an existing three-dimensional nonlinear financial system. They expand upon this system by incorporating a controller term to account for the impact of control on the overall dynamics.

On the other hand, numerous findings regarding the analysis and control of financial hyperchaotic systems have been documented in the existing literature. [Bekiros et al. \(2021\)](#) introduce an optimal mixed  $H_2/H_\infty$  control approach based on type-2 fuzzy logic for a hyperchaotic financial system. Their investigation centers around the dynamical properties of the system in the presence of coexisting attractors. [Cao \(2018\)](#) designed a four-dimensional hyperchaotic finance system, which can generate double-wing chaotic and hyperchaotic attractors with three equilibrium points. [Hajipour et al. \(2018\)](#) developed a sliding mode control strategy to regulate a hyperchaotic financial model and to ensure stability of the proposed system in the face of unwanted dynamics and disturbances. To achieve this, they applied an adaptive sliding mode control scheme that aims to drive the system's states towards desired set points.

[Xu et al. \(2021\)](#) investigate the  $H_\infty$  control problem for a hyperchaotic finance system with an energy-bounded disturbance, employing a delayed feedback controller. Through the utilization of quadratic system theory, an augmented Lyapunov functional, integral inequalities, and rigorous mathematical derivations, they establish a sufficient condition based on linear matrix inequalities. This condition ensures that the closed-loop system attains desirable performance characteristics, including boundedness,  $H_\infty$  performance, and asymptotic stability. [Li et al. \(2022\)](#) introduce a novel approach to establish adequate conditions that ensure the presence and stabilization of positive solutions in a specific hyper-chaotic financial model. Their study also investigates a nonlinear chaotic financial system with diffusion by incorporating the concepts of Laplacian semigroup and impulsive control. [Rao and Zhu \(2021\)](#)

demonstrate the theoretical importance of guiding the actual financial market. Their study highlights that implementing positive and accurate macroeconomic control measures at specific frequencies can promote market stability and result in higher positive interest rates.

Specifically, the main contributions and novelty of this study can be summarized into the following points:

1. The system consists of a total eleven terms including with sinusoidal hyperbolic non-linear variables applied to the average profit margin
2. The system exhibits multistability and coexistence attractors
3. A nonlinear feedback control approach is developed to train an adaptive neural fuzzy controller

The structure of this research article is presented as follows. First, we provide a concise description of the mathematical model for the hyperchaotic financial system. Next, we carry out a dynamic analysis of the new hyperchaotic financial system. We also discuss the multistability and coexisting hyperchaotic attractors for the new hyperchaotic financial system. As a control application, we present an adaptive neural fuzzy controller for the synchronization of the new hyperchaotic financial systems and describe the simulation results. Finally, we conclude this research article with a summary of the main results.

## MODELING OF THE NOVEL FINANCIAL RISK SYSTEM

A chaotic-based financial system due to Gao and Ma [Gao and Ma \(2009\)](#) can be expressed as follows

$$\begin{cases} \dot{z}_1 &= z_3 + (z_2 - a)z_1 \\ \dot{z}_2 &= 1 - bz_2 - z_1^2 \\ \dot{z}_3 &= -z_1 - cz_3 \end{cases} \quad (1)$$

where  $a$  represents the savings,  $b$  denotes the per investment cost, and  $c$  signifies the elasticity of commercial demands, all of which are positive constants. Considering the respective values as follows:  $a = 0.9$ ,  $b = 0.2$ ,  $c = 1.2$ , and the initial state of the system is  $(z_1(0), z_2(0), z_3(0)) = (1, 2, 0.5)$ , the system (1) exhibits chaotic behavior. The Lyapunov exponents of the Gao-Ma system (1) are calculated as  $LE_1 = 0.0833$ ,  $LE_2 = 0$  and  $LE_3 = -0.6987$ . Using these values, the Kaplan-Yorke dimension of the Gao-Ma system (1) is evaluated as follows:

$$D_{KY} = 2 + \frac{LE_1 + LE_2}{|LE_3|} = 2.1192 \quad (2)$$

Furthermore, [Yu et al. \(2012\)](#) proposed 4-D hyperchaotic finance system with added average profit margin. The 4D hyperchaotic finance system [Yu et al. \(2012\)](#) has the following dynamics:

$$\begin{cases} \dot{z}_1 &= z_3 + (z_2 - a)z_1 + z_4 \\ \dot{z}_2 &= 1 - bz_2 - z_1^2 \\ \dot{z}_3 &= -z_1 - cz_3 \\ \dot{z}_4 &= -dz_1z_2 - pz_4 \end{cases} \quad (3)$$

where parameters  $a, b, c, d, p$  are held positive. Yu *et al.* (2012) showed that the system (3) exhibits hyperchaotic behavior for the following values:  $a = 0.9, b = 0.2, c = 1.5, d = 0.2$  and  $p = 0.17$ . For MATLAB simulations, the initial state of the system (3) is chosen as  $Z(0) = (1, 2, 0.5, 0.5)$ . The Lyapunov exponents of the Hyperchaotic Yu finance system (3) are calculated as  $LE_1 = 0.0344, LE_2 = 0.0180, LE_3 = 0$  and  $LE_4 = -1.1499$ .

Using these values, the Kaplan-Yorke dimension of the hyperchaotic Yu system (3) is evaluated as follows:

$$D_{KY} = 3 + \frac{LE_1 + LE_2 + LE_3}{|LE_4|} = 3.0456 \quad (4)$$

This study proposes a new finance model by combining the Gao-Ma finance model (1) and the Yu finance model (3). Specifically, we consider the effect of hyperbolic sinusoidal nonlinearity in the  $z_4$  dynamics of the system. The new hyperchaotic finance system has the following form:

$$\begin{cases} \dot{z}_1 = z_3 + (z_2 - a)z_1 + qz_4 \\ \dot{z}_2 = 1 - bz_2 - z_1^2 \\ \dot{z}_3 = -z_1 - cz_3 \\ \dot{z}_4 = -dz_1z_2 - p \sinh(z_1) \end{cases} \quad (5)$$

Eq. (5) which represents a new financial 4-D system consists of the parameters  $a, b, c, d, p, q$  that are held as positive constants taking the following values:  $a = 0.9, b = 0.2, c = 1.5, d = 0.3, p = 0.15$  and  $q = 0.1$ . Suppose also that we consider the initial state as  $Z(0) = (1, 2, 0.5, 0.5)$ .

The calculation of Lyapunov exponents for the 4-D system (5) yields the following values:  $LE_1 = 0.0382, LE_2 = 0.0298, LE_3 = 0$  and  $LE_4 = -1.0865$  which establish the hyperchaotic behavior of the system. Using these values, the Kaplan-Yorke dimension of the new hyperchaotic financial system (5) is evaluated as follows:

$$D_{KY} = 3 + \frac{LE_1 + LE_2 + LE_3}{|LE_4|} = 3.0625 \quad (6)$$

Table 1 gives a comparison of the Lyapunov exponents, maximal Lyapunov exponent (MLE) and the Kaplan-Yorke dimension ( $D_{KY}$ ) of the three financial systems expressed by (1), (3) and (5). Table 1 demonstrates that the maximum Lyapunov exponent (MLE) value of the new system (5) is greater than that of the financial systems (1) and (3). Moreover, it is also shown that the Kaplan-Yorke dimension of the new system (5) is greater than that of the financial systems (1) and (3). These are the advantages of the proposed financial chaotic system (5). A disadvantage of the new hyperchaotic system is that it includes a hyperbolic sinusoidal nonlinearity in its dynamics and for this reason, designing an electronic circuit or field programmable gate array (FPGA) design of the new financial system (5) is complicated.

Figure 1 exhibits the plot for the strange attractors and phase portraits of system (5).

Next, we solve the following system of equations for finding the equilibrium point for system (5).

$$\begin{cases} 0 = z_3 + (z_2 - a)z_1 + qz_4 \\ 0 = 1 - bz_2 - z_1^2 \\ 0 = -z_1 - cz_3 \\ 0 = -dz_1z_2 - p \sinh(z_1) \end{cases} \quad (7)$$

**Table 1** Lyapunov Exponents, MLE and Kaplan-Yorke Dimension of Three Financial Systems

Financial System	Lyapunov Exponents (LEs)	MLE Value	$D_{KY}$
Gao-Ma Financial System (1)	$LE_1 = 0.0833$ $LE_2 = 0$ $LE_3 = -0.6987$	0.0833	2.1192
Hyperchaotic Yu System (3)	$LE_1 = 0.0344$ $LE_2 = 0.0180$ $LE_3 = 0$ $LE_4 = -1.1499$	0.0344	3.0456
New Financial System (5)	$LE_1 = 0.0381$ $LE_2 = 0.0298$ $LE_3 = 0$ $LE_4 = -1.0865$	0.0381	3.0625

By performing a straightforward calculation, it can be determined that the new financial hyperchaotic system (5) possesses a unique equilibrium point given by  $E_0 = (0, 1/b, 0, 0)$ . For the hyperchaotic case,  $b = 0.2$ . In this special case, the new financial hyperchaotic system (5) has the unique equilibrium point  $E_0 = (0, 5, 0, 0)$ . We can establish the Jacobian matrix at  $E_0 = (0, 5, 0, 0)$  to be as follows:

$$J = \begin{bmatrix} 4.10 & 0 & 1 & 0.1 \\ 0 & -0.2 & 0 & 0 \\ -1 & 0 & -1.5 & 0 \\ -1.65 & 0 & 0 & 0 \end{bmatrix} \quad (8)$$

We find that the matrix  $J$  has the eigenvalues:  $\lambda_1 = 0.0484, \lambda_2 = 3.8712, \lambda_3 = -0.2$  and  $\lambda_4 = -1.3196$ . This shows that  $E_0 = (0, 5, 0, 0)$  is a saddle point and unstable equilibrium for system (5).

## DYNAMICAL ANALYSIS

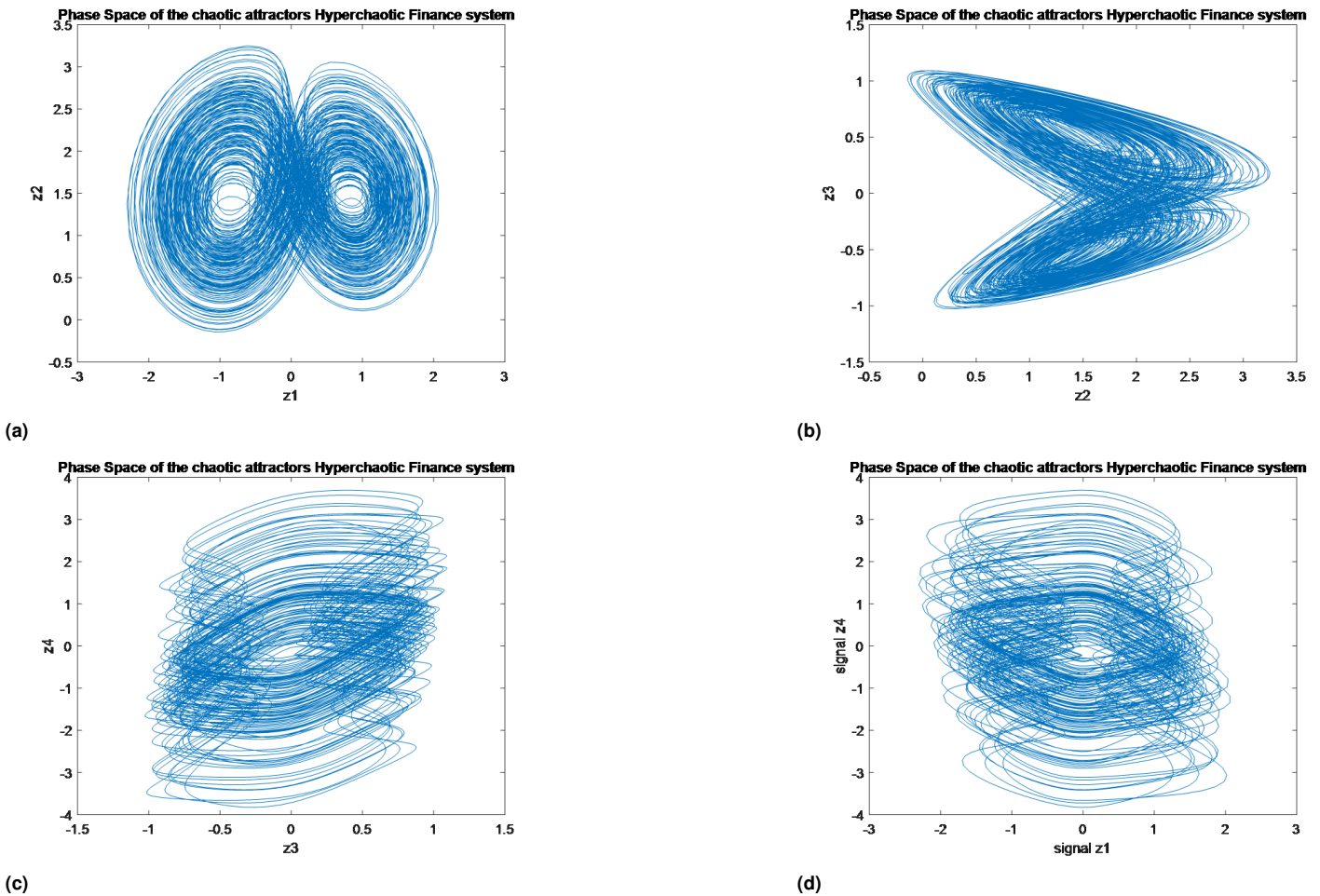
In this section, we conduct an analysis of the dynamical properties of the new hyperchaotic financial model (5) as a function of its parameters. To achieve this, we utilize various tools such as spectrum of Lyapunov exponents, bifurcation diagrams, and phase plots.

This section of the paper aims to explore how the parameters affect the behavior of the recently developed hyperchaotic finance system. To achieve this, we will utilize Lyapunov exponents spectrum, bifurcation diagrams, and phase plots. Specifically, we will focus on the case where  $Z_0 = (0.4, 0.2, 0.4, 0.4)$ .

### Bifurcation Diagram and Lyapunov Exponent

**Dynamics when  $a$  varies** Figure 2 depicts the bifurcation diagram and Lyapunov exponents spectrum of the new hyperchaotic finance system (5), where the parameter  $a$  is varied within the range  $[0, 4]$ , while the other parameters remain constant:  $b = 0.2, c = 1.5, d = 0.3, p = 0.15$ , and  $q = 0.1$ . Notably, the Lyapunov spectrum





**Figure 1** Phase portraits of the new hyperchaotic financial system (5) using MATLAB in (a)  $z_1 - z_2$  plane (b)  $z_2 - z_3$  plane, (c)  $z_3 - z_4$  plane and (d)  $z_1 - z_4$  plane

results presented in Figure 2b align with the findings obtained from the bifurcation diagram shown in Figure 2a.

When the value of  $a$  lies within the interval  $[0, 2.85]$ , the system (5) demonstrates the presence of two positive Lyapunov exponents, indicating an extreme hyperchaotic nature. The Kaplan-Yorke dimension for this behavior is measured to be  $DKY = 3.055$ . For plots, we specifically selected  $a$  to be 0.5. As a result, Figure 3a illustrates the  $z_1 - z_2$  attractor, visually representing the hyperchaotic behavior exhibited by the system (5) with the respective Lyapunov exponents having the following values:

$$\begin{pmatrix} LE_1 \\ LE_2 \\ LE_3 \\ LE_4 \end{pmatrix} = \begin{pmatrix} 0.053 \\ 0.013 \\ 0 \\ -1.042 \end{pmatrix} \quad (9)$$

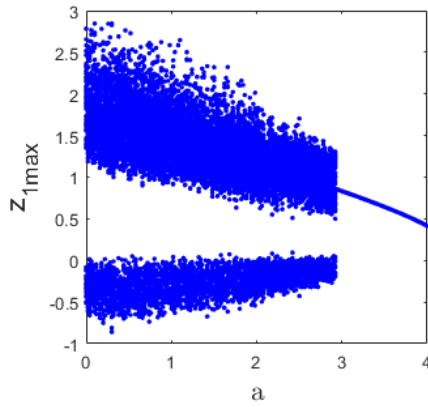
When the parameter  $a$  fall within the range  $[2.86, 3.10]$ , the system (5) demonstrates a positive maximal Lyapunov exponent, indicating the presence of chaotic behavior. The Kaplan-Yorke dimension, measured to be  $DKY = 3.011$ , further confirms the complex nature of hyperchaotic finance system (5). Specifically selecting  $a$  to be 2.95 for our plots, we observe the  $z_1 - z_2$  attractor depicted in Figure 3b, which illustrates the chaotic behavior exhibited by the system (5). The respective values for Lyapunov exponents are as follows:

$$\begin{pmatrix} LE_1 \\ LE_2 \\ LE_3 \\ LE_4 \end{pmatrix} = \begin{pmatrix} 0.0260 \\ 0 \\ -0.012 \\ -1.032 \end{pmatrix} \quad (10)$$

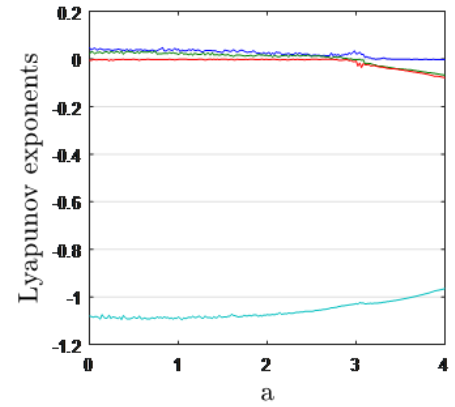
When the parameter  $a$  fall within the range  $[3.11, 4]$ , the system (5) exhibits periodic behavior without complexity. For plots, we specifically selected  $a$  to be 3.5. As a result, Figure 3c, presents the  $z_1 - z_2$  attractor, visually representing the periodic behavior displayed by the new 4D hyperchaotic finance system (5). Specific to this case, the respective Lyapunov exponents are recorded as the followings:

$$\begin{pmatrix} LE_1 \\ LE_2 \\ LE_3 \\ LE_4 \end{pmatrix} = \begin{pmatrix} 0 \\ -0.042 \\ -0.045 \\ -1.011 \end{pmatrix} \quad (11)$$

**Dynamics when  $b$  varies** In Figure 4, the bifurcation diagram and Lyapunov exponents spectrum are depicted for the finance system (5) as the parameter  $b$  changes within the range of  $[0, 0.5]$ .

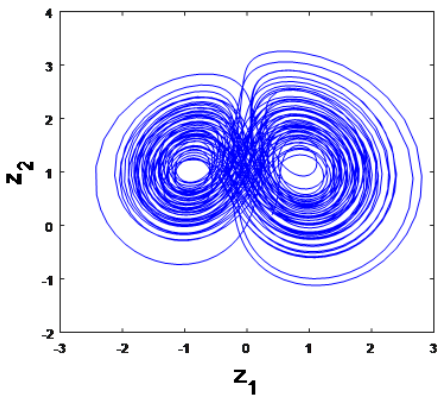


(a)

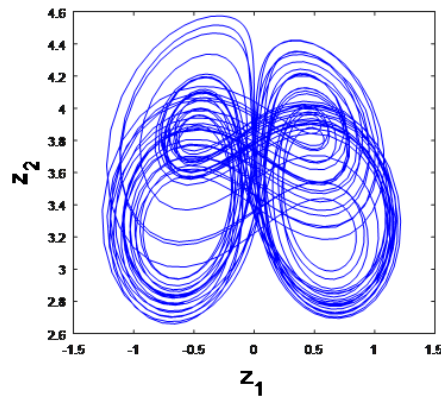


(b)

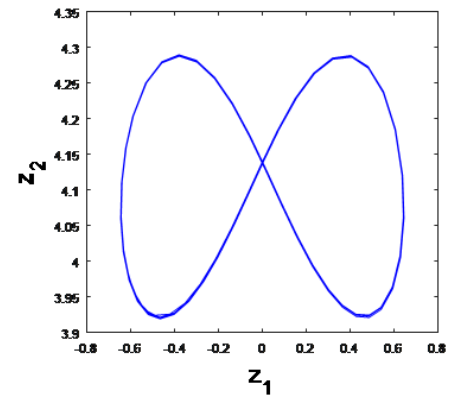
**Figure 2** Characteristics of the system (5) in terms of a) Bifurcation diagram and b) LEs spectrum when  $a \in [0, 4]$ .



(a)



(b)



(c)

**Figure 3** Output Matlab simulation (a)  $z_1 - z_2$  hyperchaotic attractor of the system (5) when  $a = 0.5$ . (b)  $z_1 - z_2$  chaotic attractor of system (3) when  $a = 2.95$  and (c)  $z_1 - z_2$  periodic orbit of the system (5) when  $a = 3.5$ .

When the parameter  $b$  falls within the range  $[0, 0.29]$ , the system (5) displays the presence of two positive Lyapunov exponents, signifying an extreme hyperchaotic nature. The Kaplan-Yorke dimension for this behavior is measured to be  $D_{KY} = 3.063$ . For plots, we specifically chose  $b$  to have a value of 0.05. Consequently, Figure 5a displays the  $z_1 - z_3$  attractor, providing a visual representation of the hyperchaotic behavior exhibited by the system (5). The associated Lyapunov exponents are as follows:

$$\begin{pmatrix} LE_1 \\ LE_2 \\ LE_3 \\ LE_4 \end{pmatrix} = \begin{pmatrix} 0.053 \\ 0.013 \\ 0 \\ -1.042 \end{pmatrix} \quad (12)$$

When the parameter  $b$  is within the range  $[0.30, 0.35]$ , the system (5) showcases a positive maximal Lyapunov exponent, indicating the presence of chaotic behavior. The measurement of the Kaplan-Yorke dimension as  $D_{KY} = 3.010$  further validates the complex nature of the system (5). For plots, we specifically selected  $b$  to have a value of 0.31. As a result, the  $z_1 - z_3$  attractor presented in Figure 5b vividly portrays the chaotic behavior exhibited by the system (5). The corresponding Lyapunov exponents are as follows:

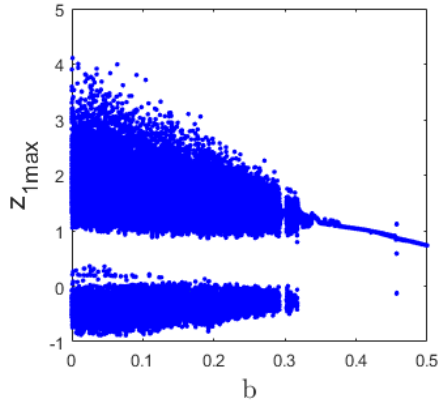
$$\begin{pmatrix} LE_1 \\ LE_2 \\ LE_3 \\ LE_4 \end{pmatrix} = \begin{pmatrix} 0.017 \\ 0 \\ -0.006 \\ -1.101 \end{pmatrix} \quad (13)$$

When the parameter  $b$  is in the range of  $[0.036, 0.5]$ , the system (5) exhibits periodic behavior without complexity. For plots, we specifically selected  $b$  to be 0.5. As a result, Figure 5c presents the  $z_1 - z_3$  attractor, visually representing the periodic behavior displayed by the system (5). The corresponding Lyapunov exponents are as follows:

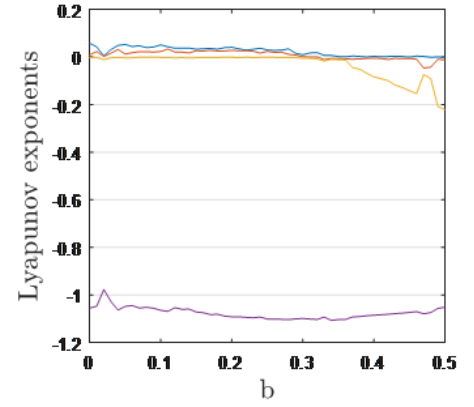
$$\begin{pmatrix} LE_1 \\ LE_2 \\ LE_3 \\ LE_4 \end{pmatrix} = \begin{pmatrix} 0 \\ -0.013 \\ -0.222 \\ -1.051 \end{pmatrix} \quad (14)$$

**Dynamics when  $c$  varies** For system (3), the Bifurcation diagram and Lyapunov exponents spectrum are depicted as in Figure 6 as the value of  $c$  ranges from 0 to 1.5.

When  $c$  belongs to the intervals  $([0, 0.84], [0.98, 1.01])$ , the system (5) has one zero and three negative Lyapunov exponents,

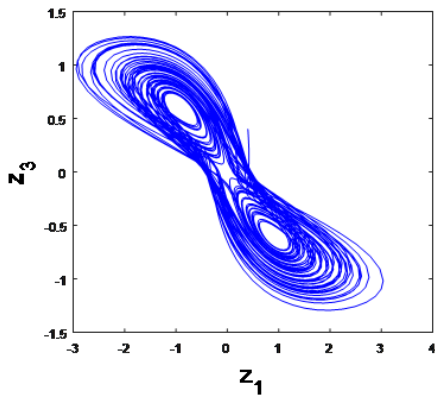


(a)

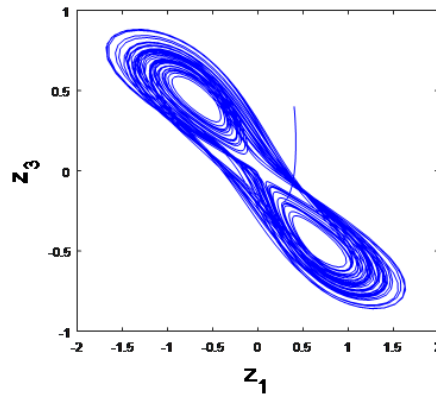


(b)

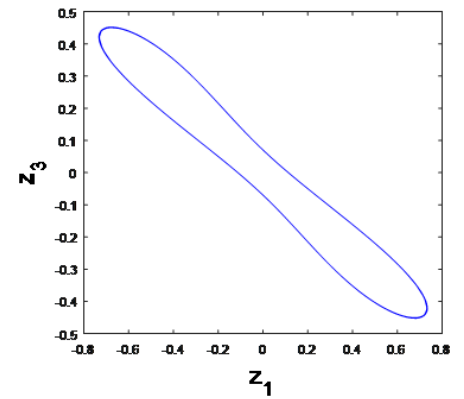
**Figure 4** Characteristics of the system (5) in terms of a) Bifurcation diagram and b) LEs spectrum when  $b \in [0, 0.5]$ .



(a)



(b)



(c)

**Figure 5** Output Matlab simulation (a)  $z_1 - z_3$  hyperchaotic attractor of system (3) when  $b = 0.5$ . (b)  $z_1 - z_3$  chaotic attractor of the system (5) when  $b = 0.31$  and (c)  $z_1 - z_3$  periodic orbit of the system (5) when  $b = 0.5$ .

indicating the emergence of periodic behavior. For plots, we have chosen the parameter  $c = 0.5$ . Subsequently, Figure 7a illustrates the  $z_2 - z_3$  attractor, which clearly demonstrates the periodic behavior of the system (5). The corresponding Lyapunov exponents are as follows:

$$\begin{pmatrix} LE_1 \\ LE_2 \\ LE_3 \\ LE_4 \end{pmatrix} = \begin{pmatrix} 0 \\ -0.025 \\ -0.133 \\ -0.134 \end{pmatrix} \quad (15)$$

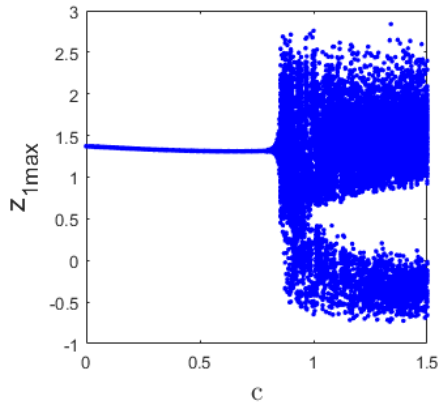
When  $c$  belongs to the intervals  $([0.84, 0.87], [0.91, 0.98], [1.01, 1.15])$ , the system (5) demonstrates a positive maximal Lyapunov exponent, and the Kaplan-Yorke dimension yields a fractional value of  $D_{KY} = 3.072$ . These characteristics indicate that the system (5) exhibits complex chaotic behavior. For plots, we have selected the parameter  $c = 1.02$ . Subsequently, Figure 7b illustrates the  $z_2 - z_3$  attractor, clearly showcasing the chaotic behavior of the system (5). The corresponding Lyapunov exponents are as follows:

$$\begin{pmatrix} LE_1 \\ LE_2 \\ LE_3 \\ LE_4 \end{pmatrix} = \begin{pmatrix} 0.061 \\ 0 \\ -0.025 \\ -0.502 \end{pmatrix} \quad (16)$$

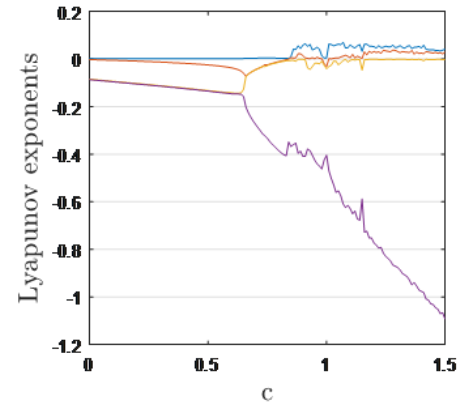
In the range where  $c$  belongs to  $([0.87, 0.91], [1.15, 1.5])$ , the system (5) showcases two positive Lyapunov exponents, indicating the presence of extreme hyperchaotic behavior. The system also possesses a fractional value of the Kaplan-Yorke dimension, with  $D_{KY} = 3.090$ . For plots, we have chosen the parameter  $c = 1.35$ . Subsequently, Figure 7c illustrates the  $z_2 - z_3$  attractor, effectively demonstrating the hyperchaotic behavior of the system (5). The corresponding Lyapunov exponents are as follows:

$$\begin{pmatrix} LE_1 \\ LE_2 \\ LE_3 \\ LE_4 \end{pmatrix} = \begin{pmatrix} 0.057 \\ 0.027 \\ 0 \\ -0.929 \end{pmatrix} \quad (17)$$

**Dynamics when  $d$  varies** For the system (5), the Bifurcation diagram and Lyapunov exponents spectrum are plotted as in Figure 8 when  $d$  varies in the region  $[-0.3, 0.3]$ .

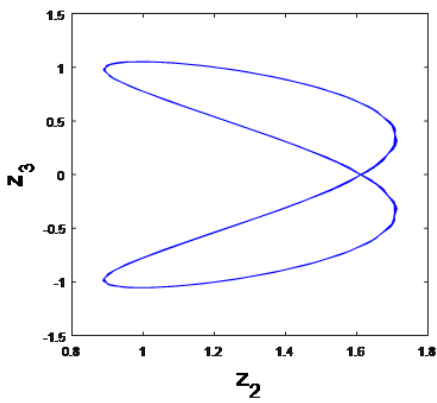


(a)

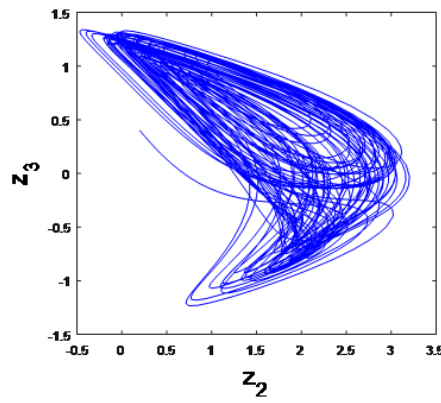


(b)

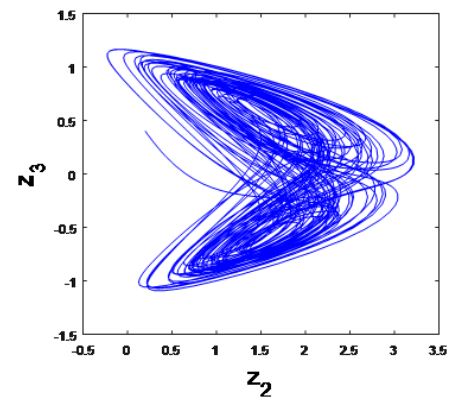
**Figure 6** Characteristics of system (3) in terms of a) Bifurcation diagram and b) LEs spectrum when  $c \in [0, 1.5]$ .



(a)



(b)



(c)

**Figure 7** Output Matlab simulation (a)  $z_2 - z_3$  hyperchaotic attractor of the system (5) when  $c = 0.5$ . (b)  $z_2 - z_3$  chaotic attractor of the system (5) when  $c = 1.02$  and (c)  $z_2 - z_3$  periodic orbit of the system (5) when  $c = 1.35$ .

When  $d$  belongs to the interval  $[-0.3, -0.14]$ , the system (5) exhibits four negative Lyapunov exponents, indicating its convergence to a stable state. Figure 9a illustrates the  $z_1 - z_4$  attractor for  $d = -0.3$ . The corresponding Lyapunov exponents are as follows:

$$\begin{pmatrix} LE_1 \\ LE_2 \\ LE_3 \\ LE_4 \end{pmatrix} = \begin{pmatrix} -0.029 \\ -0.405 \\ -0.409 \\ -1.126 \end{pmatrix} \quad (18)$$

When the value of  $d$  falls within the range  $[-0.13, 0.03]$ , the system (5) demonstrates the presence of one positive Lyapunov exponent, resulting in a fractional value of the Kaplan-Yorke dimension  $D_{KY} = 3.034$ . This indicates that the system (5) exhibits complex chaotic behavior. Figure 9b showcases the  $z_1 - z_4$  attractor for  $d = 0$ , illustrating the chaotic behavior of the system (5). The corresponding Lyapunov exponents are as follows:

$$\begin{pmatrix} LE_1 \\ LE_2 \\ LE_3 \\ LE_4 \end{pmatrix} = \begin{pmatrix} -0.055 \\ 0 \\ -0.020 \\ -1.040 \end{pmatrix} \quad (19)$$

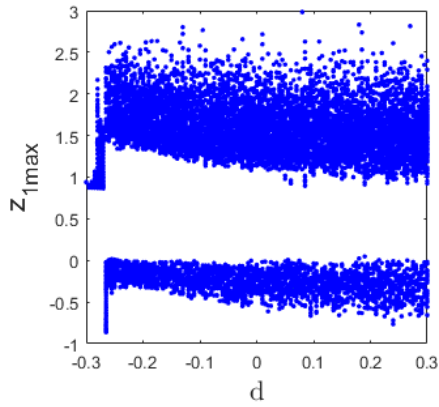
When the value of  $d$  lies within the interval  $[0.04, 0.3]$ , the sys-

tem (5) showcases two positive Lyapunov exponents, indicating its extreme hyperchaotic behavior. Moreover, the Kaplan-Yorke dimension takes on a fractional value of  $D_{KY} = 3.051$ . Figure 9c represents the plotted  $z_1 - z_4$  attractor for  $d = 0.2$ , effectively demonstrating the hyperchaotic behavior of the system (5). The corresponding Lyapunov exponents are as follows:

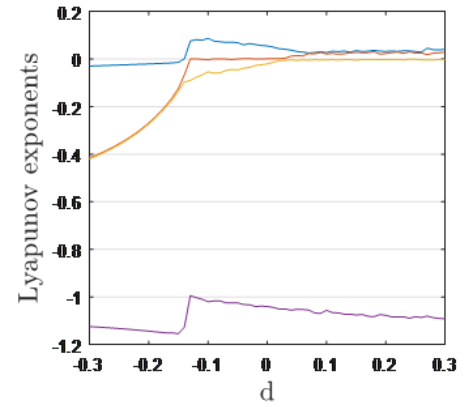
$$\begin{pmatrix} LE_1 \\ LE_2 \\ LE_3 \\ LE_4 \end{pmatrix} = \begin{pmatrix} 0.032 \\ 0.023 \\ 0 \\ -1.077 \end{pmatrix} \quad (20)$$

**Dynamics when  $p$  varies** Figure 10 illustrates the Bifurcation diagram and Lyapunov exponents spectrum of the system (5) while the value of  $p$  varies between 0 and 3.

When the parameter  $p$  falls within the range  $[0, 0.7]$ , the system (5) exhibits extreme hyperchaotic behavior. The Kaplan-Yorke dimension for this behavior is measured to be  $DKY = 3.062$ . Figure 11a displays the  $z_2 - z_4$  hyperchaotic attractor for  $p = 0.1$ . The associated Lyapunov exponents are as follows:

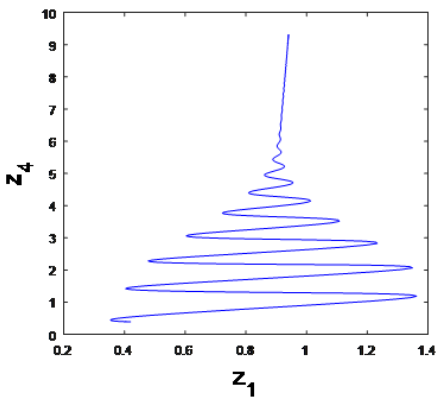


(a)

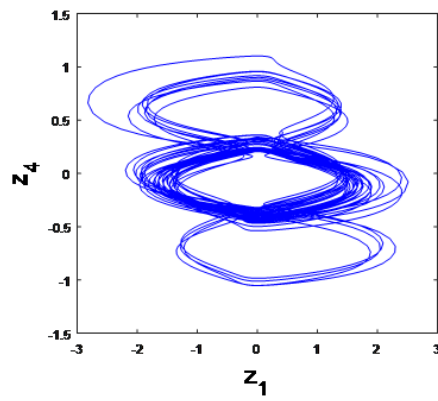


(b)

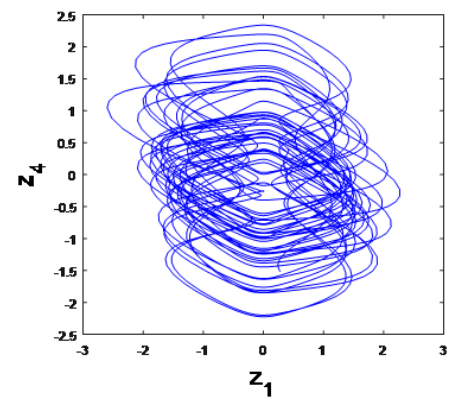
**Figure 8** Characteristics of the system (5) in terms of a) Bifurcation diagram and b) LEs spectrum when  $d \in [-0.3, 0.3]$ .



(a)



(b)



(c)

**Figure 9** Output Matlab simulation (a)  $z_1 - z_4$  hyperchaotic attractor of the system (5) when  $d = 0.5$ . (b)  $z_1 - z_4$  chaotic attractor of the system (5) when  $d = 0$  and (c)  $z_1 - z_4$  periodic orbit of the system (5) when  $d = 0.2$ .

$$\begin{pmatrix} LE_1 \\ LE_2 \\ LE_3 \\ LE_4 \end{pmatrix} = \begin{pmatrix} 0.041 \\ 0.026 \\ 0 \\ -1.086 \end{pmatrix} \quad (21)$$

When the parameter  $p$  is within the range  $[0.8, 1.7]$ , the system (5) showcases a positive maximal Lyapunov exponent, indicating the presence of chaotic behavior with  $D_{KY} = 3.033$ . Figure 11b portrait the  $z_2 - z_4$  chaotic attractor exhibited by the system (5) for  $p = 1.2$ . The corresponding Lyapunov exponents are as follows:

$$\begin{pmatrix} LE_1 \\ LE_2 \\ LE_3 \\ LE_4 \end{pmatrix} = \begin{pmatrix} 0.076 \\ 0 \\ -0.039 \\ -1.119 \end{pmatrix} \quad (22)$$

When the parameter  $p$  is in the range of  $[1.8, 3]$ , the system (5) exhibits periodic behavior without complexity. Figure 11c presents the  $z_2 - z_4$  attractor, visually representing the periodic behavior displayed by the system (5) for  $p = 3$ . The corresponding Lyapunov exponents are as follows:

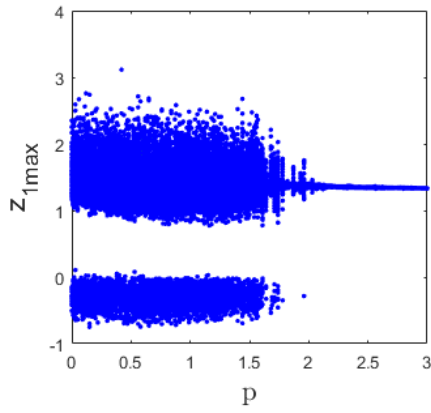
$$\begin{pmatrix} LE_1 \\ LE_2 \\ LE_3 \\ LE_4 \end{pmatrix} = \begin{pmatrix} 0 \\ -0.020 \\ -0.023 \\ -1.146 \end{pmatrix} \quad (23)$$

**Dynamics when  $q$  varies** For system (5), the Bifurcation diagram and Lyapunov exponents spectrum are illustrated as in Figure 12 as the value of  $q$  ranges from 0 to 0.5.

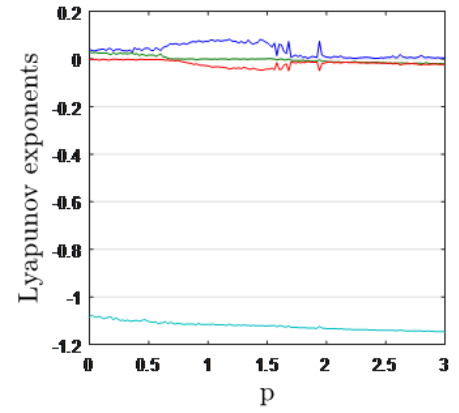
When  $q = 0$ , the system (5) exhibits periodic behavior. Figure 13a illustrates the  $z_3 - z_4$  attractor, which clearly demonstrates the periodic behavior of the system (5). The corresponding Lyapunov exponents are as follows:

$$\begin{pmatrix} LE_1 \\ LE_2 \\ LE_3 \\ LE_4 \end{pmatrix} = \begin{pmatrix} 0 \\ 0 \\ -0.010 \\ -0.947 \end{pmatrix} \quad (24)$$

When  $q$  belongs to the interval  $[0.01, 0.28]$ , system (3) exhibits complex hyperchaotic behavior with  $D_{KY} = 3.055$ . For plots, we have selected the parameter  $q = 0.2$ . Subsequently, Figure 13b illustrates the  $z_3 - z_4$  attractor. The corresponding Lyapunov exponents are as follows:

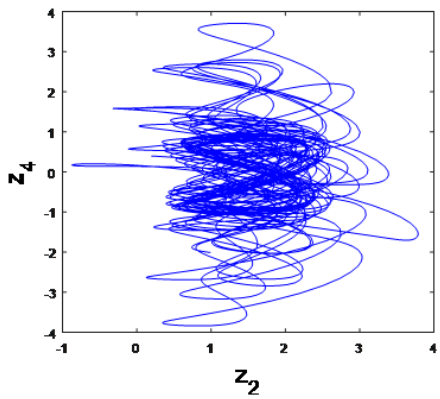


(a)

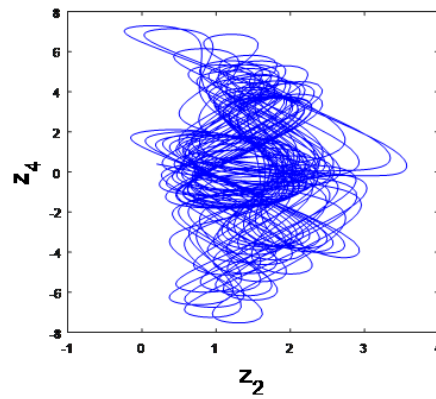


(b)

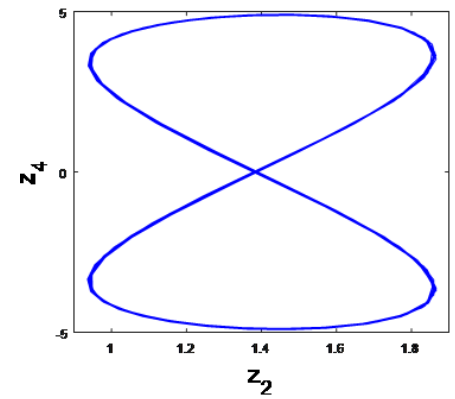
**Figure 10** Characteristics of the system (5) in terms of a) Bifurcation diagram and b) LEs spectrum when  $p \in [0, 3]$ .



(a)



(b)



(c)

**Figure 11** Output Matlab simulation (a)  $z_2 - z_4$  hyperchaotic attractor of the system (5) when  $p = 0.1$ . (b)  $z_2 - z_4$  chaotic attractor of the system (5) when  $p = 1.2$  and (c)  $z_2 - z_4$  periodic orbit of the system (5) when  $p = 3$ .

$$\begin{pmatrix} LE_1 \\ LE_2 \\ LE_3 \\ LE_4 \end{pmatrix} = \begin{pmatrix} 0.048 \\ 0.013 \\ 0 \\ -1.106 \end{pmatrix} \quad (25)$$

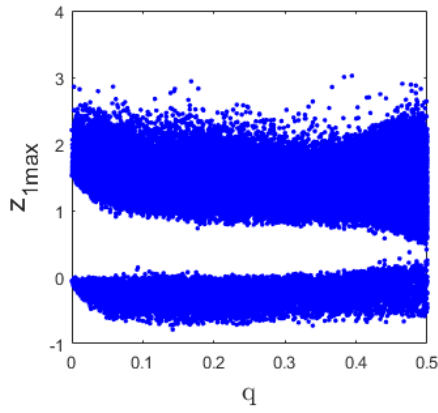
In the range where  $q$  belongs to  $[0.29, 0.5]$ , the system (5) generates chaotic behavior. The system also possesses a fractional value of the Kaplan-Yorke dimension, with  $DKY = 3.017$ . Figure 13c illustrates the  $z_3 - z_4$  attractor for  $q = 0.5$ . The corresponding Lyapunov exponents are as follows:

$$\begin{pmatrix} LE_1 \\ LE_2 \\ LE_3 \\ LE_4 \end{pmatrix} = \begin{pmatrix} 0.093 \\ 0 \\ -0.074 \\ -1.122 \end{pmatrix} \quad (26)$$

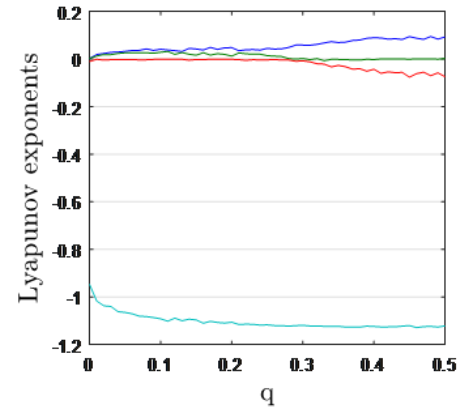
**Multistability and Coexisting Attractors** The new 4D hyperchaotic finance system (5) possesses the ability to exhibit multiple coexisting attractors. To explore this phenomenon further, we examine the system's behavior using two distinctive starting points:  $Z_{01} = (0.4, 0.2, -0.4, 0.4)$  and  $Z_{02} = (0.4, 0.2, 0.4, 0.4)$ .

When the parameters  $a = 0.9, b = 0.2, c = 1, d = 0.3, p = 0.15$ , and  $q = 0.1$  are held constant, the finance system (5) exhibits two distinct periodic behaviors based on its initial conditions, as illustrated in Figure 14. The figure showcases three separate representations denoted as (a), (b), and (c).

In the presence of parameters,  $a = 0.9, b = 0.2, c = 1.05, d = 0.3, p = 0.15$ , and  $q = 0.1$ , the finance system (5) reveals the presence of two distinct chaotic attractors, determined by the selection of initial conditions ( $Z_{01}$  or  $Z_{02}$ ), as depicted in Figure 15. The figure encompasses three different representations, labeled as (a), (b), and (c).

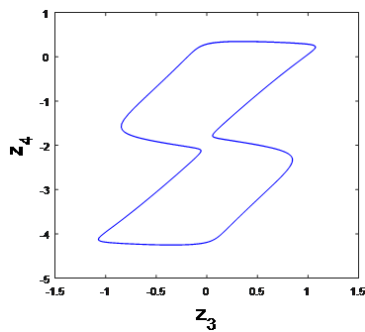


(a)

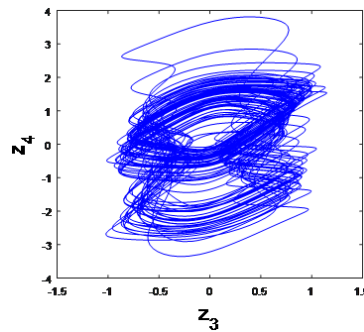


(b)

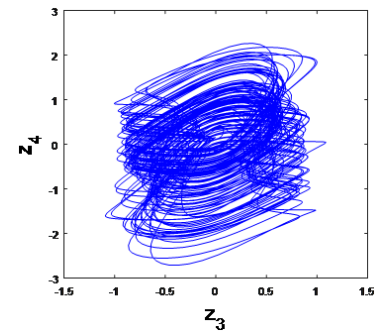
**Figure 12** Characteristics of the system (5) in terms of a) Bifurcation diagram and b) LEs spectrum when  $q \in [0, 0.5]$ .



(a)



(b)



(c)

**Figure 13** Output Matlab simulation (a)  $z_3 - z_4$  hyperchaotic attractor of the system (5) when  $q = 0.1$ . (b)  $z_3 - z_4$  chaotic attractor of the system (5) when  $q = 0.2$  and (c)  $z_3 - z_4$  periodic orbit of the system (5) when  $q = 0.5$ .

## SYNCHRONIZATION OF HYPERCHAOTIC FINANCE SYSTEM WITH GENERAL ADAPTIVE NEURAL FUZZY CONTROLLER METHOD

### Nonlinear Control Design

To synchronize two hyperchaotic financial systems modelled by the dynamics (5), first consider the following master-slave equations where index  $m$  is for master and index  $s$  is for slave.

$$\begin{cases} \dot{z}_{m1} = z_{m3} + (z_{m2} - a)z_{m1} + qz_{m4} \\ \dot{z}_{m2} = 1 - bz_{m2} - z_{m1}^2 \\ \dot{z}_{m3} = -z_{m1} - cz_{m3} \\ \dot{z}_{m4} = -dz_{m1}z_{m2} - p \sinh(z_{m1}) \end{cases} \quad (27)$$

$$\begin{cases} \dot{z}_{s1} = z_{s3} + (z_{s2} - a)z_{s1} + qz_{s4} + u_1 \\ \dot{z}_{s2} = 1 - bz_{s2} - z_{s1}^2 + u_2 \\ \dot{z}_{s3} = -z_{s1} - cz_{s3} + u_3 \\ \dot{z}_{s4} = -dz_{s1}z_{s2} - p \sinh(z_{s1}) + u_4 \end{cases} \quad (28)$$

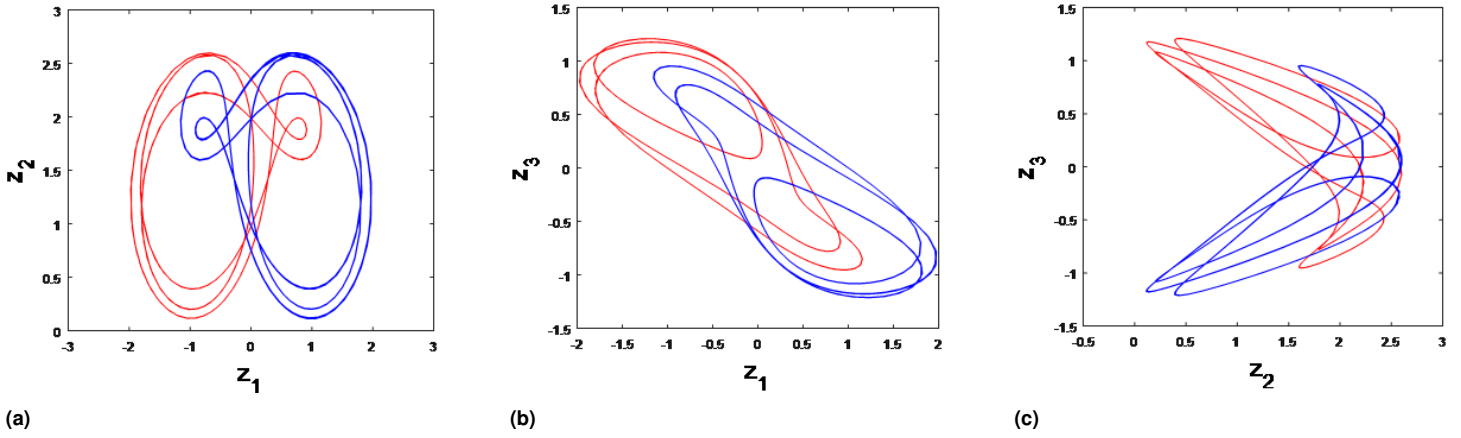
where  $u_i$  is the controller (decision variable) that should direct the equations of the slave system to the equations of the master system. Figure 16 shows that by having different values of initial conditions for the two hyperchaotic financial systems, the behavior of the system will be different.

The first goal in designing a nonlinear controller is to determine the system error equation. So:

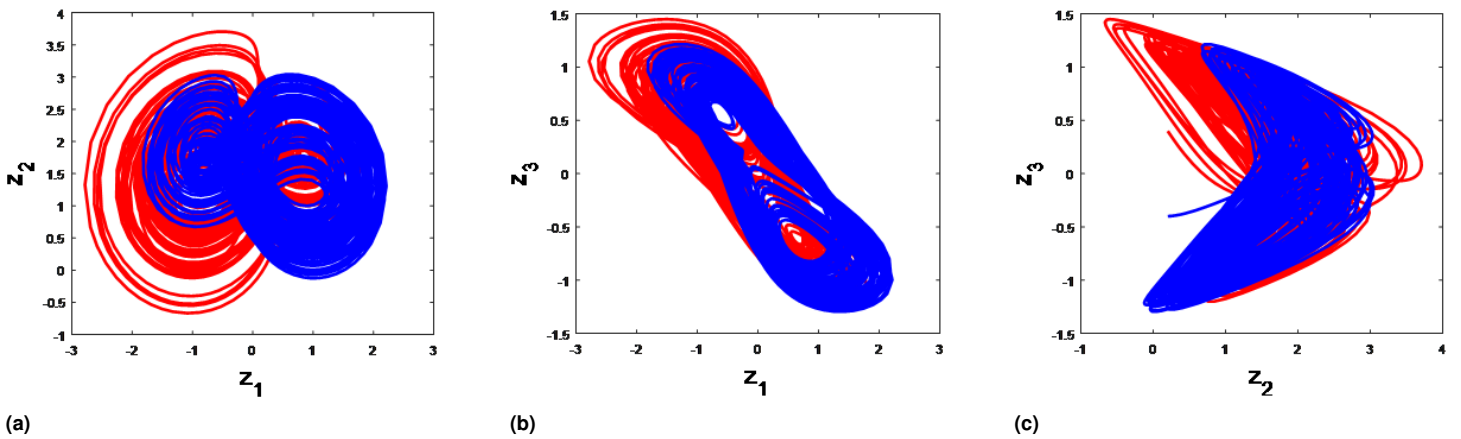
$$\begin{cases} e_1 = z_{s1} - z_{m1} \\ e_2 = z_{s2} - z_{m2} \\ e_3 = z_{s3} - z_{m3} \\ e_4 = z_{s4} - z_{m4} \end{cases} \quad (29)$$

The main goal in controller design is to reach

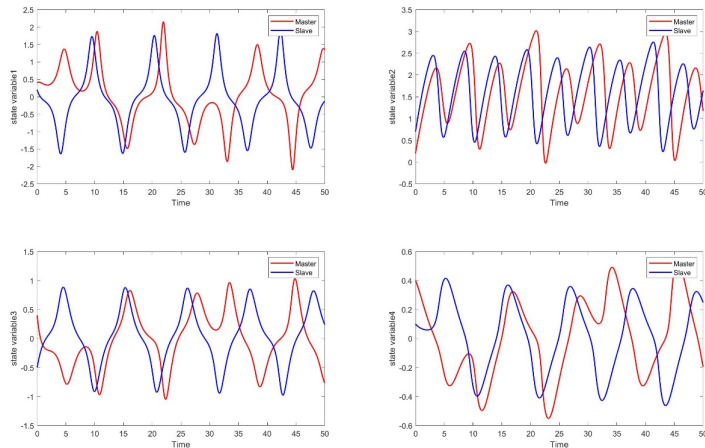
$$\lim_{t \rightarrow \infty} \|e_i(t)\| = 0 \quad (i = 1, 2, 3, 4) \quad (30)$$



**Figure 14** Matlab plots of the coexisting periodic/periodic attractors generated by the new 4D finance system (5), where the attractors generated from  $Z_{01}$  are in blue color, while attractors generated from  $Z_{02}$  are in red color. (a)  $z_1 - z_2$  plane, (b)  $z_1 - z_3$  plane and (c)  $z_2 - z_3$  plane.



**Figure 15** MATLAB plots of the coexisting chaotic/chaotic attractors generated by the new finance system (5), where the attractors generated from  $Z_{01}$  are in blue color, while the attractors generated from  $Z_{02}$  are in red color. (a)  $z_1 - z_2$  plane, (b)  $z_1 - z_3$  plane and (c)  $z_2 - z_3$  plane.



**Figure 16** Behavior of two 4D hyperchaotic systems for initial conditions  $z_{m1}(0) = 0.4, z_{m2}(0) = 0.2, z_{m3}(0) = 0.4, z_{m4}(0) = 0.4$  and  $z_{s1}(0) = 0.2, z_{s2}(0) = 0.7, z_{s3}(0) = -0.5, z_{s4}(0) = 0.1$

$$\begin{cases} \dot{e}_1 = e_3 + qe_4 + (z_{s2} - a)z_{s1} - (z_{m2} - a)z_{m1} + u_1 \\ \dot{e}_2 = -be_2 - z_{s1}^2 + z_{m1}^2 + u_2 \\ \dot{e}_3 = -e_1 - ce_3 + u_3 \\ \dot{e}_4 = -d(z_{s1}z_{s2} - z_{m1}z_{m2}) - p(\sinh(z_{s1}) - \sinh(z_{m1})) + u_4 \end{cases} \quad (31)$$

**Theorem 1.** The slave hyperchaotic finance system (28) will synchronize with the hyperchaotic finance system (27) if the controller is chosen as follows.

$$\begin{cases} u_1 = -e_3 - qe_4 - (z_{s2} - a)z_{s1} + (z_{m2} - a)z_{m1} + \lambda_1 e_1 \\ u_2 = be_2 + z_{s1}^2 - z_{m1}^2 + \lambda_2 e_2 \\ u_3 = e_1 + ce_3 + \lambda_3 e_3 \\ u_4 = d(z_{s1}z_{s2} - z_{m1}z_{m2}) + p(\sinh(z_{s1}) - \sinh(z_{m1})) + \lambda_4 e_4 \end{cases} \quad (32)$$

From equation (29), we derive:

*Proof.* To prove the stability of the candidate Lyapunov function,



it is considered as follows

$$V_i(e) = \sum_{i=1}^4 \frac{1}{2} e_i^2 = \frac{1}{2} (e_1^2 + e_2^2 + e_3^2 + e_4^2) \quad (33)$$

□

If we derive from the equation (31), we have

$$\dot{V} = e_1 \dot{e}_1 + e_2 \dot{e}_2 + e_3 \dot{e}_3 + e_4 \dot{e}_4 \quad (34)$$

By substituting equation (29) and (31) in the equation (34) and finally by substituting the proposed nonlinear controller, we have:

$$\dot{V} = \lambda_1 e_1^2 + \lambda_2 e_2^2 + \lambda_3 e_3^2 + \lambda_4 e_4^2 < 0 \quad (35)$$

where  $\lambda_i, (i = 1, 2, 3, 4)$  are the controlling gains chosen to be negative. This completes the proof. ■

### Nonlinear control design simulation results

Considering the same initial conditions as before, also the controller gain is equal to  $\lambda_i (i = 1, 2, 3, 4) = -2$ , Figure 17 shows the synchronization of two hyper-chaotic finance systems given by (27) and (28). The controller is applied to the model since  $t = 20$ . Figure 17 shows the synchronization of two hyperchaotic systems by the proposed nonlinear method.

Figure 18 shows the behavior of the non-linear controller (decision variable) that has been applied to the hyper-chaotic slave system (28) from  $T = 20$ . Figure 19 shows that the synchronization error in the proposed method tends to zero after passing a short period of time.

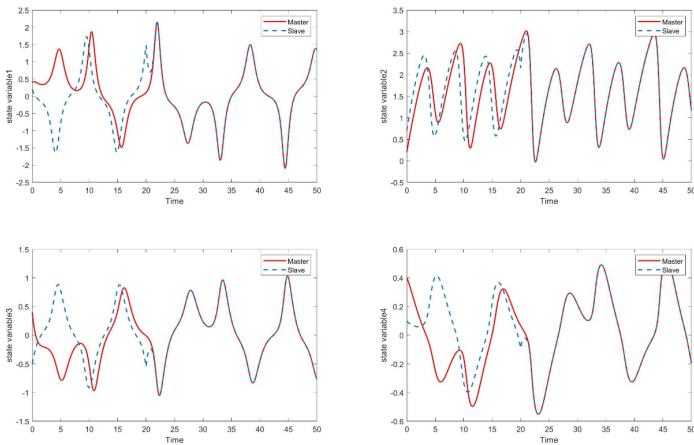


Figure 17 Synchronization of two hyperchaotic finance systems (27) and (28) in a non-linear way

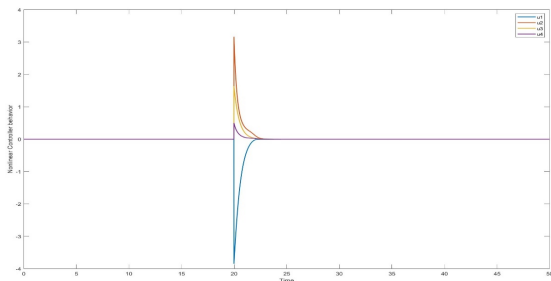


Figure 18 Non-linear controller behavior (decision variable)

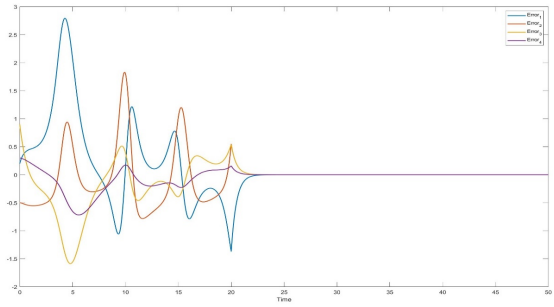


Figure 19 Synchronization error of two hyperchaotic finance systems (27) and (28) by nonlinear control method

By increasing the gain of the nonlinear controller, the convergence speed of the error can be adjusted to zero. But this issue will face problems in the real world. To prove, gains are equal to  $\lambda_i (i = 1, 2, 3, 4) = -3$  will be considered (See Figure 20). Also, to ensure the performance of the proposed method, the controller application time has also been changed. The initial conditions are unchanged. The synchronization error of two hyperchaotic systems with gains can be seen in Figure 21.

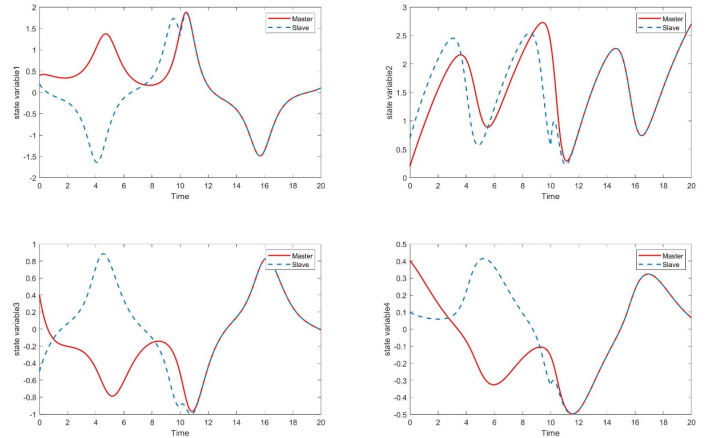


Figure 20 Synchronization of two hyperchaotic finance systems (27) and (28) with gains  $\lambda_i (i = 1, 2, 3, 4) = -3$

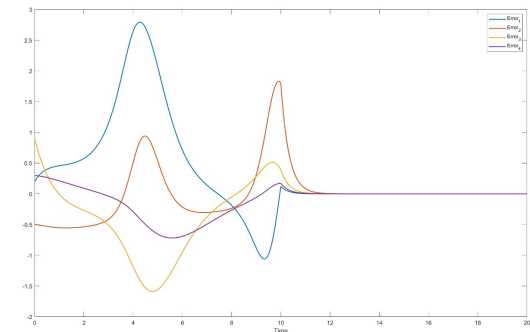
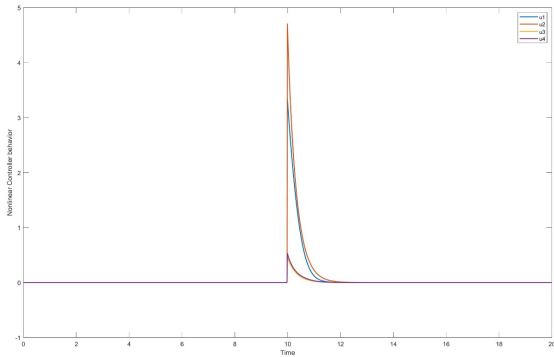


Figure 21 Synchronization error of two hyperchaotic finance systems (27) and (28) with gains

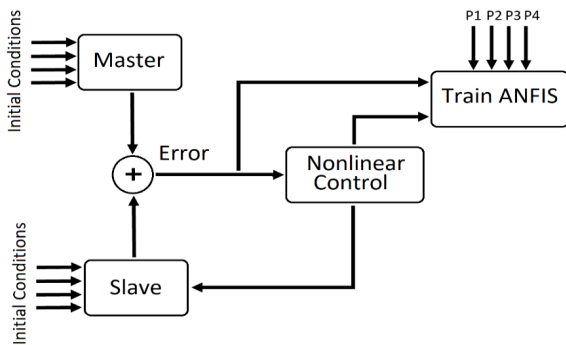


**Figure 22** Behavior of nonlinear controller with gains  $\lambda_i (i = 1, 2, 3, 4) = -3$

### Training and Test of General Adaptive Neural Fuzzy Controller

For ANFIS training, the training data must be determined first. The block diagram in Figure 23 shows how the training data is extracted from the nonlinear controller. As can be seen in Figure 23, training data is entered in ANFIS training block and training is completed by setting  $P_1$  to  $P_4$  parameters. The parameters  $P_1$  to  $P_4$  are given in Table 2. An important principle in fuzzy neural network training is what part of controller behavior and error to use for training.

In Figure 22, the controller's action time is  $t = 10$ , which has reached zero at the approximate time of  $t = 12.5$ . Also, in Figure 21, in the interval  $10 < t < 12.5$ , the system error has reached zero. Therefore, training data should be selected from time  $t$  equal to  $10 < t < 12.5$ . This is precisely the learning of the nature of hyperchaotic systems. Note that the time step is equal to 0.01.



**Figure 23** The concept of learning the adaptive neural fuzzy network with the nonlinear control method

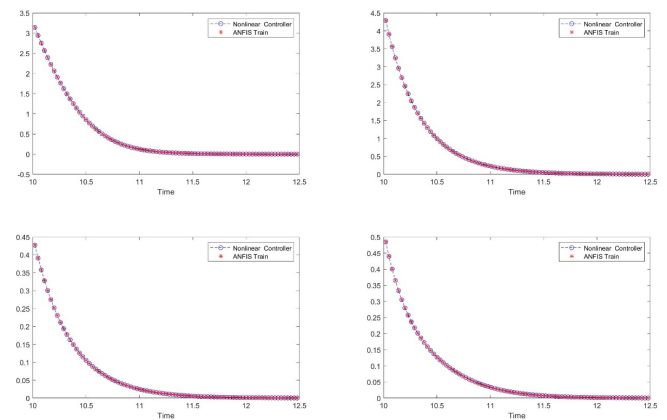
Considering that the condition for stopping training is to reach zero error or the number of epochs, in this article, the number of epochs of training has led to stopping training. Figure 24 shows that the fuzzy neural network has trained the nonlinear controller well. Figure 25 shows the error of the proposed method for training.

### Numerical Simulation and Comparison between the performance of two methods of controlling nonlinear and fuzzy adaptive neural feedback

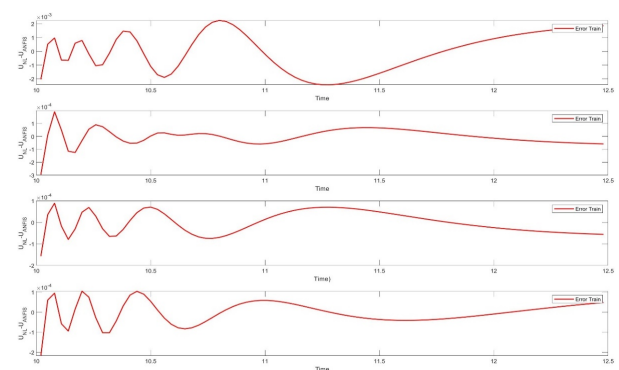
Now the exquisite controller design is finished. ANFIS controller is replaced by non-linear controller. In the numerical simulation, the initial conditions of the slave financial finance system are set equal to  $z_{s1}(0) = 0.1, z_{s2}(0) = -0.2, z_{s3}(0) = 0.1, z_{s4}(0) = 0.5$ , and

**Table 2** Proposed fuzzy neural network architecture

Total number of trainings	250
Number of training pairs	83
Number of check pairs	83
Number of test pairs	84
Number of input / output membership function (P1)	5
Input / Output Membership Function Type (P2)	'gaussmf'
epoch (P3)	80
Training error (P4)	0



**Figure 24** Comparison between the behavior of the nonlinear controller and the trained behavior of the ANFIS controller



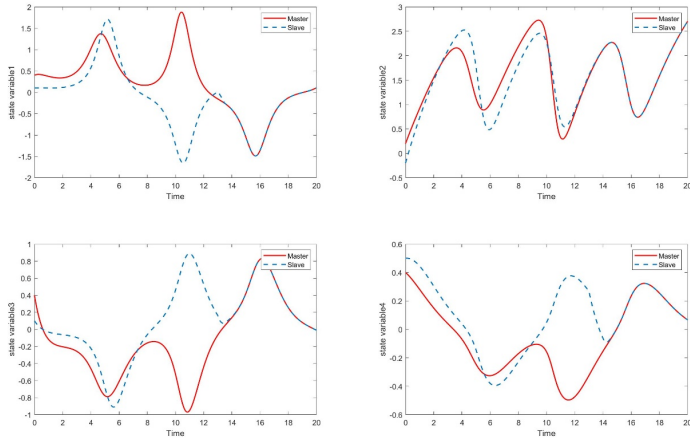
**Figure 25** ANFIS controller training error

the initial conditions for the master financial hyperchaotic system are taken as  $z_{m1}(0) = 0.4, z_{m2}(0) = 0.2, z_{m3}(0) = 0.4, z_{m4}(0) = 0.4$ . To ensure the performance of the controller, the time of its application to the system will also be changed. Figure 26 shows the synchronization of two hyperchaotic finance systems (27) and (28) using ANFIS control method. The application time of ANFIS controller is  $t = 13$ .

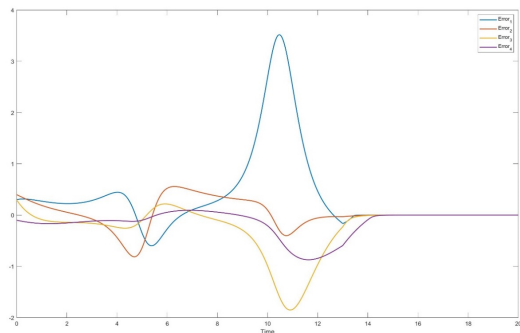
In the last part of the numerical simulation, the performance of two non-linear and infinite control methods is compared. For this purpose we regulate the initial conditions of the two hyperchaotic

**Table 3** Comparison of mean least square error

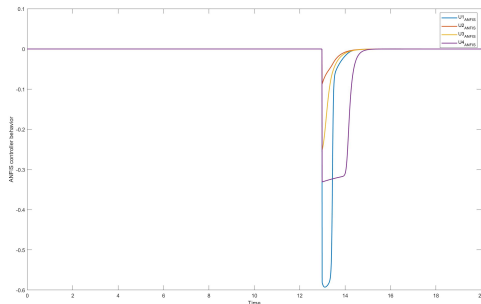
Type Control	MSE (E1)	MSE (E2)	MSE (E3)	MSE (E4)
Nonlinear	0.0983	0.1379	0.0270	0.0098
ANFIS	0.0980	0.1382	0.0273	0.0098



**Figure 26** Synchronization of two hyperchaotic finance systems (27) and (28) by ANFIS control method

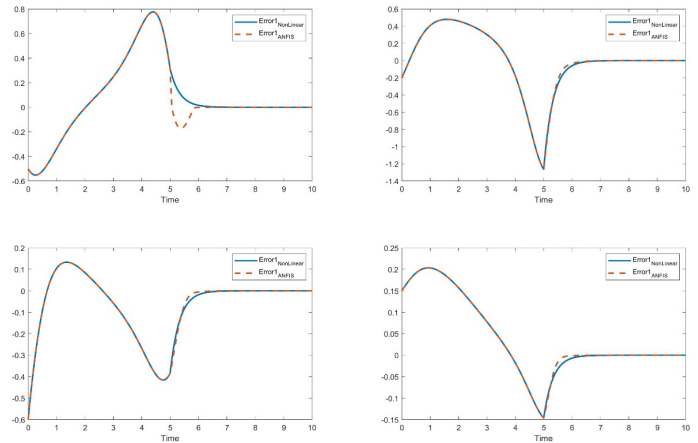


**Figure 27** Synchronization error of two hyperchaotic finance systems (27) and (28) using ANFIS control method

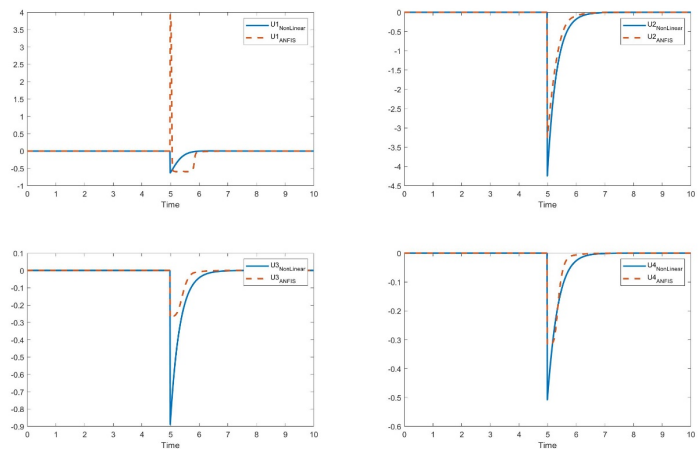


**Figure 28** ANFIS controller behavior for synchronization of two hyperchaotic finance systems (27) and (28)

finance systems (27) and (28) as unchanged, while that of the slave hyperchaotic system equals to  $z_{s1}(0) = 0.9, z_{s2}(0) = 0.4, z_{s3}(0) =$



**Figure 29** comparing the error of two controllers with the same simulation conditions



**Figure 30** The comparison of the behavior of two controllers with the same simulation conditions

$1, z_{s4}(0) = 0.25.$

The gains of the nonlinear controller are equal to  $\lambda_i (i = 1, 2, 3, 4) = -3$ . The controller is applied at time  $t=5$ . Figure 29 shows the error of two non-linear and ANFIS controllers for each variable of the financial hyper chaotic system. As can be seen from Figure 29, the error behavior in all variables of the hyperchaotic system was almost the same for both methods. Table 3 shows the mean of the least squares error for each variable.

Figure 30 shows the behavior of two nonlinear and ANFIS controllers while the simulation conditions of both were the same. Controller behavior in the real world represents implementation costs. Therefore, this behavior must be analyzed after designing the controller. In the analysis of the behavior of the controller for the first variable, the range of the ANFIS controller is much higher than the nonlinear controller, but in the fourth variable, the range of the nonlinear controller is more than the ANFIS. In the other two variables (second and third), the range of the nonlinear controller is higher.

## CONCLUSION

In this article, we investigated the new 4D hyperchaotic financial system with sinusoidal hyperbolic non-linear variables applied to the average profit margin. The bifurcation diagrams, Lyapunov exponents, and multistability, have all been used to explain the complexity behavior of new 4D hyperchaotic financial system. Finally, a nonlinear control and adaptive neural fuzzy controller are designed for demonstrate the performances of the proposed approach. The main finding is the simulation results show that the proposed neural fuzzy controller architecture well controls the synchronization of the new 4D hyperchaotic financial systems taken as master and slave systems.

## Acknowledgments

This research was funded by Universitas Padjadjaran for the project financial support.

## Availability of data and material

Not applicable.

## Conflicts of interest

The authors declare that there is no conflict of interest regarding the publication of this paper.

## Ethical standard

The authors have no relevant financial or non-financial interests to disclose.

## LITERATURE CITED

- Bekiros, S., H. Jahanshahi, F. Bezzina, and A. A. Aly, 2021 A novel fuzzy mixed  $h_2/h_\infty$  optimal controller for hyperchaotic financial systems. *Chaos, Solitons & Fractals* **146**: 110878.
- Cao, L., 2018 A four-dimensional hyperchaotic finance system and its control problems. *Journal of Control Science and Engineering* **2018**: 1–12.
- Chen, H., L. Yu, Y. Wang, and M. Guo, 2021 Synchronization of a hyperchaotic finance system. *Complexity* **2021**: 1–7.
- Gao, Q. and J. Ma, 2009 Chaos and hopf bifurcation of a finance system. *Nonlinear Dynamics* **58**: 209–216.
- Guegan, D., 2009 Chaos in economics and finance. *Annual Reviews in Control* **33**: 89–93.
- Hajipour, A., M. Hajipour, and D. Baleanu, 2018 On the adaptive sliding mode controller for a hyperchaotic fractional-order financial system. *Physica A: Statistical Mechanics and its Applications* **497**: 139–153.
- Inglada-Perez, L., 2020 A comprehensive framework for uncovering non-linearity and chaos in financial markets: Empirical evidence for four major stock market indices. *Entropy* **22**: 1435.
- Jahanshahi, H., A. Yousefpour, Z. Wei, R. Alcaraz, and S. Bekiros, 2019 A financial hyperchaotic system with coexisting attractors: Dynamic investigation, entropy analysis, control and synchronization. *Chaos, Solitons & Fractals* **126**: 66–77.
- Kai, G., W. Zhang, Z. Wei, J. Wang, A. Akgul, *et al.*, 2017 Hopf bifurcation, positively invariant set, and physical realization of a new four-dimensional hyperchaotic financial system. *Mathematical Problems in Engineering* **2017**.
- Li, X., R. Rao, and X. Yang, 2022 Impulsive stabilization on hyperchaotic financial system under neumann boundary. *Mathematics* **10**: 1866.
- Lux, T., 1998 The socio-economic dynamics of speculative markets: interacting agents, chaos, and the fat tails of return distributions. *Journal of Economic Behavior & Organization* **33**: 143–165.

- Ma, Y. and W. Li, 2020 Application and research of fractional differential equations in dynamic analysis of supply chain financial chaotic system. *Chaos, Solitons & Fractals* **130**: 109417.
- Musaev, A., A. Makshanov, and D. Grigoriev, 2022 Statistical analysis of current financial instrument quotes in the conditions of market chaos. *Mathematics* **10**: 587.
- Rao, R. and Q. Zhu, 2021 Exponential synchronization and stabilization of delayed feedback hyperchaotic financial system. *Advances in Difference Equations* **2021**: 1–13.
- Shi, J., K. He, and H. Fang, 2022 Chaos, hopf bifurcation and control of a fractional-order delay financial system. *Mathematics and Computers in Simulation* **194**: 348–364.
- Szumiński, W., 2018 Integrability analysis of chaotic and hyperchaotic finance systems. *Nonlinear Dynamics* **94**: 443–459.
- Vargas, J. A., E. Grzeidak, and E. M. Hemerly, 2015 Robust adaptive synchronization of a hyperchaotic finance system. *Nonlinear Dynamics* **80**: 239–248.
- Vogl, M., 2022 Controversy in financial chaos research and nonlinear dynamics: a short literature review. *Chaos, Solitons & Fractals* **162**: 112444.
- Xin, B., Y. Li, *et al.*, 2013 0-1 test for chaos in a fractional order financial system with investment incentive. In *Abstract and Applied Analysis*, volume 2013, Hindawi.
- Xin, L., 2009 Modified projective synchronization of a new hyperchaotic system via nonlinear control. *Communications in Theoretical Physics* **52**: 274.
- Xu, E., K. Ma, and Y. Chen, 2021  $H_\infty$  control for a hyperchaotic finance system with external disturbance based on the quadratic system theory. *Systems Science & Control Engineering* **9**: 41–49.
- Yu, H., G. Cai, and Y. Li, 2012 Dynamic analysis and control of a new hyperchaotic finance system. *Nonlinear Dynamics* **67**: 2171–2182.

**How to cite this article:** Johansyah, M. D., Hamidzadeh, S. M., Benkouider, K., Vaidyanathan, S., Sambas, A., Mohamed, M. A., and Aziz, A. A. A Novel Hyperchaotic Financial System with Hyperbolic Sinusoidal Nonlinearity: From Theoretical Analysis to Adaptive Neural Fuzzy Controller Design. *Chaos Theory and Applications*, 6(1), 26-40, 2024.

**Licensing Policy:** The published articles in *Chaos Theory and Applications* are licensed under a [Creative Commons Attribution-NonCommercial 4.0 International License](https://creativecommons.org/licenses/by-nc/4.0/).



## Chaotic and Quasi-periodic Regimes in the Covid-19 Mortality Data

Erkan Yılmaz<sup>1</sup> and Ekrem Aydiner<sup>2</sup>

\*Institute of Graduate Studies in Science, Istanbul University, 34134, İstanbul, Türkiye, <sup>a</sup>Theoretical and Computational Physics Research Laboratory, Istanbul University, 34134 İstanbul, Türkiye, <sup>a</sup>Department of Physics, Faculty of Science, Istanbul University, 34134 İstanbul, Türkiye.

**ABSTRACT** It has been reported by World Health Organization (WHO) that the Covid-19 epidemic due to the Sar-Cov-2 virus, which started in China and affected the whole world, caused the death of approximately six million people over three years. Global disasters such as pandemics not only cause deaths but also bring other global catastrophic problems. Therefore, governments need to perform very serious strategic operations to prevent both infection and death. It is accepted that even if there are vaccines developed against the virus, it will never be possible to predict very complex spread dynamics and reach a spread pattern due to new variants and other parameters. In the present study, four countries: Türkiye, Germany, Italy, and the United Kingdom have been selected since they exhibit similar characteristics in terms of the pandemic's onset date, wave patterns, measures taken against the outbreak, and the vaccines used. Additionally, they are all located on the same continent. For these reasons, the three-year Covid-19 data of these countries were analyzed. Detailed chaotic attractors analyses were performed for each country and Lyapunov exponents were obtained. We showed that the three-year times series is chaotic for the chosen countries. In this sense, our results are compatible with the results of the Covid-19 analysis results in the literature. However, unlike previous Covid-19 studies, we also found out that there are chaotic, periodic, or quasi-periodic sub-series within these chaotic time series. The obtained results are of great importance in terms of revealing the details of the dynamics of the pandemic.

### KEYWORDS

Chaotic  
Quasi-periodic  
COVID-19  
Largest lyapunov exponent  
Time delay  
Phase space  
Embedding  
dimension

### INTRODUCTION

Humanity has faced the Covid-19 epidemic, which is the biggest global disaster after the Second World War and has surrounded the whole world. The pandemic was declared by the World Health Organization (WHO) on March 11, 2020, due to the coronavirus epidemic that started in China and affected the whole world (World Health Organisation 2020). As of March 26, 2023, 761 million people were infected with coronavirus and 6.8 million people died (World Health Organisation 2023). With the beginning of mass deaths, all governments and WHO are trying to control and prevent the spread of Covid-19. As it is known until the Covid-19 vaccine was found, all countries of the world tried to prevent the

spread of this virus with a series of measures such as curfews and travel restrictions. One of the important steps to controlling the spread of Covid-19 was the mathematical modeling of the pandemic and its analysis. With the acquisition of vaccines, efforts were made to prevent the Covid-19 epidemic. As of April 2023, 69.9 percent of the world's population had at least one COVID-19 vaccine. However, despite vaccines, new virus types have emerged and caused new spreading waves. Fortunately, the end of the pandemic process, which lasted approximately three years, was announced by WHO in May 2023.

Modeling a pandemic is important for two reasons. The first of these is to find or understand the mathematical model of the spreading dynamics of the pandemic. The other is to make model-based predictions and develop strategies to take preventive measures against the pandemic. Various models have been supposed to carry out the spread dynamics of infectious diseases. One of the popular methods is the compartment method proposed by

Manuscript received: 16 January 2024,

Revised: 27 February 2024,

Accepted: 15 March 2024.

<sup>1</sup>erkany@ogr.iu.edu.tr (Corresponding author)

<sup>2</sup>ekrem.aydiner@istanbul.edu.tr

Kermack and McKendrick (Kermack and McKendrick 1927). In this method, the entire population is divided into different compartments: i) people who are prone to the disease; ii) people who are already infected and can spread the infection; iii) people who have already recovered and have developed the immune system.

This model is called as SIR model in the literature. After the Covid pandemic started, many mathematical and simulation models are proposed for the study of COVID-19 based on SIR model (Schaffer 1985; Olsen *et al.* 1988; Hethcote *et al.* 1989; Earn *et al.* 2000; Kumar *et al.* 2019; Machado *et al.* 2020; Gumel *et al.* 2004; Livadiotis 2020; Youssef *et al.* 2020; Ahmetolan *et al.* 2020). However, it is known that these models are not sufficient to predict the course of the pandemic. The validity of most predictive models relies on numerous parameters, involving biological and social characteristics often unknown or highly uncertain.

To fully understand the dynamics of the spread of such a pandemic, it is necessary to analyze the data set consisting, for example, of the number of people infected or lost their lives. Does the time series correlate? Does the time series consist of unpredictable data? Is there a pattern in the data set? The answers to these questions are important in understanding the dynamics of diffusion. Many studies have been conducted to answer these questions. For example, Mangiarotti *et al.* showed that there are chaotic attractors in the Covid-19 data of China, Japan, South Korea, and Italy (Mangiarotti *et al.* 2020). These findings indicate that the number of people infected and those who lost their lives in the pandemic is unpredictable.

It also points out that it is necessary to include the chaos theory to understand the dynamics of the pandemic. It has been previously reported that the Mexican flu and Ebola and dengue epidemics contained chaotic patterns (Speakman and Sharpley 2012; Mangiarotti *et al.* 2016; Agosto and Khan 2018). Additionally, it is also possible to see new studies in the literature supporting that the Covid-19 pandemic has chaotic spreading dynamics (Jones and Strigul 2021; Borah *et al.* 2022; Abbas *et al.* 2023; Russell *et al.* 2023; Mashuri *et al.* 2023; Wang *et al.* 2023; Debbouche *et al.* 2022; Sapkota *et al.* 2021; Gonçalves 2022).

As it is known, many parameters affect virus spreading. The most important of these are new virus variants arising from the Sars-Cov-2 virus. This causes the data to be superimposed. Therefore, it requires detailed analysis to determine the character of the wave. For example, the data may include quasi-periodic or chaotic signals. Quasi-periodic signals of this type are known as *weak* signals in the literature. These weak signals can be detected with the help of chaotic oscillators (Wang *et al.* 1999; Wang and He 2003; Liu *et al.* 2007; Raj *et al.* 1999; Birk and Pippenger 1992). However, in this study, we will analyze data as a whole and sub-series to detect quasi-periodic and chaotic regimes.

Since Covid-19 remains a potential, careful analysis of available data remains important. Even if the pandemic were to be officially declared over when we look at the records of the WHO and the Coronavirus Resource Center, it is evident that the COVID-19 outbreak still persists at a low level (World Health Organisation 2023; Coronavirus Resource Center 2024). It should not be forgotten that the world is always under the threat of a pandemic. Understanding the dynamics of the spread is crucial to combating any outbreak. Throughout history, uncontrollable pandemics have inflicted greater damage on nations than wars, and in some cases, entire states have collapsed due to epidemics. The fight against infectious diseases is not merely an epidemic issue but a strategic concern for countries. Therefore, analyzing Covid-19 data is still important to carry out the dynamics of the pandemic. In the

present study, we will analyze Covid-19 data of Türkiye, Germany, Italy, and United Kingdom in detail to discuss the spreading dynamic. We will analyze the phase spaces and calculate Lyapunov exponents for these countries' time series and different time intervals. As a main contribution, in the present works, we will show that three years Covid-19 data for the chosen countries are chaotic, and, it is the first time, we will show that the chaotic, periodic or quasi-periodic sub-series embedded as a sub regimes in these chaotic pandemic time series.

The study is organized as follows: In Section II, we briefly introduce the mathematical techniques and algorithms for the analysis of a time series. In Section III, we presented three years Covid-19 mortality data with sub-peak periods and mortality data for Türkiye, Germany, Italy, and the United Kingdom. In Section IV, we give numerical results in detail for four countries. We plotted attractors in the phase spaces and computed Lyapunov exponents of the time series of Covid-19. In this section, we show that Covid-19 data have chaotic attractors and positive Lyapunov exponents in some time intervals while they have quasi-periodic solutions in some time intervals. Finally, in the last chapter, the discussion and conclusion are given.

## CHAOTIC TIME SERIES ANALYSIS

### Time series

It is known that a time series is a series of data points indexed in time order. Time series can be obtained from data produced by a physical system, but also from discrete or a differential equation. While the discrete systems can be expressed as  $x_{n+1} = f(x_n)$ , the continuous systems can be expressed in the differential form as  $\frac{dx(t)}{dt} = F(x)$  with three or more degrees of freedom  $x(t) = [x_1(t), x_2(t), \dots, x_m(t)]$ . The time series we are interested in here is the Covid-19 mortality series of four different countries. This series consists of three years of data. Our main aim is to reveal whether these series are chaotic or not. As we will show below, we will do this both for the entire series and by dividing the series into subdivisions. We will use the same method of analysis for both cases. To perform chaotic analysis, we will need knowledge of the phase space and the Lyapunov exponent. These details will be given briefly below.

According to the classical approach of chaos theory, for a time series to be chaotic, it must be sensitive to the initial condition and be unpredictable. Since the Covid epidemic contains dynamic variables that depend on time, it should also be taken into account that it is sensitive to physical factors that change over time. However, the best way to see chaotic behavior in the data set is to perform phase space analysis and calculate the Lyapunov exponent. We will calculate these quantities using Matlab. However, we would like to briefly present the background of the calculation.

### Attractor Reconstruction

Reconstruction of phase space is very important to see the dynamic behavior of the given time series. To figure out the trajectory from a given time series is a big challenge. Fortunately, the delay time-coordinate embedding method laid by Takens (Takens 1981). The delay-coordinate method can be given as follows. From a measured time series  $x(k) = x(t_0 + k\Delta t)$  with  $\Delta t$  being the sampling interval, the following vector quantity of  $m$  components is constructed:

$$x(t) = \{x(t), x(t + \tau), \dots, x(t + (m - 1)\tau)\} \quad (1)$$

where  $t = t_0 + k\Delta t$ ,  $\tau$  is the delay time which is an integer multiple of  $\Delta t$  and  $m$  is the embedding dimension. To plot a phase space

of a given time series, it is necessary to determine the delay time  $\tau$  and embedding dimension  $m$ . Once these two parameters are determined, the reconstructed vector  $\mathbf{x}(t)$  can accurately represent the trajectory of the unknown attractor. We will not go into calculation details here. It can be seen in the details of computing these quantities in Ref. (Takens 1981).

### Lyapunov Exponent

The Lyapunov exponent is the most important quantity used to determine whether chaotic behavior exists in a dynamic system. A positive Lyapunov exponent is the strongest sign that indicates that there is chaos in the system. On the other hand, a negative Lyapunov exponent represents fixed points while a zero Lyapunov exponent denotes a limit cycle or a quasiperiodic orbit.

The Lyapunov exponent of a dynamical system or time series represents the rate of exponential divergence of an orbit from perturbed initial conditions. For example, consider an  $m$ -dimensional discrete map  $x(j)$  ( $j = 1, 2, \dots, m$ ). Let  $x_n(j)$  be its state at time  $n$ . By adding  $\delta x(j)$  to the  $x_n(j)$ , we set a new state as  $x'_n(j) = x_n(j) + \delta x(j)$ . The distance between two states changes exponentially with time

$$\|\delta x_n(j)\| \sim e^{\lambda t} \|x_{n-1}(j)\| \quad (2)$$

Then the maximal Lyapunov exponent  $\lambda_{max}$  can be obtained from Eq.(2) as

$$\lambda_{max} = \lim_{N \rightarrow \infty} \frac{1}{N} \sum_{j=0}^N \ln \frac{\|\delta x_n(j)\|}{\|\delta x_{n-1}(j)\|} \quad (3)$$

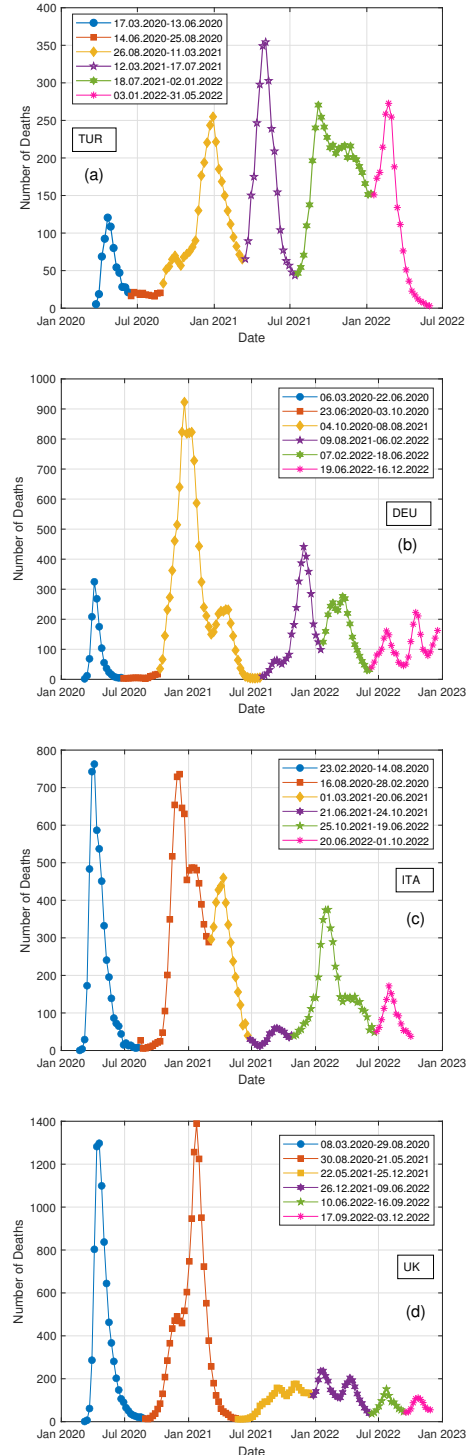
where  $\|\delta x_n(j)\| = (\sum_j^m \delta x_n(j)^2)^{1/2}$ . By using this approximation can be computed Lyapunov exponent for the dynamical systems. However, it is quite difficult to use this method in a time series analysis. Various methods have been developed to calculate the Lyapunov exponent in time series (Rosenstein *et al.* 1993; Wolf *et al.* 1985) and other methods (Meranza-Castillón *et al.* 2019; Arellano-Delgado *et al.* 2017). In this study, we will calculate Lyapunov exponents using Matlab (Inc. 2023) which based on the algorithm given in Ref. (Rosenstein *et al.* 1993). In this algorithm process, firstly time delay time  $\tau$  and embedding dimension  $m$  are computed to construct the phase space for the time series data, and then, the distance between two trajectories starts at different states.

### COVID-19 MORTALITY TIME SERIES OF FOUR COUNTRIES

In this study, as we mentioned in the introduction we will analyze the COVID-19 mortality data of Türkiye, Germany, Italy, and the United Kingdom, respectively. The data of the countries between 2020 and 2022 will be used in the analysis. The data were taken from public data of the World Health Organization and Our World in Data sites (Our World in Data Organisation 2023; World Health Organisation 2023).

Three years Covid-19 mortality data for four countries are given in Fig.1. As can be seen from Fig.1 pandemic peaks occur at different time intervals in the time series of four different countries. To conduct a systematic analysis of the data of these four countries, we divided the three-year time series into six sub-divisions for the sake of simplicity. Each peak was represented with a different color, and the start and end dates of the peaks were given in the panels. In Fig.1 the area under the peaks gives the number of people who died during that peak period. These numbers are also given in Table 1. On the other hand, it should be noted that the highest peaks were considered when determining the peak range for each country. For example, if there was no major peak in one country

and there was a high peak in another country, it was evaluated as if there was a peak in the same period. We paid attention to this generality when separating these compartments. However, the analysis of peaks is independent of the number of peaks.



**Figure 1** Mortality time series between 17.03.2020 – 31.05.2022 due to Covid-19: In (a) Türkiye, in (b) Germany, in (c) Italy, in (d) United Kingdom.

The number of deaths for each peak period for four countries is given in Table 1. It can be seen that the number of deaths varies

■ **Table 1** COVID-19 waves and mortality number of four countries.

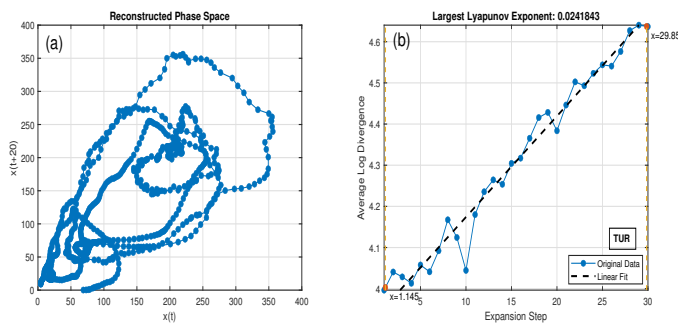
	1st		2nd		3rd		4th		5th		6th	
	Day	Deaths	Day	Deaths	Day	Deaths	Day	Deaths	Day	Deaths	Day	Deaths
Türkiye	89	4792	73	1371	198	23127	128	21198	169	32147	149	16330
Germany	106	8887	103	649	309	82247	182	26935	132	21472	181	19708
Italy	176	35265	197	62307	112	29571	126	4556	238	35895	105	9429
United Kingdom	175	57858	265	96248	218	27398	166	23374	99	7786	78	5596

dramatically within the same peak intervals. The fact that these numbers are very different from each other can be considered to vary depending on many parameters such as the elderly population, isolation strategies, and vaccination. In this study, we would like to analyze the character of the time series, not the numbers in different time intervals. Therefore, firstly, we performed the phase space analyses for three years of data for each country, and the character of the time series was determined by calculating Lyapunov exponents. Subsequently, we separately analyzed all epidemic peaks for each country. Similarly, we discussed the phase space Lyapunov exponents for each pandemic peak. Analysis results are given below.

### CHAOS ANALYSIS OF THE COVID-19 MORTALITY DATA

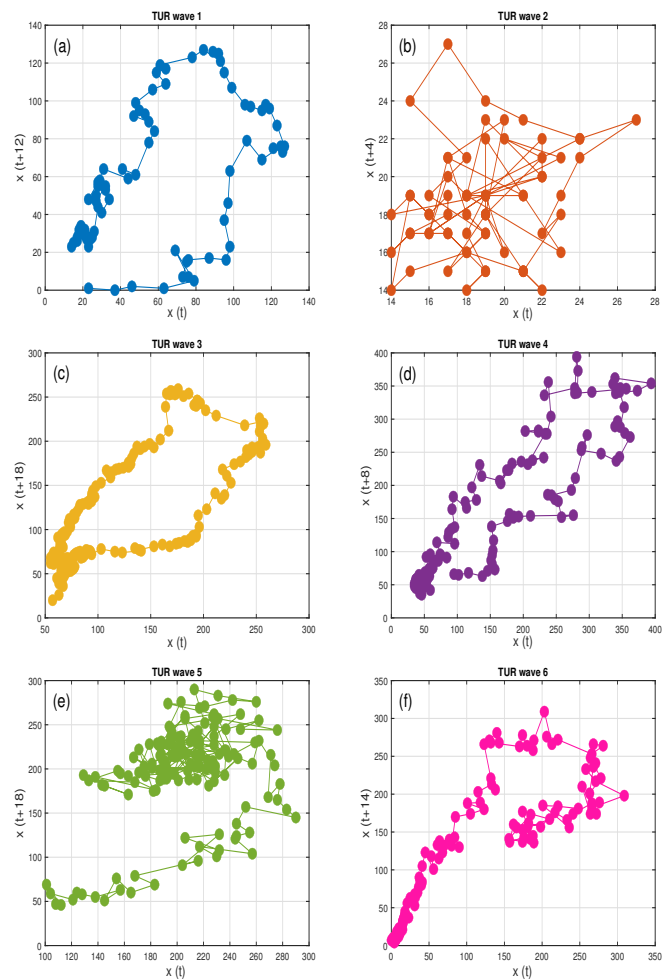
#### Türkiye

The time series showing the number of deaths due to COVID-19 in Türkiye between 2020 and 2022 is given in Fig 1(a). We obtained the embedding dimensions and delay time for this time series using the method presented in Section Chaotic time series analysis. With the help of this information, we constructed the phase space of the time series in Fig 2 (a). Although not visible in great detail, it can be seen that more than one orbit exists in the phase space. These orbits may indicate the presence of a chaotic attractor. But the attractor is not very clear, as in Lorenz, for example. Orbits may indicate the existence of a periodic or quasi-periodic solution. To see whether the orbit is chaotic or not, we calculated the Lyapunov exponent of the series with the help of MATLAB (Inc. 2023) and gave the result in Fig 2 (b).



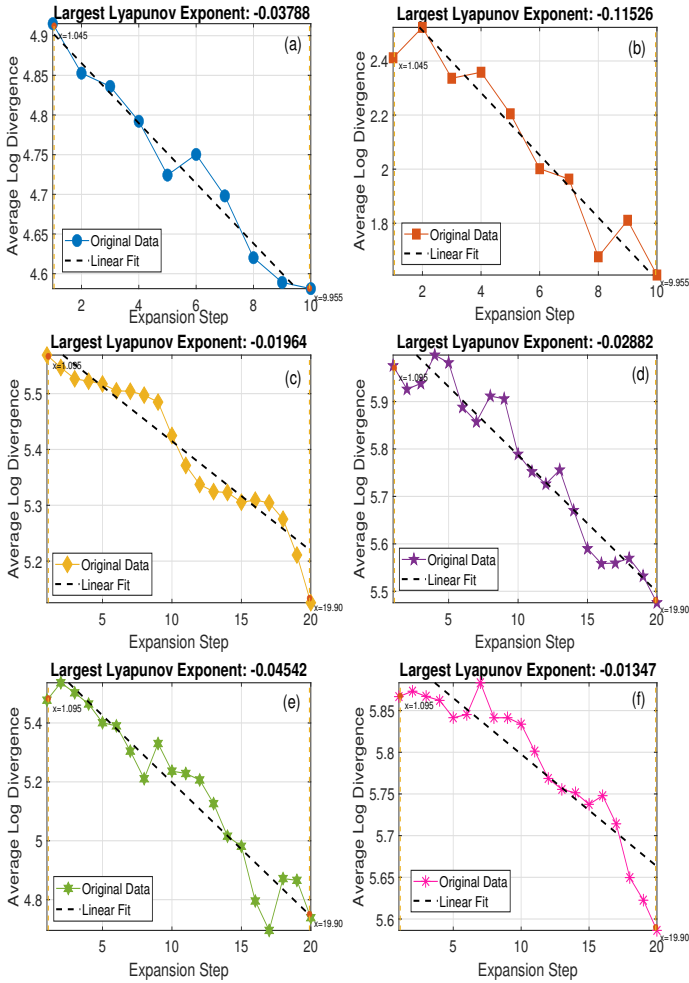
**Figure 2** COVID-19 data set of Türkiye’s reported deaths time series between 17.03.2020 – 31.05.2022. Embedding dimension  $d = 3$  and time delay  $\tau = 20$ . In (a) phase space representation, in (b) Lyapunov exponent.

As can be seen from Fig 2 (b) the Lyapunov exponent for COVID-19 three-year mortality data is positive which indicates data has chaotic behavior.



**Figure 3** Reconstructed phase space of Türkiye’s waves. In (a) 1<sup>st</sup> wave, in (b) 2<sup>th</sup> wave, in (c) 3<sup>th</sup> wave, in (d) 4<sup>th</sup> wave, in (e) 5<sup>th</sup> wave, in (f) 6<sup>th</sup> wave.





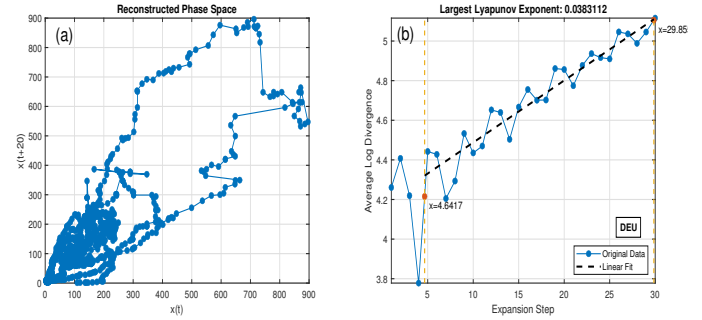
**Figure 4** Largest Lyapunov exponent of Türkiye's waves. In (a) 1<sup>st</sup> wave, in (b) 2<sup>th</sup> wave, in (c) 3<sup>th</sup> wave, in (d) 4<sup>th</sup> wave, in (e) 5<sup>th</sup> wave, in (f) 6<sup>th</sup> wave.

On the other hand, to analyze the local region in the time series, we first computed the embedding dimensions and delay times for the sub-time series corresponding to each peak, and we separately plotted the phase space diagrams for these sub-time series in Fig 3. As can be seen from this figure the single trajectory is seen in all sub-panels in Fig 3. One can see that the presence of these single orbits may indicate aperiodic orbits of the sub-time series. Lyapunov exponents of these sub-time series were calculated and given in Fig 4. As can be seen from Fig 4 all sub-time series of Türkiye have different negative Lyapunov exponents. These interesting results show that while the three-year time series of Covid-19 data is chaotic, the behavior of the sub-time series in the same period is not chaotic for Türkiye. This result is meaningful as it indicates that a time series consisting of quasi-periodic signals sub-sets can produce chaotic dynamics when evaluated as a whole.

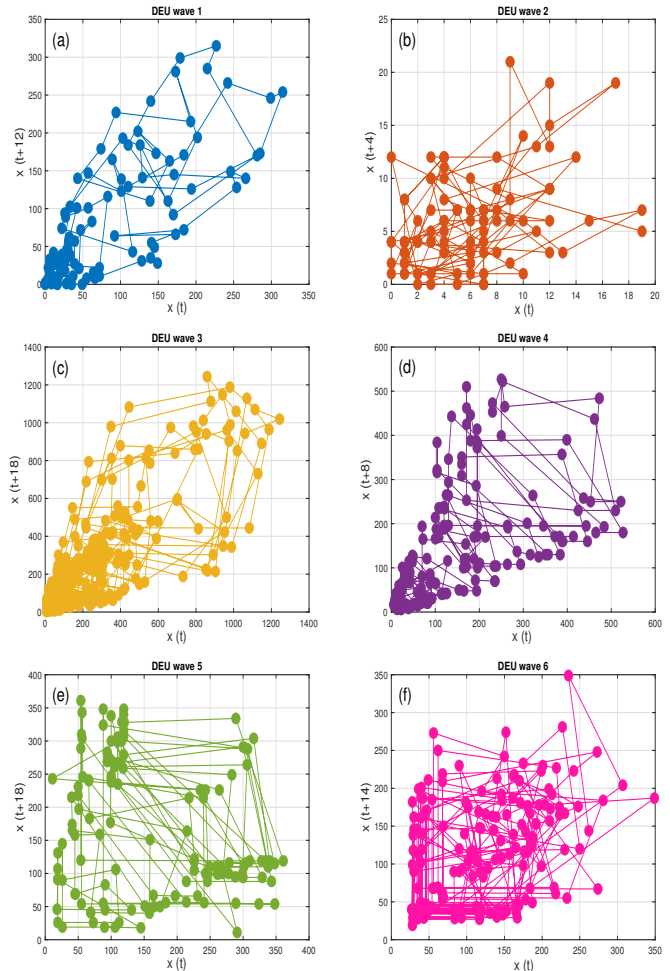
### Germany

Similarly and using the same systematics, we analyzed the three-year data of the Germany time series shown in Fig 1(b). We determined the delay time for this time series and plotted the phase space as can be seen in Fig 5(a). Contrary to Türkiye's data, we can say that there are more orbits around attractors in Germany's data. We can see from Fig 5(b) that this attractor is chaotic. Indeed,

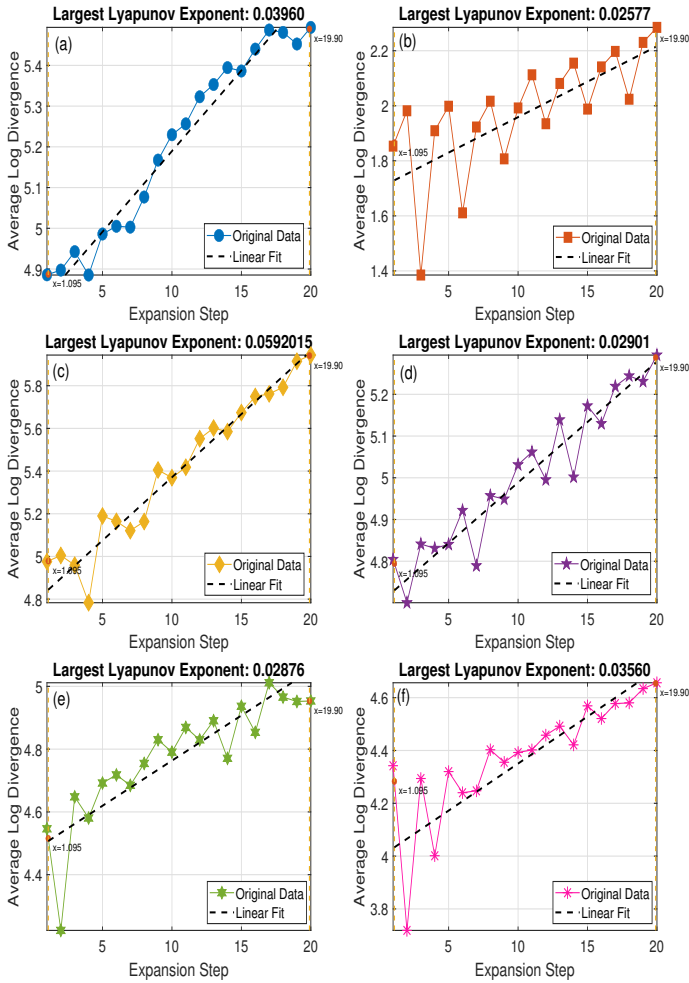
the Lyapunov exponent of this time series is positive. While the Largest Lyapunov Exponent (LLE) value is 0.038 for Germany, this value is around 0.028 for Türkiye. This difference indicates that Germany's Covid-19 time series is more chaotic than Türkiye's time series.



**Figure 5** COVID-19 data set of Germany's reported deaths time series between 09.03.2020 – 19.06.2022. Embedding dimension  $d = 3$  and time delay  $\tau = 20$ . In (a) phase space representation, in (b) Lyapunov exponent.



**Figure 6** Reconstructed Phase Space of Germany's Waves. In (a) 1<sup>st</sup> wave, in (b) 2<sup>th</sup> wave, in (c) 3<sup>th</sup> wave, in (d) 4<sup>th</sup> wave, in (e) 5<sup>th</sup> wave, in (f) 6<sup>th</sup> wave.



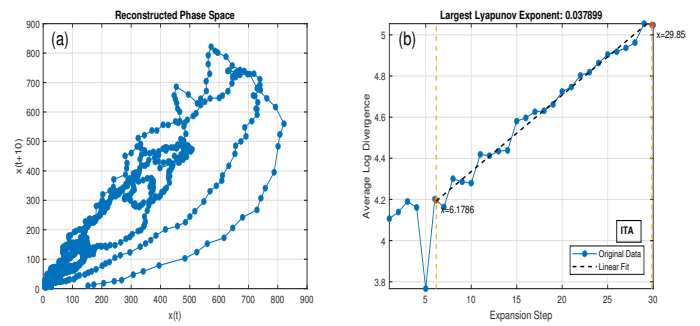
**Figure 7** Largest Lyapunov exponent of Germany's waves. In (a) 1<sup>st</sup> wave, in (b) 2<sup>th</sup> wave, in (c) 3<sup>th</sup> wave, in (d) 4<sup>th</sup> wave, in (e) 5<sup>th</sup> wave, in (f) 6<sup>th</sup> wave.

To analyze the time series of each independent peak in Germany's Covid-19 data given in Fig. 3(b), we computed embedding dimensions and delay times for each sub-data. We separately plotted the phase space diagrams for these sub-time series in Fig. 6. As can be seen from this figure more trajectories are seen in all sub-panels in Fig 6. These multi-orbits may indicate chaotic orbits of the sub-time series. Lyapunov exponents of these sub-time series were calculated and given in Fig. 7. As can be seen from Fig. 7 all sub-time series of Germany have different positive Lyapunov exponents. These interesting results show that the three-year time series and all sub-series of Covid-19 data of Germany are chaotic.

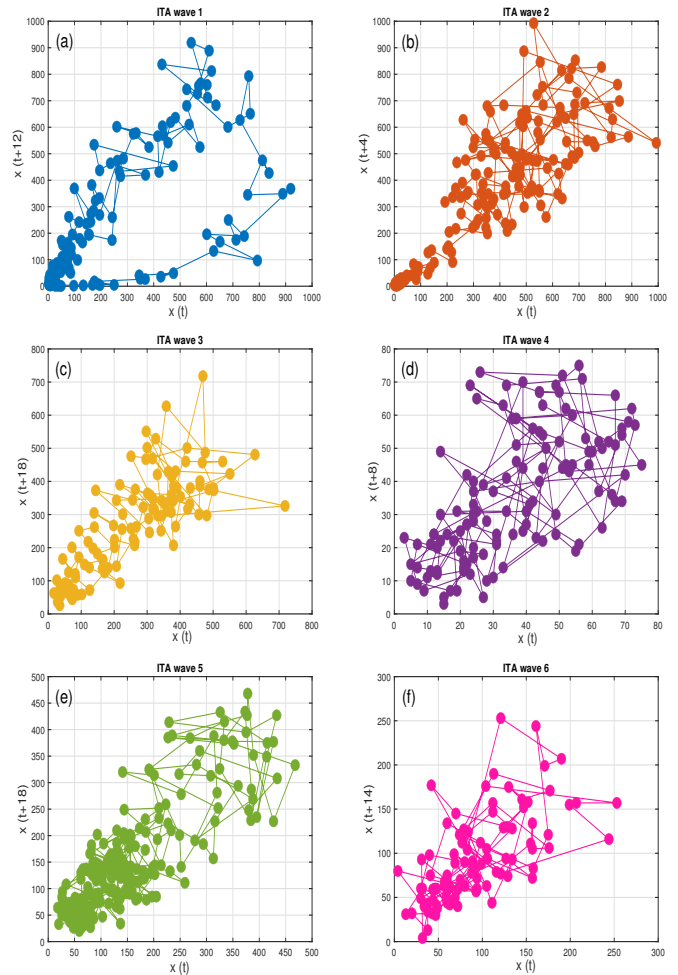
### Italy

Similarly, we compute the delay time for the three-year data of the Italy time series shown in Fig. 1(c). The chaotic attractor for this data is given in Fig. 8(a). It can be seen that there is more than one trajectory in this phase space. Additionally, we obtained the Lyapunov exponent for this data and plotted it in Fig. 8(a). The value of the Lyapunov exponent for Italy is 0.0037 which is close to the value of Germany.

To see detailed phase space attractors of the sub-series for Italy's Covid-19 data given in Fig 3(c), we computed embedding dimensions and delay times for each sub-data. We separately plotted the

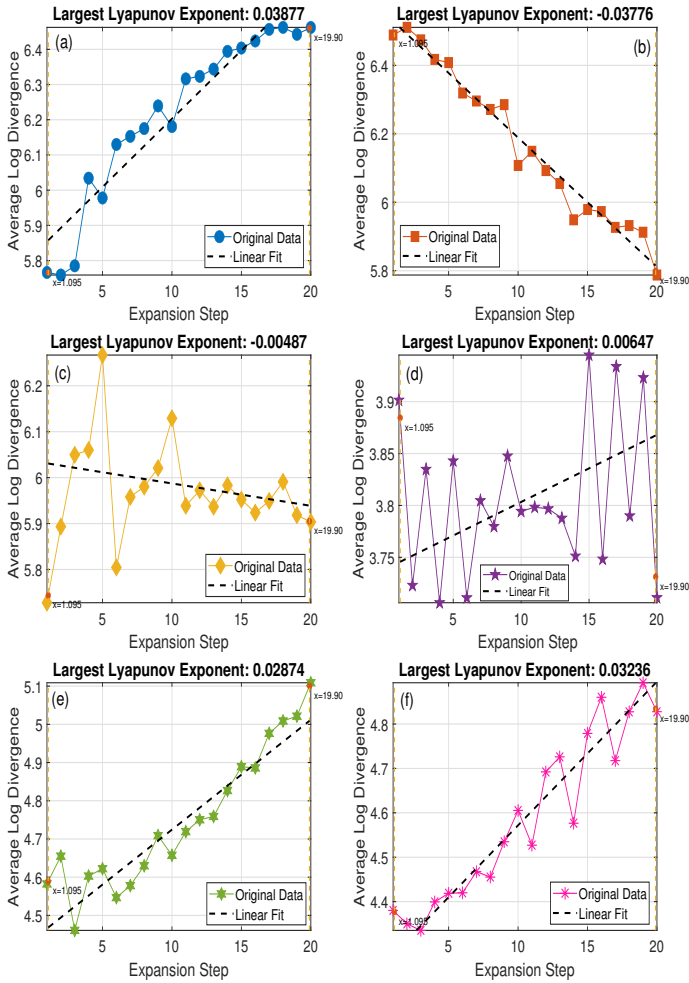


**Figure 8** COVID-19 data set of Italy's reported deaths time series between 21.02.2020 – 2.10.2022. Embedding dimension  $d = 3$  and time delay  $\tau = 10$ . In (a) phase space representation, in (b) Lyapunov exponent.



**Figure 9** Reconstructed phase space of Italy's waves. In (a) 1<sup>st</sup> wave, in (b) 2<sup>th</sup> wave, in (c) 3<sup>th</sup> wave, in (d) 4<sup>th</sup> wave, in (e) 5<sup>th</sup> wave, in (f) 6<sup>th</sup> wave.

phase space diagrams for these sub-time series in Fig 9. As can be seen from this figure more trajectories are seen in all sub-panels in Fig 9. Although there appear to be attractors in the phase space diagrams, it is difficult to say that the character of the time series can be fully understood from the orbits in the phase space. To see the dynamics of the sub-time series, Lyapunov exponents of the



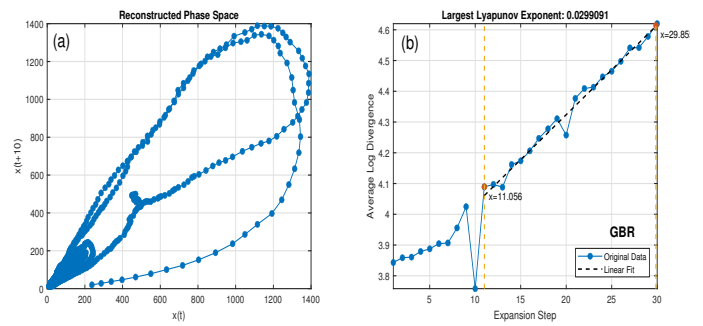
**Figure 10** Largest Lyapunov exponent of Italy's waves. In (a) 1<sup>st</sup> wave, in (b) 2<sup>th</sup> wave, in (c) 3<sup>th</sup> wave, in (d) 4<sup>th</sup> wave, in (e) 5<sup>th</sup> wave, in (f) 6<sup>th</sup> wave.

sub-time series were calculated separately and given in Fig 10. Interestingly, the second and third peaks have a negative Lyapunov exponent, while the others have a positive exponent. These results indicate that the three-year chaotic Italy series consists of a combination of chaotic and quasi-periodic sub-series.

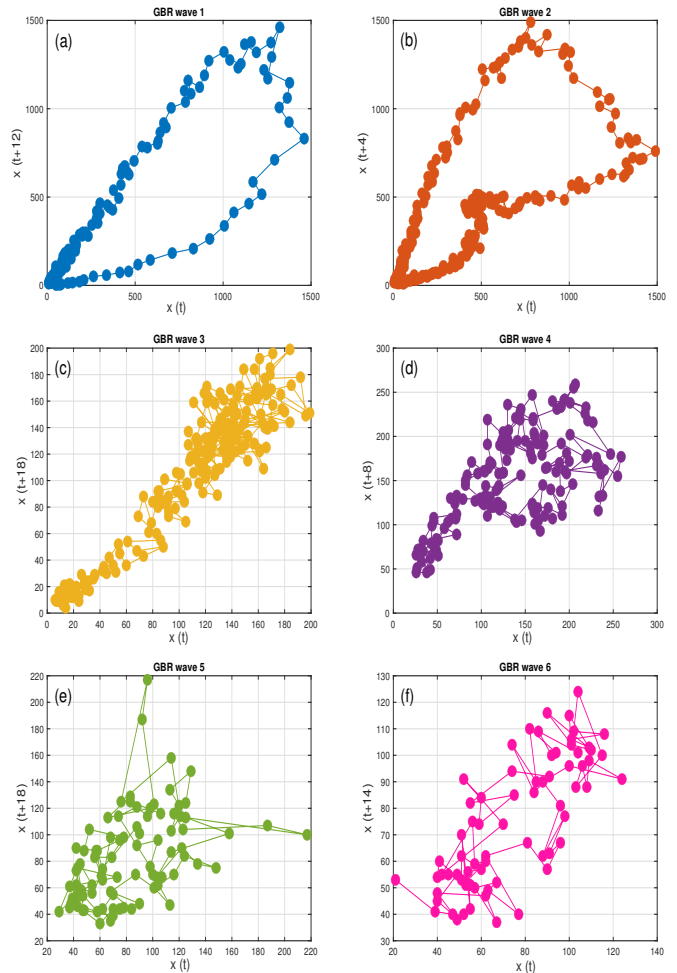
### United Kingdom

Finally, we compute the delay time for the three-year data of the United Kingdom time series shown in Fig. 1(d). The attractor for this data is given in Fig. 11(a). It can be seen that there is more than one trajectory in this phase space. Additionally, we obtained the Lyapunov exponent for this data and plotted it in Fig. 11(b). The value of the Lyapunov exponent for the United Kingdom is 0.029 which is close to the value of Türkiye.

Obtaining embedding dimensions and delay times for all sub-series for United Kingdom's Covid-19 data given in Fig 1(d). We separately plotted the phase space diagrams for these sub-time series in Fig 12. As can be seen from Fig 12 while the orbits are more distinct in the first two panels, however, the orbits are intertwined in the others. To reveal the dynamics of the sub-time series, Lyapunov exponents were calculated separately and given in Fig 13.

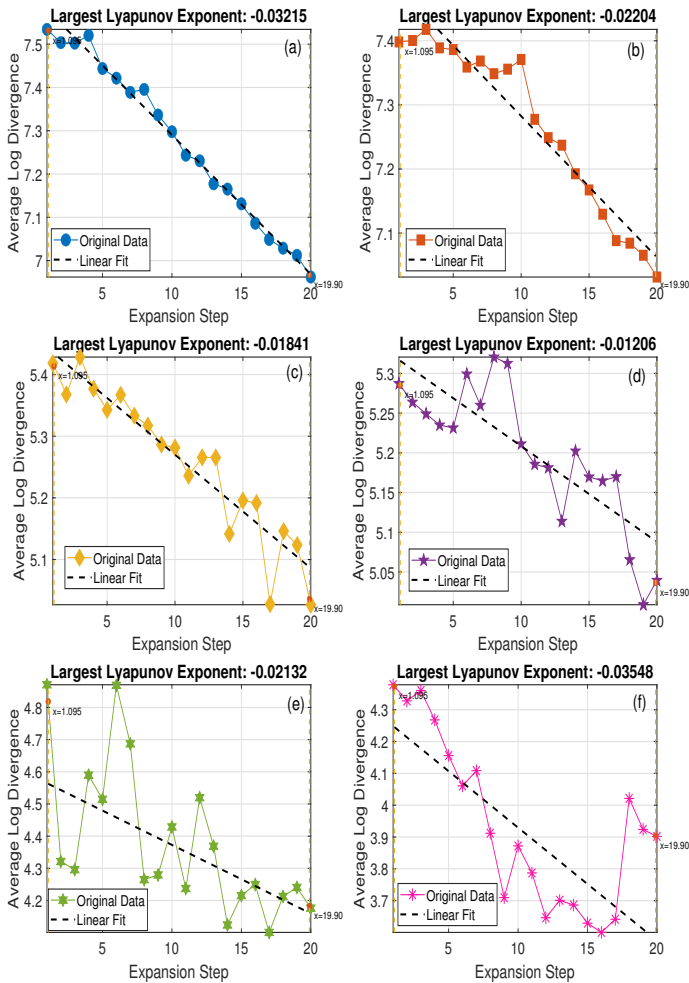


**Figure 11** COVID-19 data set of United Kingdom's reported deaths time series between 08.03.2020 – 03.12.2022. Embedding dimension  $d = 3$  and time delay  $\tau = 10$ . In (a) phase space representation, in (b) Lyapunov exponent.



**Figure 12** Reconstructed Phase Space of United Kingdom's waves. In (a) 1<sup>st</sup> wave, in (b) 2<sup>th</sup> wave, in (c) 3<sup>th</sup> wave, in (d) 4<sup>th</sup> wave, in (e) 5<sup>th</sup> wave, in (f) 6<sup>th</sup> wave.

Surprisingly, one can see that all sub-time series of the United Kingdom have a negative Lyapunov exponent. While the entire series is chaotic, the subseries behave as quasi-periodic. These results are similar to Türkiye's results.



**Figure 13** Largest Lyapunov exponent of United Kingdom's waves. In (a) 1<sup>st</sup> wave, in (b) 2<sup>th</sup> wave, in (c) 3<sup>th</sup> wave, in (d) 4<sup>th</sup> wave, in (e) 5<sup>th</sup> wave, in (f) 6<sup>th</sup> wave.

## CONCLUSION

As we mentioned in the introduction, it is very difficult to predict and make predictions about the course of the pandemic due to reasons such as its multi-parameter-dependent dynamics, the emergence of new variants, and the impact of vaccine applications. So far, it has been possible to obtain limited information about the course of the pandemic through model-based or statistical analysis-based studies. The most important possible reason for this may be that the pandemic dynamics are chaotic. Therefore, in this study, to see the presence of chaotic patterns in the Covid-19 data, we analyzed the Covid-19 mortality data of Türkiye, Germany, Italy, and the United Kingdom for three years by using the data of the WHO.

We plotted phase space diagrams of three-year mortality data of four countries and obtained Lyapunov exponents. We found positive Lyapunov exponents for all countries, which indicates phase space trajectories of the Covid-19 data are chaotic. These significant numerical results support the studies that suggest that the Covid-19 pandemic has chaotic dynamics. On the other hand, we considered the subset of data corresponding to the spreading peaks of mortality data in the time interval for three years.

Surprisingly, we found that some of the sub-time series of these countries exhibit chaotic or quasi-periodic behavior. This interest-

ing result was reported for the first time in this study. This reveals that there may be quasi-periodic *-weak-* regimes within a chaotic time series. These findings are important for a more detailed understanding of epidemics with chaotic spread dynamics.

If we summarize the results, analysis has revealed that while the Covid-19 epidemic in Türkiye was chaotic over three years, however, no peak that emerged in this period was chaotic. For example, the situation is quite different in Germany. While the three-year data in Germany behaves chaotically, it can be seen from the figure that all independent peaks in this time interval are also chaotic.

The situation in United Kingdom is the same as in Türkiye. As can be seen from the figure, all peaks are chaotic. However, in the Italy, the second and third peaks are periodic or quasi-periodic, while the others are chaotic. As is known, positive Lyapunov exponents indicate that the series behaves chaotic. In the analysis, we saw that time series that behave chaotically take different positive values. These values can be thought to reflect the degree of chaoticness of the system.

As a result, by analyzing Covid-related deaths from four countries, we showed that the series is chaotic as seen as seen Figs.2(b), 5(b), 8(b) and 11(b). In this sense, our results are compatible with the results obtained in the previous studies (Jones and Strigul 2021; Borah et al. 2022; Abbes et al. 2023; Russell et al. 2023; Sapkota et al. 2021; Gonçalves 2022). However, unlike previous Covid-19 studies, we also found out that there are chaotic, periodic or quasi-periodic sub-series within these chaotic time series. These new and novel results are reported for the first time in this study. Here we analyzed data from four countries, however, one can estimate that the time series of Covid-19 in the other countries have similar dynamics.

It can be assumed that a pandemic is a catastrophic event that occurs within a complex system (Aydiner 2020). Therefore, by its nature, the pandemic is expected to be chaotic. Indeed, it has been confirmed in the present study and previous studies that the Covid-19 pandemic is chaotic (Jones and Strigul 2021; Borah et al. 2022; Abbes et al. 2023; Russell et al. 2023; Sapkota et al. 2021; Gonçalves 2022). However, it is interesting to find periodic or quasi-periodic regimes in chaotic time series. For example; all sub-series of Türkiye and United Kingdom in Figs.4 and 13 are quasi-periodic, not chaotic.

Similarly, two sub-series for Italy in 10(b) and (c) are also quasi-periodic. Quasi-periodic regimes may indicate that the correlations between daily mortality values goes to zero which means daily mortalities are relatively independent each other.

## Availability of data and material

Not applicable.

## Conflicts of interest

The authors declare that there is no conflict of interest regarding the publication of this paper.

## Ethical standard

The authors have no relevant financial or non-financial interests to disclose.

## LITERATURE CITED

- Abbes, A., A. Ouannas, N. Shawagfeh, and H. Jahanshahi, 2023 The fractional-order discrete covid-19 pandemic model: stability and chaos. *Nonlinear Dynamics* **111**: 965–983.
- Agusto, F. and M. Khan, 2018 Optimal control strategies for dengue transmission in pakistan. *Mathematical Biosciences* **305**: 102–121.
- Ahmetolan, S., A. H. Bilge, A. Demirci, A. Peker-Dobie, and O. Ergonul, 2020 What can we estimate from fatality and infectious case data using the susceptible-infected-removed (sir) model? a case study of covid-19 pandemic. *Frontiers in Medicine* **7**.
- Arellano-Delgado, A., R. M. López-Gutiérrez, M. A. Murillo-Escobar, L. Cardoza-Avenidaño, and C. Cruz-Hernández, 2017 The emergence of hyperchaos and synchronization in networks with discrete periodic oscillators. *Entropy* **19**.
- Aydiner, E., 2020 Covid - 19 tehlikesi, karmaşık sistemler ve fizik (in turkish). İstanbul Üniversitesi, Koronavirüs özel sayı **3**: 33–49.
- Bandt, C., 2020 Entropy ratio and entropy concentration coefficient, with application to the covid-19 pandemic. *Entropy* **22**: 1315.
- Bashir, M. F., B. Ma, B. Komal, M. A. Bashir, D. Tan, *et al.*, 2020 Correlation between climate indicators and covid-19 pandemic in new york, usa. *Science of the Total Environment* **728**: 138835.
- Bauch, C. T., J. O. Lloyd-Smith, M. P. Coffee, and A. P. Galvani, 2005 Dynamically modeling sars and other newly emerging respiratory illnesses: past, present, and future. *Epidemiology* pp. 791–801.
- Birx, D. L. and S. J. Pipenberg, 1992 Chaotic oscillators and complex mapping feed-forward networks (cmffns) for signal detection in noisy environments. In [*Proceedings 1992*] *IJCNN International Joint Conference on Neural Networks*, volume 2, pp. 881–888, IEEE.
- Borah, M., A. Gayan, J. S. Sharma, Y. Chen, Z. Wei, *et al.*, 2022 Is fractional-order chaos theory the new tool to model chaotic pandemics as covid-19? *Nonlinear dynamics* **109**: 1187–1215.
- Chinazzi, M., J. T. Davis, M. Ajelli, C. Gioannini, M. Litvinova, *et al.*, 2020 The effect of travel restrictions on the spread of the 2019 novel coronavirus (covid-19) outbreak. *Science* **368**: 395–400.
- Coronavirus Resource Center, 2024 Covid-19 dashboard. The Center for Systems Science and Engineering (CSSE) at Johns Hopkins University (JHU). Available at <https://coronavirus.jhu.edu/map.html>.
- Debbouche, N., A. Ouannas, I. M. Batiha, and G. Grassi, 2022 Chaotic dynamics in a novel covid-19 pandemic model described by commensurate and incommensurate fractional-order derivatives. *Nonlinear Dyn* **109**: 33–45.
- Earn, D. J., P. Rohani, B. M. Bolker, and B. T. Grenfell, 2000 A simple model for complex dynamical transitions in epidemics. *science* **287**: 667–670.
- Fanelli, D. and F. Piazza, 2020 Analysis and forecast of covid-19 spreading in china, italy and france. *Chaos, Solitons & Fractals* **134**: 109761.
- Gonçalves, C. P., 2022 Low dimensional chaotic attractors in sars-cov-2's regional epidemiological data. medRxiv .
- Gumel, A. B., S. Ruan, T. Day, J. Watmough, F. Brauer, *et al.*, 2004 Modelling strategies for controlling sars outbreaks. *Proceedings of the Royal Society of London. Series B: Biological Sciences* **271**: 2223–2232.
- Hethcote, H. W., M. A. Lewis, and P. Van Den Driessche, 1989 An epidemiological model with a delay and a nonlinear incidence rate. *Journal of mathematical biology* **27**: 49–64.
- Inc., T. M., 2023 Matlab version: 9.13.0 (r2023b). <https://www.mathworks.com>.
- Jones, A. and N. Strigul, 2021 Is spread of covid-19 a chaotic epidemic? *Chaos, Solitons & Fractals* **142**: 110376.
- Kermack, W. O. and A. G. McKendrick, 1927 A contribution to the mathematical theory of epidemics. *Proceedings of the Royal Society of London. Series A, Containing papers of a mathematical and physical character* **115**: 700–721.
- Kumar, A., P. K. Srivastava, and R. Gupta, 2019 Nonlinear dynamics of infectious diseases via information-induced vaccination and saturated treatment. *Mathematics and Computers in Simulation* **157**: 77–99.
- Liu, Z., Y. Li, and G. Chen, 2007 The basin of attraction of the chen attractor. *Chaos, Solitons & Fractals* **34**: 1696–1703.
- Livadiotis, G., 2020 Statistical analysis of the impact of environmental temperature on the exponential growth rate of cases infected by covid-19. *PLoS one* **15**: e0233875.
- Machado, J. T., J. M. Rocha-Neves, and J. P. Andrade, 2020 Computational analysis of the sars-cov-2 and other viruses based on the kolmogorov's complexity and shannon's information theories. *Nonlinear Dynamics* **101**: 1731–1750.
- Mangiarotti, S., M. Peyre, and M. Huc, 2016 A chaotic model for the epidemic of ebola virus disease in west africa (2013–2016). *Chaos: An Interdisciplinary Journal of Nonlinear Science* **26**: 113112.
- Mangiarotti, S., M. Peyre, Y. Zhang, M. Huc, F. Roger, *et al.*, 2020 Chaos theory applied to the outbreak of covid-19: an ancillary approach to decision making in pandemic context. *Epidemiology and Infection* **148**: 1–29.
- Mashuri, A., N. M. Ali, N. S. Abd Karim, A. B. Ruslan, and N. H. Adenan, 2023 The application of chaos theory on covid-19 daily time series dataset in malaysia. *International Journal of Advanced Data Science and Intelligence Analytics* **3**.
- Meraj, G., M. Farooq, S. K. Singh, S. A. Romshoo, M. Nathawat, *et al.*, 2021 Coronavirus pandemic versus temperature in the context of indian subcontinent: a preliminary statistical analysis. *Environment, Development and Sustainability* **23**: 6524–6534.
- Meranza-Castillón, M., M. Murillo-Escobar, R. López-Gutiérrez, and C. Cruz-Hernández, 2019 Pseudorandom number generator based on enhanced hénon map and its implementation. *AEU - International Journal of Electronics and Communications* **107**: 239–251.
- Olsen, L. F., G. L. Truty, and W. M. Schaffer, 1988 Oscillations and chaos in epidemics: a nonlinear dynamic study of six childhood diseases in copenhagen, denmark. *Theoretical population biology* **33**: 344–370.
- Our World in Data Organisation, 2023 Coronavirus pandemic covid-19. OWID - 11 December 2023. Available at <https://github.com/owid/covid-19-data/tree/master/public/data>.
- Raj, S. P., S. Rajasekar, and K. Murali, 1999 Coexisting chaotic attractors, their basin of attractions and synchronization of chaos in two coupled duffing oscillators. *Physics Letters A* **264**: 283–288.
- Roosa, K., Y. Lee, R. Luo, A. Kirpich, R. Rothenberg, *et al.*, 2020 Real-time forecasts of the covid-19 epidemic in china from february 5th to february 24th, 2020. *Infectious Disease Modelling* **5**: 256–263.
- Rosenstein, M. T., J. J. Collins, and C. J. De Luca, 1993 A practical method for calculating largest lyapunov exponents from small data sets. *Physica D: Nonlinear Phenomena* **65**: 117–134.
- Russell, G., R. Lane, J. Neil, J. Advocat, E. A. Sturgiss, *et al.*, 2023 At the edge of chaos: a prospective multiple case study in australian general practices adapting to covid-19. *BMJ open* **13**: e064266.
- Sapkota, N., W. Karwowski, M. R. Davahli, A. Al-Juaid, R. Taiar,

- et al.*, 2021 The chaotic behavior of the spread of infection during the covid-19 pandemic in the united states and globally. *IEEE Access* **9**: 80692–80702.
- Sarkodie, S. A. and P. A. Owusu, 2020 Investigating the cases of novel coronavirus disease (covid-19) in china using dynamic statistical techniques. *Heliyon* **6**: e03747.
- Schaffer, W., 1985 Can nonlinear dynamics elucidate mechanisms in ecology and epidemiology? *IMA Journal of Mathematics Applied in Medicine and Biology* **2**: 221–252.
- Speakman, M. and R. Sharpley, 2012 A chaos theory perspective on destination crisis management: Evidence from mexico. *Journal of Destination Marketing & Management* **1**: 67–77.
- Takens, F., 1981 *Detecting strange attractors in turbulence*. In: *Rand DA, Young LS, eds. Symposium on Dynamical Systems and Turbulence.*, volume 898 of *Lecture Notes in Mathematics*. Berlin: Springer-Verlag.
- Wang, G., D. Chen, J. Lin, and X. Chen, 1999 The application of chaotic oscillators to weak signal detection. *IEEE Transactions on industrial electronics* **46**: 440–444.
- Wang, G. and S. He, 2003 A quantitative study on detection and estimation of weak signals by using chaotic duffing oscillators. *IEEE Transactions on Circuits and Systems I: Fundamental Theory and Applications* **50**: 945–953.
- Wang, J., W. Jiang, X. Wu, M. Yang, and W. Shao, 2023 Role of vaccine in fighting the variants of covid-19. *Chaos, Solitons & Fractals* p. 113159.
- Wolf, A., J. B. Swift, H. L. Swinney, and J. A. Vastano, 1985 Determining lyapunov exponents from a time series. *Physica D: Nonlinear Phenomena* **16**: 285–317.
- World Health Organisation, 2020 Director-general’s opening remarks at the media briefing on covid-19. WHO - 11 March 2020. Available at <https://www.who.int/director-general/speeches/detail/who-director-general-s-opening-remarks-at-the-media-briefing-on-covid-19-11-march-2020>.
- World Health Organisation, 2023 Weekly epidemiological update on covid-19. Who - 30 December 2023. Available at <https://www.who.int/emergencies/diseases/novel-coronavirus-2019/situation-reports>.
- Wu, Y., W. Jing, J. Liu, Q. Ma, J. Yuan, *et al.*, 2020 Effects of temperature and humidity on the daily new cases and new deaths of covid-19 in 166 countries. *Science of the Total Environment* **729**: 139051.
- Yousaf, M., S. Zahir, M. Riaz, S. M. Hussain, and K. Shah, 2020 Statistical analysis of forecasting covid-19 for upcoming month in pakistan. *Chaos, Solitons & Fractals* **138**: 109926.
- Youssef, H. M., N. A. Alghamdi, M. A. Ezzat, A. A. El-Bary, and A. M. Shawky, 2020 A modified seir model applied to the data of covid-19 spread in saudi arabia. *AIP advances* **10**: 125210.

**How to cite this article:** Yılmaz, E., and Aydiner, E. Chaotic and Quasi-periodic Regimes in the Covid-19 Mortality Data *Chaos Theory and Applications*, 6(1), 41-50, 2024.

**Licensing Policy:** The published articles in CHTA are licensed under a [Creative Commons Attribution-NonCommercial 4.0 International License](https://creativecommons.org/licenses/by-nc/4.0/).



## Improved Set-point Tracking Control of an Unmanned Aerodynamic MIMO System Using Hybrid Neural Networks

David Mohammed Ezekiel<sup>1</sup>, Ravi Samikannu<sup>2</sup> and Oduetse Matsebe<sup>3</sup>

<sup>\*</sup>Department of Electrical, Computer and Telecommunications Engineering, Botswana International University of Science and Technology (BIUST), Private Bag 16, Palapye, Botswana, <sup>β</sup>Department of Mechanical, Energy and Industrial Engineering, Botswana International University of Science and Technology (BIUST), Private Bag 16, Palapye, Botswana.

**ABSTRACT** Artificial neural networks (ANN), an Artificial Intelligence (AI) technique, are both bio-inspired and nature-inspired models that mimic the operations of the human brain and the central nervous system that is capable of learning. This paper is based on a system that optimizes the performance of an uncertain unmanned nonlinear Multi-Input Multi-Output (MIMO) aerodynamic plant called Twin Rotor MIMO System (TRMS). The pitch and yaw angles which are challenging to control and optimize in practice, are being used as the input to the Nonlinear Auto-Regressive with eXogenous (NARX) model, and eventually trained. The training features use the Matlab Deep Learning Toolbox. The NARX structure has its core in the neural networks' architecture. Data is collected from the TRMS testbed which is used to train the network. ANN as a Hybrid intelligent control strategy of ANN in combination with Pattern Search and Genetic Algorithm, is then utilized to optimize the parameters of the neural networks. At the end it was validated, tested and the optimized system run in simulation and compared with other intelligent and conventional controllers, with the proposed controller outperforming them, giving a very fast-tracking control, stable and optimal performance that satisfactorily met all our design requirements.

### KEYWORDS

Artificial neural network  
Nonlinear auto-regressive with eXogenous  
Twin rotor MIMO system  
Multi-input multi-output  
Aerodynamic  
Unmanned helicopter model

### INTRODUCTION

The modelling, optimization and control of rigid bodies and flexible structures/systems (Ahmad *et al.* 2000a,b; Moness and Daa-Eldeen 2017) (such as plates, shells, beams, frames, etc.) are increasingly gaining a considerable attention from researchers globally (Tavakolpour *et al.* 2010; Nasir and Tokhi 2014; TRahman *et al.* 2019). These bodies and structures are highly essential manufacturing elements in electro-mechanical, civil, marine and aerospace engineering. In this paper, the application of Feedforward Neural Networks (NN) is applied to the beam of a nonlinear uncertain system called, the TRMS. It is a highly nonlinear, high-order, complex system (Moness and Daa-Eldeen 2017; Toha and Tokhi 2009;

Alam *et al.* 2004; Toha and Tokhi 2010; Ahmad *et al.* 2016) the nonlinearities and complexities emanate from the cross-couplings between the twin-rotors. These pose as a serious challenge to effectively model, control and optimize. The modelling, control and optimization of the TRMS can be carried out in either the model-based/model-driven or data-driven approaches. The data-driven (i.e. black-box modelling) approaches for which this paper is based, requires some input/output dataset (Ljung and Gunnarsson 1990)[obtained through system simulation, offline and/or online. With this dataset, the system is identified through System Identification (SI) techniques.

The drawback of SI is that it has demonstrated a computational inadequacy with nonlinear systems, but much less uncomplicated with linear systems (Ahmad *et al.* 2000a). In spite of this, it is still indispensable and a powerful design strategy, especially if the system can be linearized about some equilibrium points. To use SI methodologies, require training of the network used in the design process, which can be parametric or non-parametric.

**Manuscript received:** 14 November 2023,

**Revised:** 16 December 2023,

**Accepted:** 21 December 2023.

<sup>1</sup>ed18100190@studentmail.biust.ac.bw

<sup>2</sup>ravis@biust.ac.bw (Corresponding author).

<sup>3</sup>matsebe@biust.ac.bw

The non-parametric SI (which is of interest here) involves the use of Artificial Intelligence, such as ANN (Sjöberg *et al.* 1994; Chu *et al.* 1990) or an Adaptive Neuro-Fuzzy Inference System (ANFIS) (Castillo *et al.* 2006). For brevity, ANN is simply referred to as NN. However, they suffer from being caught in a local minimum and a very slow convergence resulting from system complexities of nonlinear systems. To solve these problems metaheuristic methods are employed for faster convergence optimization. With this, the solution being trapped in a local minimum or local minima is prevented, thus guaranteeing an accurate solution (TRahman *et al.* 2019).

A number of these metaheuristics' approaches have been successfully used in the training of ANNs in engineering and scientific applications. Some of these methods include Symbiotic Organisms Search (SOS) scheme employed to train a feed forward NN to solve a classification problem (Wu *et al.* 2016), Genetic Algorithm (GA) (Sivadasan and Shiney 2023) Harmony Search, Simulated Annealing and Differential Evolution (DE) (Rere *et al.* 2016), a hybrid algorithm composed of Particle Swarm Optimization (PSO) used for optimization of a Convolutional NN to also solve a classification problem (Yaghini *et al.* 2013), ANN models trained for stock market price predictions/forecasts (Ghasemiyeh *et al.* 2017), the newly developed Stochastic Fractal Search Algorithm SFS by Salimi (Salimi 2015) and used to train ANNs (Mosbah and El-Hawary 2017; Khishe *et al.* 2018). Also, the successful applications of ANNs in estimating the nonlinear dynamics of dynamical systems have been reported for kinematics in (Xia and Wang 2001; Yoo *et al.* 2006; Abbas and Liu 2022) for dynamics in (Lin and Goldenberg 2001; El-Fakdi and Carreras 2013) and for control in (Xia and Wang 2001; Wai 2003; Palepogu and Mahapatra 2023)

Due to the extreme and profoundly serious (i.e., massive) nonlinearities the control of Unmanned Aerial Vehicles (UAVs), of which class the TRMS falls, is a challenging one (Agand *et al.* 2017). Rahideh *et al.* proposed a Model Inversion Control law to control a 1-DOF pitch model of the TRMS using ANN (Rahideh *et al.* 2012a). The ANN was used adaptively to tune the system model. The obtained control law was consequently used to achieve control and tracking. The scheme used an adaptive nonlinear iterative learning control (Patan and Patan 2023; Bensidhoum *et al.* 2023) for compensation of the errors due to modelling, thereby identifying the system. The use of the NARX neural networks based on a Back Propagation (BP) algorithm for network training was proposed by Tijani *et al.* in (Tijani *et al.* 2014) to solve a multi-objective optimization problem. The algorithm used a multi (or many)-objective DE algorithms to identify and control the nonlinear TRMS using real-time data from experiments. The motivation of this work stems from the fact that unlike linear systems and processes which a tremendous depth of knowledge exists on the control of such systems and processes, for nonlinear control systems are quite very challenging. Since most or nearly all control systems are nonlinear attention has shifted by researchers and control engineers globally on development of control techniques, methodologies and strategies to address these systems. Nowadays the research direction has shifted focus on Artificial Intelligence (AI) and Computational Intelligence (CI) which are at the cutting edge. From studies on the use of ANN, an AI-based technique, developing a controller using NN structure is quite very difficult, because of the dynamic nature of such systems, where the states are also dynamic in nature and constantly changing. This pose as a serious challenge to control such a system.

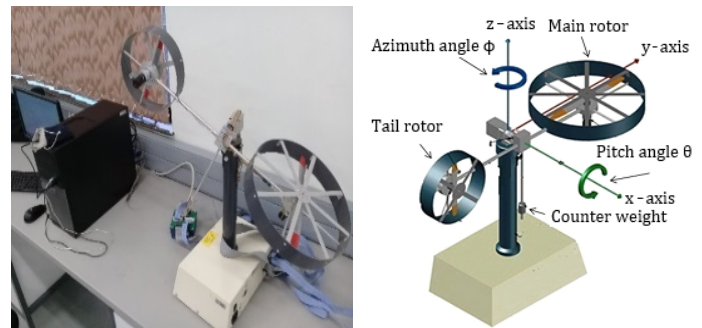
In this study, the use of Deep Neural Networks architecture using NARX Shallow NN for the ANN training is used to identify,

optimize and control the nonlinear TRMS lab-scaled helicopter. The NARX model is used here identifies/ capture the nonlinear dynamics of the nonlinear TRMS testbed. The NARX network is a feedforward neural network composed of 2 layers, with a sigmoid transfer or activation function in the hidden layer and a linear transfer function in the outer layer. Tapped delay lines are also used by the network to store previous values of the input and output sequences. Here, the outputs are fed back into the inputs through the delay lines, since if  $y(t)$  is the output, then  $y(t)$  is a function of

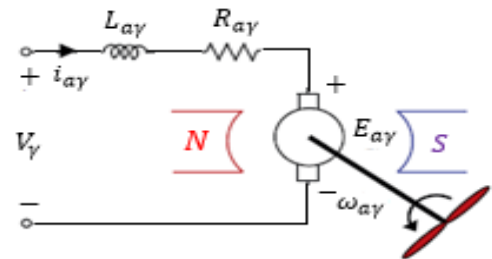
$$y(t-1), y(t-2), \dots, y(t-d). \quad (1)$$

The learning rules algorithms employed mostly are the Bayesian Regularization (trainbr), Levenberg-Marquardt (trainlm), and the Scaled Conjugate Gradient (trainscg). The first two algorithms are based on the Jacobian calculations while the last training method is based on the gradient calculations. In this paper, the 2 inputs (elevation and azimuth) and the outputs/target vectors (pitch and yaw) are composed of 181 datasets each, at random, roughly divided into 70% for the training phase, 15% for the validation phase and 15% for the test phase to generalize the network. 2 different set of numbers of hidden neurons of 10 and 1000 were used, with a tapped delay line of 4. The paper is organized as follows: Section 2 presents the experimental arrangements as well as the governing equations of motion; Section 3 presents the NN architecture and theoretical background; Section 4 gives the training results and final simulations.

## SETUP OF EXPERIMENT



**Figure 1** (a) The Real-world experimental setup at the Botswana International University of Science and Technology (BIUST), with the beam inclined at  $60^\circ$  to the horizontal at rest and showing I/O communication cables (b) Schematic graphic (Abdulwahhab and Abbas 2017; Ezekiel *et al.* 2020, 2021).



**Figure 2** The electrical circuit connection of the DC motor of the TRMS



The model of the DC motors is given in (Darus and Lokaman 2010; Rahideh et al. 2008) as:

$$\frac{di_{a\gamma}}{dt} = \frac{1}{L_{a\gamma}} (V_{\gamma} - E_{a\gamma} - R_{a\gamma}i_{a\gamma}) \quad (2)$$

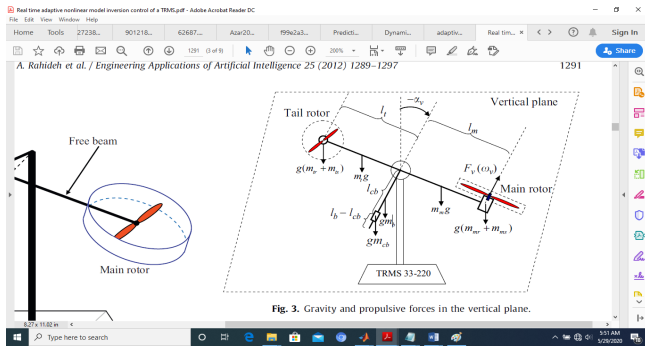
$$E_{a\gamma} = K_{a\gamma}\phi_{\gamma}\omega_{\gamma} \quad (3)$$

$$J_{\gamma r} = c_{\gamma aw} = -G_s \quad (4)$$

$$T_{e\gamma} = K_{t\gamma}i_{a\gamma} \quad (5)$$

$$T_{L\gamma} = K_{t\gamma}i_{a\gamma}|\omega_{\gamma}| \quad (6)$$

Where,  $V_{\gamma}$  is the control voltage input to either the vertical or the horizontal channel,  $E_{a\gamma}$ ,  $i_{a\gamma}$ ,  $R_{a\gamma}$ , and  $L_{a\gamma}$  are respectively the e.m.f, current, resistance, and inductance in the armature of the main/tail motor;  $k_{a\gamma}$  and  $k_{t\gamma}$  are constants;  $\phi_{\gamma}$  is the flux linkages;  $\omega_{\gamma}$  is the angular velocity of either the main or tail motor,  $T_{e\gamma}$ ,  $T_{L\gamma}$  are the magnetic torque and load torque respectively in the main/tail motor;  $J_{\gamma r}$ ,  $B_{\gamma r}$  are the moments of inertias and viscous friction damping coefficients of the rotors in the main/tail motors.



**Figure 3** Planar (vertical plane) representation of the TRMS, showing the gravity and propulsive forces (Rahideh et al. 2012b)

### Governing Equations of Motion of the TRMS

Being a dynamical system that has rotational motion, Newtonian mechanics for rotational dynamics or Lagrangian mechanics may be used to develop the dynamic equations of motion. Based on Newtonian mechanics for rotational dynamics, the dynamic equations of motion (using Newton's laws of motion for rotational dynamics) (Coelho et al. 2007a, 2008, 2007b) of the TRMS, representing the flight in the pitch (or vertical) plane and the yaw (or horizontal) plane are respectively given by:

$$\begin{aligned} \frac{dS_v}{dt} &= \frac{M_v}{J_v} = \frac{l_m F_v(\omega_m) - \Omega_v K_v + g[(A - B) \cos \alpha_v - C \sin \alpha_v]}{J_v} \\ &\quad - \frac{1}{2} \frac{\Omega_h^2 (A + B + C) \sin 2\alpha_v}{J_v} \\ &= \frac{l_m F_v(\omega_m) + g[(A - B) \cos \alpha_v - C \sin \alpha_v] - T_{\text{fric},v}}{J_v} \end{aligned} \quad (8)$$

$$\frac{dS_h}{dt} = \frac{M_h}{J_h} = \frac{l_t F_h(\omega_t) \cos \alpha_v - \Omega_h K_h}{D \sin^2 \alpha_v + E \cos^2 \alpha_v + F} = \frac{l_t F_h(\omega_t) \cos \alpha_v - \Omega_h K_h}{J_h} \quad (8)$$

where,  $\Omega_v$  and  $\Omega_h$  are the angular/rotational velocities of the rotors for the pitch and yaw orientations, respectively, given by:

$$\Omega_v = \frac{d\alpha_v}{dt} = S_v + \frac{J_{tr}\omega_t}{J_v} \quad (9)$$

$$\Omega_h = \frac{d\alpha_h}{dt} = S_h + \frac{J_{mr}\omega_m \cos \alpha_v}{J_h} = S_h + \frac{J_{mr}\omega_m \cos \alpha_v}{D \sin^2 \alpha_v + E \cos^2 \alpha_v + F} \quad (10)$$

where A, B, C, D, E, F are constants, and are given by:

$$A = \left(\frac{m_t}{2} + m_{tr} + m_{ts}\right) l_t; \quad B = \left(\frac{m_m}{2} + m_{mr} + m_{ms}\right) l_m; \quad 'L$$

$$C = \frac{m_b}{2} l_b + m_{cb} l_b; \quad D = \frac{m_b}{3} l_b^2 + m_{cb} l_{cb}^2;$$

$$E = \left(\frac{m_m}{3} + m_{mr} + m_{ms}\right) l_m^2 + \left(\frac{m_t}{3} + m_{tr} + m_{ts}\right) l_t^2;$$

$$F = m_{ms} r_{ms}^2 + \frac{m_{ts}}{2} r_{ts}^2$$

The aerodynamic propulsive forces,  $F_v(\omega_m)$  and  $F_h(\omega_t)$ , are produced by the main/tail rotors in the vertical/horizontal planes, respectively, and are given by:

$$F_v(\omega_m) = \frac{J_v \hat{\Omega}_v + g[(A - B) \cos \alpha_v - C \sin \alpha_v] - T_{\text{fric},v}}{l_m} \quad (11)$$

$$\hat{\Omega}_v = \frac{d^2 \alpha_v}{dt^2} \quad (12)$$

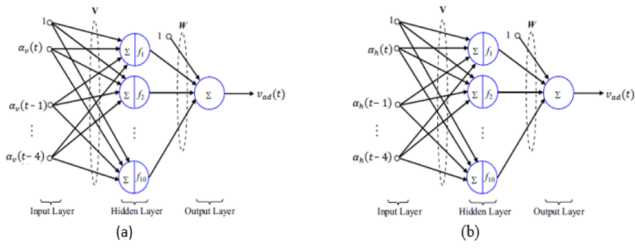
$$F_h(\omega_t) = \frac{J_h \hat{\Omega}_h - T_{\text{fric},h}}{l_t \cos \alpha_v} \quad (13)$$

$$\hat{\Omega}_h = \frac{d^2 \alpha_h}{dt^2} \quad (14)$$

The variables  $M_v$  and  $M_h$  represent the sum of moments in the pitch and yaw planes, respectively. Similarly,  $J_v$  and  $J_h$  denote the sum of moments of inertias in the vertical and horizontal planes.  $T_{\text{fric},v}$  stands for the frictional torque developed in the pitch plane. The masses  $m_{mr}$  and  $m_{tr}$  correspond to the composite mass of the Main/Tail rotor plus Main/Tail DC motor.  $m_m$  and  $m_t$  are the masses of the beam's Main/Tail portion,  $m_{cb}$  is the mass of the counterweight, and  $m_{ms}$  and  $m_{ts}$  represent the masses of the Main/Tail shield. The lengths  $l_b$ ,  $l_{cb}$ ,  $l_m$ , and  $l_t$  refer to the counterbalance beam length, the distance from the pivot joint to the counter-balance or counterweight, and the lengths of the beam's Main/Tail portion. The angles  $\alpha_v$  and  $\alpha_h$  represent the angles for the pitch and yaw, respectively.

### THE NEURAL NETWORK STRUCTURE

The NN structure presents the layers arrangements and the no. of neurons in each layer. Each of the two planes/axes of our plant in question (i.e., the pitch and yaw) are presented with a Feedforward NN structure.



**Figure 4** The NARX shallow NN for the (a) pitch (b) yaw angles (Rahideh *et al.* 2012a,b).

$$\mathbf{V} = \begin{bmatrix} b_{v,1} & \cdots & b_{v,10} \\ \vdots & \ddots & \vdots \\ v_{3,1} & \cdots & v_{3,10} \end{bmatrix} \quad \text{and} \quad \mathbf{V} = \begin{bmatrix} b_{v,1} & \cdots & b_{v,1000} \\ \vdots & \ddots & \vdots \\ v_{3,1} & \cdots & v_{3,1000} \end{bmatrix} \quad (19)$$

$$f_j(z_j) = \frac{1}{1 + e^{-\alpha_j z_j}}, \quad j = 1, 2, \dots, 10 \quad (20)$$

$$\mathbf{F} = \begin{bmatrix} 1 \\ f_1(z_1) \\ \vdots \\ f_{10}(z_{10}) \end{bmatrix} \quad (21)$$

where,  $\mathbf{X}$ = the input vector,  $\mathbf{W}$ = the network weights,  $\mathbf{V}$ = the biases matrices,  $\mathbf{F}$ = the activation function Widrow and Hoff (1960).

### Training the Network

The neural network must be trained in order for biases and weights adjustments so as to obtain the optimum system parameters. This training could be carried out in offline or online scenarios, but here the offline training is adopted. The network weights and biases are updated/adjusted with the main aim of minimizing the tracking error response of the plant (TRMS). This adjustment is done according to the following formulations (Widrow and Hoff 1960):

$$\dot{\mathbf{W}} = - \left[ (\mathbf{F} - \mathbf{FV}^T \mathbf{X}) \mathbf{r}^T + \beta \|e\| \mathbf{W} \right] \Lambda_{\mathbf{W}} \quad (22)$$

$$\dot{\mathbf{V}} = -\Lambda_{\mathbf{V}} \left[ \mathbf{X} \mathbf{r}^T \mathbf{W}^T \mathbf{F}^T + \beta \|e\| \mathbf{V} \right] \quad (23)$$

where  $\Lambda_{\mathbf{W}}, \Lambda_{\mathbf{V}}$  represent the network learning rates, and with  $\beta > 0$  ensures tracking the error of the system  $e$  and the neural networks weights are bounded uniformly.  $e$  is given by:

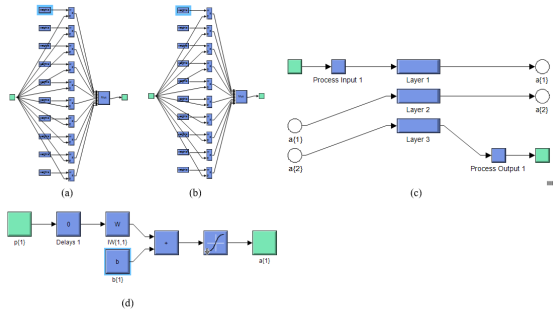
$$e = \begin{bmatrix} \alpha_{v,\text{ref}} - \alpha_v \\ \dot{\alpha}_{v,\text{ref}} - \dot{\alpha}_v \end{bmatrix} \quad (24)$$

$$\mathbf{F} = \begin{bmatrix} 0 & 0 & \cdots & 0 \\ \frac{\partial f_1(z_1)}{\partial z_1} & 0 & \cdots & 0 \\ 0 & \frac{\partial f_2(z_2)}{\partial z_2} & \cdots & \vdots \\ 0 & \cdots & \ddots & \frac{\partial f_2(z_2)}{\partial z_2} \\ 0 & \cdots & 0 & 0 \end{bmatrix} \quad (25)$$

$$\mathbf{r}^T = (\mathbf{e}^T \mathbf{P} \mathbf{B})^T \quad (26)$$

where,  $\mathbf{P}$  is the Lyapunov candidate solution for the nonlinear equation:

$$\mathbf{A}^T \mathbf{P} + \mathbf{P} \mathbf{A} + \mathbf{Q} = 0 \quad (27)$$



**Figure 5** The actual NARX shallow (1-layered) NN controllers for the (a) pitch (b) yaw, each having 10 neurons with network weights attached as seen above (c) the configuration showing the single-input single-output network (d) the feedforward configuration for both pitch and yaw angles.

### The Feedforward Neural Network

For the first NARX shallow Neural Networks (Fig. 4a) having one hidden layer with 10 hidden neurons, since 4 input tapped delays are employed for this research work, then the pitch angle of the beam is the inputs to the NN at the current time, and delayed 1, 2, 3, and 4 samples, i.e.,  $\alpha_v(t), \alpha_v(t-1), \alpha_v(t-2), \alpha_v(t-3), \alpha_v(t-4)$ . In a similar vein, the second NARX NN model is for the yaw angle with inputs at the current time instant, and those delayed by 1, 2, and 3 samples, i.e.,  $\alpha_h(t), \alpha_h(t-1), \alpha_h(t-2), \alpha_h(t-3), \alpha_h(t-4)$ . For both models, the output  $v_{ad}(t)$  is expressed as:

$$v_{ad}(t) = b_w + \sum_{j=1}^n w_j f_j \left( b_{vj} + \sum_{i=1}^3 v_{ij} x_i \right) = \mathbf{W}^T \mathbf{F}(\mathbf{V}^T \mathbf{X}) \quad (15)$$

$$\mathbf{X} = \begin{bmatrix} 1 \\ x_1 \\ x_2 \\ x_3 \end{bmatrix} \quad (16)$$

$$x_i = \alpha_v(t-i+1) = \alpha_h(t-i+1), \quad i = 1, 2, 3 \quad (17)$$

$$\mathbf{W} = \begin{bmatrix} w_1 \\ w_2 \\ \vdots \\ w_n \end{bmatrix}, \quad n = 10, 1000 \quad (18)$$

where  $Q$  must be a positive-definite matrix (i.e.,  $Q > 0$ ),  $A$  and  $B$  are matrices for the tracking error ( $e$ ), given by:

$$A = \begin{bmatrix} 0 & 1 \\ -k_p & -k_d \end{bmatrix} \quad (28)$$

$$B = \begin{bmatrix} 0 \\ 1 \end{bmatrix} \quad (29)$$

### Validation of the Model

The tools used for validating the nonlinear model of the TRMS include, One Step-Ahead (OSA) Prediction, Mean Squared Error (MSE), Correlations Tests (Autocorrelation and cross-correlation functions) and Normalization.

### OSA Prediction

The OSA prediction for the NARX network or model occurs when the feedback loop of the network is open. The NARX network/model thus predicts the next value of the output  $v_{\alpha d}(t)$  from the previous ones of  $v_{\alpha d}(t)$  and the input  $\alpha_\gamma(t)$ . For a Multi-Step-Ahead prediction, the feedback loop must necessarily be closed. The OSA is a measure of the accuracy in modeling. It is given by:

$$\hat{v}_{\alpha d}(t) = f[\alpha_\gamma(t), \alpha_\gamma(t-1), \dots, \alpha_\gamma(t-n_{\alpha_\gamma}), v_{\alpha d}(t-1), \dots, v_{\alpha d}(t-n_{v_{\alpha d}})] \quad (30)$$

where,  $f$  is a nonlinear function approximator,  $\alpha_\gamma, v_{\alpha d}$  represent the input/output respectively,  $\hat{v}_{\alpha d}(t)$  is the prediction value and  $\gamma$  represents pitch or yaw. The OSA is an extension of the NARX model, where the NARX model is given by:

$$v_{\alpha d}(t) = f[v_{\alpha d}(t-1), \dots, v_{\alpha d}(t-n_{v_{\alpha d}}), \alpha_\gamma(t-1), \dots, \alpha_\gamma(t-n_{\alpha_\gamma})] \quad (31)$$

$$e_{\text{res}} = v_{\alpha d}(t) - \hat{v}_{\alpha d}(t) \quad (32)$$

### Mean Squared Error (MSE)

The MSE (Mean Squared Error) is a validation test, providing the average of the sum of mean squares of the differences between the actual and predicted outputs ( $v_{\alpha d}(t), \hat{v}_{\alpha d}(t)$ ) of the TRMS system. The outputs are generated using the input and the optimized parameters of the network. MSE is given by:

$$\text{MSE} = f(e) = \frac{1}{n} \sum_{i=1}^n |e_{\text{res}}|^2 = \frac{1}{n} \sum_{i=1}^n |v_{\alpha d}(t) - \hat{v}_{\alpha d}(t)|^2 \quad (33)$$

where,  $n$  is the number of input/output samples.

The MSE (Mean Squared Error) algorithm helps in adjusting the network weights and biases, minimizing the MSE. Fortunately, the MSE performance indicator is a quadratic function, which will either have a global minimum, a weak minimum, or no minimum at all, determined by the nature of the input vectors. Hence, a unique solution may or may not exist. The MSE algorithm, or Widrow-Hoff learning algorithm (Demuth and Beale 2000), approximates MSE based on the steepest descent algorithm at each iteration.

Taking the partial derivatives of the MSE with respect to weights and biases at the  $k$ th iteration, we get:

$$\frac{\partial e_{\text{res}}^2(k)}{\partial w_{ij}} = 2e_{\text{res}}(k) \frac{\partial e_{\text{res}}(k)}{\partial w_{ij}}, \quad j = 1, 2, \dots, R \quad (34)$$

$$\frac{\partial e_{\text{res}}^2(k)}{\partial b} = 2e_{\text{res}}(k) \frac{\partial e_{\text{res}}(k)}{\partial b} \quad (35)$$

Taking the partial derivative w.r.t error

( $e_{\text{res}}$ )

$$\frac{\partial e_{\text{res}}(k)}{\partial w_{i,j}} = \frac{\partial}{\partial w_{i,j}} [t(k) - \alpha(k)] = \frac{\partial}{\partial w_{i,j}} [t(k) - (Wp(k) + b)] \quad (36)$$

or

$$\frac{\partial e_{\text{res}}(k)}{\partial w_{i,j}} = \frac{\partial}{\partial w_{i,j}} [t(k) - \left( \sum_{i=1}^R w_{1,i} p_i(k) + b \right)] \quad (37)$$

where,  $p_i(k)$  is the  $i$ th element of the input vector at the  $k$ th iteration.

Further simplification yields:

$$\left. \begin{aligned} \frac{\partial e_{\text{res}}(k)}{\partial w_{i,j}} &= -p_j(k) \\ \frac{\partial e_{\text{res}}(k)}{\partial b} &= -1 \end{aligned} \right\} \quad (38)$$

### The Correlations Tests

These tests are statistical tests for bivariate dataset composed of the autocorrelation and cross-correlation functions (Darus and Lokaman 2010), given by:

$$\left. \begin{aligned} \phi_{\varepsilon\varepsilon}(\tau) &= E[\varepsilon(t-\tau)\varepsilon(t)] = \delta(t) \\ \phi_{x\varepsilon}(\tau) &= E[x(t-\tau)\varepsilon(t)] = 0 \quad \forall \tau \\ \phi_{x^2\varepsilon}(\tau) &= E[(x^2(t-\tau) - \bar{x}^2(t))\varepsilon(t)] = 0 \quad \forall \tau \\ \phi_{x^2\varepsilon^2}(\tau) &= E[(x^2(t-\tau) - \bar{x}^2(t))\varepsilon^2(t)] = 0 \quad \forall \tau \\ \phi_{\varepsilon(\varepsilon x)}(\tau) &= E[\varepsilon(t)\varepsilon(t-1-\tau)x(t-1-\tau)] = 0 \quad \tau \geq 0 \end{aligned} \right\} \quad (39)$$

where,  $\phi_{\varepsilon\varepsilon}(\tau)$  and  $\phi_{x\varepsilon}(\tau)$  are the autocorrelation and cross-correlation functions between  $x(t)$  and  $\varepsilon(t)$ , and  $\varepsilon(t)$  is the error of the prediction sequence.

### Normalization

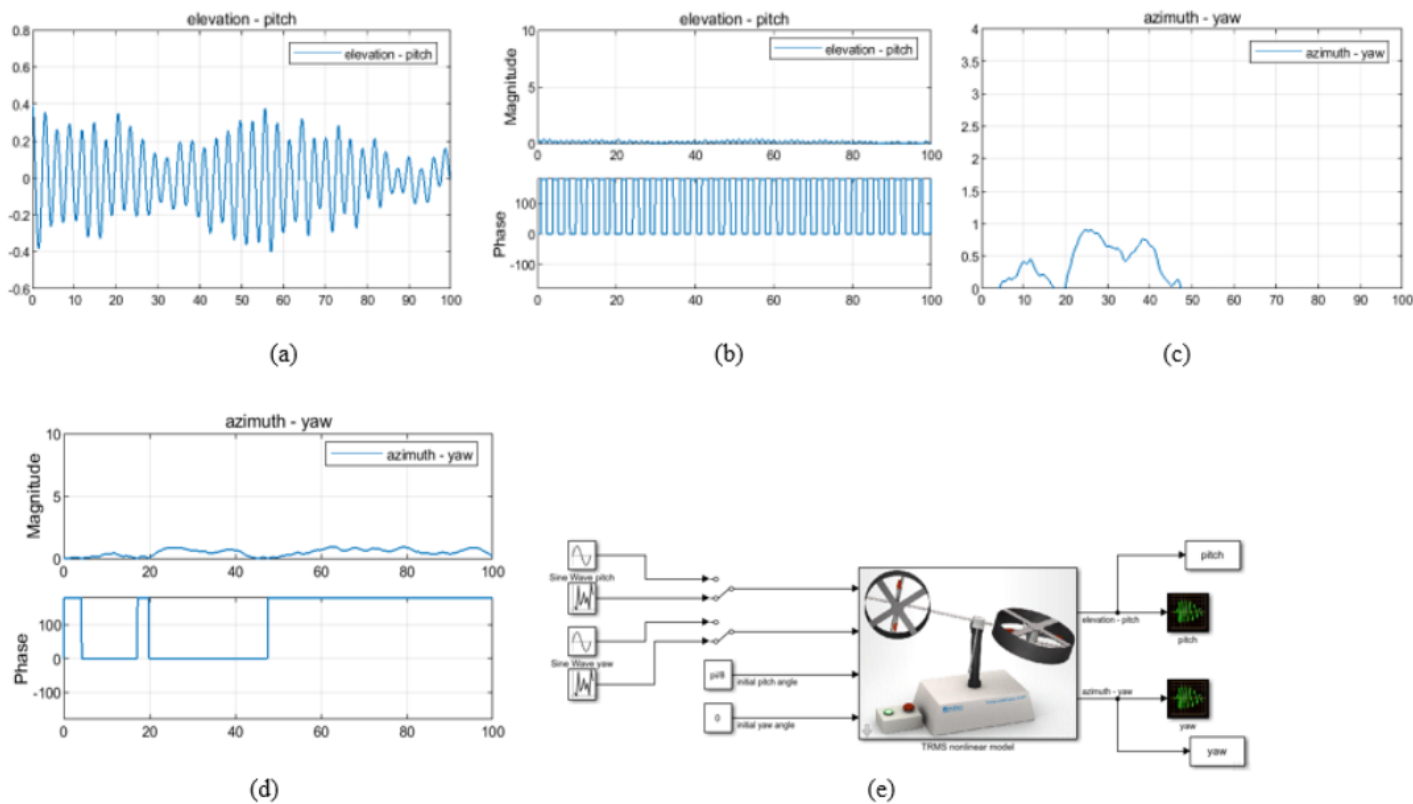
In practice, the correlations computed are normalized to ensure all the values fall within a given bandwidth and/or range. The normalized correlation function between two sequences  $\psi_1(t)$  and  $\psi_2(t)$  is given by:

$$\hat{\phi}_{\psi_1\psi_2}(\tau) = \frac{\sum_{i=1}^{N-\tau} \psi_1(t)\psi_2(t-\tau)}{\sqrt{\sum_{i=1}^N \psi_1^2(t) \sum_{i=1}^N \psi_2^2(t)}} \quad (40)$$

## RESULTS AND DISCUSSION

### The Nonlinear TRMS Modelling

The method employed in this research work involves the use of a time-domain closed-loop control approach. Here, the NARX shallow Neural Networks modelling is used as a compensator to train the network and provide the closed-loop control signal. The input signals to the TRMS and the NN are a uniform random signal, exciting both the pitch and yaw subsections of the plant/system. The Simulink model of the TRMS as well as the signals are given below.



**Figure 6** Simulation of the TRMS (a) Pitch Random signals for the input (b) Its Log/Magnitude (c) Yaw Random signals for the input (d) Its Log/Magnitude (e) Simulink model of the nonlinear TRMS

### Shallow NN Modelling

**Training with Levenberg-Marquardt (LM)** It is known that for every neural network structure designed/implemented as a solution to e.g. a control problem, the correction error functions must lie within an acceptable predefined region which is depicted in figs 7 (a - e), otherwise the control design objective will not be achievable. Also, the Best validation performance for our design must occur at an epoch where the best value falls the parameterized training, validation and testing performance scores. And as can be clearly seen, these were obtained at various epochs for individual runs of the TRMS plant, forming the available simulation data to the NN. 3 different runs each for 10 neurons (figs. 7 (g - i)) and for 1000 neurons (figs. 7 (j - l)) were used in order to show data integrity from the TRMS Simulink model obtained from first principles. For the training, testing and validation of the NN structure, Levenberg-Marquardt training algorithm was used throughout this research and the step-by-step procedure is giving above in fig. 7 (m) in Matlab.using the nntool command.

**Further Discussions** Figs 9 – 13 below show the results obtained from different controllers employed in this study. In Fig. 9, Classical PID control was used for simulation times of (a) 50 (b) 100 seconds, while in Fig. 10, ANN controllers were generated and deployed for simulation times of (a) 50 (b) 100 seconds. In Fig. 11, the developed ANN controllers were combined with meta-heuristic approaches of Pattern Search (PS) and Latin Hyperbole (LH) to improve on the neural controller. In Fig. 12, the ANN controllers were combined with PS and Genetic Algorithm (GA) this time to obtain highly improved tracking control performances for simulation times of (a) 50 (b) 100 seconds. Fig. 13 is merely

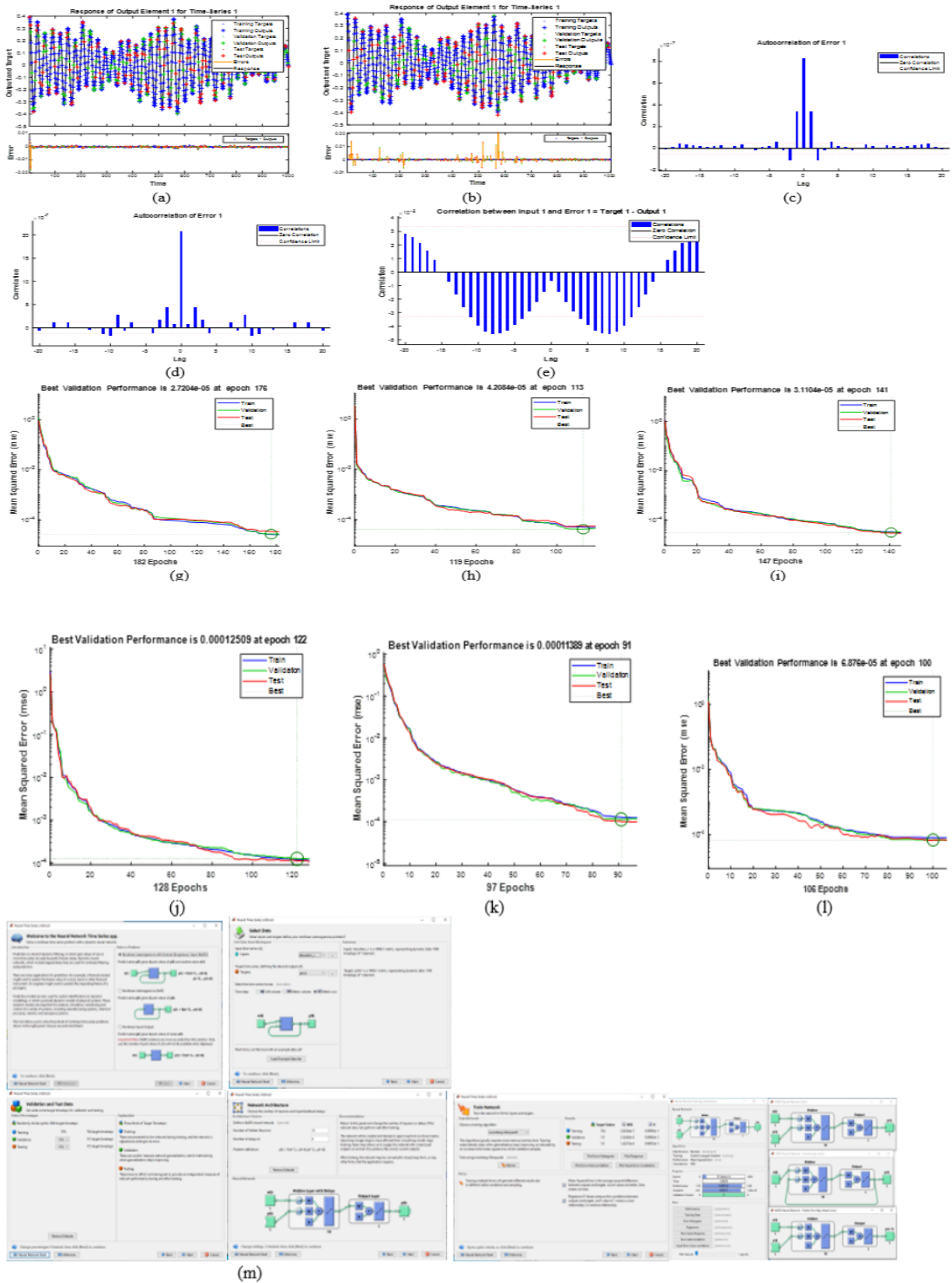
a comparison of these techniques above, combined, to depict the strength of the ANN + PS + GA strategy over the other methods in setpoint tracking of the commanded input to the TRMS prototype helicopter.

Since the performance measures can be given in terms of time-domain or frequency-domain specifications, here the performance indices are expressed in terms of the usual time-domain specification: rise time  $\tau_r$ , settling time  $\tau_s$ , and steady-state error  $e_{ss}$ . These results have been presented and tabulated in Tables 1 and 2 below. Note that the ISE and RMSE are functions of the squares of  $e_{ss}$  error coefficients, statistically designed as indices of performances of the control simulations. Since the results are presented in a composite fashion, the combined  $e_{ss}$  for the pitch and yaw angles for ANN + PS + GA is negligibly small compared to the other methods used, as seen in Fig. 12 and Table 1. This explains the best tracking performance and low control energy required.

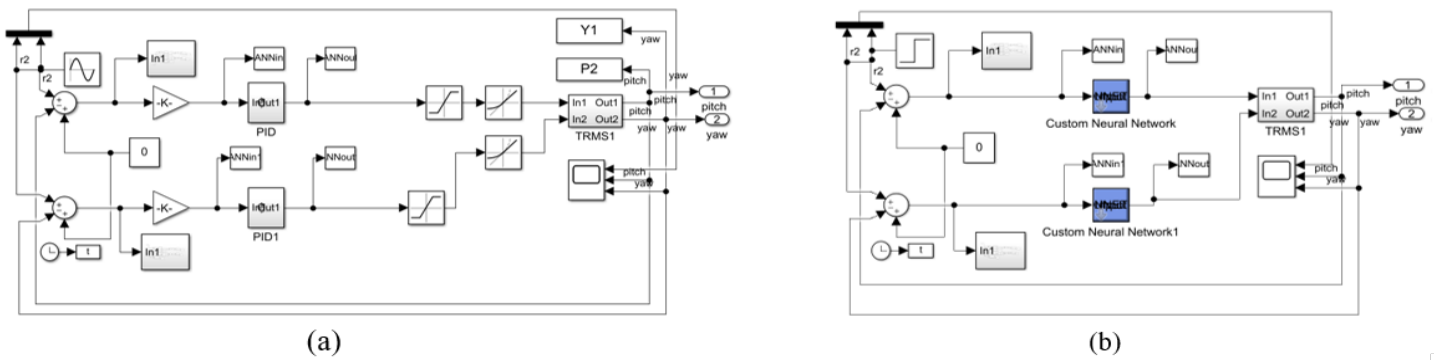
Note: PS = Pattern Search; LH = Latin Hyperbole;  $\tau_r$ =rise time;  $\tau_s$ =Settling time;  $e_{ss}$ =Steady-state error

Note: PS = Pattern Search; LH = Latin Hyperbole;  $\tau_r$ =rise time;  $\tau_s$ =Settling time;  $e_{ss}$ =Steady-state error; ISE = Integral Squared Error; RMSE = Root Mean Squared error

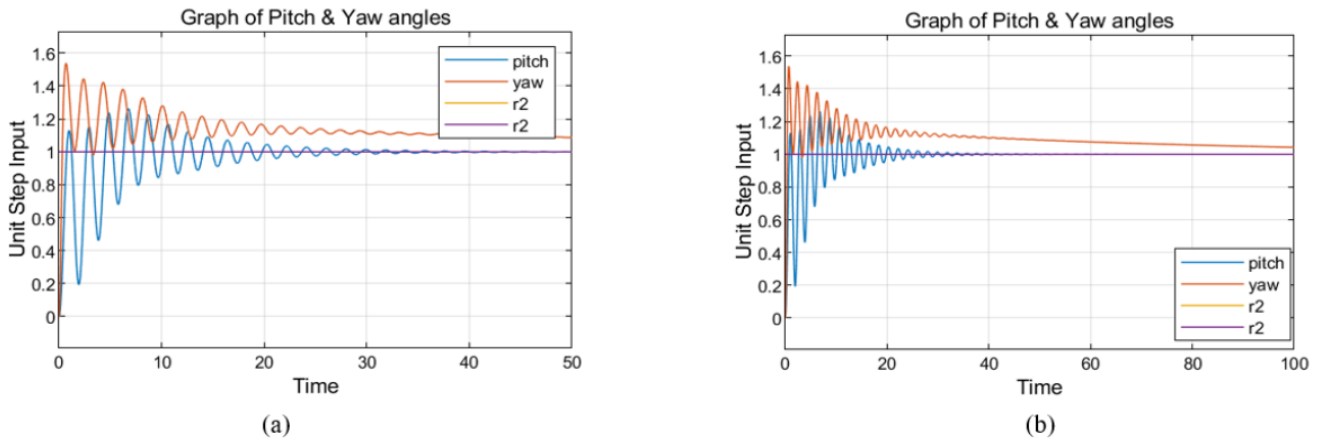
The TRMS plant is a highly uncertain and highly nonlinear plant with high-frequency oscillations, particularly with the pitch angle. This can pose as a serious control challenge in efforts to remove the rippling oscillations. This is shown in the scope of the designed control system using the conventional PID controllers (Fig. 9). For the real system, this evidently would affect the plant operation in the inability of the plant to settle within acceptable limits specified for effective control. The need, therefore, for im-



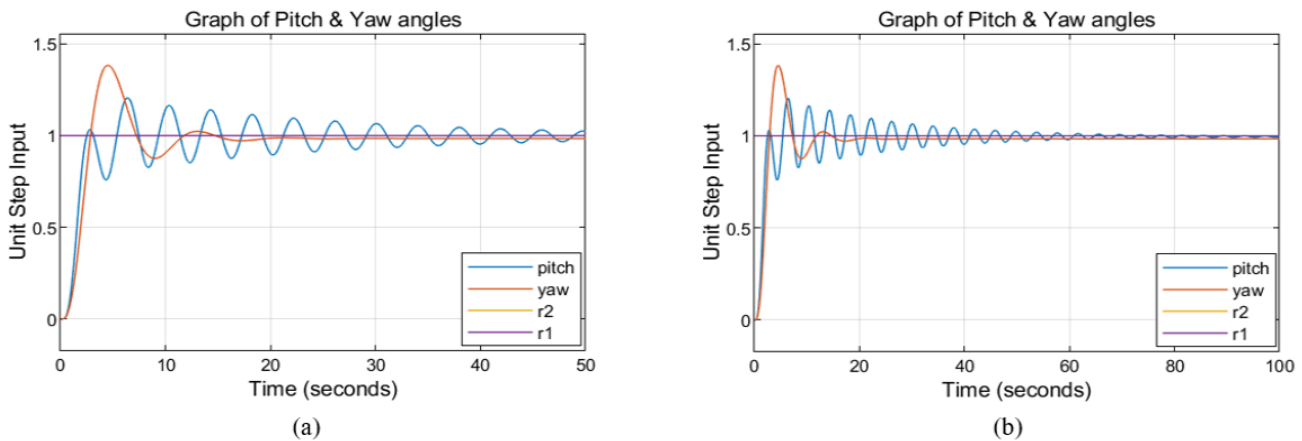
**Figure 7** Levenberg-Marquardt training with (a) 10 (b) 1000 hidden neurons; Autocorrelation Error for (c) 10 (d) 1000 hidden neurons; Input-Error Correlation for (e) 10 (f) 1000 hidden neurons; Best validation performance for (g)-(i) 10 (j) – (l) 1000 hidden neurons (m) Matlab nntool NARX NN GUI programming and execution.



**Figure 8** Control system designed to implement step input signal tracking control using (a) conventional PID controller (b) neural networks controllers generated using the 'gensim' command



**Figure 9** The tracking control for the elevation (pitch)-red and azimuth (yaw)-blue trackings of the TRMS using PID controllers for a simulation time of (a) 50 (b) 100 seconds

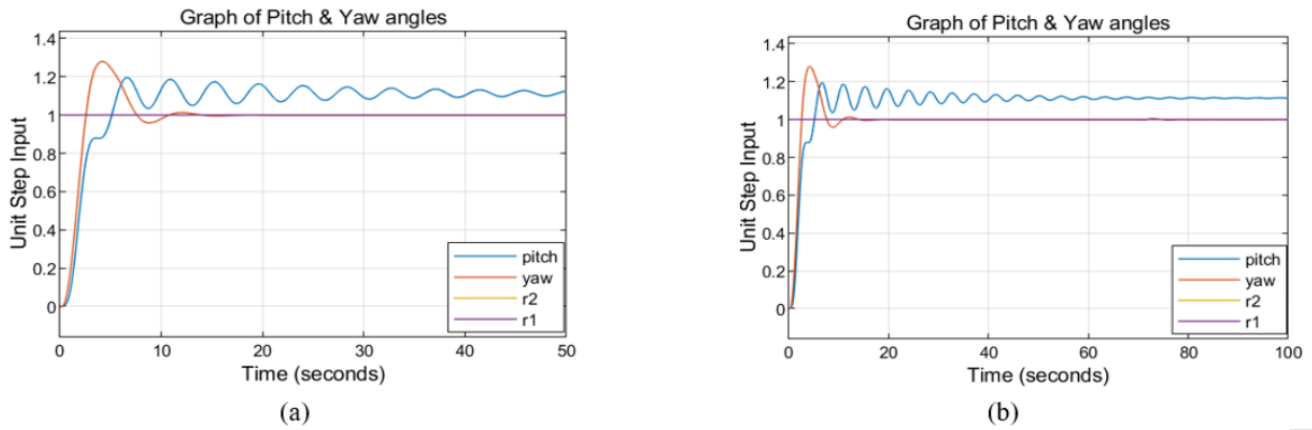


**Figure 10** The final actual output shown for the elevation (pitch)-red and azimuth (yaw)-blue trackings of the TRMS using ANN controllers realized using the "gensim" command for a simulation time of (a) 50 (b) 100 seconds

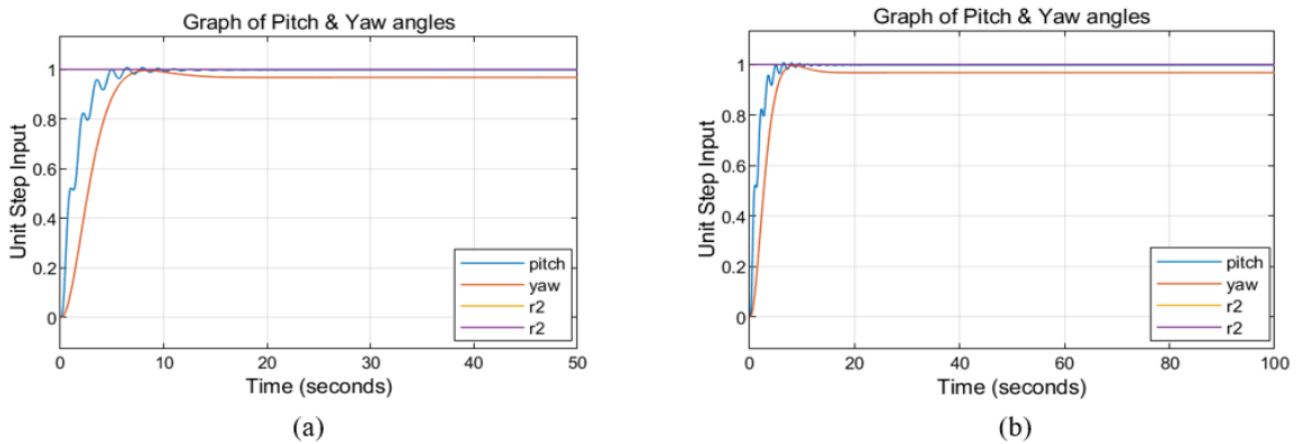
proved tracking becomes indispensable for such a safety-critical system.

This informed the use of the neural networks (NN) controllers (Fig. 10). The NN controllers were able to eliminate the undesirable oscillations or ripples in the final outputs for the yaw angle at first glance (Fig. 10), though with a large overshoot. When the network

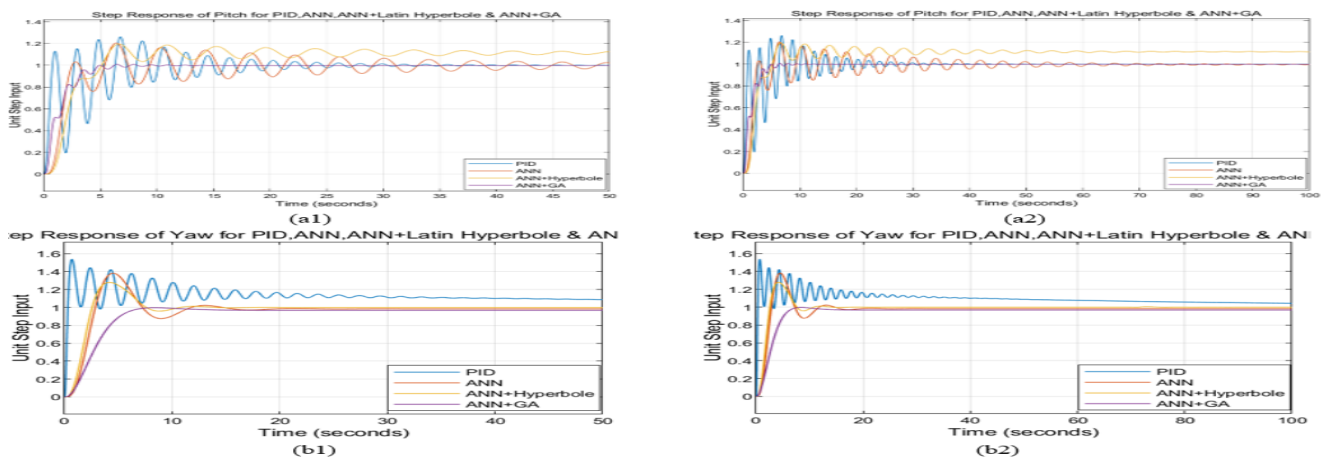
weights of the ANN controllers were optimized using intelligent schemes of Pattern Search with Latin Hyperbole (ANN + PS + LH) and Pattern Search with Genetic Algorithm (ANN + PS + GA), the GA-based ANN controllers completely eliminated the ripples for both angles and brought the system within acceptable bandwidths of control (Fig. 12) and fast tracking simulation time of 10 seconds.



**Figure 11** Improved step input tracking control for the pitch and yaw angles using neural networks controllers optimized using Pattern Search + Latin Hyperbole for a simulation time of (a) 10 (b) 100 seconds



**Figure 12** Final Improved step input tracking control for the pitch and yaw angles using neural networks controllers optimized using Pattern Search + GA for a simulation time of (a) 10 (b) 100 seconds



**Figure 13** Comparisons of the different controllers employed above for a step input tracking response for the (a) pitch and (b) yaw angles, for a simulation time of (a1 & b1) 50 (a2 & b2) 100 seconds

The ANN + PS + LH also performed well with a fast tracking response but with a very high overshoot for the yaw angle and a large steady-state error ( $e_{ss}$ ) (Fig. 11).

The best-performing algorithm as evidenced in Table 2 above is the proposed ANN + PS + GA, with the best settling time for the pitch angle ( $\tau_s = 5.14$ ) and the second-best settling time for the

■ **Table 1** Quantitative comparison of time-domain specifications between the proposed ANN + Pattern Search + GA controller, and the 3 other controllers design strategies for pitch & yaw angles

Controller Method	Horizontal plane ( $\phi$ angle )			Vertical plane ( $\theta$ angle )		
	$\tau_r$	$\tau_s$	$e_s$	$\tau_r$	$\tau_s$	$e_{ss}$
	PID	0.24	100	0.04	0.48	25.00
ANN	1.18	14.5	0.02	1.32	56	0.00
ANN + PS + LH	1.55	9.9	0.99	4	37	0.11
ANN + PS + GA	3.85	14.42	0.03	2.79	5.14	0.002

■ **Table 2** Quantitative comparison of performance indices between the proposed ANN + Pattern Search + GA controller, and 3 other controllers design strategies for pitch & yaw angles.

Controller Method	Horizontal plane ( $\phi$ angle )		Vertical plane ( $\theta$ angle )	
	ISE	RMSE	ISE	RMSE
	PID	1.402	0.087	1.135
ANN	1.862	0.016	1.556	0.223
ANN + PS + LH	1.835	0.002	2.243	0.123
ANN + PS + GA	2.034	0.032	72.36	0.758

yaw angle, as well as good rise times, i.e., very fast responses and good steady-state errors for both the pitch and yaw angles.

## CONCLUSION

Results for the NARX Feedforward NN methodology in the modeling of the nonlinear TRMS have been presented in this report. It has also been shown that different solutions are obtained for every NN training undergone. This is due to the differing initial weights conditions and biases as well as the arbitrary (i.e., random) division of the dataset into training, validation, and testing in the given ratios of 0.7, 0.15, 0.15. To ensure accuracy of the modeling results, retraining should be performed several times.

The final output results for the ANN and Pattern Search with Genetic Algorithm (ANN + PS + GA) show satisfactory control for the optimized performance of the nonlinear plant, outperforming three other controllers employed, as proven by the statistical and graphical results presented. The proposed controller met all our design requirements of within 5% of settling time, below 1% ( $\gg 1\%$ ) of overshoot, as well as excellent rise times, i.e., very fast (aggressive) responses for both the pitch and yaw angles, and no steady-state error for the pitch angle, and a negligible steady-state error for the yaw angle. Also of note was the minimum control energy used by the controller in achieving these objectives.

The neural controllers designed were based on SISO control architecture of the neural networks, each for the decoupled and independent pitch and yaw subsystems. For future work, a more robust and adaptive MIMO neural networks controller can be developed/ designed without going through the rigours of decoupling the TRMS helicopter model where some dynamics could be lost due to system approximations and simplification in modelling. The MIMO neural controller should automatically determine the network gains and biases for a neural networks structure with two-inputs two-outputs in a reasonable amount of time.

## Acknowledgments

Authors David Mohammed Ezekiel, Ravi Samikannu, and Matsebe Oduetse received initiation research grants from Botswana International University of Science and Technology (BIUST) to carry out this research work. Grant No: Ref/DVC/RDI/2/1/7 V (8) Account Project Code: S00170.

## Availability of data and material

Not applicable.

## Conflicts of interest

The authors declare that there is no conflict of interest regarding the publication of this paper.

## Ethical standard

The authors have no relevant financial or non-financial interests to disclose.

## LITERATURE CITED

- Abbas, N. and X. Liu, 2022 A mixed dynamic optimization with  $\mu$ -synthesis (dk iterations) via optimal gain for varying dynamics of decoupled twin-rotor mimo system based on the method of inequality (moi). *Journal of Control Engineering and Applied Informatics* **24**: 13–23.
- Abdulwahhab, O. W. and N. H. Abbas, 2017 A new method to tune a fractional-order pid controller for a twin rotor aerodynamic system. *Arabian Journal for Science and Engineering* **42**: 5179–5189.
- Agand, P., M. A. Shoorehdeli, and A. Khaki-Sedigh, 2017 Adaptive recurrent neural network with lyapunov stability learning rules for robot dynamic terms identification. *Engineering applications of artificial intelligence* **65**: 1–11.
- Ahmad, M., A. Ali, and M. A. Choudhry, 2016 Fixed-structure  $h_\infty$  controller design for two-rotor aerodynamical system (tras). *Arabian Journal for Science and Engineering* **41**: 3619–3630.
- Ahmad, S. M., A. J. Chipperfield, and M. O. Tokhi, 2000a Dynamic modelling and control of a 2-dof twin rotor multi-input multi-output system. In *2000 26th Annual Conference of the IEEE Industrial Electronics Society, IECON 2000. 2000 IEEE International Conference on Industrial Electronics, Control and Instrumentation. 21st Century Technologies*, volume 2, pp. 1451–1456, IEEE.
- Ahmad, S. M., A. J. Chipperfield, and O. Tokhi, 2000b Dynamic modeling and optimal control of a twin rotor mimo system. In *Proceedings of the IEEE 2000 National Aerospace and Electronics Conference. NAECON 2000. Engineering Tomorrow (Cat. No. 00CH37093)*, pp. 391–398, IEEE.
- Alam, M. S., F. M. Aldebrez, and M. O. Tokhi, 2004 Adaptive command shaping using genetic algorithms for vibration control. In *Proceedings of IEEE SMC UK-RI Third Workshop on Intelligent Cybernetic Systems*, pp. 7–8, IEEE.



- Bensidhoum, T., F. Bouakrif, and M. Zasadzinski, 2023 A high order p-type iterative learning control scheme for unknown multi input multi output nonlinear systems with unknown input saturation. *International Journal of Computational and Applied Mathematics & Computer Science* **3**: 27–31.
- Castillo, E., B. Guijarro-Berdinas, O. Fontenla-Romero, A. Alonso-Betanzos, and Y. Bengio, 2006 A very fast learning method for neural networks based on sensitivity analysis. *Journal of Machine Learning Research* **7**.
- Chu, S. R., R. Shoureshi, and M. Tenorio, 1990 Neural networks for system identification. *IEEE Control systems magazine* **10**: 31–35.
- Coelho, J., R. Neto, D. Afonso, C. Lebres, H. Fachada, *et al.*, 2007a Helicopter system modelling and control with matlab. CEE'07-2nd INTERNATIONAL CONFERENCE ON ELECTRICAL ENGINEERING pp. 110–117.
- Coelho, J., R. M. Neto, C. Lebres, H. Fachada, N. M. Ferreira, *et al.*, 2007b Application of fractional algorithms in the control of a helicopter system. In *Symposium on Applied Fractional Calculus*, pp. 1–12.
- Coelho, J., R. M. Neto, C. Lebres, V. Santos, N. M. Ferreira, *et al.*, 2008 Application of fractional algorithms in the control of a twin rotor multiple input-multiple output system. ENOC 08 pp. 1–8.
- Darus, I. Z. M. and Z. A. Lokaman, 2010 Dynamic modelling of twin rotor multi system in horizontal motion. *Jurnal Mekanikal*.
- Demuth, H. B. and M. H. Beale, 2000 *Neural Network Toolbox: For Use with MATLAB®*. MathWorks.
- El-Fakdi, A. and M. Carreras, 2013 Two-step gradient-based reinforcement learning for underwater robotics behavior learning. *Robotics and Autonomous Systems* **61**: 271–282.
- Ezekiel, D. M., R. Samikannu, and O. Matsebe, 2021 Pitch and yaw angular motions (rotations) control of the 1-dof and 2-dof trms: A survey. *Archives of Computational Methods in Engineering* **28**: 1449–1458.
- Ezekiel, D. M., R. Samikannu, and M. Oduetse, 2020 Modelling of the twin rotor mimo system (trms) using the first principles approach. In *2020 International Conference on Computer Communication and Informatics (ICCCI)*, pp. 1–7, IEEE.
- Ghasemiyeh, R., R. Moghdani, and S. S. Sana, 2017 A hybrid artificial neural network with metaheuristic algorithms for predicting stock price. *Cybernetics and systems* **48**: 365–392.
- Khishe, M., M. R. Mosavi, and A. Moridi, 2018 Chaotic fractal walk trainer for sonar data set classification using multi-layer perceptron neural network and its hardware implementation. *Applied Acoustics* **137**: 121–139.
- Lin, S. and A. A. Goldenberg, 2001 Neural-network control of mobile manipulators. *IEEE Transactions on Neural Networks* **12**: 1121–1133.
- Ljung, L. and S. Gunnarsson, 1990 Adaptation and tracking in system identification—a survey. *Automatica* **26**: 7–21.
- Moness, M. and T. Daa-Eldeen, 2017 Experimental nonlinear identification of a lab-scale helicopter system using mlp neural network. In *2017 13th International Computer Engineering Conference (ICENCO)*, pp. 166–171, IEEE.
- Mosbah, H. and M. E. El-Hawary, 2017 Optimization of neural network parameters by stochastic fractal search for dynamic state estimation under communication failure. *Electric Power Systems Research* **147**: 288–301.
- Nasir, A. N. K. and M. O. Tokhi, 2014 A novel hybrid bacteria-chemotaxis spiral-dynamic algorithm with application to modelling of flexible systems. *Engineering Applications of Artificial Intelligence* **33**: 31–46.
- Palepogu, K. R. and S. Mahapatra, 2023 Pitch orientation control of twin-rotor mimo system using sliding mode controller with state varying gains. *Journal of Control and Decision* pp. 1–11.
- Patan, K. and M. Patan, 2023 Fault-tolerant design of non-linear iterative learning control using neural networks. *Engineering Applications of Artificial Intelligence* **124**: 106501.
- Rahideh, A., A. H. Bajodah, and M. H. Shaheed, 2012a Real time adaptive nonlinear model inversion control of a twin rotor mimo system using neural networks. *Engineering Applications of Artificial Intelligence* **25**: 1289–1297.
- Rahideh, A., A. H. Bajodah, and M. H. Shaheed, 2012b Real time adaptive nonlinear model inversion control of a twin rotor mimo system using neural networks. *Engineering Applications of Artificial Intelligence* **25**: 1289–1297.
- Rahideh, A., M. H. Shaheed, and H. J. C. Huijberts, 2008 Dynamic modelling of a trms using analytical and empirical approaches. *Control Engineering Practice* **16**: 241–259.
- Rere, L. R., M. I. Fanany, and A. M. Arymurthy, 2016 Metaheuristic algorithms for convolution neural network. *Computational intelligence and neuroscience*.
- Salimi, H., 2015 Stochastic fractal search: a powerful metaheuristic algorithm. *Knowledge-based systems* **75**: 1–18.
- Sivadasan, J. and J. R. J. Shiney, 2023 Modified nondominated sorting genetic algorithm-based multiobjective optimization of a cross-coupled nonlinear pid controller for a twin rotor system. *Journal of Engineering and Applied Science* **70**: 133.
- Sjöberg, J., H. Hjalmarsson, and L. Ljung, 1994 Neural networks in system identification. *IFAC Proceedings Volumes* **27**: 359–382.
- Tavakolpour, A. R., M. Mailah, I. Z. M. Darus, and O. Tokhi, 2010 Self-learning active vibration control of a flexible plate structure with piezoelectric actuator. *Simulation Modelling Practice and Theory* **18**: 516–532.
- Tijani, I. B., R. Akmeliawati, A. Legowo, and A. Budiyo, 2014 Nonlinear identification of a small scale unmanned helicopter using optimized narx network with multiobjective differential evolution. *Engineering Applications of Artificial Intelligence* **33**: 99–115.
- Toha, S. F. and M. O. Tokhi, 2009 Dynamic nonlinear inverse-model based control of a twin rotor system using adaptive neuro-fuzzy inference system. In *2009 Third UKSim European Symposium on Computer Modeling and Simulation*, pp. 107–111, IEEE.
- Toha, S. F. and M. O. Tokhi, 2010 Augmented feedforward and feedback control of a twin rotor system using real-coded moga. In *IEEE Congress on Evolutionary Computation*, pp. 1–7, IEEE.
- TRahman, T. A., A. As'array, N. A. Jalil, and R. Kamil, 2019 Dynamic modelling of a flexible beam structure using feedforward neural networks for active vibration control. *International Journal of Automotive and Mechanical Engineering* **16**: 6263–6280.
- Wai, R. J., 2003 Tracking control based on neural network strategy for robot manipulator. *Neurocomputing* **51**: 425–445.
- Widrow, B. and M. E. Hoff, 1960 Adaptive switching circuits. In *IRE WESCON convention record*, volume 4, pp. 96–104.
- Wu, H., Y. Zhou, Q. Luo, and M. A. Basset, 2016 Training feedforward neural networks using symbiotic organisms search algorithm. *Computational intelligence and neuroscience*.
- Xia, Y. and J. Wang, 2001 A dual neural network for kinematic control of redundant robot manipulators. *IEEE Transactions on Systems, Man, and Cybernetics, Part B (Cybernetics)* **31**: 147–154.
- Yaghini, M., M. M. Khoshraftar, and M. Fallahi, 2013 A hybrid algorithm for artificial neural network training. *Engineering Applications of Artificial Intelligence* **26**: 293–301.
- Yoo, S. J., Y. H. Choi, and J. B. Park, 2006 Generalized predictive

control based on self-recurrent wavelet neural network for stable path tracking of mobile robots: adaptive learning rates approach. *IEEE Transactions on Circuits and Systems I: Regular Papers* **53**: 1381–1394.

**How to cite this article:** Ezekiel, D. M., Samikannu, R., and Matsebe, O. Improved Set-point Tracking Control of an Unmanned Aerodynamic MIMO System Using Hybrid Neural Networks. *Chaos Theory and Applications*, 6(1), 51-62, 2024.

**Licensing Policy:** The published articles in *Chaos Theory and Applications* are licensed under a [Creative Commons Attribution-NonCommercial 4.0 International License](https://creativecommons.org/licenses/by-nc/4.0/).



# Future Prediction for Tax Complaints to Turkish Ombudsman by Models from Polynomial Regression and Parametric Distribution

Mehmet Niyazi Çankaya <sup>1</sup> and Murat Aydın <sup>2</sup>

\*Faculty of Applied Sciences, Department of International Trading and Finance, Uşak University, Uşak, Türkiye, <sup>α</sup>Faculty of Applied Sciences, Department of Accounting Finance and Management, Uşak University, Uşak, Türkiye.

**ABSTRACT** The aim of this study is to forecast the amount of tax complaints filed with the Turkish Ombudsman in the future and whether or not policymakers require a specific tax Ombudsman. The polynomial regression for discrete data set is proposed to fit the number of events of tax complaints in the period from years 2013 to 2021. The artificial data set is generated by models which are polynomial regression and parametric distribution. The location, scale and shape parameters are determined according to the smallest value between the observed and predicted dependent variable. After determining the smallest value for the tried values of shape parameter and the parameters of polynomial regression, the best value determined by grid search for shape parameter is around 1.07. Thus, the heavy-tailed form of exponential power distribution is gained. The artificial data sets are generated and sorted from the smallest to biggest ones. The maximum values are around 700 and 800 which can be regarded as future prediction because the distance among observations is taken into account by models from polynomial regression and parametric distribution. Since the polynomial regression and the parametric models are used simultaneously for modelling, the distance among observations can also be modelled by parametric model as an alternative approach provided.

**KEYWORDS**  
Estimation  
Inference  
Public economics  
Parametric models  
Simulation

## INTRODUCTION

Estimation is a challenging topic that needs to be improved by advancing the tools in the statistical literature. Many data sets in the applied sciences should be modelled efficiently. For example, the number of Ombudsman who hear complaints from citizens about failures, actions and decisions by public authorities is discrete data such that natural numbers are used to represent these kind of data sets. The main aim of the Ombudsman is to fight against abuse of rights, omissions, wrong decisions and delays for citizens. As the institution of the ombudsman is important, a design for estimating the number of Ombudsman will be an important issue in the near future. A combination of polynomial regression as a parametric model based on the regression case and the parametric distribution, for example the exponential power distribution, based on the

distributional form of dependent variable or any variable can be proposed to set an approach for forecasting (Mineo and Ruggieri 2005). Note that if the data set is discrete, the discrete models such as binomial, generalized form of binomial, etc. can be used to fit the data set. If the data set is continuous, the continuous parametric model such as exponential power distribution and its variants such as skew, model, trimodal family for a known parametric models can be generated and used. The compound forms of distributions are also derived to model the data set more efficiently as far as we can do (Balakrishnan and Nevzorov 2004).

In the working principle of nature providing the observed values after the experiment has been performed, it is not easy to imply that a data set can be only one parametric model. There is a hard indeterminacy in the nature of data formation. For this reason, the regression form can be a bridge for us to fit the data if we insist on driving the tools as alternative objectives in this study. Since estimation is a fluctuation around function  $f$  used for the representation of parametric model such as exponential power distribution, that is, we can get  $\hat{f}$  representing the estimated form of  $f$  due to the

**Manuscript received:** 19 January 2024,

**Revised:** 4 March 2024,

**Accepted:** 20 March 2024.

<sup>1</sup>mehmet.cankaya@usak.edu.tr

<sup>2</sup>murat.aydin@usak.edu.tr (Corresponding author).

finite sample points of  $f$ , it is logical to suggest that a regression form can be used for data to perform a modelling instead of using directly parametric model to fit the data set (Vila *et al.* 2020, 2022).

Especially, since we have small sample size of data, it can be a gate for us to overcome the problem about the case where we have few data that will be needed to fit precisely as far as we can achieve the joint work between polynomial regression as a parametric model and the parametric distribution when compared by the non-parametric forms (Härdle *et al.* 2004; Hunter 2023). Thus, we can have an applicable form when we use the computational tool for this marriage. Especially when the sample size is small, the parametric models cannot be very powerful because we do not have enough data where the data set comes from or it is very rough to know how the real data set has occurred while the experiment is being conducted.

Note that a data set can show a regression or a polynomial movement/pattern. Since we are proposing to use the regression equation in order to model the data set observed over time, the time series form can be suggested as a regression case. On the other hand, the bulk of the data at each time throughout the time period cannot be a fixed variance. In particular, it is reasonable to observe that a non-identical distributed data throughout time is indispensable observed in the nature of the data set. That is, there may be heteroscedasticity (Mokhtari *et al.* 2022). Such non-identical movement or heteroscedasticity can be modelled by using the peakedness parameter  $p$  in the exponential power distribution when the regression case is used. On the other hand, there is a struggle between the chosen parametric model for the distribution of the error term of the regression equation to determine whether or not there is heteroscedasticity in reality. There may be another reason to imply the existence of heteroscedasticity if we change the analytical form of the regression model.

In the regression equation, the square of the error term, known as the estimated variance, is used to generate the artificial dataset, that is, we want to estimate the scale parameter for the dataset using the regression approach with parametric model based on the peakedness parameter  $p$ . This approach is an alternative if we want to estimate the scale parameter for the data set. Since the discrepancy can be detected by the error term in the regression, the generation for artificial data can also be done by using the peakedness parameter of the exponential power distribution (Mineo and Ruggieri 2005). On the other hand, it is reasonable to expect that the peakedness ( $p$ ) and scale ( $\sigma$ ) parameters can interact, because they are parameters which are responsible for changing the shape of the function. Note that the interaction can lead to occur the heteroscedasticity. The main problem is about the future prediction of tax complaints when the polynomial regression and parametric model are used together. Thus, we can perform an efficient fitting by using not only a trend as regression (location) but also the error terms of polynomial regression model which are modelled by exponential power distribution. It should be noted that heteroscedasticity can be modelled as an alternative approach if the parametric distribution is used.

Taxation is an important and effective way to manage government resources fairly. There are many studies to model the tax of governments which use the distribution assumption to model the tax managed by governments. The role of tax is investigated and the different suggestion on the tax regulation in the management modelling or planning in the government have been carried out in the different and directions which are still investigating what the government policy should be or some markers in the financial markets push or drive the policy management to increase the

efficiency and correctness on the process improvement (Bala and Biswas 2005). It is generally accepted that the tax management is very problematic and the Ombudsman is an inevitable community for the set and built law system to touch the correct and effective decision in the timing period in the tax system. We believe that the Ombudsman should be supported and improved by means of using different directions. Thus, the role of tax management can be improved and more accurate decision can be reached by the responsible drivers in the system of government policy.

These improvements, such as rotations, directions, suggestions, etc., make an automatic control and checked feedback in the working principle of the set system, which should be improved simultaneously, no matter when it finally stops. In other words, it should be a system which is a rounding around itself and it should be controlled by independent communities which can work out independently and put their suggestions briefly touching every point of the picture carefully and do not cover any potential uncovered parts in the tax system management. Such a situation can be achieved by carrying out the stricter effective analysing procedure which will not be influenced and touched. The reality of the current system should have its clarifications in order to discover the hidden parts in the system. For this purpose, the Ombudsman is a key institute for us to round up the system and so the quality control can be tried to be guaranteed (Serrano 2007).

Basically, this institution listens to taxpayers' complaints and solves their problems. It also improves the organisation of the tax service. In America, for example, the name is even more different. The Taxpayer Advocate Service is an institution in the US that intervenes when the Internal Revenue Service does not want to do so. There is at least one local Taxpayer Advocate in every state. There is no such thing as a tax ombudsman in US tax law. In Spain, as in other countries, there is a tax ombudsman who depends on the government. He balances the relationship between the taxpayer and the administration. In the Law of Taxpayers' Rights there are five functions of the Tax Ombudsman. These are; informative action, democratic control, alternative dispute resolution, and improving the moving legal system (Bala and Biswas 2005).

The organization of the paper is as follows: Section for preliminaries introduces the parametric model and the estimation method. In next section, the problem is solved by using models from polynomial regression and parametric distribution. The numerical results and figures are given as a separate section. The last section is divided for the conclusions.

## PRELIMINARIES

### Parametric model

The normal distribution is commonly used and it is a popular distribution. The generalisation of the normal distribution and the different probable directions are proposed by (Çankaya 2018). The exponential power distribution is one of them and it has a peakedness parameter being responsible for determining the peak of the function. The empirical distribution of the data can be a way to observe how the shape of the function behaves.

The analytical expression of the exponential power distribution is given by the following form:

$$f(x; \mu, \sigma, p) = \frac{1}{2\sigma p^{1/p} \Gamma(1 + 1/p)} \exp\left\{-\left|\frac{x - \mu}{p^{1/p} \sigma}\right|^p\right\} \quad (1)$$

$\mu \in \mathbb{R}, \sigma > 0, p > 0$  represents parameters for location, scale and peakedness of the function, respectively. The exponential power distribution is the special form of asymmetric bimodal exponential power distribution (Mineo and Ruggieri 2005; Çankaya 2018).

### Estimation method: Maximum likelihood estimation

If there is a distribution of the error terms in the regression model, or the error terms are assumed to have a distribution such as normal, Student t, exponential power, asymmetric bimodal exponential power distribution (Çankaya 2018) etc., then the error terms can be a member of a parametric model. If a distribution is used in the regression model as the location of the parametric model, then maximum likelihood estimation is preferred to estimate the parameters of the regression model. There are important properties which are efficiency, consistency, minimum variance, etc. when maximum likelihood estimation method is used (Lehmann and Casella 2006).

The function `lmp` in 'normalp' at RStudio 2023.09.1+494 free open statistical software is used to fit a regression model with the dependent variable  $y$  and the independent variables  $x_1, x_2, \dots, x_k$ . It can be used when the errors are distributed as an exponential power distribution (Mineo and Ruggieri 2005; Lehmann and Casella 2006). The maximum likelihood estimation method gives us advantage of using the assumed parametric model to estimate the regression parameters when the errors are distributed as the corresponding parametric model. Each observation can be considered as an output, i.e. there can be a regression expression that can be applied to find the relationship between the observations in the period. The next section provides the detailed discussion and methodological contribution to assess the distribution of the variable  $y$  and the variable  $\varepsilon$ . Thus, the regression expression, as a fixed part that tries to represent how a real relationship exists between variables, can be used to determine the distribution of the error term  $\varepsilon$ .

### DESCRIPTION OF THE PROBLEM

There is a potential overlap between the chosen regression model, with its corresponding distribution of the error term of the regression model, and the chosen kernel smoothing techniques which are based on the parametric or semi-parametric approaches. In modelling, not only the assumed regression model but also the distribution of the error terms are two components that influence each other. Thus, if we can determine what the distribution of the error term can be, then the distribution of the observation term  $y$  as a dependent variable will also be determined. Each data is the replication of the previous case or there is a potential dependence among the previous cases of the data set, as in the case of the random walk in the stochastic process (Iacus *et al.* 2008). The data set can be reorganised by using the regression approach which we can consider to apply. It is logical to expect that a data set can be represented by a polynomial approach. Since a polynomial approach can be performed on the data set, the future prediction can be performed by polynomial regression. In the context of the artificial data set, it is reasonable to perform a random number generation procedure to observe which data can be artificially observed.

In order to fit the data set via the proposed function, the polynomial regression approach can be used. Secondly, a parametric model for error term of regression can be suggested. After the regression case can be done, the peakedness parameter of the exponential power distribution can be determined by using the grid search approach. Since we perform such an approach to determine the value of the peakedness parameter  $p$  for peakedness, the computational cost of simultaneously estimating the location, scale and peakedness parameters can be solved as an alternative approach for modelling. This is an important contribution when the sample size is small and we need to use a parametric model to generate the artificial dataset. Why do we need to generate an

artificial dataset? The future prediction or the probable numerical values for the questionnaire of phenomena can be determined, as an alternative approach if the regression case is not the only solution for the future prediction.

In other words, it is logical to observe that each data can be a member of a polynomial movement in the forthcoming situation in an experiment. Even if we assume that each data is independently distributed, it is reasonable to perform a polynomial motion among the data set. Independence can be a restrictive approach, or an alternative comment, is that it is already well known that a number can be made to belong to a polynomial function. A rounding around a data can be produced by another data, which shows that it is possible to carry out modelling using a polynomial approach based on the regression case. In the statistical literature, this approach should be preferred when the computational cost increases as the number of parameters to be estimated increases. In our approach, the first step was to determine the peakedness parameter using the grid search algorithm. The second step is the estimation of the location and scale parameters when the peakedness parameter  $p$  is given as a fixed value determined by using the case of regression with polynomial motion. Finally, random numbers are generated for the estimated values of the position and scale parameters. The maximum likelihood estimation method is used to obtain the estimators of the parameters when the fixed value of the peakedness parameter  $p$  determined by the polynomial approach is given.

Econometricians search for regression models to fit the data set based on the time series sense. Statisticians make the overlap between the chosen regression model and the error term ( $\varepsilon$ ) of the regression model. Both scientists try to find the best strategy for modelling the data set. The advantage of being a statistician may be more beneficial because a statistician focuses on the distribution of the error term. The distribution of the error term in the equation (2) corresponds to the distribution of the variable  $y$  which represents the observed value. Even if the nature of the observed value of tax complaints is discrete, the polynomial regression model can also be proposed to fit the number of events in the period. In this case, since the events  $y(t) := y_t$ , where  $t$  represents time, depend on time as in the case of the random walk in the stochastic process, there can be a potential correspondence from the discrete data to the continuous data.

For further discussion, the tax complaints occur due to many reasons based on the continuous observations from the government money process. The currency and the economic indicators are responsible tools that lead to have the continuous observations. That is, in other words, when we make a projection where the discrete data comes from, it is observable to detect that the continuous observations touch occurring the discrete data sets. Even if the binomial regression or the corresponding counterparts are used to model the discrete data sets, the continuous case is more flexible to generate artificial data sets; because the peakedness parameter is more important to determine the distribution of the data set. On the other hand, the continuous data already represents the discrete data as a neighbourhood framework. In addition, the binomial distribution converges to the normal distribution with peakedness parameter  $p = 2$  in the exponential power distribution. In this direction, there can be a transfer from the discrete data to the continuous data (Sicuro *et al.* 2015).

It should be noted that even if the discrete data are analysed in the regression case, the continuous distribution can be used for the application; because there is a correspondence between the polynomial function and the gamma function (Alzer and Grinshpan 2007).

In this sense, as discussed above, the peakedness parameter plays a key role in determining the distribution of the data. The exponential power distribution is symmetric around the location parameter and so the general tendency of the economic indicators is assumed to be symmetric due to the nature of the experiments; because the government applies the tax rule equally balanced on the people in the country and the symmetric distribution can play the role for modelling the data sets output by many reasons occurred on the economic indicators (Haberman 1989; Coles *et al.* 2001; Mineo and Ruggieri 2005; Çankaya 2018; Çankaya and Arslan 2020).

## Materials and Methods

**Regression model** Regression models are generally used to set the relationship between at least two variables. The nature of the dependent and independent variables can be determined according to what a researcher investigates. When the observations from the experiments are measured, they are analysed according to the researcher's objective. In our framework, a polynomial regression equation is used to model the observations by using the sequence occurred over time. In other words, in mathematical terms, the set of data or observations can be expressed in terms of the movement over time.

The assumed regression model for representation of reality is as follow:

$$y = a_0 + a_1x^{p_1} + a_2x^{p_2} + a_3x^{p_3} + \varepsilon \quad (2)$$

where  $\varepsilon$  is a random variable assumed to have an exponential power distribution. The parameters  $p_1$ ,  $p_2$  and  $p_3$  are responsible for the different degrees of the polynomial function in the equation (2).  $a_0$ ,  $a_1$ ,  $a_2$  and  $a_3$  are regression parameters estimated using the `lmp` function with different trial values of the peakedness parameter  $p$ .

The sampling form of the equation (2) is given by

$$y_t = a_0 + a_1x_t^{p_1} + a_2x_t^{p_2} + a_3x_t^{p_3} + \varepsilon_t, t = 1, 2, \dots, n \quad (3)$$

where  $x_t = t$  as an explanatory variable representing the time (year) and  $n$  is the number of sample size.

It should be noted that since the polynomial movement among the data sets is assumed to be expressed by the polynomial regression case, it should be preferred to model the upcoming events. It is important to note that the distribution of the error term  $\varepsilon$  begins to play a role in determining the value of the peakedness parameter in the parametric model used. In the general setting, it is logical to propose a parametric model that has a peakedness parameter. Thus, using the role of the peakedness parameter will give us an advantage in determining the tail movement and thus we can have a chance for future prediction instead of using the regression case in future prediction. Such an approach makes an alternative suggestion/contribution to the statistical literature to determine the value of the peakedness parameter  $p$  as an alternative approach. On the other hand, the peakedness parameter  $p$  and the powers  $p_1$ ,  $p_2$  and  $p_3$  in the regression model can play same role when there is a conceptual equivalence and the definition of the regression, i.e.,  $\mathbb{E}(Y/X = x)$  with the non-fixed value of scale parameter (or with heteroscedasticity), takes into account, i.e.,  $Y \sim D(\mathbb{E}(Y/X = x_t), \sigma(X = x_t))$ . Since the number of samples is small, it will not be easy to determine the almost exact peakedness of the assumed parametric model. For this reason, we have provided an alternative approach to determine the peakedness parameter from the data set. The assumed model for the distribution of  $\varepsilon$  is the exponential power one.

The nature of the occurred phenomena tricks our approach, because tax complaints can have a heavy tailed distribution due to the nature of the tax complaints (Jenkins 2017).

**Algorithmic schema for computational procedure** The following steps show the schematic algorithm how the computational procedure is conducted to reach the value of peakedness of parameter  $p$  if the polynomial regression in equation (2) is used (see Appendices).

1. Determine the peakedness parameter  $p$  by using `lmp` function in the `normalp` package in RStudio 2023.09.1+494 software
2. Try different values of the parameters  $p$  to get the different probable the smallest difference between the predicted  $y$ , i.e.  $\hat{y}$ , and the observed  $y$  as data
3. Use the polynomial regression in equation (2)
4. Set a vector for the tried values of peakedness parameter  $p$
5. For each values of  $p_1$ ,  $p_2$  and  $p_3$  which are (0,75,1.25], (1.75,2.25] and (2.75,3.25], respectively, the values of peakedness parameter  $p$  are determined according to the smallest value, i.e. predicted error ( $\hat{\varepsilon} = y - \hat{y}$ ), of the distance between the predicted  $y$ , i.e.  $\hat{y}$ , and the observed  $y$ . If an appropriate  $p$  value which satisfies the smallest value for  $\hat{\varepsilon}$  is determined, then the determined value of  $p$  in the 125 000 times due to `set1=50`, `set2=50` and `set3=50` makes the probable appropriate values of  $p$ , which is obtained by each values of  $p_1$ ,  $p_2$  and  $p_3$

If the number of degree of power parameter in the polynomial regression in equation (3) is increased according to `for` loop given above, the different forms of the values of  $p_1$ ,  $p_2$  and  $p_3$  in regression equation can be tried to model the movement among the observations. The role of sensitivity of higher order powers  $p_2$  and  $p_3$  should be applied to fit the observations more precisely, because the degree of polynomial regression can be versatile due to the chosen values of  $p_2$  and  $p_3$  especially. Note that it is possible to apply different polynomial regression with higher order polynomial power; however, the dependence structure among the right hand side of regression equation (3) can start to be a problem, leading to a multicollinearity problem. The dependence can be tricked according to the chosen values of parameters  $p_1$ ,  $p_2$  and  $p_3$ . To avoid the more biased estimation for the parameters  $a_0$ ,  $a_1$ ,  $a_2$  and  $a_3$  due to the probable structure of the dependence among the variables  $x^{p_1}$ ,  $x^{p_2}$  and  $x^{p_3}$ , we continue to follow the regression equation in (3). That is, the new variable  $x^{p_4}$  or other variables have not been added to the regression model, because the degree of perturbation should be avoided for mathematical reasons as well (Montgomery *et al.* 2021).

Since the nature of the polynomial approach can have the negative estimated values for the parameters, the forecast in the forthcoming numbers for the occurred events from tax complaints cannot be determined by using the regression approach directly. On the other side of the picture, since we have few data sets for applying the regression case, the rank problem can occur due to the number of regression parameters starting to be close to the number of sample size  $n = 9$  in our case (Stanimirović 2017). For this reason, we prefer to use two steps for the approach in the future prediction instead of doing the prediction using the regression equation.

## NUMERICAL RESULTS

### Tools: polynomial regression and correlation

The numerical results with illustrative representations are provided to observe how the regression equation produces the results which are the estimated values for correlation, standard deviation and their empirical probability density function (pdf) computed by means of the `EnvStats` package with kernel functions (such as Refs. (Härdle et al. 2004; Hunter 2023)) in RStudio 2023.09.1+494 software.

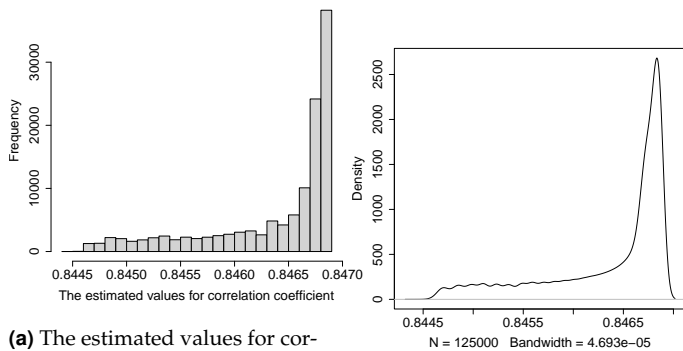
The parameters  $a_0, a_1, a_2$  and  $a_3$  in regression model at equation (3) can be estimated and provided by the following form:

$$\hat{y} = \hat{a}_0 + \hat{a}_1 x^{p_1} + \hat{a}_2 x^{p_2} + \hat{a}_3 x^{p_3} \quad (4)$$

where  $x$  is independent variable having numerical values from 1 to the sample size  $n$  and  $p_1, p_2$  and  $p_3$  are power parameters which are responsible to make a flexible fitting on the data.

The equation (4) is used to get the predicted  $\hat{y}$ . The correlation values are computed by using the correlation formula for the observed  $y$  and the predicted  $\hat{y}$  values (Lehmann and Casella 2006). According to the codes in appendix, the estimated values for the correlation coefficient are given by figure 1. Figure 1 informs us for the estimated values of correlation coefficients between the observed values of  $y$  and the estimated values of  $\hat{y}$  given by equation 4.

The performance of future prediction depends on the degree of the values of correlation. That is, we have success at the degree %85 for trusting the numerical values generated artificially. For this aim, the values at the figure 2a should be preferable to represent the non-identically case of distributed data set, i.e., if the estimated values of scale parameter are big, then we can have values being far from the bulk of the data.



(a) The estimated values for correlation coefficient between the predicted and the observed values of  $y$  (b) Empirical pdf of the estimated values for correlation coefficient

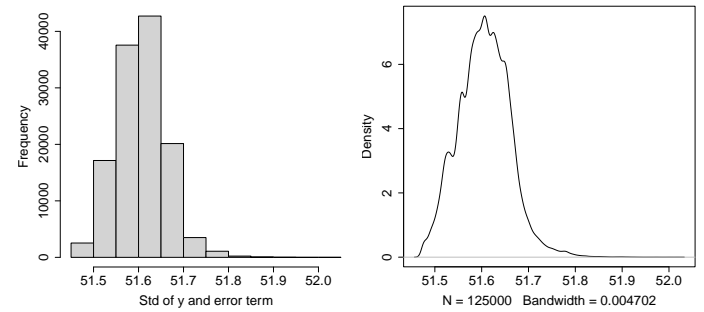
Figure 1  $\hat{\rho}$ : The estimated values for the correlation coefficient

Figures 1a and 1b represent the histograms and the smoothed form of empirical pdf according to the frequency when the bandwidth from kernel estimation in `EnvStats` package is determined automatically as nearly as being small. The same illustrations are given by forthcoming figures 2-5 and 7.

### The statistics for scale parameter as a dispersion measure

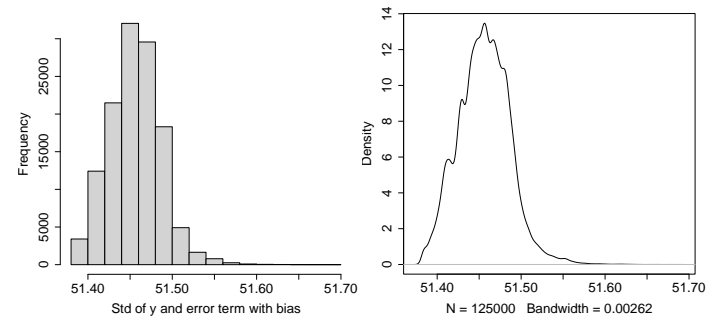
The following figures represent the numerical values generated at random from the exponential power distribution with the determined value of the peakedness parameter  $p = 1.07$ . These

numerical values are sorted from smallest to largest. They are then plotted according to these sorted values. Each sorted value is replicated and the number of replication is 10 000. Since we have the sorted values, we have the advantage of being able to plot the values that are the maximum and the previous ones which are represented by  $(-1), (-2), (-3)$ , etc. Thus, the probable values which are maximum and the previous values before maximum can be observed. It is important to note that since we are replicating, the random data may have different values for each replication. For such a design, there may be some cases where there are the same numerical results in the simulation given by Figure 8.



(a)  $\sqrt{\text{Var}(y) + \text{Var}(\hat{\epsilon})}$  from  $\hat{y}$  and  $\hat{\epsilon}$  (b) Empirical pdf of  $\sqrt{\text{Var}(y) + \text{Var}(\hat{\epsilon})}$  at the chosen values of parameter  $p$

Figure 2 Histogram and empirical pdf for  $n - k$  in computation of the estimated error,  $\hat{\epsilon}$



(a)  $\sqrt{\text{Var}(y) + \text{Var}(\hat{\epsilon})}$  from  $\hat{y}$  and  $\hat{\epsilon}$  (b) Empirical pdf of  $\sqrt{\text{Var}(y) + \text{Var}(\hat{\epsilon})}$  at the chosen values of parameter  $p$

Figure 3 Histogram and empirical pdf for  $n$  in computation of the estimated error,  $\hat{\epsilon}$

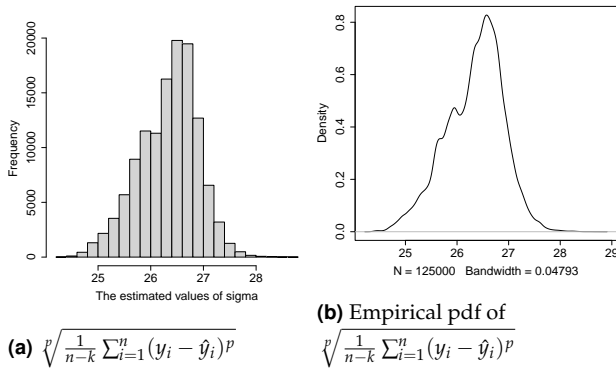
The distance between the observed variable  $y$  and the predicted variable  $\hat{y}$  is defined as the variation. It is also called as error term  $\epsilon$ . The sampling form of  $\epsilon$ , i.e.,  $\hat{\epsilon}$ , is given by the following expression for the exponential power distribution:

$$\hat{\epsilon} = \frac{1}{n} \sum_{t=1}^n (y_t - \hat{y}_t)^p \quad (5)$$

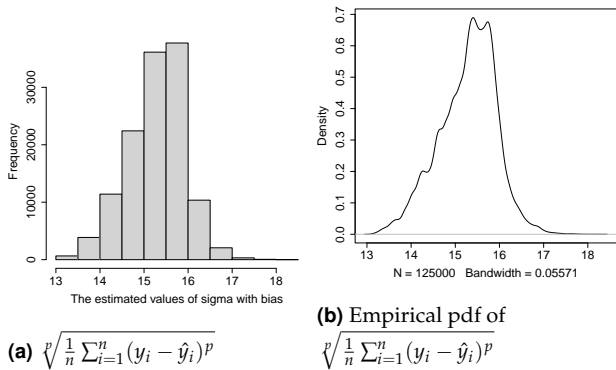
$$\hat{\epsilon} = \frac{1}{n - k} \sum_{t=1}^n (y_t - \hat{y}_t)^p \quad (6)$$

Comparing figures 2 and 3, the values in figure 3 are smaller than those in figure 2 because the formula for the error term,  $\epsilon$ , is

$\frac{1}{n} \sum_{t=1}^n (y_t - \hat{y}_t)^p$  for exponential power distribution. For the figure (2),  $\frac{1}{n-k} \sum_{t=1}^n (y_t - \hat{y}_t)^p$ , where  $k$  is the number of the estimated parameter. Note that the error term can also be considered as a scale parameter. Then we have the estimated values of the parameter  $\sigma$ , given by the figures 4 and 5.



**Figure 4** Histogram of  $\hat{\sigma}$  and empirical pdf for  $n - k$  in computation of the estimated error,  $\hat{\varepsilon}$



**Figure 5** Histogram of  $\hat{\sigma}$  and empirical pdf for  $n$  in computation of the estimated error,  $\hat{\varepsilon}$

Since the determined value for the parameter  $p$  is around 1.07 (see figure 7a), the behaviour of the exponential power distribution is a heavy-tailed one. Thus, the future prediction may be more representative for the target in which we can safely use it, taking into account the predictive performance of our approach for the probable cases in the future. Since the number of sample size  $n$  is 9, it cannot be enough to suggest numerical values from the regression model in equation (2), because the polynomial movement cannot be enough to evaluate how the future occurs. It is possible to use other methods based on the mode movement that can also be taken into account to model and analyse the real data set. In this case, there can be parametric and non-parametric models that can produce the light-tailed movement. In such a case, we can have the numerical values that cannot be far from the location as the central tendency of the empirical data set. In our statistical analysis, the year 2100 can also be proposed for the future prediction.

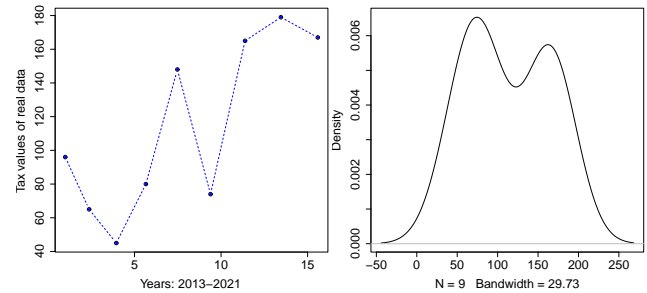
In each replication, the number of samples is 100. According to the estimated values used for the location and scale parameters, we can have the negative values due to the nature of the parametric model used, which is the exponential power distribution with  $p =$

1.07. Since the awareness of the population about the Ombudsman system is reflected in different areas of the tax and financial system, the numbers that represent the case of the Turkish Ombudsman consulted for the tax complaints can be increased. It is surprisingly important to note that the results in the 2013-2021 period provide the analysis results that give the heavy-tailed function, which can provide an advantage for future prediction even if the numerical values are discrete.

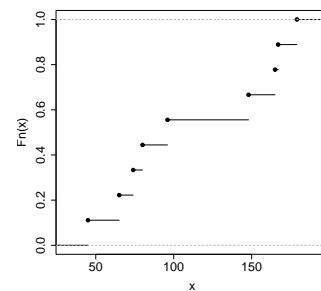
It is known that the discrete data can show the representation of a continuous case if the number of replications of events in the experiments is increased or the big law of large numbers is applied as an asymptotic behaviour. For example, the binomial distribution approaches the normal distribution (Lehmann and Casella 2006). The figure 6a showing the scatter plot shows a polynomial movement, which may be one approach we propose to model the data set.

### Illustrative purposes for observing behaviour of artificial and real data sets

Figure 6 shows the scatter plot, the empirical probability and the empirical cumulative distributions of real data set with sample size  $n = 9$ . Figure 6b shows that there can be a bimodality on the data set. However, even if data is discrete and shows a bimodality, this is an extra situation needed to investigate. In our approach, we keep to follow polynomial regression and one-mode parametric model called as exponential power distribution, because the tax and the related part being Ombudsman can have a movement based on the time series.



**(a)** Scatter plot of real data in years 2013-2021 **(b)** Empirical pdf (Density) of real data



**(c)** Empirical cdf ( $F_n(x)$ ) of real data

**Figure 6** Illustrative representation for real data



Figure 7 shows the histogram, empirical and cumulative distributions of the determined values of the peakedness parameter  $p$  of the exponential power distribution. Cumulative distribution function (cdf) is the cumulated form of probability density function (pdf). Note that the bimodality in figure 6b can also be modelled by bimodal distribution. However, the main aim is to determine the tail behaviour in order to where the maximum values can be around. It should be noted that the empirical distribution of the determined values of the parameter  $p$  can be modelled using the smooth kernel estimation method (Härdle *et al.* 2004); however, the chosen kernel plays the role of determining the probabilities.

Instead of using the location estimation for the parameter  $p$  in its probable empirical distribution, we use the mean of the determined values of the peakedness parameter  $p$  with a sample size of 125 000; because we generate the artificial data set when the parameter  $p$  is close to upper values of 1, which will not affect the more accurately generated probable random numbers (see figure 8). On the other hand, since the maximum likelihood estimation method is used, the distribution of the determined values of  $p$  is expected to be asymptotically normal, which may allow to use the arithmetic mean as a statistic for the values of  $p$  (see figure 7b) (Lehmann and Casella 2006).

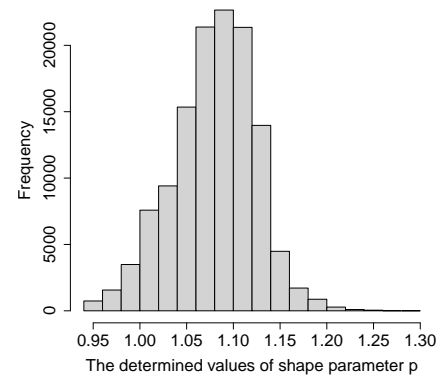
On the other hand, the values for the parameter  $p$  is around 1.07, which means that the synthetic data can get values from the tails, that is, it is possible to observe the values which is bigger than the real values, 179 as a maximum value. In such scenario, we add the role of distance among observations while performing the analysing on the data set. If the values of  $p$  tends going to 1 which leads to get reaching more degree of heavy tails for the exponential power distribution, it is reasonable to observe the values which can be bigger than 800. The codes in the appendices can be used to generate the synthetic data sets.

Figures 8 and 9 show the different numbers of estimated values generated by the exponential power distribution. In figure 9, the estimated value of the scale parameter is larger than in figure 8, which is why the estimated values from the simulation for the Ombudsman are around 800. An additional comment is that after sorting the synthetic dataset from smallest to largest, the previous values that come before the maximum value of the dataset are also given by the  $y$ -axis of Figures 8 and 9, labelled with the last value (-1) of the synthetic. (-1), (-2) and (-3) represent the ordered data. Note that the data set is sorted from the smallest to the biggest one, the last three values are chosen and they are represented by (-1), (-2) and (-3).

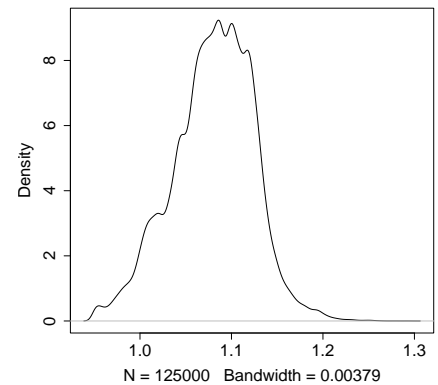
In addition, the fact that the trending slope looks away from the  $x$ -axis can be interpreted as an evidence that these artificially generated data will increase the necessity of the Ombudsman in the future. Note that even though the maximum value of real data sets is the number 179, the generated values for the artificial data sets are close to 800 as a maximum value; because we suggest to use the role of scale parameter as a dispersion measure which provides very important indicator for determining the behaviour of the data sets in any phenomena at the applied field of science. Thus, the role of scale parameter is an inevitable situation to touch more precisely the process in phenomena.

Note that the peakedness parameter  $p$  plays role as well importantly. Thus, the scale and peakedness playing role for determining tail behaviour of the function are in the class to determine the shape of function (Lehmann and Casella 2006; Arslan and Genç 2009; Çankaya 2018; Çankaya *et al.* 2019).

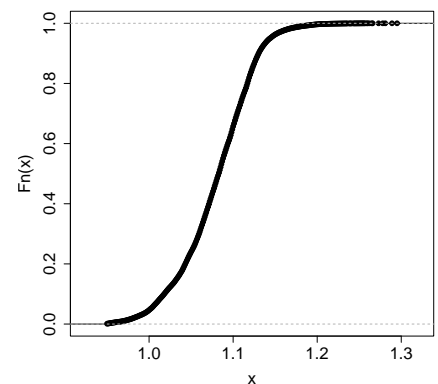
In figures 1-5 and 7, it should be noted that for the sake of the fact that representation of the frequency and the smoothed



(a) Histogram of  $p$



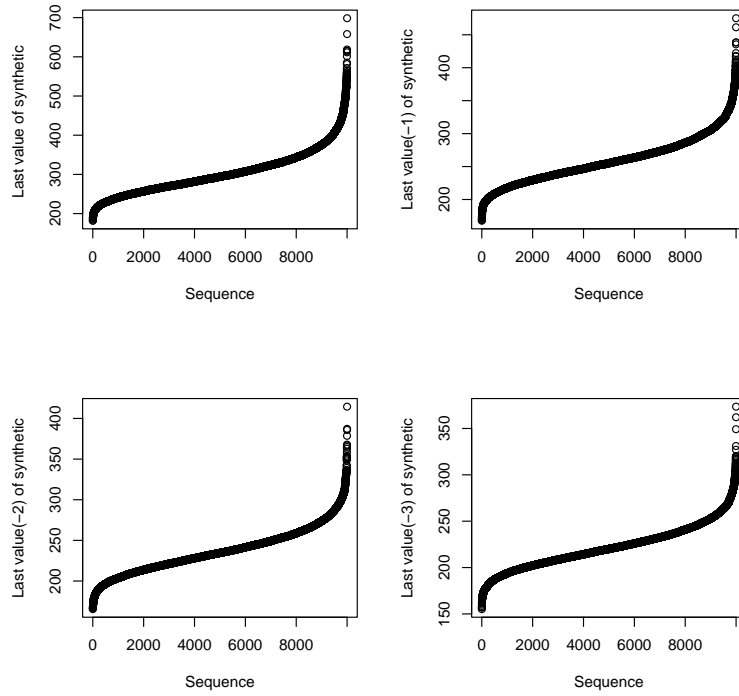
(b) Empirical pdf (Density) of the determined values of parameter  $p$



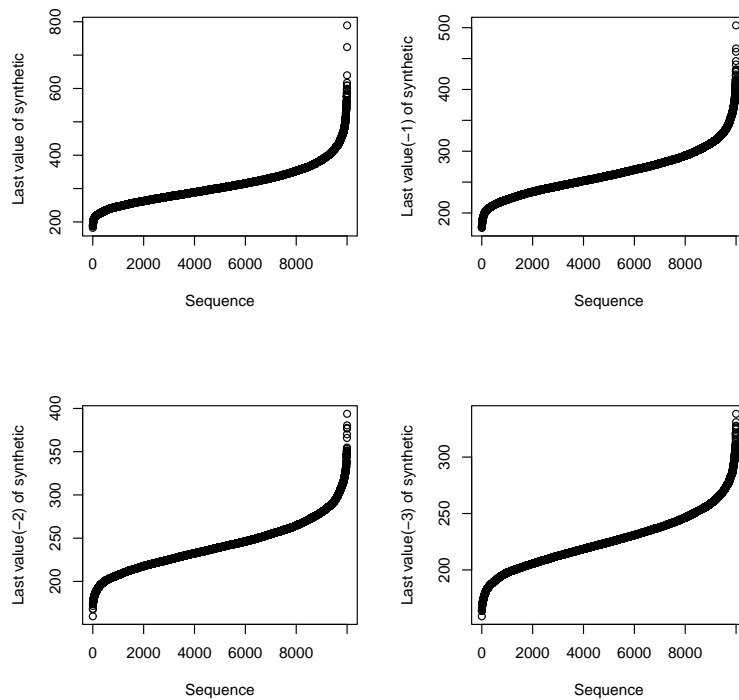
(c) Empirical cdf ( $F_n(x)$ ) of the determined values of parameter  $p$

**Figure 7** Illustrative representation for the values of parameter  $p$  computed by  $lmp$  function with the smallest estimated error,  $\hat{\varepsilon}$

form can be more feasible, the histogram and smooth form of pdf are given separately at different scaling form of the cartesian coordinates.



**Figure 8** Case 1: The last values and previous ones of the replicated synthetic data for the ordered form of data for 10000 replication with  $\hat{\sigma}$  from values represented by figure 2a



**Figure 9** Case 2: The last values and previous ones of the replicated synthetic data for the ordered form of data for 10000 replication with  $\hat{\sigma}$  from values represented by figure 3a

## CONCLUSION

The polynomial regression models providing a relationship among observations have been proposed to help determining the distribution of the observations as well. That is, the distribution of the error term  $\varepsilon$  corresponds to the distribution of the variable  $y$ . Such an approach is important; because, when the small number of sample size is given, it is not an easy task to propose a parametric model to analyse the dataset accurately. The correlation between the observed  $y$  and the predicted  $y$  can be increased if the values of  $p$  from exponential power distribution and the power parameters  $p_1$ ,  $p_2$  and  $p_3$  in regression model can play same role in fitting data well. Note that the parameters  $p$ ,  $p_1$ ,  $p_2$  and  $p_3$  are conceptually in same framework when the heteroscedasticity is taken into account. Such an approach provides a novelty for the study.

For example, using a distribution for discrete data cannot be an easy task to perform a precise modelling on the data set. The determined parametric model based on the regression models has been a special case of the exponential power distribution. Thus, we can have an advantage to generate the artificial data set to perform a prospective overview for modelling. If the peakedness parameter is around 1.07, the function is called the heavy-tailed form for the exponential power distribution. Since we have a heavy-tailed distribution, it is observable to get the numerical values which can come from tail parts of the function. For this reason, the synthetically generated numerical values are around 700 and 800 at most. Thus, we have suggested that the probable projection for the future prediction can provide numbers for the tax complaints upto year 2100. Future studies are in progress to suggest different materials, such as applying the heavy-tailed distributions and estimation methods for future projections of tax complaints in the Ombudsman (Çankaya 2021; De Gregorio *et al.* 2023).

## APPENDIX

### The main codes in the numerical evaluation for computation and regression case

The smallest value of  $|y - \hat{y}|$  is used to determine the best value for the peakedness parameter  $p$ , because the best prediction performance can be gained, which means that the distribution of observation  $y$  can be determined by means of the distribution of error term which is equivalent to the observation  $y$ . The values of  $p_1$ ,  $p_2$  and  $p_3$  are generated by using the following schema.

```
set1=50;set2=50;set3=50;pw11=0.75;pw12=1.75;pw13=2.75;
indx=replicate(set1, numeric(set2));
ppval=replicate(set1, numeric(set2));
indx3ar<-array(c(indx, indx), dim = c(set1,set2,set3));
ppval3ar<-array(c(ppval, ppval), dim = c(set1,set2,set3));
pvariable=seq(0.95,1.35,0.001);
replication = length(pvariable);
for (i1 in 1:set1)
{
pw11 = pw11 + 0.01;
for (i2 in 1:set2)
{
pw12 = pw12 + 0.01/set1;
for (i3 in 1:set3)
{
pw13 = pw13 + 0.01/(set1*set2);
for (i in 1:replication)
{
regp<-lmp(y~x, p = pvariable[i]);
```

```
coefa <- regp$coefficients;
ypredict[i,] <- xx %*%
matrix(c(coefa[1],coefa[2],coefa[3],coefa[4]),4,1);
errorry[i,] <- abs(y - ypredict[i,]);
meanerrorry[i] <- sum(errorry[i,])/n;
}
indx3ar[i1,i2,i3]=min(which(sumerrorry == min(sumerrorry)));
ppval3ar[i1,i2,i3]=pvariable[indx3ar[i1,i2,i3]];
}
}
}
```

### Estimation of error term distributed as the exponential power

Let us provide the codes showing how the equations (5) and (6) are adopted to the simulation in free open source statistical software RStudio 2023.09.1+494.

```
for (i1 in 1:set1)
{
pw11 = pw11 + 0.01;
for (i2 in 1:set2)
{
pw12 = pw12 + 0.01/set1;
for (i3 in 1:set3)
{
pw13 = pw13 + 0.01/(set1*set2);
indx3ar[i1,i2,i3]=min(which(sumerrorry == min(sumerrorry)));
ppval3ar[i1,i2,i3]=pvariable[indx3ar[i1,i2,i3]];
regp <- lmp(y~x, p = ppval3ar[i1,i2,i3]);
coefp <- regp$coefficients;
y_last_predict <- xx %*%
matrix(c(coefp[1],coefp[2],coefp[3],coefp[4]),4,1);
cor_vals3ar[i1,i2,i3] <- cor(y,y_last_predict);
var_n_eps3ar[i1,i2,i3] <-
sum(abs(y - y_last_predict)^ppval3ar[i1,i2,i3]) / n;
sig_n_eps3ar[i1,i2,i3] <-
(sum(abs(y - y_last_predict)^ppval3ar[i1,i2,i3]) / n) ^
(1/ppval3ar[i1,i2,i3]);
var_eps3ar[i1,i2,i3] <-
sum(abs(y - y_last_predict)^ppval3ar[i1,i2,i3]) /
(n - (dim(x)[2]+1));
sig_eps3ar[i1,i2,i3] <-
(sum(abs(y - y_last_predict)^ppval3ar[i1,i2,i3]) /
(n - (dim(x)[2]+1)))^(1/ppval3ar[i1,i2,i3]);
}
}
}
```

### Random number generation for the design

The normalp package is used to generate random number. The estimated values for location, scale and peakedness parameters are plug into the function rnormp given by:

```
rnormp(n, mu, sigma, p , method = c("def", "chiodi"))
```

Note that mu, sigma and p are parameters which are estimated by using the empirical distribution produced by the regressional form.

## Acknowledgments

We appreciate the editorial board's and reviewers' valuable comments on the paper.

## Availability of data and material

Not applicable.

## Conflicts of interest

The authors declare that there is no conflict of interest regarding the publication of this paper.

## Ethical standard

The authors have no relevant financial or non-financial interests to disclose.

## LITERATURE CITED

- Alzer, H. and A. Z. Grinshpan, 2007 Inequalities for the gamma and  $q$ -gamma functions. *Journal of Approximation Theory* **144**: 67–83.
- Arslan, O. and A. I. Genç, 2009 The skew generalized  $t$  distribution as the scale mixture of a skew exponential power distribution and its applications in robust estimation. *Statistics* **43**: 481–498.
- Bala, S. K. and P. K. Biswas, 2005 Tax-ombudsman in bangladesh: an analytical review of the regulatory framework. *Cost and Management* **33**: 27–40.
- Balakrishnan, N. and V. B. Nevzorov, 2004 *A primer on statistical distributions*. John Wiley & Sons.
- Çankaya, M. N., 2018 Asymmetric bimodal exponential power distribution on the real line. *Entropy* **20**: 23.
- Çankaya, M. N. and O. Arslan, 2020 On the robustness properties for maximum likelihood estimators of parameters in exponential power and generalized  $t$  distributions. *Communications in Statistics-Theory and Methods* **49**: 607–630.
- Çankaya, M. N., A. Yalçınkaya, Ö. Altındağ, and O. Arslan, 2019 On the robustness of an epsilon skew extension for burr iii distribution on the real line. *Computational Statistics* **34**: 1247–1273.
- Çankaya, M. N., 2021 Derivatives by ratio principle for  $q$ -sets on the time scale calculus. *Fractals* **29**: 2140040.
- Coles, S., J. Bawa, L. Trenner, and P. Dorazio, 2001 *An introduction to statistical modeling of extreme values*, volume 208. Springer.
- De Gregorio, J., D. Sanchez, and R. Toral, 2023 Entropy estimators for markovian sequences: A comparative analysis. arXiv preprint arXiv:2310.07547 .
- Haberman, S. J., 1989 Concavity and estimation. *The Annals of Statistics* pp. 1631–1661.
- Härdle, W., M. Müller, S. Sperlich, A. Werwatz, et al., 2004 *Nonparametric and semiparametric models*, volume 1. Springer.
- Hunter, D. R., 2023 Unsupervised clustering using nonparametric finite mixture models. *Wiley Interdisciplinary Reviews: Computational Statistics* p. e1632.
- Iacus, S. M. et al., 2008 *Simulation and inference for stochastic differential equations: with R examples*, volume 486. Springer.
- Jenkins, S. P., 2017 Pareto models, top incomes and recent trends in uk income inequality. *Economica* **84**: 261–289.
- Lehmann, E. L. and G. Casella, 2006 *Theory of point estimation*. Springer Science & Business Media.
- Mineo, A. and M. Ruggieri, 2005 A software tool for the exponential power distribution: The normalp package. *Journal of Statistical Software* **12**: 1–24.
- Mokhtari, F., R. Rouane, S. Rahmani, and M. Rachdi, 2022 Consistency results of the  $m$ -regression function estimator for stationary continuous-time and ergodic data. *Stat* **11**: e484.

- Montgomery, D. C., E. A. Peck, and G. G. Vining, 2021 *Introduction to linear regression analysis*. John Wiley & Sons.
- Serrano, F., 2007 The taxpayer's rights and the role of the tax ombudsman: an analysis from a spanish and comparative law perspective. *Intertax* **35**.
- Sicuro, G., P. Tempesta, A. Rodríguez, and C. Tsallis, 2015 On the robustness of the  $q$ -gaussian family. *Annals of Physics* **363**: 316–336.
- Stanimirović, I., 2017 *Computation of generalized matrix inverses and applications*. CRC Press.
- Vila, R., L. Alfaia, A. F. Menezes, M. N. Çankaya, and M. Bourguignon, 2022 A model for bimodal rates and proportions. *Journal of Applied Statistics* pp. 1–18.
- Vila, R., L. Ferreira, H. Saulo, F. Prata, and E. Ortega, 2020 A bimodal gamma distribution: properties, regression model and applications. *Statistics* **54**: 469–493.

**How to cite this article:** Çankaya, M. N., and Aydın, M. Future Prediction for Tax Complaints to Turkish Ombudsman by Models from Polynomial Regression and Parametric Distribution *Chaos Theory and Applications*, 6(1), 63-72, 2024.

**Licensing Policy:** The published articles in CHTA are licensed under a [Creative Commons Attribution-NonCommercial 4.0 International License](https://creativecommons.org/licenses/by-nc/4.0/).

